Cell wall profiling of tobacco leaves and grapes in the context of *Botrytis cinerea* infection

by

Florent Weiller

Dissertation presented for the degree of
Doctor of Philosophy (Agricultural Sciences)

at
Stellenbosch University
Department of Viticulture and Oenology, Faculty of AgriSciences

Supervisor: Dr JP Moore
Co-supervisors: Profs MA Vivier and A Driouich

March 2021

Declaration

By submitting this dissertation electronically, I declare that the entirety of the work contained therein is my own, original work, that I am the sole author thereof (save to the extent explicitly otherwise stated) that reproduction and publication thereof by Stellenbosch University will not infringe any third party rights and that I have not previously in its entirety or in part submitted it for obtaining any qualification.

Date: March 2021

Summary

The plant cell wall has been shown to be at the centre of plant-biotic stress interactions. In the case of a pathogen encounter (e.g. fungi), the cell wall acts as the second barrier after the cuticle to stop pathogen penetration and tissue colonisation. The plant cell wall matrix composition and architecture influences the nature of resistance and susceptible responses to fungal pathogens.

Botrytis cinerea, the fungus responsible for grey mold disease, causes worldwide crop losses. Understanding factors that differentiate susceptible from resistant plants is essential to develop new plant protection strategies against *B. cinerea*. In this study, genetically engineered plants with known resistance phenotypes, compared to the untransformed controls (with susceptible phenotypes) were used to understand the leaf cell wall changes either afforded by the transgenes introduced and/or the Botrytis infection process. The approach to investigate cell wall changes during Botrytis infection was also expanded to grapevine berry fruit. The method of choice was Comprehensive Microarray Polymer Profiling (CoMPP) technology, a high-throughput method for tracking cell wall matrix polysaccharide and protein composition and it was combined with monosaccharide profiling and various imaging tools.

In the first part of this study, the leaves of nine tobacco (*Nicotiana tabacum*) lines: four overexpressing the known defence gene, grapevine polygalacturonase-inhibiting protein 1 (*VviPGIP1*), four overexpressing another known defence gene, the tobacco cinnamyl alcohol dehydrogenase 14 (*NtCAD14)* and the wild type SR1 were screened for cell wall compositional differences due to genetic overexpression in the absence of infection. Total lignin and monolignols were assayed using Py-GC-MS, but results showed limited variations between the different plant lines. CoMPP and GC-MS analysis for cell wall composition and monosaccharide content showed variation in homogalacturonan (HG) methylesterification patterning between the various transgenic plant lines. Arabinogalactan proteins (AGPs) and extensins increased in the majority of the VviPGIP1 lines. These results suggest that PGIP overexpression probably influences pectinmethylesterase (PME) enzyme activity and affects glycoprotein organisation.

Following these results, more in-depth analysis continued during infection of PGIP plants. Infection experiments were conducted using *B. cinerea* on leaves of VviPGIP1 tobacco lines, compared to the wild type as control. Lesion size differences were observed from 96 hours post inoculation (hpi) with reduced lesions in the transgenic lines compared to the wild type, confirming the known resistance responses of the transgenic plants to the fungus. Cell wall alterations were followed in the 72 hpi period, showing HG degradation with RG-I signal increase, whereas the cellulose-xyloglucan network was mostly unaffected. Extensins and AGPs accumulated at and

around the lesions, while distal non-infected leaves showed matrix changes from 72 hpi, with reorganisation of the cellulose/xyloglucan network and in the homogalacturonan methylesterification patterning, indicative of a systemic response. A typical Botrytis infection with cell wall depectination exposed less hemicellulose polysaccharides. In parallel, the plant seemed to build a defensive response to the infection with accumulation of defence related proteins at the lesion and in distal leaves. Unlike the wild type, the transgenic plants response was efficient in restricting Botrytis progression from 72 hpi onwards.

In the last part of this study berries, at three developmental stages (veraison, post-veraison and ripe), from four *Vitis vinifera* cultivars (Cabernet Sauvignon, Sauvignon Blanc, Dauphine and Barlinka grape berries), were infected with *B. cinerea*. Ripe grapes from all four cultivars developed symptoms and showed cell wall degradation with cultivar differences were noted, while very few successful *B. cinerea* infections on veraison and post-veraison grapes were observed. This is in line with the generalised view that grapevine berries display ontogenic resistance in the greener developmental stages, although there are known exceptions. Cabernet Sauvignon was the least susceptible cultivar to *B. cinerea* and displayed a delayed lesion development in our experimental conditions. The infected grapes from all the cultivars were characterised by altered HG methylesterification patterning, extensin reorganisation, as well as glucan accumulation as the infection progressed.

This work has brought new insights to existing efforts to fully characterise the role of the grapevine *PGIP1* gene in plant cell wall modifications, in the presence and absence of *B. cinerea* infection. It provides further proof that small changes in the cell wall matrix contribute to the possible priming of plants to resist and overcome infection. Moreover, the similarities and differences observed between tobacco leaves and grape berry cell walls during Botrytis infection will help to conduct targeted experiments and to complement the existing models on plant cell wall – *B. cinerea* interactions.

Opsomming

Die plant selwand is al aangewys as die eppisentrum van plant-biotiese stress interaksies. In die geval van patogeen teëkoming (bv. swamme), tree die selwand op as ‘n tweede versperring, na die kutikula, om patogeen penetrasie en kolonisering te stop. Die plant selwand matriks samestelling en argitektuur beïnvloed die aard van weerstand of vatbare reaksies op swampatogene.

Botrytis cinerea, die swam verantwoordelik vir vaalrot, veroorsaak oes verliese wêreldwyd. Dit is van kardinale belang om die fakotre wat vatbare van weerstandbiedige plante van mekaar onderskei te verstaan om sodoende nuwe plant beskermingsstrategieë te ontwikkel teen *B. cinerea.* In hierdie studie, word geneties gemanipuleerde plante met bekende weestandsfenotipes, in vergelyking met die ongetransformeerde kontroles (met vatbare fenotipes) gebruik om die blaar selwand veranderinge te verstaan wat deur die transgene toegeein kan word en/of deur die *Botrytis* infeksie proses. Hierdie benadering om die selwand veranderinge tydens die *Botrytis* infeksie te bestudeer was verder uitgebrei na wingerdvrugte. Die voorgekeurde metode was Omvattende Mikro-sikking Polimeer Profilering tegnologie, ‘n hoë deursettings methode vir die analisering van selwand matriks polisakkaried en proteïen samestelling en dit was ook gekombineer met monosakkaried profilering en verskillende beeldhulpmiddels.

In die eerste gedeelte van hierdie studie was die blare van nege tabaklyne (*Nicotiana tabacum*): vier wat die bekende weerstandsgeen, *Vitis vinifera* poligalakturonase-inhiberende proteïen 1 (*VviPGIP1*), vier wat ‘n ander bekende weerstandsgeen ooruitdruk, die tabak kanielalkohol dehydrogenase 14 (*NtCAD14*) en die wilde tipe SR1 almal gekeur vir selwand samestellingsverskille as gevolg van die genetiese ooruitdrukking in die afwesigheid van infeksie. Totale lignien en monolignole was getoets deur Pirolise Gas Chromatografie Massaspektrometrie (Py-GC-MS), maar die resultate het egter beperkte variasies tussen die plantlyne getoon. Omvattende Mikro-sikking Polimeer Profilering tegnologie en GC-MS analise vir selwand samestelling en monosakkaried inhoud het variasie geroon in die homogalakturonaan (HG) metielverestering patroon tussen die verskillende transgeniese plantlyne. Arabinogalaktan proteïene (AGPs) en ekstensien het toegeneem in die meerderheid van die VviPGIP1 lyne. Die resultate stel voor dat PGIP ooruitdrukking moontlik die pektienmetielesterase (PME) ensiem aktiwiteit beïinvloed en die glukoproteïen organisasie affekteer.

Na aanleiding van hierdie resultate was ‘n verdere diepgaande ontleding voortgesit tydens die infeksie van die PGIP plante. Infeksie eksperimente was uitgevoer met *B. cinerea* op die blare van die VviPGIP1 tabak plantlyne en vergelykk met die wilde tipe as kontrole. Verskille in letsel grootte

was waargeneem vanaf 96 ure na inoculasie (uni) met verminderde letsels in die transgeniese lyne in vergelyking met die wilde tipe wat die bekende weerstand reaksie van die transgeniese plante teenoor die fungus bevestig. Veranderinge in die selwand was gevolg gedurende die 72 uni periode, wat HG-agteruitgang getoon het met rhamnogalakturonaan I (RG-I) onthulling, terwyl die sellulose-xiloglukaan netwerk die meeste geaffekteer was. Ekstensins en AGPs het opgehoop by en rondom die letsels, terwyl distale nie-geïnfekteerde blare, matriks veranderinge getoon het op 72 uni, met herorganisasie van die sellulose/xiloglukaan netwerk en in die homogalakturonaan metielverestering patroon, aanduidend van 'n sistemiese reaksie. ‘n Tipiese Botrytis infeksie met selwand depektinasie het minder hemisellulose blootgestel. In parallel, wil dit voorkom asof die plant 'n verdedigende reaksie opbou teenoor die infeksie, met ophoping van weerstand verwante proteïene by die letsel en by verre blare. Anders as die wilde tipe, was die reaksie van die transgeniese plante doeltreffend genoeg om die vordering van die Botrytis te beperk vanaf 72 uni en verder.

In die laaste gedeelte van hierdie studie was druiwebessies, by drie verskillende ontwilkkelingsfases (veraison, na-veraison en ryp), van vier *Vitis vinifera* kultivars (Cabernet Sauvignon, Sauvignon Blanc, Dauphine and Barlinka druiwebessies), geïnfekteer met *B. cinerea.* Ryp druiwe van al vier kultivars het simptome ontwikkel en selwand degradasie getoon met opgemerkte kultivarverskille, terwyl baie min suksesvolle *B. cinerea* infeksies op veraison en na-veraison druiwe opgemerk was. Dit is in lyn met die algemene sienning dat wingerd druiwebessies ontogeniese weerstand toon in die groen ontwikkelingsfases, hoewel daar wel bekende uitsonderings is. Cabernet Sauvignon was die minste vatbare kultivar teen *B. cinerea* en het ‘n vertraagde letsel ontwikkeling getoon met ons eksperimentele toestande. Die geïinfekteerde druiwe van al die kultivars was gekenmerk deur veranderde HG-metielverestering patrone, ekstensin herorganisasie so wel as glukaan akkumulasie soos die infeksie gevorder het.

Hierdie werk het nuwe insigte gebring tot die bestaande pogings om die rol van die wingerd *PGIP1* geen ten volle te karaktariseer in plant selwand aanpassings, in die teenwoordigheid en afwesigheid van *B. cinerea* infeksie. Dit verskaf ook verdere bewyse dat klein aanpassings in die selwand matriks bydra tot die moontlike verdedigingsvoorvoerding (“priming”) van plante om infeksie te weerstaan en te oorkom. Daarbenewens, die ooreenkomstes en verskille wat opgemerk was tussen tabakblare en wingerd druiwebessie selwande tydens *Botrytis* infeksie sal help om geteikende eksperimente uit te voer en sal die bestaande modelle op plant selwand – *B. cinerea* interaksies aanvul.

This dissertation is dedicated to
my Parents

Biographical sketch

Florent Weiller was born on 20 January 1987 in Mont Saint Aignan, Normandy, France. He enrolled in 2007 at the Université de Rouen (Rouen, France) for a Licence (BSc) Sciences, Technologie, Santé specialised in Sciences de la Vie, de la Terre et de l'Environnement. He graduated in 2010 and got accepted in a research Master (MSc) specialised in Biologie cellulaire. During this MSc he realised two internships of six months each at the Institute for Wine Biotechnology (Stellenbosch University, South Africa) to conduct a research project and obtain laboratory experience. These internships led to a publication. Following his graduation in 2012, he enrolled in 2013 for a PhD in Wine biotechnology in the same institute.

Acknowledgements

I wish to express my sincere gratitude and appreciation to the following persons and institutions:

- Dr John Moore, for his supervision, advices and help during all my thesis. For the long discussions about sciences, and the chitchats. And for his constant support during the up and downs.

- Prof Melané Vivier for giving me the opportunity to start this PhD and for her co-supervision and advices during this thesis.

- Prof Azeddine Driouich for connecting me with Stellenbosch and for his advices and support in all the phases of this thesis.

- The University of Stellenbosch, the SAGWRI and Winetech for financial support.

- Karin Vergeer for her constant help from my first day in Stellenbosch till now! Admin always felt easy with you and it was a great pleasure to come for a question or a chitchat.

- Varsha, Ilse, Mukani, Kari, Helmien, Carin, Anscha and Fanny for making the plantlab such a friendly place and accompanying me through that adventure.

- Anke and Chandré for making the Viticulture lab a warm place despite the liquid nitrogen and for all the chitchats.

- Other lab colleagues and academics for all their advices and friendliness.

- Sophie Bernard, Lucky Mokwena, Madelaine Frazenburg and Miranda Waldron for their technical support and guidance.

- Tania, Egon, Judith for keeping the environment clean despite all our mess and for their friendliness.

- Lorette and the admin people for their help.

- Marisa for her friendship, help and for making me discover South African culture and wine.

- Lalo, Jay, Sophia for making such a great group of friends.

- Lalitha for her constant support, encouragements and help.

- Pierre, Jason, Morgan, Roxane, Elodie, Had and all my friends from France South Africa and abroad for their support.

- My family for being always here when needed and for their constant encouragements.

- Helena for making my life so luminous since you entered it! For your unlimited support and encouragements. For bringing back a smile in the bad days. For making my figures look so much more beautiful and for your advices and help in the final rush! Every new day with you around is an adventure. I love you!

- My Parents for making me feel I can lift the world. For your unshakable support. For everything you have done for me. For believing in me. You raised me and guided me to become the person I am and I am forever grateful for all your love and care!!!

Preface

This dissertation is presented as a compilation of six chapters. Chapter 3 has been published in the journal Vaccines. Chapter 5 has been submitted for publication to Annals of Botany and written according to the style of the journal.

Chapter 1 **General Introduction and project aims**

Chapter 2 **Literature review**
The plant cell wall, its components, models and their role in response to pathogens

Chapter 3 **Research results**
Overexpression of VviPGIP1 and NtCAD14 in tobacco screened using glycan microarrays reveals cell wall reorganisation in the absence of fungal infection

Chapter 4 **Research results**
VviPGIP1 transgenic tobacco leaves infected by *Botrytis cinerea* results in localised degradation as well as AGP and extensin reorganisation at the lesion site

Chapter 5 **Research results**
Tracking cell wall changes in wine and table grapes undergoing *Botrytis cinerea* infection using glycan microarrays

Chapter 6 **General discussion and conclusions**

I hereby declare that, with the exception of the contributions by others stated below, I was responsible for and performed the infection experiments, sampling and tissue processing. I performed the microscopical observations under the guidance of Mrs Madelaine Frazenburg and Mrs Miranda Waldron (Chapter 4-5). The CT-scan observations were performed under the guidance of Prof Anton du Plessis (Chapter 5). I prepared the samples for GC-MS, they were run by Mr Lucky Mockwena, I integrated and analysed the peaks (Chapters 3-4-5). The CoMPPs were outsourced, AIR tissue was sent to Dr Jonatan Fangel, Dr Julia Schückel and Prof William Willats that performed the technique (Chapters 3-4-5). The Py-GC-MS (Chapter 3) was performed by Dr Lorenz Gerber. Prof Martin Kidds assisted in some of the statistical analyses and Prof Johan Trygg trained and advised me on the SIMCA software. I analysed all the results, extracted the information and structured the results in a contextualised logical way. I drafted the thesis. My supervisor Dr John Moore was involved in this study design with Prof Melané Vivier and Prof Azeddine Driouich. He also accompanied me through all the steps of this thesis with critical discussions and advises, he reviewed and corrected my manuscripts. Prof Melané Vivier acted as cosupervisor and complimented Dr Moore's inputs and thesis corrections. Prof Azeddine Driouich welcomed me in France for a three months training, shared his expertise and contributed in the manuscript revision.

Table of Contents

Abbreviations

AGP : Arabinogalactan protein
Ara : Arabinose
AIR : Alcohol insoluble residues
BK : Barlinka
CAD : Cinnamyl alcohol dehydrogenase
CBMs : Carbohydrate-binding modules
CDTA : Cyclohexane diamine tetra acetic acid
CoMPP : Comprehensive microarray polymer profiling
CS : Cabernet Sauvignon
CT : Computed tomography.
CWDEs : Cell wall degrading enzymes
DAMP : Damage associated molecular pattern
DE : Degree of esterification
Dp : Degree of polymerisation
DP : Dauphine
EL : Eichhorn and Lorenz
ELISA : Enzyme-Linked Immunosorbent Assay
ESI : Electrospray ionization
ePG : endo-Polygalacturonases
Fuc : Fucose
Gal : Galactose
GalA : Galacturonic acid
GC : Gas Chromatography
Glc : Glucose
GlcA : Glucuronic acid
HG : Homogalacturonan
Hi : High infection
HILIC : hydrophilic interaction liquid chromatography
HMDS : Hexamethyldisilazane
HPAEC : High performance anion-exchange chromatography
hpi : Hours post infection
HR : Hypersensitive response
HRGP : Hydroxyproline-rich glycoprotein
JIM : John Innes *Monoclonal* Antibodies
L : leaf
Li : Light infection
LM : Leeds Monoclonal Antibodies
LSD : Least significant difference
mAbs : Monoclonal antibody MAMP : Microbe associated molecular pattern
Man : Mannose
MAPK : Mitogen-activated protein kinase
ME : Methylesterification
Mi : Moderate infection
MS : Mass spectrometry
MTI : MAMP-triggered immunity
Ni : No-infection Defined twice
NW : No wax
OG : Oligogalacturonide
OIV : International Organisation of Vine
PAMP : Pathogen Associated Molecular Pattern
PC1 : First dimension principal component
PCA : Principal component analysis
PG : Polygalacturonases
PGA : Polygalacturonic acid
PGIP : Polygalacturonase inhibiting protein
PMEs : Pectin methylesterases
PMEIs : Pectin methyl-esterase inhibitor
PNL : Pectin lyase
PR : Pathogenesis-related
PRR : Pattern recognition receptor
PV : Post-Veraison
Py-GC–MS : Pyrolysis gas chromatography mass spectrometry
R : Ripe
RG : Rhamnogalacturonan
Rha : Rhamnose
ROS : Reactive oxygen species
SB : Sauvignon Blanc
SEM : Scanning electron microscopy
S/G ratio : Syringyl to guaiacyl ratio
TFA : Trifluoroacetic acid
TMCS : Trimethylsilyl chloride
V : Veraison
XET : Xyloglucan endotransglycosylase
XTH : Xyloglucan endotransglucosylase/hydrolase
XyG : Xyloglucan
Xyl : Xylose

Chapter 1

General introduction and project aims

General introduction and project aims

1.1.Introduction

Crop loss due to diseases poses a serious threat to agricultural yields and food security globally. Research has led to the development of pesticides that have drastically reduced the damage caused. However, the widespread use of pesticides has been shown to produce adverse and alarming effects such as soil contamination, pollinator poisoning and possible toxic effects on human health (Hernández *et al.* 2013; Czerwinski and Sadd 2017). The added negative social and environmental effects linked to pesticide use have been estimated in 2014 to cost 9.6 billion dollars in the USA alone (Pimentel and Burgess 2014). Consequently, a certain number of pesticides have been or are in the process of being banned leading to the need for more sustainable alternatives.

Grapevines are one of the most planted fruit crops worldwide (FAO, http://www.fao.org/faostat/en/#data; accessed: 01/11/2020). However, due to centuries of selection for quality-associated traits and vegetative propagation strategies that precluded the natural adaptation of the selected plants to pests and diseases, the commercial *Vitis vinifera* cultivars, most commonly used for wine and table grape production are sensitive to a variety of diseases. For example, during the 19th century, European grapevines were severely devastated after the accidental introduction of the North American aphid *Phylloxera vestatrix* and only saved due to the development of grafting *Vitis vinifera* scions onto resistant American rootstocks (Cantu *et al.* 2016). Currently vineyard pests and diseases are mostly controlled with chemical pesticides, although resistance breeding programmes around the world are providing a growing list of new, more resistant cultivars that could help to lessen the industry's dependence on chemicals. Currently, on average French grapevines are sprayed eight times per year against downy mildew, caused by the oomycete *Plasmopara viticola* (Chen *et al.* 2020).

1.2.The Botrytis – PGIP-cell wall nexus in pathogen infections and plant defence

Among the many pathogens responsible for pre- and post-harvest loss, the necrotrophic fungi such as *Botrytis cinerea* that feed on dead tissue (in contrast to biotrophic fungi e.g. the mildews) are particularly destructive (van Kan 2006). Significant research efforts including the identification of pathogen infection strategies and virulence factors (Petrasch, Silva, *et al.* 2019; Faris and Friesen 2020) are being conducted to understand pathogen infection processes and how they overcome the plants natural defence mechanisms (Pandey *et al.* 2016).

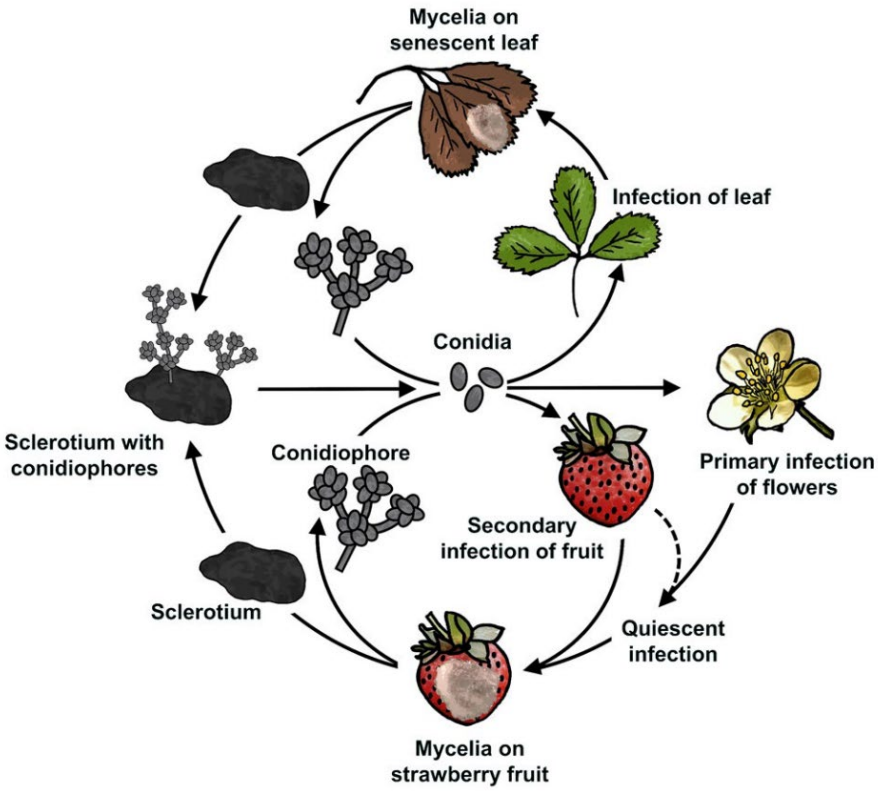

Figure 1.1: Disease cycle of *Botrytis cinerea* infection in strawberry. Flowers primary infections and fruit secondary infections are depicted (From Petrasch *et al.* 2019).

Research strategies have highlighted the necessity to focus on the identification and characterisation of molecules involved in successful plant defence responses. Saijo *et al.* (2018) reviewed the current knowledge on biotic stress perception by plants. They listed the known cell wall receptors and the downstream signalling pathways they activate to trigger untargeted or specific plant defence responses. Bacete *et al.* (2018) described how cell wall receptors can also sense products of cell wall degradation, generated during a pathogen attack, and trigger defence responses. Cell wall proteins have been shown to be crucial in plant protection against pathogens. They act at different levels by either targeting directly the pathogen and its effectors; acting as a shield to protect the plant cell wall components from fungal pathogen enzyme degradation; or by detecting and signalling the pathogen presence to trigger plant defence responses, as reviewed by Ferreira *et al.* (2007). Identification of resistance factors such as cell wall changes that limit pathogen enzyme efficiency i.e. methylesterification (Lionetti *et al.* 2017; Silva-Sanzana *et al.* 2019) or acetylation (Nafisi *et al.* 2015) have also been reported. Of importance are studies on plant cell wall composition, as it constitutes the first protective barrier during infection (Houston *et al.* 2016). Cell wall characterisation and comparison between sensitive and resistant plants have been typically conducted using mutant plants with an impaired cell wall trait. These studies have provided clues to perform more targeted analysis in order to identify cell wall components essential for resistance/susceptibility (Molina *et al.* 2020).

Polygalacturonase-inhibiting proteins (PGIPs) are one of the most studied proteins involved in protection against necrotrophic fungi, combining polygalacturonase (PGs) inhibitory action and a signalling role (Kalunke *et al.* 2015). A PGIP isolated from grapevine (*Vitis vinifera* cv. Pinotage) (De Ascensao 2001), encoded by *VviPGIP1*, showed *in vivo* inhibitory activity against *B. cinerea* PGs (Joubert *et al.* 2007). When overexpressed in tobacco (*Nicotiana tabacum*), the plants showed reduced susceptibility to *B. cinerea* (Joubert *et al.* 2006). In addition to the PGs inhibitory activity, it was shown that these transgenic tobacco plants displayed gene expression modifications prior to any fungal infection (Alexandersson *et al.* 2011). Amongst the changes observed, was modification of the cell wall matrix, namely the arabinoxyloglucan polymers, seemingly linked to downregulation of XET/XTH genes. The transgenic lines also displayed an increase in lignin deposition in their stems, linked with upregulation of lignin metabolism genes including a cinnamyl alcohol dehydrogenase (CAD), which is a protein that catalyses some of the final steps of lignin precursor biosynthesis (Vanholme *et al.* 2019). Finally, hormonal changes were also observed with an increase of auxin levels, and a stronger jasmonic acid response linked to *B. cinerea* infection (Alexandersson *et al.* 2011; Nguema-Ona *et al.* 2013). These results were suggestive of a primed state, due to the overexpression of the *VviPGIP1* gene. To assess the possible role of lignin in the resistance phenotype, the *NtCAD14* gene, upregulated in the VviPGIP1 tobacco plants, was overexpressed and characterised in newly engineered *NtCAD14* tobacco lines. These transgenic plants also displayed reduced sensitivity to *B. cinerea* during a leaf infection (Mbewana 2010) and increased CAD enzyme activity in the stems of the plants, but cell wall structure analysis and lignin assays were not completed on these plants, leaving some unanswered questions in terms of the observed phenotypes.

1.3. Project aims

This study aims:

(1) To make progress towards a better understanding of the cell wall matrix of tobacco leaves from plant lines that display susceptible and resistance phenotypes against *B. cinerea* (without infection, as well as during infection).

(2) To improve current knowledge on the *B. cinerea* infection process in the context of cell wall changes of grapevine fruits.

For aim 1: PGIP and CAD proteins have been shown to play a role in plant defence. However, the full extent of their action on cell wall composition or remodelling hasn't been investigated. The first aim of this study is to complete the characterisation of PGIP and CAD activity on cell wall composition and matrix rearrangement, by investigating available PGIP and CAD overexpressing tobacco lines. Cell wall characterisation of uninfected PGIP and CAD tobacco plants will supplement the initial

analyses performed previously (Alexandersson *et al.* 2011; Nguema-Ona *et al.* 2013) and particularly to test the role of lignification in the resistance phenotypes. This data will also provide a baseline to further analyse the effect of PGIP1 overexpression on cell wall remodelling upon infection with *B. cinerea* in the VviPGIP1 tobacco - *B. cinerea* pathosystem.

For aim 2: *B. cinerea* is a very adaptable fungus that can infect more than 1000 different plant species and modifies its infection strategies depending on the target host (Veloso and van Kan 2018). *V. vinifera* berries are a natural host for this pathogen albeit susceptibility differences are observed between cultivars. Current knowledge on grape berry cell wall modifications during infections are scarce. Therefore, we aim to investigate how cell wall compositions from different grape berry cultivars might change during an infection with *B.* cinerea and 'track' pathogen infection progression.

To track cell wall composition and changes, comprehensive microarray polymer profiling (CoMPP) is a promising and a recently developed technology. This profiling method provides a comprehensive analysis of cell wall matrix polysaccharides and glycoproteins composition using monoclonal antibodies and carbohydrate binding modules in a high-throughput format. CoMPP was chosen as the main analysis technology of this thesis, in association with imaging and quantification techniques. With the wide range of of monoclonal antibodies now available to detect cell wall components, it will help to identify those that might be used for future immunolocalisation studies.

This thesis has been written as three research chapters based on the following plants and pathosystems studied:

- VviPGIP1 (lines 24, 37, 45 and 47) and NtCAD14 (lines 4, 32, 38 and 42) overexpressing tobacco lines were profiled using a screening approach that included Py-GC-MS for lignin analysis, followed by CoMPP profiling analysis in conjunction with GC-MS for monosaccharide sugar composition (presented in Chapter 3).

- Two VviPGIP1 tobacco lines (37 and 45) with leaves infected with *B. cinerea* (using a hypervirulent grape strain (Atwell *et al.* 2015)) were followed by detailed cell wall analyses using CoMPP profiling in conjunction with GC-MS monosaccharide sugar composition at the infection lesion, on areas adjacent to the infection spot, as well as on uninfected distal leaves, during a time-course analysis over the first 72 hours of the infection (presented in Chapter 4).

- Berries from two wine grape (the red Cabernet Sauvignon and the white Sauvignon Blanc) and two table grape (the black Barlinka and the white Dauphine) cultivars at véraison, post-véraison and ripe developmental stages were infected by *B. cinerea* (hypervirulent grape

strain or BO.5.10) under controlled conditions. Infection was monitored using imaging techniques followed by CoMPP analysis in conjunction with GC-MS monosaccharide sugar composition (presented in Chapter 5).

The thesis also includes a condensed literature review (Chapter 2) and General Discussion and Conclusion section, presented in Chapter 6.

1.4.References

Alexandersson E, Becker JVW, Jacobson D, *et al.* 2011. Constitutive expression of a grapevine polygalacturonase-inhibiting protein affects gene expression and cell wall properties in uninfected tobacco. *BMC Research Notes* **4**: 493.

De Ascensao A. **2001**. Isolation and characterization of a polygalacturonase-inhibiting protein (PGIP) and its encoding gene from Vitis vinifera. *PhD thesis, Stellenbosch University, South Africa,*.

Atwell S, Corwin JA, Soltis NE, Subedy A, Denby KJ, Kliebenstein DJ. **2015**. Whole genome resequencing of *Botrytis cinerea* isolates identifies high levels of standing diversity. *Frontiers in Microbiology* **6**: 996.

Bacete L, Mélida H, Miedes E, Molina A. **2018**. Plant cell wall-mediated immunity: cell wall changes trigger disease resistance responses. *Plant Journal* **93**: 614–636.

Cantu D, Roper MC, Powell ALT, Labavitch JM. **2016**. Problematic crops: 1. Grape: to long life and good health: untangling the complexity of grape diseases to develop pathogen-resistant varieties In: *Plant Pathogen Resistance Biotechnology*. John Wiley and Sons, Inc., Hoboken, New Jersey, 193–215.

Chen M, Brun F, Raynal M, Makowski D. **2020**. Delaying the first grapevine fungicide application reduces exposure on operators by half. *Scientific Reports* **10**: 1–12.

Czerwinski MA, Sadd BM. **2017**. Detrimental interactions of neonicotinoid pesticide exposure and bumblebee immunity. *Journal of Experimental Zoology Part A: Ecological and Integrative Physiology* **327**: 273–283.

Faris JD, Friesen TL. **2020**. Plant genes hijacked by necrotrophic fungal pathogens. *Current Opinion in Plant Biology* **56**: 74–80.

Hernández AF, Parrón T, Tsatsakis AM, Requena M, Alarcón R, López-Guarnido O. **2013**. Toxic effects of pesticide mixtures at a molecular level: Their relevance to human health. *Toxicology* **307**: 136–145.

Houston K, Tucker MR, Chowdhury J, Shirley N, Little A. **2016**. The plant cell wall: a complex and dynamic structure as revealed by the responses of genes under stress conditions. *Frontiers in Plant Science* **7**: 984.

Joubert DA, Kars I, Wagemakers L, *et al.* 2007. A polygalacturonase-inhibiting protein from grapevine reduces the symptoms of the endopolygalacturonase BcPG2 from *Botrytis cinerea* in *Nicotiana benthamiana* leaves without any evidence for in vitro interaction. *Molecular Plant-Microbe Interactions* **20**: 392–402.

Joubert DA, Slaughter AR, Kemp G, *et al.* 2006. The grapevine polygalacturonase-inhibiting protein (VvPGIP1) reduces Botrytis cinerea susceptibility in transgenic tobacco and differentially inhibits fungal polygalacturonases. *Transgenic Research* **15**: 687–702.

Kalunke RM, Tundo S, Benedetti M, Cervone F, De Lorenzo G, D'Ovidio R. **2015**. An update on polygalacturonase-inhibiting protein (PGIP), a leucine-rich repeat protein that protects crop plants against pathogens. *Frontiers in Plant Science* **6**: 146.

van Kan JAL. **2006**. Licensed to kill: the lifestyle of a necrotrophic plant pathogen. *Trends in Plant Science* **11**: 247–53.

Lionetti V, Fabri E, De Caroli M, *et al.* 2017. Three pectin methylesterase inhibitors protect cell wall integrity for Arabidopsis immunity to *Botrytis*. *Plant Physiology* **173**: 1844–1863.

Mbewana S. **2010**. Functional analysis of a lignin biosynthetic gene in transgenic tobacco. *MSc thesis, Stellenbosch University, South Africa,*.

Molina A, Miedes E, Bacete L, *et al.* 2020. Arabidopsis cell wall composition determines disease resistance specificity and fitness. *bioRxiv*: 2020.05.21.105650.

Nafisi M, Stranne M, Fimognari L, *et al.* 2015. Acetylation of cell wall is required for structural integrity of the leaf surface and exerts a global impact on plant stress responses. *Frontiers in Plant Science* **6**: 550.

Nguema-Ona E, Moore JP, Fagerström AD, *et al.* 2013. Overexpression of the grapevine PGIP1 in tobacco results in compositional changes in the leaf arabinoxyloglucan network in the absence of fungal infection. *BMC Plant Biology* **13**: 46.

Pandey D, Rajendran SRCK, Gaur M, Sajeesh PK, Kumar A. **2016**. Plant defense signaling and responses against necrotrophic fungal pathogens. *Journal of Plant Growth Regulation* **35**: 1159–1174.

Petrasch S, Knapp SJ, van Kan JAL, Blanco-Ulate B. **2019**. Grey mould of strawberry, a devastating disease caused by the ubiquitous necrotrophic fungal pathogen *Botrytis cinerea*. *Molecular Plant Pathology* **20**: 877–892.

Petrasch S, Silva CJ, Mesquida-Pesci SD, *et al.* 2019. Infection strategies deployed by *Botrytis cinerea*, *Fusarium acuminatum*, and *Rhizopus stolonifer* as a function of tomato fruit ripening stage. *Frontiers in Plant Science* **10**: 1–17.

Pimentel D, Burgess M. **2014**. Environmental and economic costs of the application of pesticides primarily in the United States In: *Integrated Pest Management*. Springer Netherlands, 47–71.

Saijo Y, Loo EP iian, Yasuda S. **2018**. Pattern recognition receptors and signaling in plant–microbe interactions. *Plant Journal* **93**: 592–613.

Silva-Sanzana C, Celiz-Balboa J, Garzo E, *et al.* 2019. Pectin methylesterases modulate plant homogalacturonan status in defenses against the aphid *Myzus persicae*. *Plant Cell* **31**: 1913–1929.

Vanholme R, De Meester B, Ralph J, Boerjan W. **2019**. Lignin biosynthesis and its integration into metabolism. *Current Opinion in Biotechnology* **56**: 230–239.

Veloso J, van Kan JAL. **2018**. Many shades of grey in *Botrytis*–Host plant interactions. *Trends in Plant Science* **23**: 613–622.

Chapter 2

Literature review

The plant cell wall, its components, models and their role in response to pathogens

Chapter 2
Literature review

2.1. The plant cell wall, an introduction

The plant cell wall is the outer layer of the plant cells beyond the plasma membrane, and interacts with the cuticle and wax layers on the outer surfaces (Albersheim *et al.* 2011). It is an important cellular component for plants which provides support and plasticity/elasticity during plant growth and development, as well as rigidity and resistance to mechanical constraints and turgor pressure (Höfte and Voxeur 2017). With the cuticle, it also acts as the first barrier against various types of pathogen attack (e.g. fungi) and is very important for plant disease resistance in general (Underwood 2012).

The plant cell wall forms a complex and dynamic matrix which can, in general, be divided into three parts, the middle lamella, the primary cell wall and the secondary cell wall (Albersheim *et al.* 2011) (Fig 2.1). Each of these interconnected polysaccharide and glycoprotein networks vary depending on the tissue, developmental stage and the plant species in question (Albersheim *et al.* 2011).

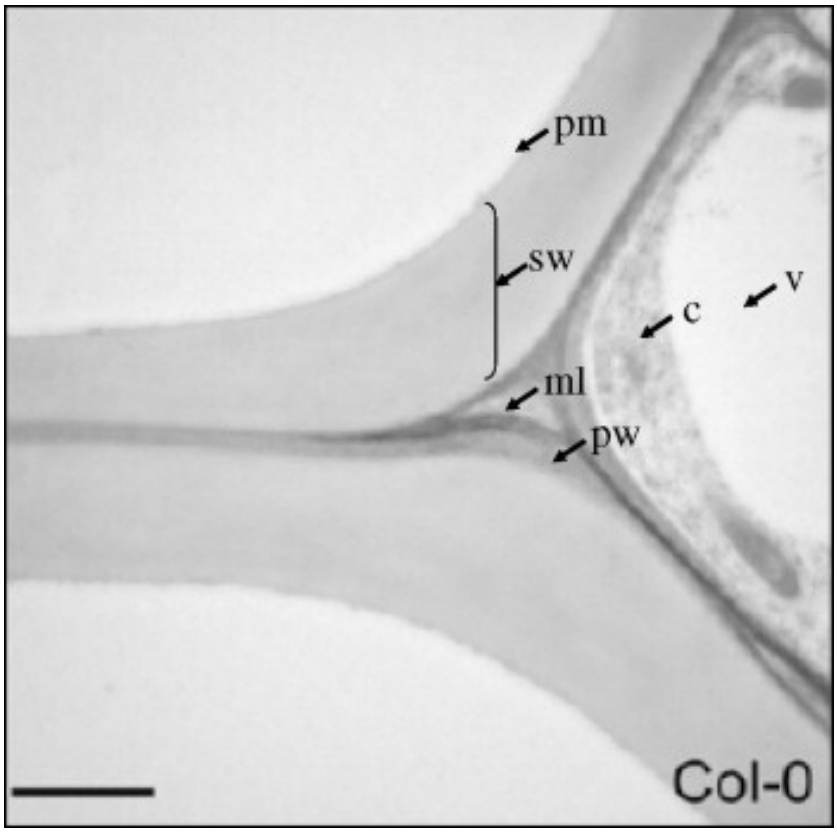

Figure 2.1: Transmission electron micrograph of *Arabidopsis thaliana* Columbia-O cell wall. The micrograph is centered on a middle lamella (ml), the primary cell wall (pw) and the secondary cell wall (sw). The plasma membrane (pm), cytosol (c) and vacuole (v) are also reported. Scale bar = 2 µM. From Caffall and Mohnen (2009)

The middle lamella is located at the interface between cells and plays a role in cellular adhesion and tissue cohesion. It is rich in pectins which act as the 'cement' between the cells from the moment they are formed during cytokinesis (Albersheim *et al.* 2011). The primary cell wall is the first cell wall formed during plant growth (Cosgrove and Jarvis 2012). It brings support and flexibility to the growing cells. The middle lamella is hydrophilic (composed of 60% fresh weight water), and rich in cellulose (30% dry weight i.e. insoluble cell wall residue), pectin (25-30%) and hemicellulose, which are mostly xyloglucan (20%) (Fry 2018). The secondary cell wall is formed in some specialised tissues like the xylem cells and woody vasculature when cells reach their maximum size (Somerville *et al.* 2004). It is located between the primary cell wall and the plasma membrane and brings rigidity and disease resistance to the plant tissue (Miedes *et al.* 2014). Secondary cell walls are a primary source of cellulose which account for up to 50% of their dry weight, whereas their hemicellulose is mostly composed of glucuronoxylans (20-30%) and their pectin content is very low (Fry 2018). Secondary cell walls are more hydrophobic and in some tissues like the xylem, they are additionally lignified (Fry 2018). This literature review will focus on the primary cell wall of dicotyledons such as *Arabidopsis thaliana,* the molecular model plant species. The main primary cell wall polysaccharide-protein components will first be described. Then the various plant cell wall architecture models, which have been proposed over the years, will be presented, before describing cell wall components role in plant immunity against biotic stresses, particularly pathogenic fungi such as *Botrytis cinerea*.

2.2 The cell wall components

2.2.1. Cellulose

Cellulose is a polymer of β-(1-4)-D-glucopyranoses linear chains. The chains are composed from 250 to 15000 neutral glucose residues and are linked together through hydrogen bonds to form microfibrils. Known as the most abundant biopolymers on earth, they are synthesised in the plasma membrane by cellulose synthase complexes (Somerville 2006). As presented in the different models, they are the main blocks of the matrix bringing rigidity and general structure to the cell wall. The orientation of cellulose fibres shapes the resistance and elongation direction of the wall (Thomas *et al.* 2013; Cosgrove 2014). Cellulose can be found in different forms, from crystalline to amorphous, depending on the "order", hydrogen bonds and hydrophobicity of the fibres. Their state will determinate their properties and degradability (Lynd *et al.* 2002; Arantes and Saddler 2010).

2.2.2. Hemicellulose

Hemicellulose consists of a heterogeneous group of polysaccharides that group together the non-cellulosic and non-pectic polysaccharides. They are composed of mono- and heteropolymeric chains which can be substituted or associated with side chains. The monopolymeric hemicelluloses have their main chains composed of xylose, mannose and glucose for the xylan, mannan or β-glucan

families respectively (Ebringerová *et al.* 2005; Fry 2011). In the primary cell wall of eudicotyledons, xylan is mostly found as glucuronoarabinoxylan where xylan chains are substituted with glucuronic acid and arabinose residues (about 5% of dry weight). Arabino- and glucuronoxylan can also be found. Xylan substitution can vary a lot between species, tissues and developmental stages, xylose residues can also be acetylated (Scheller and Ulvskov 2010).

Mannans as monopolymers are minor in primary cell wall of eudicotyledons. Their mannose backbone can be substituted with galactose forming galactomannans. Most of the mannans are found as glucomannans, a heteropolymer with alternating mannose and glucose residues (3-5% of cell wall dry weight). Mannose can also be substituted with galactose (galactoglucomannans). Mannans and glucomannans can be acetylated on mannose residues, (Scheller and Ulvskov 2010; Pauly *et al.* 2013). Xylan and mannan's role in secondary cell walls where they are more abundant has been shown to be linked with structure/strengthening for xylan and seed storage for galactomannans but their role in the primary cell walls remains largely unknown (Scheller and Ulvskov 2010).

Xyloglucans represent the major hemicellulose in eudicotyledons primary cell walls (20-25% of cell wall dry weight). Its backbone is formed of (1,4)-β-D-glucose residues largely substituted with α-D-xyloses. A nomenclature, based on xyloglucan substitution was created, it can be described as a succession of letters, each representing the last substituted sugar (if substituted). Xyloglucan from vascular plants are mainly substituted by three xyloses out of four glucoses forming a XXXG unit, consequently they are usually grouped as oligomers of four units (whereas grass xyloglucans have a XXGG base unit). Xylose residues can also be substituted with an additional sugar such as β-D-galactose (L) and/or α-L-arabinose (S). Galactose residues can be in turn substituted by α-L-fucose residues (F). With less common substitutions, 24 combinations have been identified to date. Additionally, some of the monosaccharides can be acetylated (Scheller and Ulvskov 2010; Pauly and Keegstra 2016). As described previously, xyloglucan have been shown to play a structural role in the cell wall architecture by cross-linking cellulose microfibrils. Therefore, xyloglucan modifications can act on the cell wall matrix properties and cohesion. By cutting xyloglucan chains, the matrix can be loosened. That process has been shown to occur and be important during plant growth or fruit ripening (Chebli and Geitmann 2017; Witasari *et al.* 2019). It is done by xyloglucan endotransglucosylase/hydrolase (XTH), a family of enzymes that can cleave xyloglucan chains with either hydrolase (XEH) or endotransglycosylase (XET) activity (Van Sandt *et al.* 2007; Miedes *et al.* 2013; Shinohara *et al.* 2017).

2.2.3. Pectin

The pectic polymers are complex and diverse polysaccharides, they represent about 30% of the primary cell wall in eudicotyledons and have various functions (Caffall and Mohnen 2009). They are composed of different structural "domains", covalently linked together (Atmodjo *et al.* 2013), often discussed as separate polymers. They are galacturonic acid-rich and are composed of up to 17 different sugars involving 20 known linkages (Voragen *et al.* 2009). They can be described as four different structures in eudicotyledons which are homogalacturonan, xylogalacturonan and rhamnogalacturonan 1 and 2 as represented in Figure 2.2.

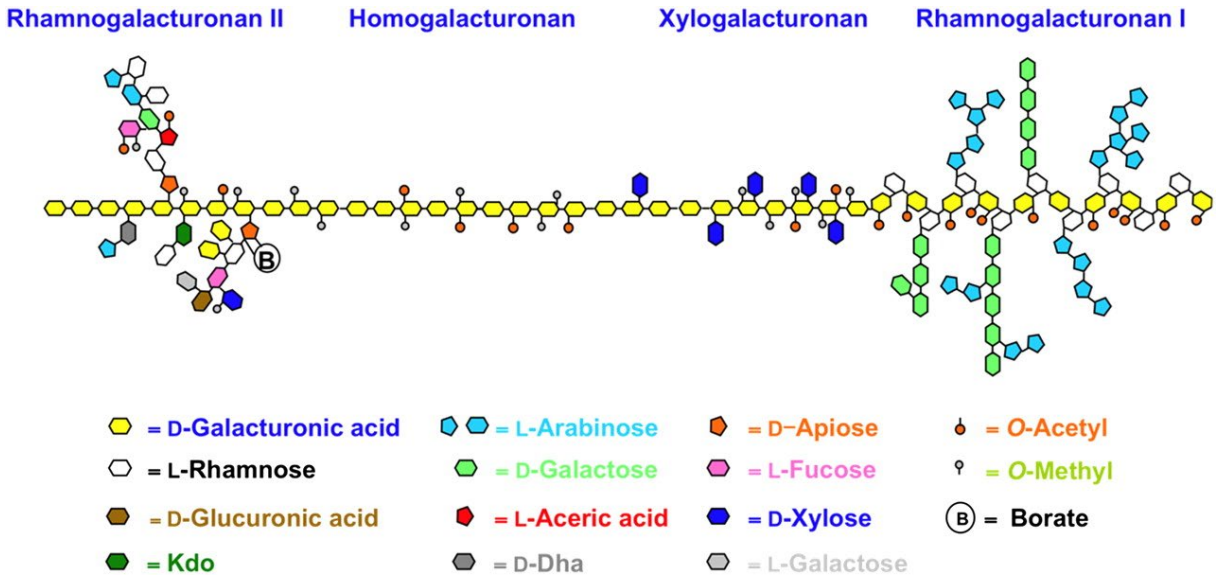

Figure 2.2: Schematic arrangement of the four pectin polysaccharides. Kdo: 3-Deoxy-D-manno-2-octulosonic acid; DHA: 3-deoxy-D-lyxo-2-heptulosaric acid. (From Harholt *et al.* (2010))

Homogalacturonan (HG) is the major pectin polysaccharide representing up to 65% of the primary cell wall pectins (Mohnen 2008). It is a homopolymer composed of α-1,4-linked D-galacturonic acid residues from 85 to 230 units which can be methyl esterified or acetylated. The degree of methyl-esterification, by modifying the charge of the chain, will affect HG solubility, its capacity to act as a gel and the cell wall biochemical and biomechanical properties (Levesque-Tremblay *et al.* 2015). This influences the cell wall porosity (Mohnen 2008). Stretches of non-methylated HG portions, which are negatively charged, can be linked together through calcium ions bridges (Liners *et al.* 1989). Those structures, called "egg-box motifs", are thought to play a role in cell adhesion as the middle lamella is pectin rich (Wolf *et al.* 2009) and might play a role against pathogen penetration as they induce cell wall tightening. HG has been shown to play different roles in morphogenesis (Chebli and Geitmann 2017), fruit maturation and softening (Wang *et al.* 2018) or defence against pathogens.

HG can be substituted by single or disaccharides of xylose forming xylogalacturonans (less than 10% of pectin), mostly found in reproductive tissues. Notably, in monocotyledons, HG can be substituted by apiofuranose residues, forming apiogalacturonans (Fry 2018).

The HG backbone can also be substituted with at least four different side chains composed of twelve different glycosyl residues (17 with stereoisomers), bound together by twenty different linkages (O'Neill *et al.* 2004). This domain is called rhamnogalacturonan II (RG-II) and forms the most complex polysaccharide in the plant cell wall, representing 1 to 4% of the primary cell wall components. The side chains are composed of classic and rare glycosyl residues such as aceric acid, 2-*O*-methyl fucose, 2-*O*-methyl xylose, apiose, 3-deoxy-D-manno-2-octulosonic acid (Dha), 3-deoxy-D- lyxo-2-heptulosonic acid (KDO) (see Figure 2.2). Rhamnogalacturonan-II are often found as dimers cross-linked by borate di-ester bonds (Kobayashi *et al.* 1996; Chormova and Fry 2016) and they can be covalently linked to HG (Ishii and Matsunaga 2001). RG-II is considered as highly conserved, though small chains variations were reported in *Vitis vinifera* cultivar Merlot and *A. thaliana* (Pabst *et al.* 2013; Buffetto *et al.* 2014). Rhamnogalacturonan-II boron links are essential for plant growth; in the Arabidopsis, the *mur1* mutant with a modified RG-II side chain unable to dimerise, leads to dwarf plants (O'Neill *et al.* 2004).

The last pectin domain, termed rhamnogalacturonan-I (RG-I), accounts for 20 to 35% of the primary cell wall pectins. It has a backbone composed of a succession of (1,2)-α-L-Rha-(1,4)-α-D-GalA disaccharides. Rhamnose residues can be substituted (from 20 to 80%) with very diverse neutral side chains composed of galactan, arabinan or arabinogalactan either linear or branched, fucose and glucuronic acid were also observed in minor quantities (Mohnen 2008; Fry 2018). Rhamnogalacturonan-I can be acetylesterified, mostly on its GalA residues, while methylesterification is still under investigation (Yapo 2011b). Long arabinan and/or galactan side chains are capable to bind to cellulose through hydrogen bonding which suggests an important role as a structural polysaccharide (Zykwinska *et al.* 2007).

2.2.4. Cell wall proteins

The primary cell wall is also composed of many structural and functional proteins that represent about 10% of its mass. Many of those proteins possess enzymatic activity to remodel the cell wall matrix, depending on the tissue needs (growth, maturation, senescence) and could include hydrolases, esterases, peroxidases, invertases or lyases, such as XTH, polygalacturonase (PG), pectin methyl-esterase (PME) and pectate lyase (PL) enzymes (Showalter 1993; Duruflé *et al.* 2017). To control these cell wall remodelling enzymes, enzyme inhibitors are also present such as PG inhibiting proteins (PGIPs) and PME inhibitors (PMEIs). These proteins inhibit plant enzymes when required but are also involved in plant protection by inhibiting pathogen cell wall degrading enzymes (CWDEs) or by promoting the production of functional damage associated molecular patterns (DAMPs) to trigger a strong or specialised defence response (Kalunke *et al.* 2015; Lionetti *et al.*

2017; Bacete *et al.* 2018) (see section 2.6 for more details). Other functional proteins of importance include expansins which loosen the plant cell wall by non-enzymatically removing hydrogen bonds between cellulose and xyloglucan (Cosgrove 2015; Marowa *et al.* 2016). The most important structural proteins are composed of the hydroxyproline-rich glycoprotein (HRGP) family (Showalter 1993; Cassab 1998). These proteins can be structurally classified in different groups, the extensins, arabinogalactan proteins (AGPs), Hyp/proline-rich proteins and glycine-rich proteins (Hijazi *et al.* 2014; Czolpinska and Rurek 2018). Among them, extensins and AGPs have been extensively studied.

2.2.5. Extensins

Extensins are HRGP characterised by a repeating pentapeptide sequence Ser-$(Hyp)_4$, but other repeating units that vary between species are usually also present. Extensins are *O*-glycosylated with most of the Hyp substituted with arabinose chains of one to five residues. Ser can also be substituted with one or two Gal residues (Hijazi *et al.* 2014). They form a rod-like glycoprotein with a left-handed poly-Pro-II helix (Lamport *et al.* 2011). Extensins possess tyrosine residues that can be oxidised and transformed into isodityrosines to cross-link; this can modify the protein conformation or commonly leading to extensins cross-links forming a protein network (Brady *et al.* 1998). They are believed to be able to link with pectin through their opposite electrostatic interactions, or with other glycoproteins such as AGPs (Valentin *et al.* 2010; Tan *et al.* 2018). Extensins are known to be involved in many functions such as cell morphogenesis and growth (Baumberger *et al.* 2001; Velasquez *et al.* 2011; Herger *et al.* 2019) or response to mechanical stresses (Merkouropoulos and Shirsat 2003; Vlad *et al.* 2007).

2.2.6. AGPs

AGPs are proteoglycans belonging to the HRGP family (Showalter 2001). Although their structure can vary a lot, “classical AGPs” are rich in Hyp, Ala, Ser, Thr and Gly amino acids. They are composed of at least 90% of carbohydrates (mass) forming side-chains. Those chains are arabinose and galactose rich, often forming short arabinan chains, or the typical arabinogalactan chain II (also found in RG-I). Many AGPs possess a glycosylphosphatidylinositol lipid anchor at the C-terminal which allows them to be anchored to the plasma membrane (Seifert and Roberts 2007; Tan *et al.* 2012). AGPs are therefore found in the plasma membrane, in the cell wall, and are even secreted. AGPs have been found to possess functions involving them in a wide range of biological process. In apple fruits, AGPs presence was found to increase with ripening, their conformation and mass varying, while their proper conformation was shown to be essential for cell wall assembly (Leszczuk *et al.* 2020). Several studies pointed out their role in plant morphogenesis and growth with functions in cell division and expansion, root and shoot development, programmed cell death, plant reproduction, embryogenesis or pollen germination as extensively reviewed by Ellis *et al*. (2010), Seifert and Roberts (2007) and Su and Higashiyama (2018).

2.3. Current perspectives on plant primary cell wall models

The plant cell wall is a complex and dynamic matrix that is not fully understood, even after 50 years of concerted efforts. In order to reconcile research data with cell wall structure and functioning, various plant cell wall models have been developed and refined, evolving as new research methods and approaches are adopted.

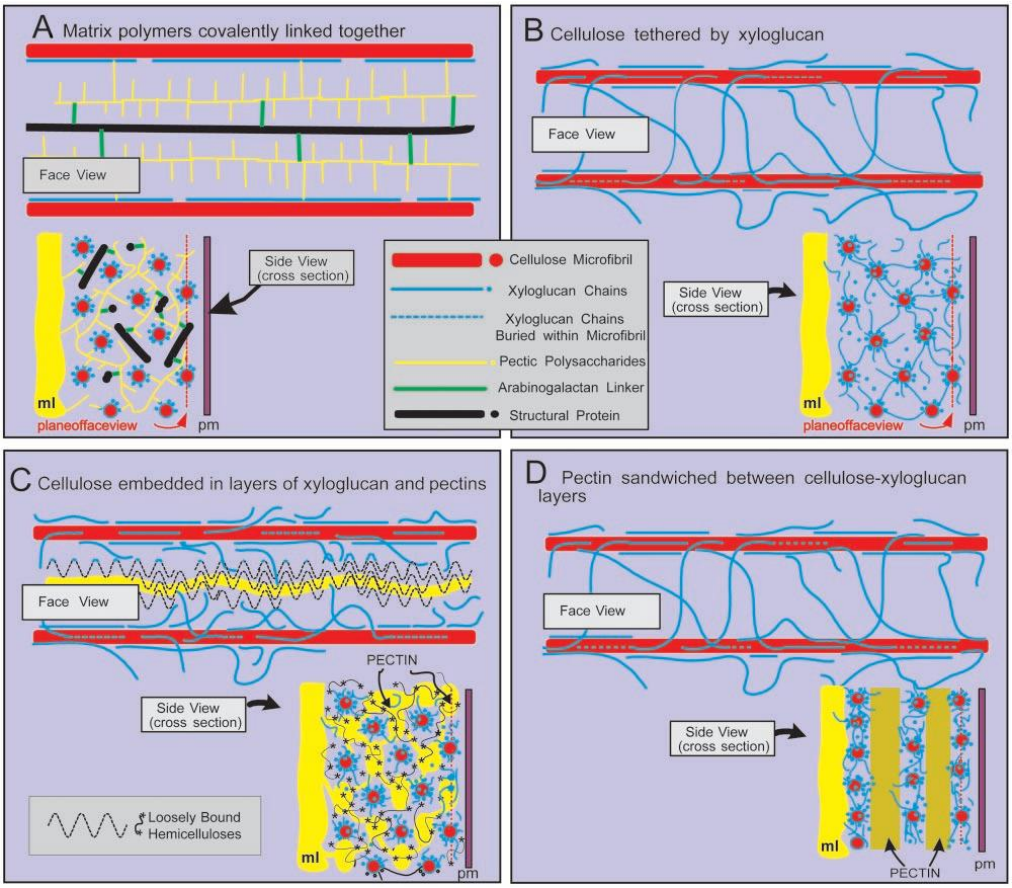

Figure 2.3: Different cell wall structure models. **A**: Keegstra model – Cellulose is linked to xyloglucan by hydrogen bonds. The other polymers from the matrix are covalently linked to one another. **B**: "Tethered Network" model – Cellulose is tethered together by single xyloglucan chains that cross the gap between microfibrils, while pectic polysaccharides (not represented) occupy the space within the xyloglucan chains. **C**: "Multicoat" model – Cellulose is embedded in layers of matrix polymers that get successively looser. Cite **D**: "Stratified" model – Cellulose microfibril – xyloglucan chains layers alternate with pectin polysaccharides layers, resembling a sandwich. cite pm: Plasma membrane; ml: middle lamella. From Cosgrove (2001)

Based on sycamore cell suspension cultures, one of the first cell wall models was proposed by Keegstra *et al.* in 1973. Keegstra *et al.* (1973) proposed that pectin, cell wall proteins and xyloglucan were covalently attached to each other and that xyloglucan was linked to cellulose through hydrogen bonds (Figure 2.3A). This model was later refined by Fry (1988) and Hayashi (1989) with the 'tethered network model'. They proposed xyloglucan as linking (tethering) cellulose microfibrils that act as "load bearing" polymers within the cell wall framework (Figure 2.3B). Pectin is then embedded with other hemicelluloses and cell wall proteins within the framework. This model

was reviewed and extended to primary and secondary cell walls of grasses, monocotyledonous, as well as dicotyledonous flowering plants and contextualised for expanding cells by Carpita and Gibeaut (1993). Alternative models based on the “tethered network” were proposed such as the “multicoat” model from Talbott and Ray (1992) where pectins are forming looser layers in the interface between cellulose-hemicellulose layers (Figure 2.3C). Alternatively, the “stratified model” described a cell wall where layers of cross-linking cellulose microfibrils are stacked, bringing rigidity and separated by gel-like pectins (Figure 2.3D) (Ha *et al.* 1997). These various models were described and reviewed in Cosgrove (2001), see Figure 2.3 for a schematic description and Figure 2.4 for an up to date tethered network model.

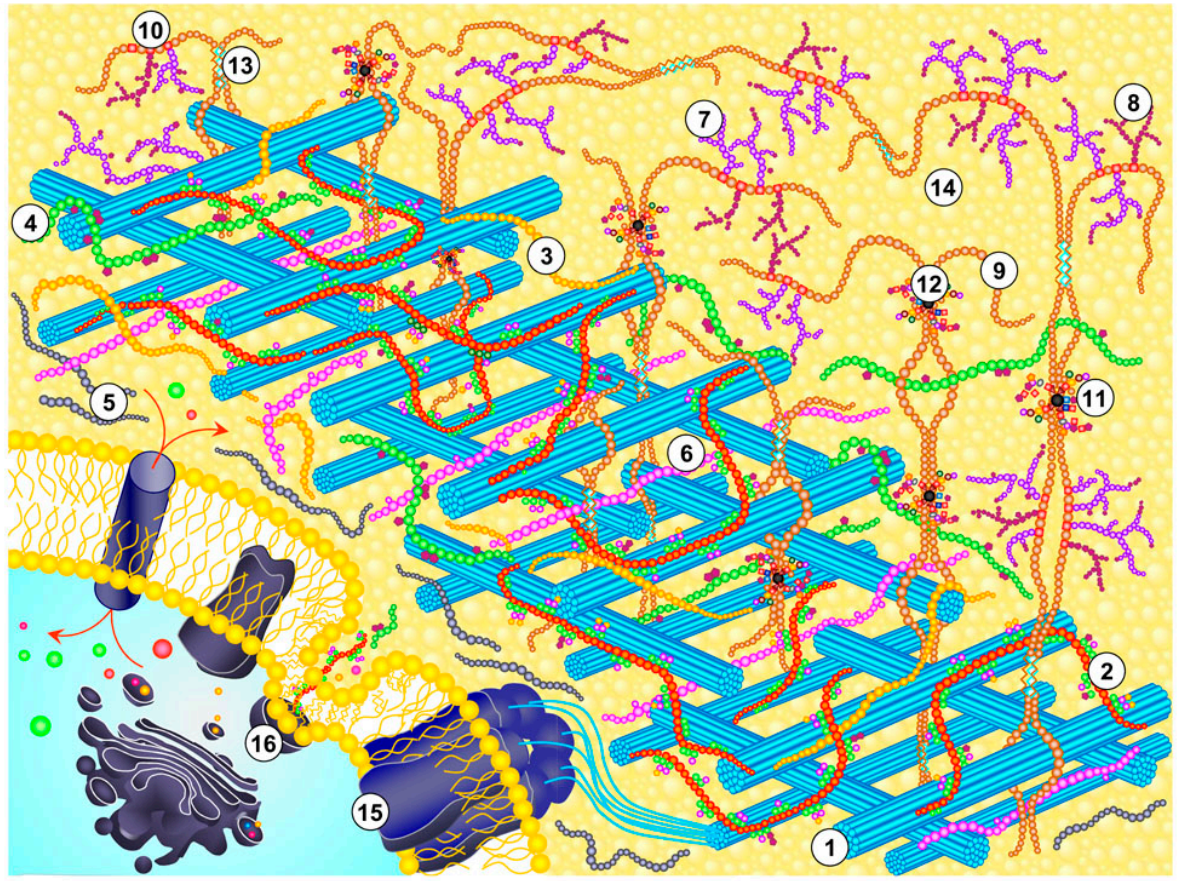

Figure 2.4: Model of plant cell wall with polysaccharides and proteins matrix representation **1**: Cellulose microfibrils; 2–6: Hemicelluloses: **2**: xyloglucan; **3**: mixed-linkage glucan; **4**: xylan and related heteroxylans; **5**: callose; **6**: mannan and related heteromannans; 7–11: Pectins: **7**: galactan; **8**: arabinan; **9**: homogalacturonan; **10**: rhamnogalacturonan-1; **11**: rhamnogalacturonan-2; **12**: boron bridge; **13**: ‘egg-box’ motif with calcium bridges; 14–16: Non-polysaccharide components: **14**: enzymes and structural proteins; **15**: cellulose synthase complex; **16**: transport vesicles. (From Franková and Fry 2013)

More recent findings have indeed shown that the matrix is much more interlinked than suggested previously. In potato and sugar beet, arabinan and galactan side chains of RG-I were found to be able to stick to cellulose microfibrils (Zykwinska *et al.* 2007). Xyloglucan in rose suspension cells and many other angiosperm cell cultures were found to be covalently linked to (acidic) pectin (Thompson and Fry 2000; Popper and Fry 2005), showing that the polysaccharides

are much more interlinked together. This was also shown by Cavalier *et al.* (2008), using *Arabidopsis thaliana* xyloglucan deficient mutants. In these plants, which had two xylosyltransferase genes disrupted, xyloglucan epitopes were not detected and while mechanical properties were altered, the viability of the plants were not affected, as could have been expected with the tethered model. These results suggested the presence of alternative supporting/linking polysaccharides than xyloglucan. Park and Cosgrove (2012) also showed that the xyloglucan "load bearing domains" were short and bringing cellulose microfibrils almost in contact with one another, leading scientists to question the validity of the tethered network model (Cosgrove and Jarvis 2012; Cosgrove 2014). These contradicting results and insights lead to the development of a new cell wall model termed the "biomechanical hotspots model" (Park and Cosgrove 2015; Cosgrove 2018), presented in comparison with the tethered network model in Figure 2.5.

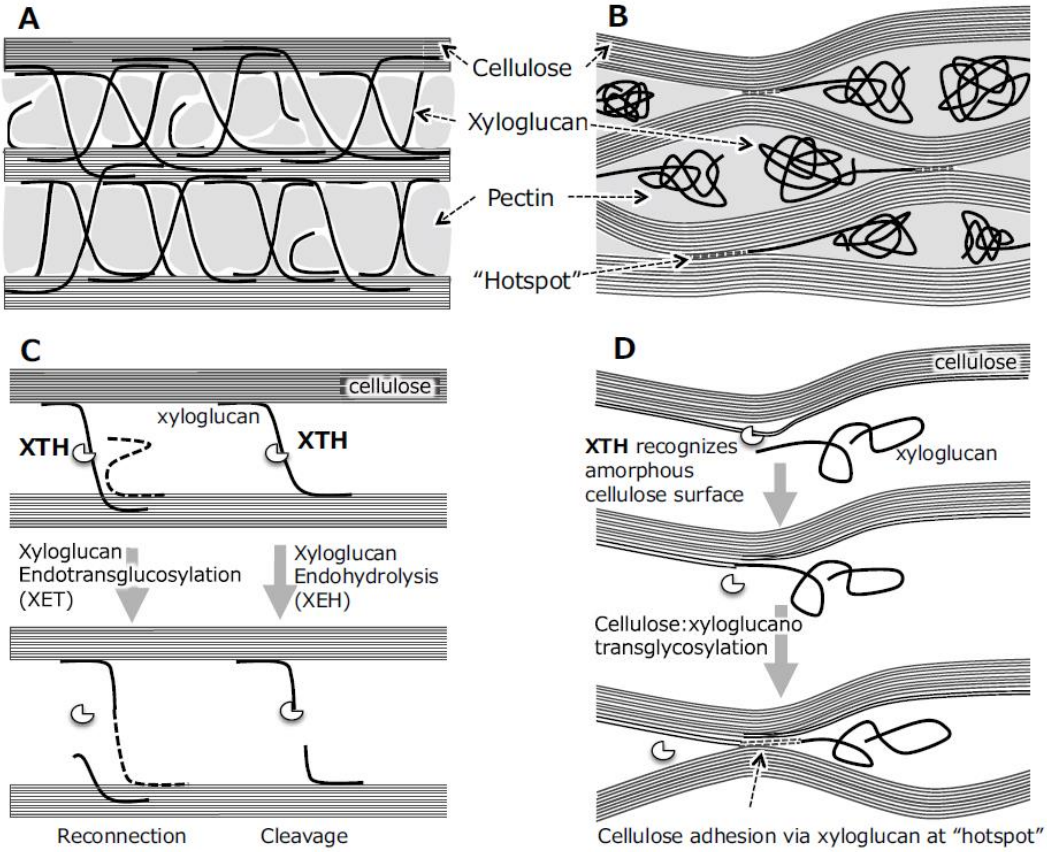

Figure 2.5: Model for integration of both "Tethered Network" (A) and "Biomechanical hotspot" (B) models. In (C) XTHs and XETs cleave and reconnect xyloglucan tethers; or in (D) XTH is responsible for cellulose adhesion via xyloglucan "hotspots". XET, xyloglucan endo-transglycosylase; XTH, Xyloglucan endotransglucosylase/hydrolases (presented by Kazuhiko Nishitani at the 8th Plant Biomechanics International Conference, Nagoya, Japan).

While this model, represented in Figure 2.6, is relatively new and not widely accepted, it highlights the cell wall matrix complexity and the dynamism of cell wall focused research. Even though the structural models and the interactions between cell wall components remain to be fully understood, the biochemical composition of plant cell walls has been elucidated. In the next section, the known roles of the major cell wall components in plant cell wall biotrophic immunity will be described.

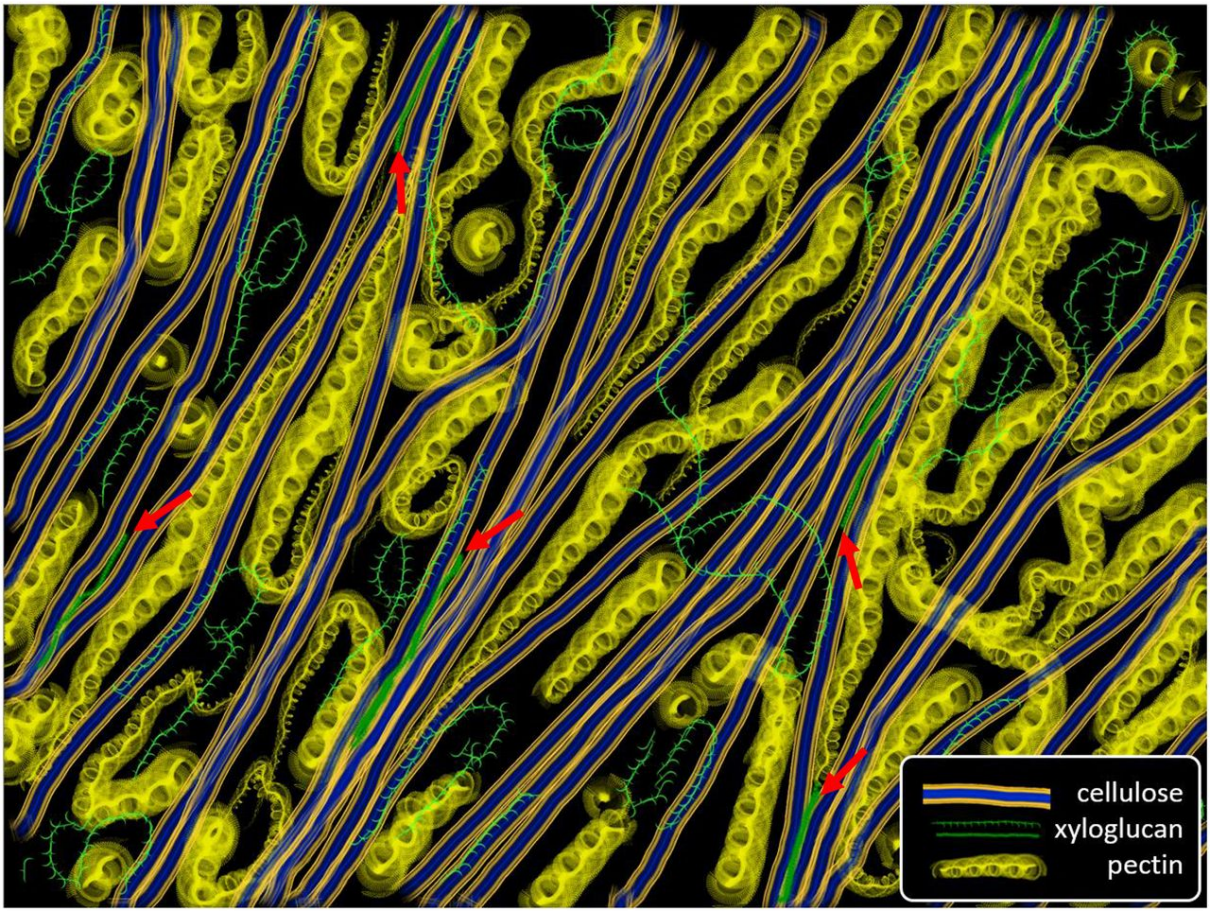

Figure 2.6: Representation of primary cell wall structural arrangement from Cosgrove (2018). Cellulose microfibrils are grouped by direct contact and at cellulose–xyloglucan tight junctions. Xyloglucan is solvated in both coiled and extended confirmations and can binds to the hydrophobic part of cellulose or can be entrapped between microfibrils. Coiled pectins fill the gaps between cellulose, binding to the hydrophilic surface of cellulose. Cellulose microfibrils (thick blue for hydrophobic core and orange coat for hydrophilic side), xyloglucan (green), pectins (yellow), cellulose-xyloglucan-cellulose cell wall loosening junctions (red arrow).

2.4. The plant cell wall against pathogen degrading enzymes

The success of plants to resist biotic aggressions often reside in their capacity to block pathogen tissue penetration. Many pathogens such as necrotrophic fungi will secrete enzymes to breach the plant cell wall (Prins *et al.* 2000; Veloso and van Kan 2018). Necrotrophic fungi such as *B. cinerea* secrete a wide range of CWDEs that target most of the cell wall components (Tudzynski and Kokkelink 2009). As part of the plant-pathogen co-evolution, plants have developed strategies to

protect their cell wall components from fungal enzymes, mostly by protecting cleavage sites, or with enzymes inhibitors (Blanco-Ulate *et al.* 2015).

Cellulose degradation usually requires a combination of enzymes, endocellulases, exocellulases and glucosidases, as reviewed by Lakhundi *et al*. (2015) with different enzymatic systems. In the effort to degrade ligno-cellulosic biomass for biofuel production, a cellulase activity was discovered using oxidative system such as cellobiose dehydrogenase and the recently found lytic polysaccharide monooxygenases (Beeson *et al.* 2015; Garajova *et al.* 2016). Degradation of cellulose, especially in crystalline form, is not easy, as microfibrils are tightly associated together or covered by hemicelluloses and degradation sites not accessible. Kang and Buchenauer (2000) showed with ultrastructural studies on wheat infected by *Fusarium culmorum*, that pectinase activity was higher the first three days of infection than xylanases and cellulases, suggesting a difference in secretion timing or activity between the different enzymes. During pathogen attacks, the pathogens first have to enter through the middle lamella, a pectin-rich layer before accessing the cellulose-rich layer which might explain this timing difference. In addition to its structural properties, cellulose is directly or indirectly associated to the response to pathogen attacks through signalling associated properties (described later). Cellulose-binding domains are motifs found in all cellulases. They don't possess any degrading activity but the Cellulose-Binding Elicitor Lectin from *Phytophthora parasitica* was found to elicit necrotic lesion and induce defence gene expression on tobacco and *A. thaliana* (Gaulin *et al.* 2006; Dumas *et al.* 2008).

Xyloglucan integrity and remodelling have been shown to be important for plant resistance against pathogens. XTHs expression were shown to be inhibited in tomato and apple and their XET activity decreased after infection by *Penicillium expansum* Link. A. (Miedes and Lorences 2007; Muñoz-Bertomeu and Lorences 2014). However, in those cases, as during tomato infection by the holoparasitic angiosperm *Cuscuta* (Olsen *et al.* 2016), it wasn't possible to say if XTH inhibition was aiding the plant defence, or the pathogen due to its dual enzymatic activity (XEH/XET).

Transgenic tobacco expressing a grapevine polygalacturonase inhibiting protein (*VviPGIP1*), which were found to have increased resistance to *B. cinerea*, had a downregulated XTH that was suggested to lead to a more cross-linked cellulose-xyloglucan network (Alexandersson *et al.* 2011; Nguema-Ona *et al.* 2013). XTH from celery and *Arabidopsis* were also suggested to be involved in protection against aphid infestation (Divol *et al.* 2007). Other xyloglucan degrading enzymes such as *Aspergillus aculeatus* xyloglucan β-1,4 endoglucanases (XEGs) were inhibited by tomato XEG inhibiting proteins during fungal infection (Qin *et al.* 2003). Independently of its structural role and XTH activity, in tobacco BY-2 cells, xyloglucan oligomer application alter gene expression including the upregulation of stress related genes (González-Pérez *et al.* 2014).

Plant can also protect their cell wall components using post-transcriptional modifications. This is the case for HG which ability to block pathogen penetration (therefore acting as a barrier) is

dependent on its degree of methyl-esterification or acetylation. Those modifications will either modify the wall properties as mentioned, or limit pathogen enzyme degrading activities. It was shown that during infestation of Arabidopsis by the aphid *Myzus persicae*, PMEI activity was essential in resistance, since AtPMEI13 mutants were more sensitive to infestation than the wild type (Silva-Sanzana *et al.* 2019). During infection by *B. cinerea*, Arabidopsis mutants AtPMEI11, AtPMEI12 and AtPMEI13 were similarly more sensitive to the necrotrophic fungi that the wild-type (Lionetti *et al.* 2017). In wheat, a differential expression of PMEs was reported between sensitive and resistant plants during *Fusarium graminearum* infection, suggesting its importance for resistance (Zega and D'Ovidio 2016). Many other cases of the influence of methyl-esterification in HG resistance against biotic (and abiotic) stresses were compiled by Lionetti *et al.* (2012) and Levesque-Tremblay *et al.* (2015). It was also highlighted that PMEs expression, can either favour or impair resistance depending on the pathosystem and that PME-specific, rather than total activity, was crucial for resistance (Bethke *et al.* 2014). In addition, the pattern of methyl-esterification (random or blockwise) was shown to influence plant susceptibility, as found between susceptible (blockwise) and resistant (random) wheat lines against the wheat stem rust fungus *Puccinia graminis f. sp. tritici* (Wiethölter *et al.* 2003). This is linked to the degrading activity of PG (Lionetti *et al.* 2014).

These enzymes with glycosyl hydrolase activity, naturally present in the plants for cell wall remodelling activity (during fruit maturation for example) are also secreted by pathogens to breach the plant cell wall. Deletion of *Bcpg2* lead to 50 to 85% decrease of lesion expansion rate during tomato and broad beans infection by *B. cinerea* (Kars *et al.* 2005) confirming its importance as virulence factors. *Pseudomonas syringae* has also been shown to upregulate a gene stimulating Arabidopsis PG activity, increasing its sensitivity to the bacteria (Wang *et al.* 2017). In addition, to protect HG degradation with methylesterification, plants have evolved PGIPs to counter the PG pectinolytic activity.

Acetylation has been much less studied but it is getting more attention as it was found to impact plant pathogen resistance (Pauly and Ramírez 2018). A reduction of pectin acetylation through the mutation of a reduced wall acetylation (RWA) protein, or the expression of *Aspergillus nidulans* acetylesterases were found to increase resistance to *B. cinerea* in Arabidopsis and Brachypodium mutants (Manabe *et al.* 2011; Pogorelko *et al.* 2013; Nafisi *et al.* 2015). Conversely, a pectin acetyltransferase mutant (PAE9) was shown to improve Arabidopsis response to aphids (Kloth *et al.* 2019) and the mutation of a putative pectin acetyltransferase gene leads to resistance against powdery mildew (*Golovinomyces cichoracearum*), but induces increased sensitivity to *B. cinerea* in Arabidopsis, highlighting the complex plant-pathogen specific interaction mechanisms (Chiniquy *et al.* 2019).

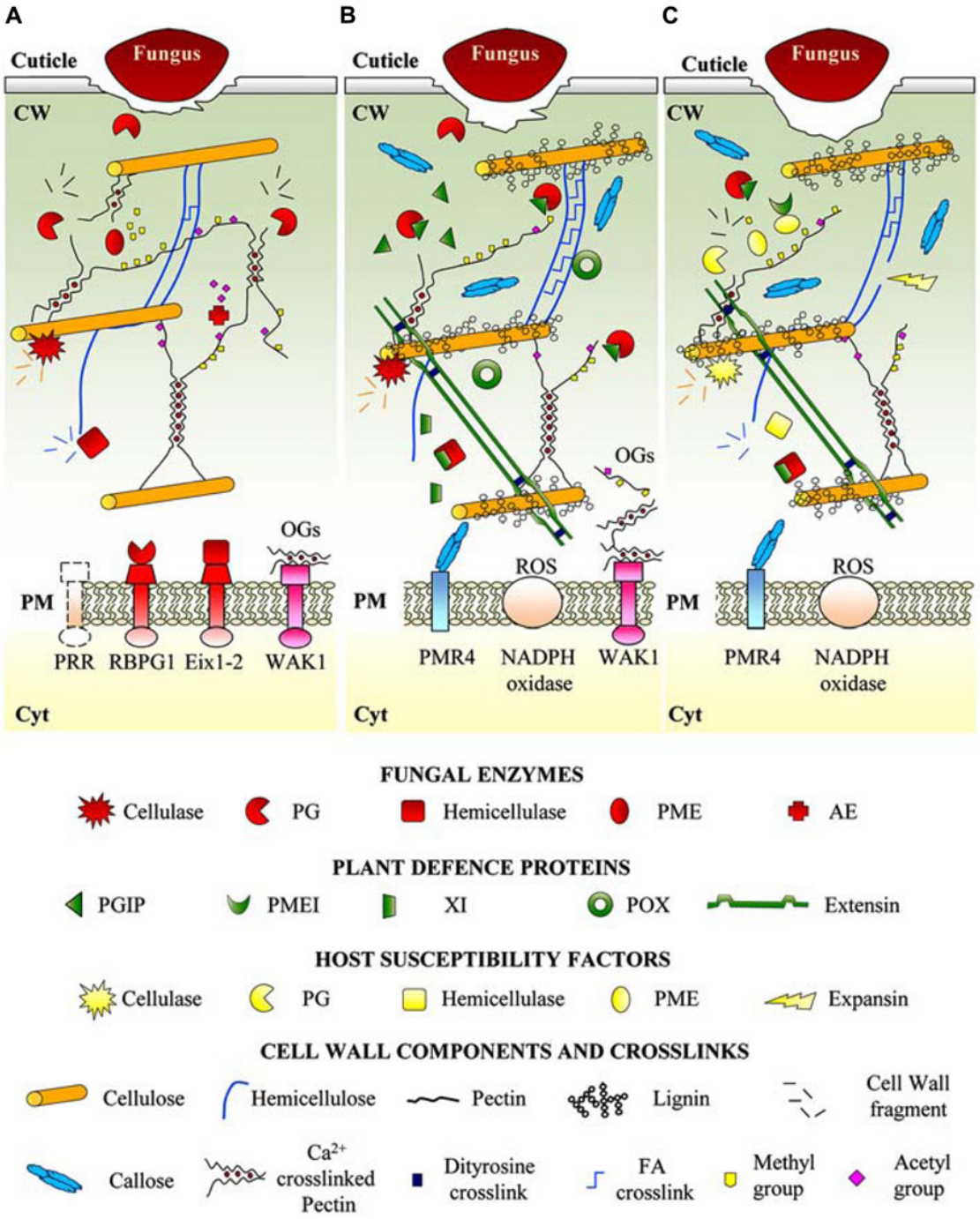

Figure 2.7: Cell Wall interplay with a necrotrophic fungi. **A**: Upon attack, necrotrophic fungi produce diverse cell wall degrading enzymes that are secreted in the apoplastic space, leading to CW breaching and facilitating nutrients acquisition. Fungal enzymes can act as MAMPs and be recognised by the membrane receptors RBPG1 and Eix1-2. **B**: MAMPs recognition triggers a first line defense with the production of CWDE inhibitors, like PGIPs. It also triggers specific signalling pathways leading to a restructuration of cell wall as reinforcement by deposition of callose and lignin, and induction of peroxidases/ROS-mediated crosslinks between cell wall structural proteins and polysaccharides. **C**: Depending on the susceptibility to the pathogen, fungi can manipulate the cell to beneficiate from plant cellulases, expansins, PGs and PMEs. Aes: acetyl esterases; $Ca^{2+:}$ calcium ions; CW: cell wall; Cyt: cytoplasm; Eix1-2: receptors of ethylene induced xylanases; FA: ferulic acid; Ogs: oligogalacturonides; PGs: polygalacturonases; PGIPs: polygalacturonase inhibitors; PM: plasma membrane; PME: pectin methylesterases; PMEI: pectin methylesterase inhibitor; PMR4: Powdery mildew resistant 4; POX: peroxidase; PRR: pattern recognition receptor; RBPG1: Responsiveness to Botrytis PG1; ROS: reactive oxygen species; XI: xylanase inhibitor; WAK1: wall associated kinase 1. (From Bellincampi *et al.* 2014).

Xylan acetylation, similarly to other cell wall components, has been shown to trigger defence responses, or increase resistance to pathogen infections (Manabe *et al.* 2011; Pogorelko *et al.* 2013; Escudero *et al.* 2017). However, the major effects are observed on the secondary cell wall where xylan is a major constituent, while on the primary cell wall it is much more subtle.

Alternatively, fungal enzymes can be countered by limiting their access to their target catalytic sites. For example, xylogalacturonans synthesis has been shown to be stimulated during various pathogen attacks, suggesting that they could substitute/reinforce HG in order to limit endopolygalacturonases degrading actions (Jensen *et al.* 2008).

High complexity in the walls might also protect from fungal enzymes. Rhamnogalacturonan-II, with its numerous and uncommon sugars, has been found to be resistant to a wide range of pectinolytic enzymes (Doco *et al.* 1997) and is capable to bind to heavy metals (Pellerin and O'Neill 1998). Despite being in limited amounts in the primary cell wall, all those properties suggest an important role in resistance against various biotic and abiotic stresses. The difficulty to produce RG-II binding antibodies has rendered studies quite difficult to be conducted leading to limited knowledge on the functional roles of RG-II (Yapo 2011a).

Cell wall components are not limited to a barrier function, glycoproteins can play a more active role in stopping pathogen invasion (Deepak *et al.* 2010). Extensins, as HRGP proteins, have been thought to play a role in response to pathogens for a long time, but their mode of action is only now starting to be investigated. It was shown that an Arabidopsis mutant for extensin arabinosylation had impaired defence elicitation and was more sensitive to *Phytophthora parasitica* root colonisation (Castilleux *et al.* 2020). Extensin genes were also more expressed in roots during banana infection by *Fusarium oxysporum* (Wu *et al.* 2017). Recent knowledge leading to their involvement in plant defence was discussed by Castilleux et al. (2018) and Rashid, (2016). Evidence for the involvement of AGPs as cell wall protective proteins are scarce. In the root, AGPs were shown to be abundantly present at the cell surface or secreted to interact with the rhizosphere (Nguema-Ona *et al.* 2013). AGPs synthesis was stimulated during infection from various pathogens and they were found to interact and inhibit *Aphanomyces euteiches* in pea and *Brassica napus* (Cannesan *et al.* 2012). After injection of *Penicillium spinulosum* in apple (*Malus x domestica*), AGPs distribution around the injection area increased and upon AGP inactivation using the β-glucosyl Yariv reagent the infection progressed much faster (Leszczuk *et al.* 2019). The topic is only starting to attract attention and recent knowledge was reviewed by Mareri *et al.* (2018) but more remains to be elucidated.

2.5. The plant cell wall becomes a highly dynamic structure during pathogen infection

As described previously, the cell wall acts as a physical barrier to block pathogen penetration. It is a dynamic matrix that undergoes modifications as needed. During biotic stress, those modifications are induced after recognition of a pathogen attack. This signalling role is the other important feature in cell wall defence against pathogen attacks. Pathogen and microbe associated molecular patterns (PAMPs and MAMPs) are molecules from the pathogen that are recognised by plants and act as stress signals to trigger defence responses (Gust *et al.* 2017; De Lorenzo *et al.* 2019). In addition to these molecules, products of cell wall degradation, called DAMPs also serve as plant defence elicitors (Vaahtera *et al.* 2019) (Figure 2.7). Most DAMPs are derived from pectins; once degraded by pathogen enzymes, HG fragments, called oligogalacturonides (OGs), act as DAMPs and trigger defence responses (Ferrari *et al.* 2013). Oligogalacturonides have been shown to be released, after HG demethylesterification, under the action of PGs or PLs and promoted by PGs interactions with PGIPs (Benedetti *et al.* 2015). Oligogalacturonides length seems to be important for plant defence initiation and many studies showed that OGs with a degree of polymerisation (DP) between 10 and 15 were the most active to trigger plant defence responses (Ferrari *et al.* 2013; De Lorenzo *et al.* 2018). Short OGs (DP =3) were recently shown to also induce defence response similarly to long OGs, except for reactive oxygen species (ROS) production (Davidsson *et al.* 2017). Interestingly, another recent study showed that OGs generated with pectin lyases (PNL) in Arabidopsis were mostly methyl- or acetylesterified and representing about 80% of total OGs produced during *B. cinerea* infection (Voxeur *et al.* 2019). Those OGs had a DP of 2 to 5 and longer OGs were shown to be rapidly hydrolysed into shorter OGs once in contact with *B. cinerea*. Oligogalacturonides are recognised by pattern recognition receptors (PRR), membrane receptors from the receptor-like kinase family (RLK) (Li *et al.* 2016; Boutrot and Zipfel 2017), the wall-associated receptor-like kinases (WAKs) (Wolf 2017). WAK1 was shown to bind to OGs and its overexpression increased resistance against *B. cinerea* (Brutus *et al.* 2010). As described by Kohorn (2012, 2016), WAKs bind to galacturonic acid based polymers such as HG, OG and RG (I and II). They were shown to be required for cell expansion and involved in stress response. They are believed to activate downstream pathways leading to different genes up or down regulation. While the transduction pathways are still largely unknown, one of the identified pathways includes different mitogen-activated protein kinases (MAPKs) (Figure 2.8). Through a phosphorylation cascade, MAPKs such as MPK3 and MPK6 have been shown to trigger different defence responses by phosphorylating transcription factors; those are different from the signalling pathway activated with MPK4, highlighting the diversity and specificity of the signal perception and responses (Meng and Zhang 2013; Thulasi Devendrakumar *et al.* 2018).

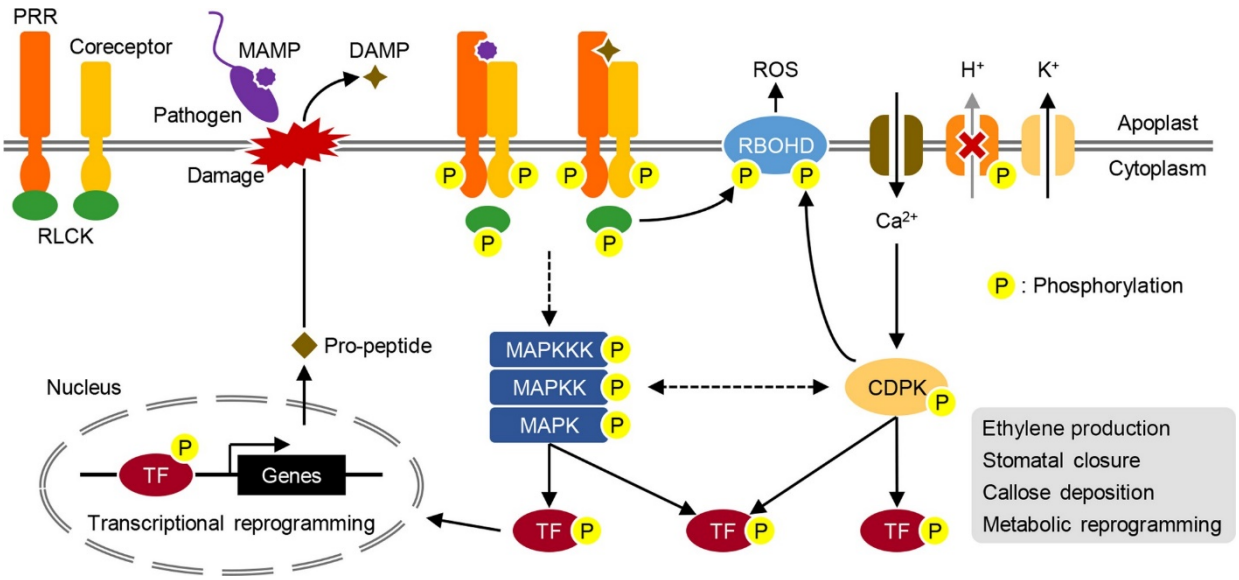

Figure 2.8: Schematic overview of pattern-triggered immunity. Pattern recognition receptors (PRR) coupled with receptor-like cytoplasmic kinases (RLCK) perceive Microbe/Damage-associated molecular pattern (MAMPs/DAMPs). Transphosphorylation of this complex triggers downstream signaling, that can be transmitted via phosphorylation cascades and calcium-dependent protein kinases (CDPKs) to downstream targets including ATPases and transcriptional factors (TFs). (From Saijo *et al.* 2018)

The signalling role of cell wall components is currently receiving significant research attention. DAMPs, together with pathogen fragments recognised as non-self, the MAMPs act as signals (Gust *et al.* 2017; Engelsdorf *et al.* 2018; De Lorenzo *et al.* 2018; Hou *et al.* 2019). Cellobiose, a dimer from cellulose degradation, was recently shown to be perceived as a stress signal, triggering some plant immune response, similarly to other well-known elicitors. No ROS production, nor callose deposition were observed, suggesting the need of a combined signal with other elicitors for complete plant response (de Azevedo Souza *et al.* 2017). Purified xyloglucan oligomers were also found to induce numerous plant defence responses and increase resistance to *B. cinerea in* Arabidopsis and grapevine, suggesting its capacity to act as a DAMP (Claverie *et al.* 2018).

Oligogalacturonides, cellobiose or xyloglucan are recognised as DAMPs and it is quite possible that other polysaccharide fragments will be identified similarly. Rhamnogalacturonan-I fragments from tomato, injected into new tomato fruits, were recently found to increase glucanase, chitinase and peroxidase activity, showing a plant response to the treatment and a probable role as a DAMP molecule (Jiménez-Maldonado *et al.* 2018).

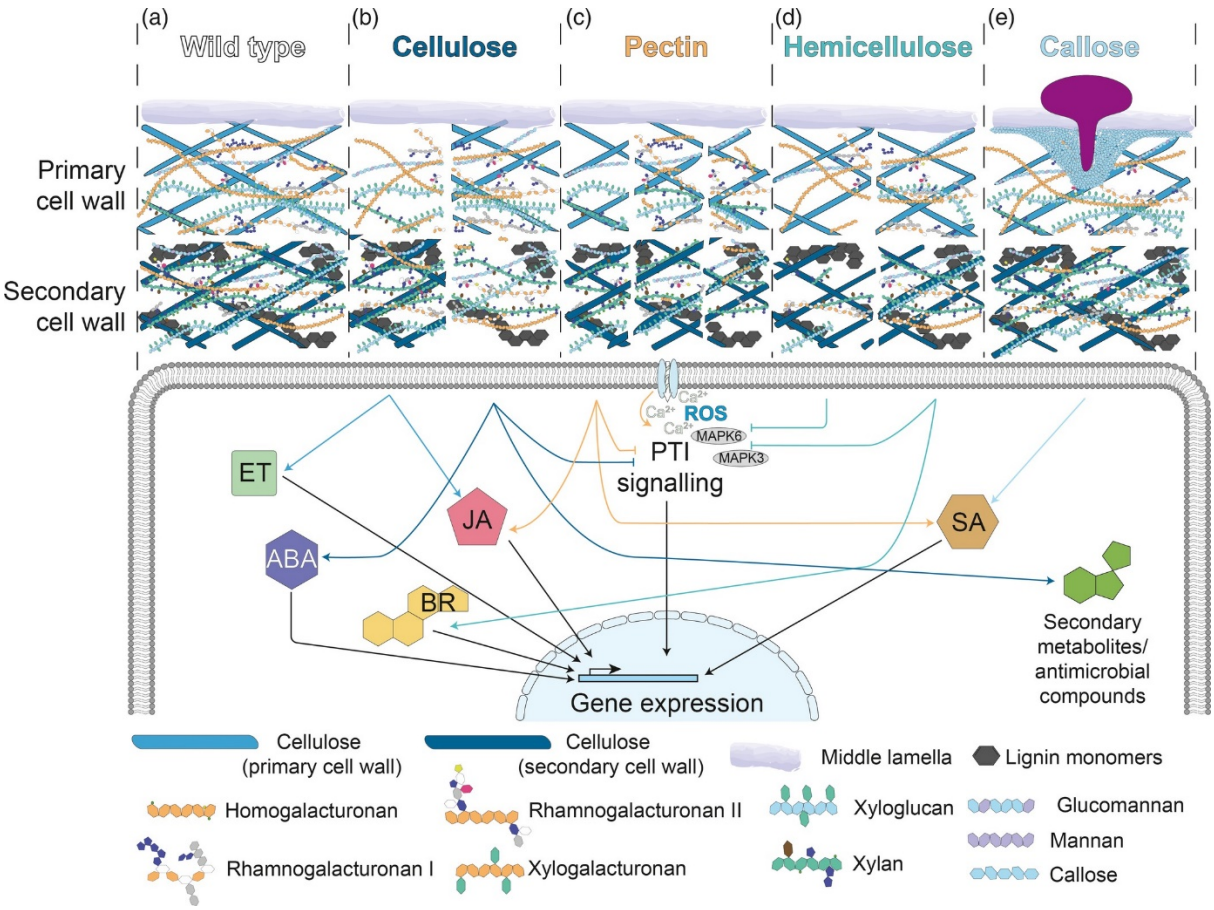

Figure 2.9: Schematic representation of a degraded *Arabidopsis thaliana* cell wall and the associated disease resistance responses. **a**: Wild type cell wall. Primary cell wall composed of cellulose, homogalacturonan, rhamnogalacturonan-1 and rhamnogalacturonan-2, xyloglucan, xylan, mannan and glucomannan. Secondary cell wall presence depends on the plant tissue and is composed of cellulose, xylans and lignin. **b**: Cellulose biosynthesis alteration triggers defensive responses mediated by the hormones JA, ET or ABA; or can attenuate PTI response. **c**: Modification of pectin content (left), degree of acetylation (center) or methylation (right), activate responses regulated by JA or SA, and can trigger PTI responses. **d**: Hemicellulose degree of acetylation (left) or overall content (right) alteration, trigger responses like activation of BR and ABA signalling pathways but can also attenuate PTI. **e**: Callose is deposited in pathogen cell wall penetration sites, strenghtening it and probably activating SA defensive pathways. ABA, abscisic acid; BR, brassinosteroid; ET, ethylene; JA, jasmonic acid; PTI, pattern triggered immunity; ROS, reactive oxygen species; SA, salycylic acid. (From Bacete *et al.* 2018).

These molecules are recognised by membrane receptors such as the PRR and will induce the MAMP-triggered immunity (MTI) formerly termed pattern-triggered immunity (PTI), a non-specific plant immune response (Trdá *et al.* 2015; Li *et al.* 2016; Boutrot and Zipfel 2017; Saijo *et al.* 2018). MTI will induce the production of ROS, callose deposition or lignification (Figure 2.9). Callose deposition is typical of the hypersensitive response, it was shown to be induced by flagellin 22 and chitosan, two MAMPs, and is correlated with hydrogen peroxide levels and can be stimulated or repressed by abscisic acid (Luna *et al.* 2011). A strong and early response is capable to stop many pathogens as observed with early and increased callose deposition in an Arabidopsis mutant against a variety of powdery mildew strains (Ellinger *et al.* 2013). However, many pathogens have developed strategies to evade or utilise MTI to their advantage like necrotrophic fungi that benefit from plant cell death or have been shown to secrete small RNAs to silence specific plant defence genes (Govrin

and Levine 2000; Chaloner *et al.* 2016). Plants have therefore a second layer of defence called effector-triggered immunity (ETI) that involves more specific responses (Malinovsky *et al.* 2014; Peng *et al.* 2018). It is based on the recognition of specific pathogen effectors at the plasmic membrane, or intracellularly using nucleotide-binding leucine-rich-repeat proteins. It is often associated with the hypersensitive response, the induction of specific defence genes or the stimulation of some phytohormone pathways (Toruño *et al.* 2016). From the different effectors and signalling pathways that have been identified until now, it is clear that some effectors activate RLKs shown to also regulate plant growth. The RLK THESEUS1 was shown to sense cellulose deficiency and inhibit growth while FERONIA is required for normal cell elongation and involved in the response to mechanical stresses (Wolf 2017). It is widely observed that infected plants stop or drastically reduce their growth. At a cellular level, the trade-off between growth and defence seems to involve cell wall integrity surveillance and maintenance (Wolf *et al.* 2012; Voxeur and Höfte 2016; Wolf 2017; Vaahtera *et al.* 2019).

2.6. Comprehensive microarray polymer profiling, a powerful tool for cell wall analysis

Common analytical approaches to decipher cell wall component localisation or quantification are based on microscopy and biochemical analysis. Localisation studies have been using a wide range of cell wall targeting probes such as monoclonal antibodies (mAbs) and carbohydrate-binding modules (CBMs), observed using immunofluorescence microscopy. Monoclonal antibodies are generated by injecting into a target animal (usually a rat or a mouse) an antigen containing the epitope of interest that needs to be recognised. The animal serum is collected and analysed after confirming animal immunisation. Potential antibodies are isolated and further tested as described in Willats *et al.* (1998). Monoclonal antibodies are mostly used for *in situ* localisation of specific molecules or epitopes using immunofluorescence experiments. For example, Silva-Sanzana *et al.* (2019) used the HG binding mAbs LM19 and LM20 to show that aphid infestation induced HG demethylesterification in Arabidopsis. A recent review from Rydahl *et al.* (2018) presents the latest antibodies available and the various approach they can be employed.

Taking advantage of the large range of mAbs and CBMs available and their almost comprehensive albeit not complete coverage of cell wall polymers, a technique called CoMPP was developed to characterise the cell wall polysaccharide composition in a profiling technique (Moller *et al.* 2007). This high throughput method allows to focus on the relative availability of polysaccharides to interact with mAbs and CBM. Termed Comprehensive Microarray Polymer Profiling (CoMPP), it was published in 2007. This technology uses a wide range of mAbs and CBMs, targeting specific cell wall motifs to obtain an overview of the matrix polysaccharides and glycoproteins composition (Moller *et al.* 2007). It is based on microarray technology allowing a high number of samples to be

processed simultaneously (high throughput) using a small amount (10 mg) of material as shown in Figure 2.10.

Plant material preparation requires tissue grinding and processing for Alcohol Insoluble Residue (AIR). All AIR samples follow a sequential extraction first using CDTA to obtain a pectin-rich fraction. The pellet is subsequently incubated with NaOH to obtain a hemicellulose-rich fraction. These two fractions are printed on microarray nitrocellulose membranes and probed with a selection of mAbs and or CBMs as needed. Microarray plates are then scanned and the produced images are analysed for signal quantification and data processing.

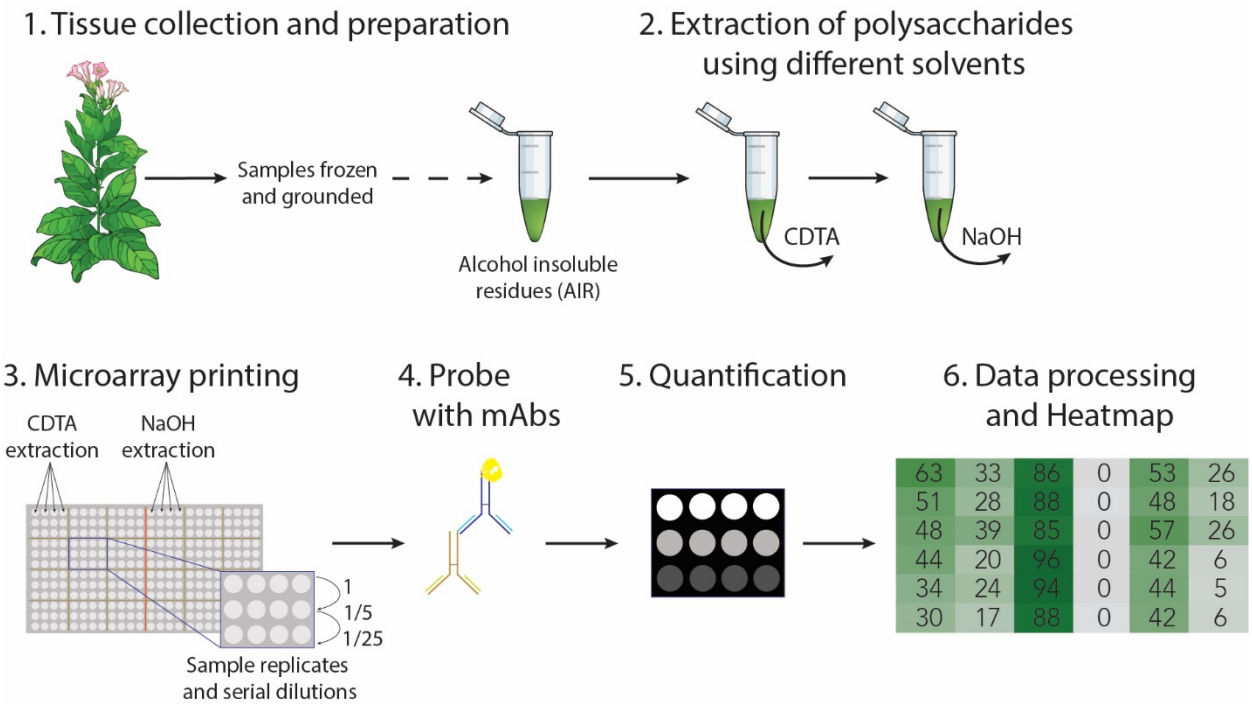

Figure 2.10: Overview of the main steps followed during a CoMPP analysis from sample preparation to data presentation.

Its potential utility was quickly demonstrated on *A. thaliana* mutants (Moller *et al.* 2007, 2008) and a methods paper was published for the community (Moller *et al.* 2012), with a recent update by Kračun *et al.* (2017).

The increased used of CoMPP allowed for some new insights; for example to understand the influence of arbuscular mycorrhizal colonisation on tomato fruit and root cell walls (Chialva *et al.* 2019); or to show that the fungus “garden” in symbiosis with the leaf cutting ants *Acromyrmex echinatior*, by preferentially degrading pectin, xyloglucan and xylan (Moller *et al.* 2011). With the selection of specific antibodies, CoMPP was also used for the characterisation of some Metazoan organisms, showing its potential use on animal tissue (Salmeán *et al.* 2017). Growing interest for the technique led to its adaptation such as performed by Wood *et al.* (2017) that added association

mapping, using SNP detection and gene expression to bring a transcriptomic dimension to the technology. With a similar approach, Salmeán *et al.* (2018) combined CoMPP high-throughput capabilities with medium throughput protein expression system to develop a Double Blind CoMPP platform, used to further characterise algal cell wall polysaccharides.

This literature review has presented an overview of the biology of plant cell walls and their involvement in plant immunity (i.e. response to pathogens such as fungi). However, current research is mostly focused on the identification of a specific trait or process. Informations on the overall cell wall dynamics during development and biotic stresses remain scarce. The use of CoMPP capabilities, associated with other analytical and observation methods, can provide valuable information on cell wall, its dynamic characterisation and polysaccharides composition and remodelling during pathogen attack. This new insight will fill the gap on current cellular knowledge to develop more accurate cell wall dynamic matrix models. The use of CoMPP will also help to identify antibodies of interest to conduct further immunolocalisation studies (*i.e.* using light or electron microscopy).

2.7. References

Albersheim P, Darvill AG, Roberts K, Sederoff R, Staehelin A. **2011**. Cell walls and plant anatomy In: *Plant Cell Walls*. Garland Science, New York, USA, 1–42.

Alexandersson E, Becker JVW, Jacobson D, *et al.* 2011. Constitutive expression of a grapevine polygalacturonase-inhibiting protein affects gene expression and cell wall properties in uninfected tobacco. *BMC Research Notes* **4**: 493.

Arantes V, Saddler JN. **2010**. Access to cellulose limits the efficiency of enzymatic hydrolysis: the role of amorphogenesis. *Biotechnology for Biofuels* **3**: 4.

Atmodjo MA, Hao Z, Mohnen D. **2013**. Evolving views of pectin biosynthesis. *Annual Review of Plant Biology* **64**: 747–79.

de Azevedo Souza C, Li S, Lin AZ, *et al.* 2017. Cellulose-derived oligomers act as damage-associated molecular patterns and trigger defense-like responses. *Plant Physiology* **173**: 2383–2398.

Bacete L, Mélida H, Miedes E, Molina A. **2018**. Plant cell wall-mediated immunity: cell wall changes trigger disease resistance responses. *Plant Journal* **93**: 614–636.

Baumberger N, Ringli C, Keller B. **2001**. The chimeric leucine-rich repeat/extensin cell wall protein LRX1 is required for root hair morphogenesis in *Arabidopsis thaliana*. *Genes and Development* **15**: 1128–1139.

Beeson WT, Vu V V., Span EA, Phillips CM, Marletta MA. **2015**. Cellulose degradation by polysaccharide monooxygenases. *Annual Review of Biochemistry* **84**: 923–946.

Bellincampi D, Cervone F, Lionetti V. **2014**. Plant cell wall dynamics and wall-related susceptibility in plant-pathogen interactions. *Frontiers in Plant Science* **5**: 228.

Benedetti M, Pontiggia D, Raggi S, *et al.* 2015. Plant immunity triggered by engineered *in vivo* release of oligogalacturonides, damage-associated molecular patterns. *Proceedings of the National Academy of Sciences of the United States of America* **112**: 5533–5538.

Bethke G, Grundman RE, Sreekanta S, Truman W, Katagiri F, Glazebrook J. **2014**. Arabidopsis *PECTIN METHYLESTERASEs* contribute to immunity against *Pseudomonas syringae*. *Plant Physiology* **164**: 1093–1107.

Blanco-Ulate B, Labavitch JM, Vincenti E, Powell ALT, Cantu D. **2015**. Hitting the wall: Plant cell walls

during *Botrytis cinerea* infections In: *Botrytis – the Fungus, the Pathogen and its Management in Agricultural Systems*. Cham: Springer International Publishing, Switzerland, 361–386.

Boutrot F, Zipfel C. **2017**. Function, discovery, and exploitation of plant pattern recognition receptors for broad-spectrum disease resistance. *Annual Review of Phytopathology* **55**: 257–286.

Brady JD, Sadler IH, Fry SC. **1998**. Pulcherosine, an oxidatively coupled trimer of tyrosine in plant cell walls : its role in cross-link formation. *Phytochemistry* **47**: 0–4.

Brutus A, Sicilia F, Macone A, Cervone F, De Lorenzo G. **2010**. A domain swap approach reveals a role of the plant wall-associated kinase 1 (WAK1) as a receptor of oligogalacturonides. *Proceedings of the National Academy of Sciences of the United States of America* **107**: 9452–9457.

Buffetto F, Ropartz D, Zhang XJ, Gilbert HJ, Guillon F, Ralet MC. **2014**. Recovery and fine structure variability of RGII sub-domains in wine (*Vitis vinifera* Merlot). *Annals of Botany* **114**: 1327–1337.

Caffall KH, Mohnen D. **2009**. The structure, function, and biosynthesis of plant cell wall pectic polysaccharides. *Carbohydrate Research* **344**: 1879–1900.

Cannesan MA, Durand C, Burel C, *et al.* 2012. Effect of arabinogalactan proteins from the root caps of pea and *Brassica napus* on *Aphanomyces euteiches* zoospore chemotaxis and germination. *Plant Physiology* **159**: 1658–1670.

Carpita NC, Gibeaut DM. **1993**. Structural models of primary cell walls in flowering plants: consistency of molecular structure with the physical properties of the walls during growth. *The Plant Journal* **3**: 1–30.

Cassab GI. **1998**. Plant cell wall proteins. *Annual Review of Plant Physiology and Plant Molecular Biology* **49**: 281–309.

Castilleux R, Plancot B, Gügi B, *et al.* 2020. Extensin arabinosylation is involved in root response to elicitors and limits oomycete colonization. *Annals of Botany* **125**: 751–763.

Castilleux R, Plancot B, Ropitaux M, *et al.* 2018. Cell wall extensins in root–microbe interactions and root secretions. *Journal of Experimental Botany* **69**: 4235–4247.

Cavalier DM, Lerouxel O, Neumetzler L, *et al.* 2008. Disrupting two *Arabidopsis thaliana* xylosyltransferase genes results in plants deficient in xyloglucan, a major primary cell wall component. *Plant Cell* **20**: 1519–1537.

Chaloner T, van Kan JAL, Grant-Downton RT. **2016**. RNA 'information warfare' in pathogenic and mutualistic interactions. *Trends in Plant Science* **21**: 738–748.

Chebli Y, Geitmann A. **2017**. Cellular growth in plants requires regulation of cell wall biochemistry. *Current Opinion in Cell Biology* **44**: 28–35.

Chialva M, Fangel JU, Novero M, *et al.* 2019. Understanding changes in tomato cell walls in roots and fruits: The contribution of arbuscular mycorrhizal colonization. *International Journal of Molecular Sciences* **20**: 1–17.

Chiniquy D, Underwood W, Corwin J, *et al.* 2019. PMR5, an acetylation protein at the intersection of pectin biosynthesis and defense against fungal pathogens. *The Plant Journal* **100**: 1022–1035.

Chormova D, Fry SC. **2016**. Boron bridging of rhamnogalacturonan-II is promoted *in vitro* by cationic chaperones, including polyhistidine and wall glycoproteins. *New Phytologist* **209**: 241–251.

Claverie J, Balacey S, Lemaître-Guillier C, *et al.* 2018. The cell wall-derived xyloglucan is a new DAMP triggering plant immunity in *Vitis vinifera* and *Arabidopsis thaliana*. *Frontiers in Plant Science* **871**: 1725.

Cosgrove DJ. **2001**. Wall structure and wall loosening. A look backwards and forwards. *Plant Physiology* **125**: 131–134.

Cosgrove DJ. **2014**. Re-constructing our models of cellulose and primary cell wall assembly. *Current Opinion in Plant Biology* **22**: 122–131.

Cosgrove DJ. **2015**. Plant expansins: diversity and interactions with plant cell walls. *Current Opinion in Plant Biology* **25**: 162–172.

Cosgrove DJ. **2018**. Diffuse growth of plant cell walls. *Plant Physiology* **176**: 16–27.

Cosgrove DJ, Jarvis MC. **2012**. Comparative structure and biomechanics of plant primary and secondary cell walls. *Frontiers in Plant Science* **3**: 204.

Czolpinska M, Rurek M. **2018**. Plant glycine-rich proteins in stress response: An emerging, still prospective story. *Frontiers in Plant Science* **9**: 302.

Davidsson P, Broberg M, Kariola T, Sipari N, Pirhonen M, Palva ET. **2017**. Short oligogalacturonides induce pathogen resistance-associated gene expression in *Arabidopsis thaliana*. *BMC Plant Biology* **17**: 19.

Deepak S, Shailasree S, Kini RK, Muck A, Mithöfer A, Shetty SH. **2010**. Hydroxyproline-rich glycoproteins and plant defence. *Journal of Phytopathology* **158**: 585–593.

Divol F, Vilaine F, Thibivilliers S, Kusiak C, Sauge MH, Dinant S. **2007**. Involvement of the xyloglucan endotransglycosylase/hydrolases encoded by celery XTH1 and Arabidopsis XTH33 in the phloem response to aphids. *Plant, Cell & Environment* **30**: 187–201.

Doco T, Williams P, Vidal S, Pellerin P. **1997**. Rhamnogalacturonan II, a dominant polysaccharide in juices produced by enzymic liquefaction of fruits and vegetables. *Carbohydrate Research* **297**: 181–186.

Dumas B, Bottin A, Gaulin E, Esquerré-Tugayé MT. **2008**. Cellulose-binding domains: cellulose associated-defensive sensing partners? *Trends in Plant Science* **13**: 160–164.

Duruflé H, Clemente HS, Balliau T, Zivy M, Dunand C, Jamet E. **2017**. Cell wall proteome analysis of *Arabidopsis thaliana* mature stems. *Proteomics* **17**: 1–16.

Ebringerová A, Thomas H, Hromádková Z, Heinze T. **2005**. Hemicellulose. *Advances in Polymer Science* **186**: 1–67.

Ellinger D, Naumann M, Falter C, *et al.* 2013. Elevated early callose deposition results in complete penetration resistance to powdery mildew in Arabidopsis. *Plant Physiology* **161**: 1433–1444.

Ellis M, Egelund J, Schultz CJ, Bacic A. **2010**. Arabinogalactan-proteins: key regulators at the cell surface? *Plant Physiology* **153**: 403–19.

Engelsdorf T, Gigli-Bisceglia N, Veerabagu M, *et al.* 2018. The plant cell wall integrity maintenance and immune signaling systems cooperate to control stress responses in *Arabidopsis thaliana*. *Science Signaling* **11**: eaao3070.

Escudero V, Jordá L, Sopeña-Torres S, *et al.* 2017. Alteration of cell wall xylan acetylation triggers defense responses that counterbalance the immune deficiencies of plants impaired in the β-subunit of the heterotrimeric G-protein. *The Plant Journal* **92**: 386–399.

Ferrari S, Savatin D V, Sicilia F, Gramegna G, Cervone F, Lorenzo G De. **2013**. Oligogalacturonides: plant damage-associated molecular patterns and regulators of growth and development. *Frontiers in Plant Science* **4**: 49.

Franková L, Fry SC. **2013**. Biochemistry and physiological roles of enzymes that “cut and paste” plant cell-wall polysaccharides. *Journal of Experimental Botany* **64**: 3519–3550.

Fry SC. **1988**. The growing plant cell wall: chemical and metabolic analysis In: *The growing plant cell wall: chemical and metabolic analysis*. Longman Group Limited, Harlow, UK, 333.

Fry SC. **2011**. Plant cell walls. From chemistry to biology. *Annals of Botany* **108**: viii–ix.

Fry SC. **2018**. Cell wall polysaccharide composition and covalent crosslinking. *Annual Plant Reviews online* **41**: 1–42.

Garajova S, Mathieu Y, Beccia MR, *et al.* 2016. Single-domain flavoenzymes trigger lytic polysaccharide monooxygenases for oxidative degradation of cellulose. *Scientific Reports* **6**: 28276.

Gaulin E, Dramé N, Lafitte C, *et al.* 2006. Cellulose binding domains of a *Phytophthora* cell wall protein are novel pathogen-associated molecular patterns. *Plant Cell* **18**: 1766–1777.

González-Pérez L, Perrotta L, Acosta A, *et al.* 2014. In tobacco BY-2 cells xyloglucan oligosaccharides alter the expression of genes involved in cell wall metabolism, signalling, stress responses, cell division and transcriptional control. *Molecular Biology Reports* **41**: 6803–6816.

Govrin EM, Levine A. **2000**. The hypersensitive response facilitates plant infection by the necrotrophic pathogen *Botrytis cinerea*. *Current Biology* **10**: 751–757.

Gust AA, Pruitt R, Nürnberger T. **2017**. Sensing danger: key to activating plant immunity. *Trends in Plant Science* **22**: 779–791.

Ha MA, Apperley DC, Jarvis MC. **1997**. Molecular rigidity in dry and hydrated onion cell walls. *Plant Physiology* **115**: 593–598.

Harholt J, Suttangkakul A, Scheller HV. **2010**. Biosynthesis of pectin. *Plant Physiology* **153**: 384–395.

Hayashi T. **1989**. Xyloglucans in the primary cell wall. *Annual Review of Plant Physiology and Plant Molecular Biology* **40**: 139–168.

Herger A, Dünser K, Kleine-Vehn J, Ringli C. **2019**. Leucine-rich repeat extensin proteins and their role in cell wall sensing. *Current Biology* **29**: R851–R858.

Hijazi M, Velasquez SM, Jamet E, Estevez JM, Albenne C. **2014**. An update on post-translational modifications of hydroxyproline-rich glycoproteins: Toward a model highlighting their contribution to plant cell wall architecture. *Frontiers in Plant Science* **5**: 395.

Höfte H, Voxeur A. **2017**. Plant cell walls. *Current biology* **27**: 865–870.

Hou S, Liu Z, Shen H, Wu D. **2019**. Damage-associated molecular pattern-triggered immunity in plants. *Frontiers in Plant Science* **10**: 646.

Ishii T, Matsunaga T. **2001**. Pectic polysaccharide rhamnogalacturonan II is covalently linked to homogalacturonan. *Phytochemistry* **57**: 969–974.

Jensen JK, Sørensen SO, Harholt J, *et al.* 2008. Identification of a xylogalacturonan xylosyltransferase involved in pectin biosynthesis in *Arabidopsis*. *Plant Cell* **20**: 1289–1302.

Jiménez-Maldonado MI, Tiznado-Hernández ME, Rascón-Chu A, *et al.* 2018. Analysis of rhamnogalacturonan I fragments as elicitors of the defense mechanism in tomato fruit. *Chilean Journal of Agricultural Research* **78**: 339–349.

Kalunke RM, Tundo S, Benedetti M, Cervone F, De Lorenzo G, D'Ovidio R. **2015**. An update on polygalacturonase-inhibiting protein (PGIP), a leucine-rich repeat protein that protects crop plants against pathogens. *Frontiers in Plant Science* **6**: 146.

Kang Z, Buchenauer H. **2000**. Ultrastructural and cytochemical studies on cellulose, xylan and pectin degradation in wheat spikes infected by *Fusarium culmorum*. *Journal of Phytopathology* **148**: 263–275.

Kars I, Krooshof GH, Wagemakers L, Joosten R, Benen JAE, Van Kan JAL. **2005**. Necrotizing activity of five *Botrytis cinerea* endopolygalacturonases produced in *Pichia pastoris*. *The Plant Journal* **43**: 213–225.

Keegstra K, Talmadge KW, Bauer WD, Albersheim P. **1973**. The structure of plant cell walls: III. A model of the walls of suspension-cultured sycamore cells based on the interconnections of the macromolecular components. *Plant Physiology* **51**: 188–197.

Kloth KJ, Abreu IN, Delhomme N, *et al.* 2019. PECTIN ACETYLESTERASE9 affects the transcriptome and metabolome and delays aphid feeding. *Plant Physiology* **181**: 1704–1720.

Kobayashi M, Matoh T, Azuma JI. **1996**. Two chains of rhamnogalacturonan II are cross-linked by borate-diol ester bonds in higher plant cell walls. *Plant Physiology* **110**: 1017–1020.

Kohorn BD. **2016**. Cell wall-associated kinases and pectin perception. *Journal of Experimental Botany* **67**: 489–494.

Kohorn BD, Kohorn SL. **2012**. The cell wall-associated kinases, WAKs, as pectin receptors. *Frontiers in plant science* **3**: 88.

Kračun SK, Fangel JU, Rydahl MG, Pedersen HL, Vidal-Melgosa S, Willats WGTGT. **2017**. Carbohydrate microarray technology applied to high-throughput mapping of plant cell wall glycans using comprehensive microarray polymer profiling (CoMPP) In: *Lauc G., Wuhrer M. (eds) High-Throughput Glycomics and Glycoproteomics. Methods in Molecular Biology*. Humana Press, New York, NY, 147–165.

Lakhundi S, Siddiqui R, Khan NA. **2015**. Cellulose degradation: a therapeutic strategy in the improved treatment of *Acanthamoeba* infections. *Parasites and Vectors* **8**: 23.

Lamport DTA, Kieliszewski MJ, Chen Y, Cannon MC. **2011**. Role of the extensin superfamily in primary cell wall architecture. *Plant Physiology* **156**: 11–9.

Leszczuk A, Pieczywek PM, Gryta A, Frąc M, Zdunek A. **2019**. Immunocytochemical studies on the distribution of arabinogalactan proteins (AGPs) as a response to fungal infection in *Malus x domestica* fruit. *Scientific Reports* **9**: 1–15.

Leszczuk A, Zając A, Kurzyna-Szklarek M, Cybulska J, Zdunek A. **2020**. Investigations of changes in the arabinogalactan proteins (AGPs) structure, size and composition during the fruit ripening process. *Scientific Reports* **10**: 1–15.

Levesque-Tremblay G, Pelloux J, Braybrook SA, Müller K. **2015**. Tuning of pectin methylesterification: consequences for cell wall biomechanics and development. *Planta* **242**: 791–811.

Li L, Yu Y, Zhou Z, Zhou JM. **2016**. Plant pattern-recognition receptors controlling innate immunity. *Science China Life Sciences* **59**: 878–888.

Liners F, Letesson J-J, Didembourg C, Van Cutsem P. **1989**. Monoclonal antibodies against pectin. *Plant Physiology* **91**: 1419–1424.

Lionetti V, Cervone F, Bellincampi D. **2012**. Methyl esterification of pectin plays a role during plant-pathogen interactions and affects plant resistance to diseases. *Journal of Plant Physiology* **169**: 1623–30.

Lionetti V, Cervone F, De Lorenzo G. **2014**. A lower content of de-methylesterified homogalacturonan improves enzymatic cell separation and isolation of mesophyll protoplasts in *Arabidopsis*. *Phytochemistry* **112**: 188–194.

Lionetti V, Fabri E, De Caroli M, *et al.* 2017. Three pectin methylesterase inhibitors protect cell wall integrity for Arabidopsis immunity to *Botrytis*. *Plant Physiology* **173**: 1844–1863.

De Lorenzo G, Ferrari S, Cervone F, Okun E. **2018**. Extracellular DAMPs in plants and mammals: immunity, tissue damage and repair. *Trends in Immunology* **39**: 937–950.

De Lorenzo G, Ferrari S, Giovannoni M, Mattei B, Cervone F. **2019**. Cell wall traits that influence plant development, immunity, and bioconversion. *The Plant Journal* **97**: 134–147.

Luna E, Pastor V, Robert J, Flors V, Mauch-Mani B, Ton J. **2011**. Callose deposition: A multifaceted plant defense response. *Molecular Plant-Microbe Interactions* **24**: 183–193.

Lynd LR, Weimer PJ, van Zyl WH, Pretorius IS. **2002**. Microbial cellulose utilization: fundamentals and biotechnology. *Microbiology and Molecular Biology Reviews* **66**: 506–577.

Malinovsky FG, Fangel JU, Willats WGT. **2014**. The role of the cell wall in plant immunity. *Frontiers in Plant Science* **5**: 178.

Manabe Y, Nafisi M, Verhertbruggen Y, *et al.* 2011. Loss-of-function mutation of *REDUCED WALL ACETYLATION2* in Arabidopsis leads to reduced cell wall acetylation and increased resistance to *Botrytis cinerea*. *Plant Physiology* **155**: 1068–1078.

Mareri L, Romi M, Cai G. **2019**. Arabinogalactan proteins: actors or spectators during abiotic and biotic stress in plants? *Plant Biosystems* **153**: 173–185.

Marowa P, Ding A, Kong Y. **2016**. Expansins: roles in plant growth and potential applications in crop improvement. *Plant Cell Reports* **35**: 949–965.

Meng X, Zhang S. **2013**. MAPK cascades in plant disease resistance signaling. *Annual Review of Phytopathology* **51**: 245–266.

Merkouropoulos G, Shirsat AH. **2003**. The unusual *Arabidopsis* extensin gene *atExt1* is expressed throughout plant development and is induced by a variety of biotic and abiotic stresses. *Planta* **217**: 356–366.

Miedes E, Lorences EP. **2007**. The implication of xyloglucan endotransglucosylase/hydrolase (XTHs) in tomato fruit infection by *Penicillium expansum* Link. A. *Journal of Agricultural and Food Chemistry* **55**: 9021–9026.

Miedes E, Suslov D, Vandenbussche F, *et al.* 2013. Xyloglucan endotransglucosylase/hydrolase (XTH) overexpression affects growth and cell wall mechanics in etiolated Arabidopsis hypocotyls. *Journal of Experimental Botany* **64**: 2481–97.

Miedes E, Vanholme R, Boerjan W, Molina A. **2014**. The role of the secondary cell wall in plant resistance to pathogens. *Frontiers in Plant Science* **5**: 358.

Mohnen D. **2008**. Pectin structure and biosynthesis. *Current Opinion in Plant Biology* **11**: 266–277.

Moller IE, de Fine Licht HH, Harholt J, Willats WGT, Boomsma JJ. **2011**. The dynamics of plant cell-wall polysaccharide decomposition in leaf-cutting ant fungus gardens. *PLoS ONE* **6**: e17506.

Moller I, Marcus SE, Haeger A, *et al.* 2008. High-throughput screening of monoclonal antibodies against plant cell wall glycans by hierarchical clustering of their carbohydrate microarray binding profiles. *Glycoconjugate Journal* **25**: 37–48.

Moller IE, Pettolino FA, Hart C, Lampugnani ER, Willats WGT, Bacic A. **2012**. Glycan profiling of plant cell wall polymers using microarrays. *Journal of Visualized Experiments* **70**: e4238.

Moller I, Sørensen I, Bernal AJ, *et al.* 2007. High-throughput mapping of cell-wall polymers within and between plants using novel microarrays. *The Plant Journal* **50**: 1118–28.

Muñoz-Bertomeu J, Lorences EP. **2014**. Changes in xyloglucan endotransglucosylase/hydrolase (XTHs) expression and XET activity during apple fruit infection by *Penicillium expansum* Link. A. *European Journal of Plant Pathology* **138**: 273–282.

Nafisi M, Stranne M, Fimognari L, *et al.* 2015. Acetylation of cell wall is required for structural integrity of the leaf surface and exerts a global impact on plant stress responses. *Frontiers in Plant Science* **6**: 550.

Nguema-Ona E, Moore JP, Fagerström AD, *et al.* 2013. Overexpression of the grapevine PGIP1 in tobacco results in compositional changes in the leaf arabinoxyloglucan network in the absence of fungal infection. *BMC Plant Biology* **13**: 46.

Nguema-Ona E, Vicré-Gibouin M, Cannesan MA, Driouich A. **2013**. Arabinogalactan proteins in root-microbe interactions. *Trends in Plant Science* **18**: 1360–1385.

O'Neill MA, Ishii T, Albersheim P, Darvill AG. **2004**. Rhamnogalacturonan II: structure and function of a borate cross-linked cell wall pectic polysaccharide. *Annual Review of Plant Biology* **55**: 109–139.

Olsen S, Popper ZA, Krause K. **2016**. Two sides of the same coin: Xyloglucan endotransglucosylases/hydrolases in host infection by the parasitic plant *Cuscuta*. *Plant Signaling & Behavior* **11**: e1145336.

Pabst M, Fischl RM, Brecker L, *et al.* 2013. Rhamnogalacturonan II structure shows variation in the side chains monosaccharide composition and methylation status within and across different plant species. *The Plant Journal* **76**: 61–72.

Park YB, Cosgrove DJ. **2012**. A revised architecture of primary cell walls based on biomechanical changes induced by substrate-specific endoglucanases. *Plant Physiology* **158**: 1933–43.

Park YB, Cosgrove DJ. **2015**. Xyloglucan and its interactions with other components of the growing cell wall. *Plant & Cell Physiology* **56**: 180–94.

Pauly M, Gille S, Liu L, *et al.* 2013. Hemicellulose biosynthesis. *Planta* **238**: 627–642.

Pauly M, Keegstra K. **2016**. Biosynthesis of the plant cell wall matrix polysaccharide xyloglucan. *Annual Review of Plant Biology* **67**: 235–259.

Pauly M, Ramírez V. **2018**. New insights into wall polysaccharide o-acetylation. *Frontiers in Plant Science* **9**: 1210.

Pellerin P, O'Neill MA. **1998**. The interaction of the pectic polysaccharide Rhamnogalacturonan II with heavy metals and lanthanides in wines and fruit juices. *Analusis* **26**: 32–36.

Peng Y, van Wersch R, Zhang Y. **2018**. Convergent and divergent signaling in PAMP-triggered immunity and effector-triggered immunity. *Molecular Plant-Microbe Interactions* **31**: 403–409.

Pogorelko G, Lionetti V, Fursova O, *et al.* 2013. Arabidopsis and *Brachypodium distachyon* transgenic plants expressing *Aspergillus nidulans* acetylesterases have decreased degree of polysaccharide acetylation and increased resistance to pathogens. *Plant Physiology* **162**: 9–23.

Popper ZA, Fry SC. **2005**. Widespread occurrence of a covalent linkage between xyloglucan and acidic polysaccharides in suspension-cultured angiosperm cells. *Annals of Botany* **96**: 91–99.

Prins TW, Tudzynski P, von Tiedemann A, *et al.* 2000. Infection strategies of *Botrytis cinerea* and related necrotrophic pathogens In: *Kronstad J.W. (eds) Fungal Pathology*. Dordrecht: Springer, Dordrecht, The

Netherlands, 33–64.

Qin Q, Bergmann CW, Rose JKC, *et al.* 2003. Characterization of a tomato protein that inhibits a xyloglucan-specific endoglucanase. *The Plant Journal* **34**: 327–338.

Rashid A. **2016**. Defense responses of plant cell wall non-catalytic proteins against pathogens. *Physiological and Molecular Plant Pathology* **94**: 38–46.

Rydahl MG, Hansen AR, Kračun SK, Mravec J. **2018**. Report on the current inventory of the toolbox for plant cell wall analysis: Proteinaceous and small molecular probes. *Frontiers in Plant Science* **9**: 581.

Saijo Y, Loo EP iian, Yasuda S. **2018**. Pattern recognition receptors and signaling in plant–microbe interactions. *Plant Journal* **93**: 592–613.

Salmeán AA, Guillouzo A, Duffieux D, *et al.* 2018. Double blind microarray-based polysaccharide profiling enables parallel identification of uncharacterized polysaccharides and carbohydrate-binding proteins with unknown specificities. *Scientific Reports* **8**: 1–11.

Salmeán AA, Hervé C, Jørgensen B, Willats WGT, Mravec J. **2017**. Microarray glycan profiling reveals algal fucoidan epitopes in diverse marine metazoans. *Frontiers in Marine Science* **4**: 293.

Van Sandt VSTT, Suslov D, Verbelen J-PP, Vissenberg K. **2007**. Xyloglucan endotransglucosylase activity loosens a plant cell wall. *Annals of Botany* **100**: 1467–1473.

Scheller HV, Ulvskov P. **2010**. Hemicelluloses. *Annual Review of Plant Biology* **61**: 263–289.

Seifert GJ, Roberts K. **2007**. The biology of arabinogalactan proteins. *Annual Review of Plant Biology* **58**: 137–161.

Shinohara N, Sunagawa N, Tamura S, *et al.* 2017. The plant cell-wall enzyme AtXTH3 catalyses covalent cross-linking between cellulose and cello-oligosaccharide. *Scientific Reports* **7**: 46099.

Showalter AM. **1993**. Structure and function of plant cell wall proteins. *The Plant Cell* **5**: 9–23.

Showalter AM. **2001**. Arabinogalactan-proteins: structure, expression and function. *Cellular and Molecular Life Sciences* **58**: 1399–1417.

Silva-Sanzana C, Celiz-Balboa J, Garzo E, *et al.* 2019. Pectin methylesterases modulate plant homogalacturonan status in defenses against the aphid myzus persicae. *Plant Cell* **31**: 1913–1929.

Somerville C. **2006**. Cellulose synthesis in higher plants. *Annual Review of Cell and Developmental Biology* **22**: 53–78.

Somerville C, Bauer S, Brininstool G, *et al.* 2004. Toward a systems approach to understanding plant cell walls. *Science* **306**: 2206–2211.

Su S, Higashiyama T. **2018**. Arabinogalactan proteins and their sugar chains: functions in plant reproduction, research methods, and biosynthesis. *Plant Reproduction* **31**: 67–75.

Talbott LD, Ray PM. **1992**. Molecular size and separability features of pea cell wall polysaccharides: Implications for models of primary wall structure. *Plant Physiology* **98**: 357–368.

Tan L, Showalter AM, Egelund J, Hernandez-Sanchez A, Doblin MS, Bacic A. **2012**. Arabinogalactan-proteins and the research challenges for these enigmatic plant cell surface proteoglycans. *Frontiers in Plant Science* **3**.

Tan L, Tees D, Qian J, Kareem S, Kieliszewski MJ. **2018**. Intermolecular interactions between glycomodules of plant cell wall arabinogalactan-proteins and extensins. *The Cell Surface* **1**: 25–33.

Thomas LH, Trevor Forsyth V, Šturcová A, *et al.* 2013. Structure of cellulose microfibrils in primary cell walls from collenchyma. *Plant Physiology* **161**: 465–476.

Thompson JE, Fry SC. **2000**. Evidence for covalent linkage between xyloglucan and acidic pectins in suspension-cultured rose cells. *Planta* **211**: 275–286.

Thulasi Devendrakumar K, Li X, Zhang Y. **2018**. MAP kinase signalling: interplays between plant PAMP- and effector-triggered immunity. *Cellular and Molecular Life Sciences* **75**: 2981–2989.

Toruño TY, Stergiopoulos I, Coaker G. **2016**. Plant-pathogen effectors: cellular probes interfering with plant defenses in spatial and temporal manners. *Annual Review of Phytopathology* **54**: 419–441.

Trdá L, Boutrot F, Claverie J, Brulé D, Dorey S, Poinssot B. **2015**. Perception of pathogenic or beneficial bacteria and their evasion of host immunity: pattern recognition receptors in the frontline. *Frontiers in Plant Science* **6**: 219.

Tudzynski P, Kokkelink L. **2009**. *Botrytis cinerea*: Molecular aspects of a necrotrophic life style In: Deising HB, ed. *Deising H.B. (eds) Plant Relationships. The Mycota (A Comprehensive Treatise on Fungi as Experimental Systems for Basic and Applied Research),*. Springer, Berlin, Heidelberg, 29–50.

Underwood W. **2012**. The plant cell wall: a dynamic barrier against pathogen invasion. *Frontiers in Plant Science* **3**: 85.

Vaahtera L, Schulz J, Hamann T. **2019**. Cell wall integrity maintenance during plant development and interaction with the environment. *Nature Plants* **5**: 924–932.

Valentin R, Cerclier C, Geneix N, *et al.* 2010. Elaboration of extensin-pectin thin film model of primary plant cell wall. *Langmuir* **26**: 9891–9898.

Velasquez SM, Ricardi MM, Dorosz JG, *et al.* 2011. O-glycosylated cell wall proteins are essential in root hair growth. *Science* **332**: 1401–1403.

Veloso J, van Kan JAL. **2018**. Many shades of grey in *Botrytis*–Host plant interactions. *Trends in Plant Science* **23**: 613–622.

Vlad F, Spano T, Vlad D, Bou Daher F, Ouelhadj A, Kalaitzis P. **2007**. Arabidopsis prolyl 4-hydroxylases are differentially expressed in response to hypoxia, anoxia and mechanical wounding. *Physiologia Plantarum* **130**: 471–483.

Voragen AGJ, Coenen GJ, Verhoef RP, Schols HA. **2009**. Pectin, a versatile polysaccharide present in plant cell walls. *Structural Chemistry* **20**: 263–275.

Voxeur A, Habrylo O, Guénin S, *et al.* 2019. Oligogalacturonide production upon *Arabidopsis thaliana-Botrytis cinerea* interaction. *Proceedings of the National Academy of Sciences of the United States of America* **116**: 19743–19752.

Voxeur A, Höfte H. **2016**. Cell wall integrity signaling in plants: “To grow or not to grow that’s the question.” *Glycobiology* **26**: 950–960.

Wang X, Hou S, Wu Q, *et al.* 2017. IDL6-HAE/HSL2 impacts pectin degradation and resistance to *Pseudomonas syringae* pv tomato DC3000 in Arabidopsis leaves. *Plant Journal* **89**: 250–263.

Wang D, Yeats TH, Uluisik S, Rose JKC, Seymour GB. **2018**. Fruit Softening: Revisiting the Role of Pectin. *Trends in Plant Science* **23**: 302–310.

Wiethölter N, Graeßner B, Mierau M, Mort AJ, Moerschbacher BM. **2003**. Differences in the methyl ester distribution of homogalacturonans from near-isogenic wheat lines resistant and susceptible to the wheat stem rust fungus. *Molecular Plant-Microbe Interactions* **16**: 945–952.

Willats WGT, Marcus SE, Knox JP. **1998**. Generation of a monoclonal antibody specific to (1→5)-α-l-arabinan. *Carbohydrate Research* **308**: 149–152.

Witasari LD, Huang FC, Hoffmann T, Rozhon W, Fry SC, Schwab W. **2019**. Higher expression of the strawberry xyloglucan endotransglucosylase/hydrolase genes *FvXTH9* and *FvXTH6* accelerates fruit ripening. *Plant Journal* **100**: 1237–1253.

Wolf S. **2017**. Plant cell wall signalling and receptor-like kinases. *Biochemical Journal* **474**: 471–492.

Wolf S, Hématy K, Höfte H. **2012**. Growth control and cell wall signaling in plants. *Annual Review of Plant Biology* **63**: 381–407.

Wolf S, Mouille GG, Pelloux JJ. **2009**. Homogalacturonan methyl-esterification and plant development. *Molecular Plant* **2**: 851–860.

Wood IP, Pearson BM, Garcia-Gutierrez E, *et al.* 2017. Carbohydrate microarrays and their use for the identification of molecular markers for plant cell wall composition. *Proceedings of the National Academy of Sciences of the United States of America* **114**: 6860–6865.

Wu Y, Fan W, Li X, *et al.* 2017. Expression and distribution of extensins and AGPs in susceptible and resistant banana cultivars in response to wounding and *Fusarium oxysporum*. *Scientific Reports* **7**: 42400.

Yapo BM. **2011a**. Pectin rhamnogalacturonan II: On the “Small Stem with Four Branches” in the primary cell walls of plants. *International Journal of Carbohydrate Chemistry* **2011**: 1–11.

Yapo BM. **2011b**. Pectic substances: From simple pectic polysaccharides to complex pectins - A new hypothetical model. *Carbohydrate Polymers* **86**: 373–385.

Zega A, D’Ovidio R. **2016**. Genome-wide characterization of pectin methyl esterase genes reveals members differentially expressed in tolerant and susceptible wheats in response to *Fusarium graminearum*. *Plant Physiology and Biochemistry* **108**: 1–11.

Zykwinska AW, Thibault J-F, Ralet M-C. **2007**. Organization of pectic arabinan and galactan side chains in association with cellulose microfibrils in primary cell walls and related models envisaged. *Journal of Experimental Botany* **58**: 1795–1802.

Chapter 3

Research chapter 1

Overexpression of VviPGIP1 and NtCAD14 in tobacco screened using glycan microarrays reveals cell wall reorganisation in the absence of fungal infection

This chapter was published in **Vaccines** and has been formatted according to their guideline rules

vaccines

MDPI

Article

Overexpression of VviPGIP1 and NtCAD14 in Tobacco Screened Using Glycan Microarrays Reveals Cell Wall Reorganisation in the Absence of Fungal Infection

Florent Weiller [1], Lorenz Gerber [2,†], Johan Trygg [3], Jonatan U. Fangel [4,‡], William G.T. Willats [5], Azeddine Driouich [6], Melané A. Vivier [1] and John P. Moore [1,*]

[1] South African Grape and Wine Research Institute, Department of Viticulture and Oenology, Stellenbosch University, Stellenbosch 7602, South Africa; florent@sun.ac.za (F.W.); mav@sun.ac.za (M.A.V.); moorejp@sun.ac.za (J.P.M.)

[2] Department of Plant Sciences, Swedish Agricultural University, 75007 Uppsala, Sweden; lorenzottogerber@gmail.com

[3] Computational Life Science Cluster, Department of Chemistry, University of Umeå, 901 87 Umea, Sweden; johan.trygg@umu.se

[4] Department of Plant and Environmental Sciences, University of Copenhagen, 1165 Copenhagen, Denmark; jonatanfangel@gmail.com

[5] School of Agriculture, Food and Rural Development, Newcastle University, Newcastle-Upon-Tyne NE1 7RU, UK; william.willats@newcastle.ac.uk

[6] Laboratoire de Glycobiologie et Matrice Extracellulaire Végétale (GlycoMEV), University of Rouen, 76821 Mont Saint Aignan, France; Azeddine.Driouich@univ-rouen.fr

* Correspondence: moorejp@sun.ac.za; Tel.: +27-21-808-2733

† Present Address: Genome Institute of Singapore, Singapore.

‡ Present Address: Novozymes, Copenhagen, Denmark.

Received: 29 June 2020; Accepted: 14 July 2020; Published: 15 July 2020

Abstract: The expression of *Vitis vinifera* polygalacturonase inhibiting protein 1 (VviPGIP1) in *Nicotiana tabacum* has been linked to modifications at the cell wall level. Previous investigations have shown an upregulation of the lignin biosynthesis pathway and reorganisation of arabinoxyloglucan composition. This suggests cell wall tightening occurs, which may be linked to defence priming responses. The present study used a screening approach to test four VviPGIP1 and four NtCAD14 overexpressing transgenic lines for cell wall alterations. Overexpressing the tobacco-derived cinnamyl alcohol dehydrogenase (*NtCAD14*) gene is known to increase lignin biosynthesis and deposition. These lines, particularly PGIP1 expressing plants, have been shown to lead to a decrease in susceptibility towards grey rot fungus *Botrytis cinerea*. In this study the aim was to investigate the cell wall modulations that occurred prior to infection, which should highlight potential priming phenomena and phenotypes. Leaf lignin composition and relative concentration of constituent monolignols were evaluated using pyrolysis gas chromatography. Significant concentrations of lignin were deposited in the stems but not the leaves of NtCAD14 overexpressing plants. Furthermore, no significant changes in monolignol composition were found between transgenic and wild type plants. The polysaccharide modifications were quantified using gas chromatography (GC–MS) of constituent monosaccharides. The major leaf polysaccharide and cell wall protein components were evaluated using comprehensive microarray polymer profiling (CoMPP). The most significant changes appeared at the polysaccharide and protein level. The pectin fraction of the transgenic lines had subtle variations in patterning for methylesterification epitopes for both VviPGIP1 and NtCAD14 transgenic lines versus wild type. Pectin esterification levels have been linked to pathogen defence in the past. The most marked changes occurred in glycoprotein

abundance for both the VviPGIP1 and NtCAD14 lines. Epitopes for arabinogalactan proteins (AGPs) and extensins were notably altered in transgenic NtCAD14 tobacco.

Keywords: cell wall; lignin; pectin; extensin; PGIP; CAD; tobacco

1. Introduction

Pathogens such as necrotrophic or biotrophic plant pathogenic fungi have to break through/disrupt the host cell wall before colonising and feeding can begin. The first line of defence against the invading organism is the plant cell wall, which is a 'dynamic' glycan-matrix, composed of pectins-phenolics-proteins and hemicellulose layers depending on the plant species [1]. The plant cell wall matrix of fruits is a co-evolved pectin-protein-phenolic matrix, which aids in both the protection and dispersal of encapsulated seeds. Plant cell wall composition can be very different between fruits, such as grapes containing cell walls rich in pectin, grasses (i.e., monocotyledon) with secondary cell walls composed of mainly xylan-abundant polymers, or root tissues that are rich in xylogalacturonans [1,2]. The plant is able through pathogen detection systems to then modify its wall composition in response to a perceived stressor [3]. Callose deposition, lignification, and pectin esterification alterations are common responses at local points of contact between the pathogen and plant [1,3]. Invariably, this must mean that the plant pathogen (e.g., fungus) must also develop a molecular toolkit of weapons, such as enzymes, which are able to overcome and degrade the cell wall to access the host organism [1,4]. In addition to polysaccharides, cell wall proteins such as extensins have been shown to be plant–pathogen response macromolecules with an important role for arabinosylation in cross-linking these proteins at the site of deposition presumably impeding infection [5,6]. Plant pathogens can also use mechanical force via an appressorium [7], or use a wide range of plant cell wall degrading enzymes (CWDEs) to a good effect [8,9] to overcome the plant cell wall barrier.

One of the first enzymes released, and essential to fungal pathogenicity, are endo-polygalacturonases (ePGs) [10,11] in common terminology. That is not to say for example that CWDEs such as ePGs are more important than pectate lyases or pectin methyl esterases (PMEs) [12,13], but it is clear that they have been studied for the longest time in plant defence. ePGs hydrolyse the O-glycosyl bonds of α-1,4-linked galacturonic acid residues that form polygalacturonan chains. To counter the action of these fungal enzymes as well as regulate the plants own cell wall remodelling enzymatic process [14], plants have proteins with inhibiting properties such as the polygalacturonase inhibiting proteins (PGIPs), a conserved leucine rich repeat protein with ePG inhibiting activity [15–17]. PGIPs seem to have evolved to protect plants against fungal pathogens. However, the conserved leucine rich repeat pattern of the protein also suggests that the protein has indirect signalling roles in plants and may no longer function in a direct inhibiting action [18]. In some cases, selected PGIPs might have evolved to such a degree to have functions completely removed from directly inhibiting ePGs but rather in modulating molecular signalling pathways by activating seemingly unrelated plant pathways.

Moving back to the well-established idea of a direct role for PGIPs in inhibiting ePGs activity [19] a clear mechanism is still lacking. Docking studies by Federici et al. [20] have shown that PGIP2 from *Phaseolus vulgaris* can inhibit *Fusarium moniliforme* PG1 by a 'dual' action. Sicilia et al. [21] also showed that inhibition of *Botrytis cinerea* PG1 (*Bc*PG1) was achievable using PGIP2 isolated from *Phaseolus vulgaris*. Liu et al. [22,23] also showed with docking studies that PGIP1 can interact with various ePGs with specific binding sites depending of the ePG. However, no in vitro interaction evidence could be detected between *Bc*PG2 and *Vitis vinifera* PGIP1 (*Vvi*PGIP1) despite a reduction of symptoms observed during *Nicotiana benthamiana* co-infiltration experiments [19,24]. It was further suggested that PGIPs can interact directly with pectins to protect them from the action of the fungal enzymes via a competitive interaction process [25]. PGIPs have also been thought to stimulate plant defence responses by favouring the accumulation of oligogalacturonides [26]. Oligogalacturonides

(OGs) are α-1,4-galacturonic acid oligomers released after the action of ePGs on homogalacturonans (HG). These OGs function as damage-associated molecular patterns (DAMPs) and are therefore potentially capable of activating various plant defence responses [27–31].

VviPGIP1 may also be activating defence pathways indirectly of the enzyme-inhibitor protein direct interaction paradigm [17]. Overexpressing VviPGIP1 in a useful patho-system, *Nicotiana tabacum* (tobacco), resulted in changes in cell wall gene expression and lignin specific staining in leaves and stems of wild type compared to transgenic plants [18]. VviPGIP1 was also studied at the promoter level showing its regulation is inducible via defence response triggers and signaling pathways [32]. Constitutive expression of *Vvipgip1* in tobacco leads to alteration in phytohormone levels but also in some cell wall components [18]. One of the genes found to be altered in the microarray datasets was a cinnamyl alcohol dehydrogenase (CAD). CAD is a key enzyme in lignin biosynthesis, and indeed, when upregulated resulted in stem lignification of transgenic tobacco. In order to investigate a possible role for CAD upregulation in cell wall strengthening a number of transgenic lines of tobacco plants overexpressing NtCAD14 was generated [33]. However based on pathogen 'challenge' datasets, CAD activity alone appears insufficient to impart resistance to transgenic tobacco plants [33].

VviPGIP1 expression clearly influences polysaccharide remodelling. This was supported from microarray and additional cell wall datasets. Xyloglucan endotransglycosylase/hydrolase (XET/XTH) genes showed altered expression compared to wild types. The use of CoMPP (comprehensive microarray polymer profiling) with fractionation and enzymatic data focused on the changes found in the arabinoxyloglucan components of transgenic versus wild-type plants [18,34]. A model was proposed in Nguema-Ona et al. [34] where the plant became 'primed' due to VviPGIP1 expression, which produced a lignified and tightened xyloglucan network better able to resist infection by a fungal pathogen such as *Botrytis cinerea* [34]. More recently the role of xyloglucan as a new DAMP in plant–pathogen interactions in *Arabidopsis* and *V. vinifera* has been uncovered [35] supporting the Nguema-Ona et al. [34] study. Given a set of VviPGIP1 overexpressing lines are available and the CAD tobacco lines produced in the Mbewana [33] study, it was thought a screening study would be most useful and informative. In the CAD lines for example does the expression of the gene also lead to cell wall alterations in the absence of a pathogen? This for example remains unclear. Therefore, both the VviPGIP1 and CAD tobacco lines were investigated using pyrolysis gas chromatography mass spectrometry (Py-GC–MS) to more accurately dissect the lignin and phenolic differences/similarities. Using a survey screening approach, the variation in cell wall polysaccharide composition and organisation was investigated by performing CoMPP and monosaccharide analysis (GC–MS) of all available transgenic tobacco lines.

2. Materials and Methods

2.1. Plant Material

The transgenic tobacco lines used in this study were generated using *Nicotiana tabacum* cv Havana petit SR1 that either constitutively express the *VviPGIP1* gene as described in Joubert et al. [24], or the *NtCAD14* gene as described in Mbewana [33]. The *VviPGIP1* transformants and the CAD32, CAD38, and CAD42 lines did not show any phenotypical difference with the SR1 control. The CAD4 line had a delayed growth in the developmental time of the experiment though fully developed plants reach the equivalent size as SR1. See Table 1 for additional information.

Table 1. Table summarizing known information on the transgenic lines used in this study.

Plant Line	Promotor	Percentage of Successful Infections per Plant Line	Average Lesion Diameter (mm) *	Percentage Decrease in Disease Susceptibility (Compared to SR1) *, **	Experiments Conducted on Those Lines	Reference
SR1	-	97%	24.0 ± 7.3 (11 dpi)	0		
CAD 4	CaMV 35Sp	93%	17.7 ± 5.2	27%	CAD enzyme activity assay	
CAD 32		93%	14.5 ± 3.4	40%	Whole plant infection assay	[33]
CAD 38		-	-	-		
CAD 42		97%	16.4 ± 3.6	32%		
SR1	-	75%	40.94 ± 3.5 (15 dpi)	0	Detached leaves and whole plant infection assay	[24]
					Gene expression analysis on infected and uninfected leaf tissue On uninfected leaves:	[18]
					XTH activity	
					Phytohormones analysis	
					Lignin staining	[36]
PGIP 24	CaMV 35Sp	83%	15.43 ± 0.9	62%	Monosaccharide composition	
PGIP 37		83%	12.60 ± 1.1	69%	Volatile organic compound analysis	
PGIP 45		92%	21.84 ± 3.1	47%	CoMPP	[34]
PGIP 47		92%	36.77 ± 3.2	10%	Arabinoxyloglucan analysis	

* Calculated 11 dpi for the CAD lines and 15 dpi for the VviPGIP1 lines. ** The decrease in disease susceptibility was calculated by comparing the average lesion diameter at 11 dpi for the CAD lines and 15 dpi for the VviPGIP1 lines to that of the untransformed control (SR1).

2.2. Plant Growth Conditions

Seeds (wild type tobacco *Nicotiana tabacum* cv Havana petit SR1) were surface sterilised [37] and sown on MS medium [38]. Transgenic seeds [24,33] were sown under Kanamycin resistance. Seedlings were hardened off in peat moss plugs (Jiffy Products International, AS, Norway) before they were transferred into pots containing an equal mixture of soil, peat moss, and vermiculite. The plants were grown in a clima-room (artificial light intensity of 120 $\mu mol.m^{-2}.s^{-1}$) with a sixteen hours light and eight hours dark photoperiod at 23 °C. Organic fertilizer (Nitrosol, Fleuron (Pty) Ltd., South Africa) was added during watering once every two weeks. Plant material was harvested when six leaves had fully expanded (see Supplementary Materials Figure S1). Leaves were labelled leaf position 3 (L3) to leaf position 6 (L6) as outlined in previous studies such as Nguema-Ona et al. [34] and where leaf 1 is nearest to the shoot apical meristem. A biological sample consisted of three leaves at a specific leaf position (e.g., leaf 3) was harvested from four different plants at the same time and immersed into liquid nitrogen. Hence, the sampling was a form of biological composite representative sampling to ensure sufficient material was available for downstream analysis.

2.3. Cell wall Isolation Protocol

The selected leaves were processed for alcohol insoluble residue (AIR) preparations as described in Nguema-Ona et al. [34,39]. Leaf material was plunge frozen with liquid nitrogen and then ground to a fine powder using a Retsch Mixer Mill (30 rounds per minute, 60 s, Retsch, Haan, Germany). After boiling the tissue powder for 20 min in 80% aqueous ethanol (reagent grade) to deactivate enzymes, the insoluble material was washed with methanol for two hours on a rotating wheel. After centrifugation at 3000 rpm for 3 min, the pellets were sequentially washed twice with a (1:1)

methanol/chloroform solution for 2 h to remove plant oils/lipids and then rinsed with acetone for another 2 h before being air-dried. The extracted material was resuspended in distilled water and freeze-dried to obtain cell wall AIR. Samples were destarched using a combination of thermostable alpha-amylase, amyloglucosidase and pullulanase (from Megazyme). The AIR material was used for all further analytical experiments. All solvents used were from (Sigma-Aldrich, MO, USA) at reagent grade.

2.4. Pyrolysis Gas Chromatography Mass Spectrometry (Py-GC–MS) for Lignin Analysis

The AIR samples were analysed according to Gerber et al. [40]. Briefly, the analytical setup consisted of an oven pyrolyser equipped with an auto sampler (PY-2020iD and AS-1020E, Frontier-Labs, Japan) mounted on a GC–MS system (Agilent, 7890A/5975C, Agilent Technologies AB, Sweden). The pyrolysis oven was set to 450 °C, the interface to 340 °C and the injector to 320 °C. The injector was operated with a split ratio of 16:1, with helium as the carrier gas. The pyrolysate was separated on a DB-5MS capillary column (30 m × 0.25 mm i.d., 0.25 μm film thickness; J&W, Agilent Technologies AB, Sweden). The GC temperature program was as follows: the analysis was started at 40 °C and was then increased by 32 °C min^{-1} to 100 °C, followed by 6 °C min^{-1} to 120 °C, by 15 °C min^{-1} to 250 °C and finally by 32 °C min^{-1} to 320 °C where the temperature was kept for a further 3 min. The MS interface was kept at 280 °C. The quadrupole mass spectrometer (operated at unit mass resolution) recorded spectra in the range from 35 to 250 m/z. Quantification of lignin in particular was performed by calculating integrated peak areas from selected m/z channels.

2.5. Gas Chromatography–Mass Spectrometry (GC–MS) for Monosaccharides

Monosaccharide composition of the tobacco AIR isolated was determined using GC–MS according to the method of York et al. [41]. 5 mg of AIR was hydrolysed with 2 M TFA at 110 °C for 2 h. After centrifugation, the supernatant containing the monosaccharides was converted to methoxy sugars using an application of 1 M methanolic HCl at 80 °C for 16 h. Silylation was performed on the methoxy sugars by addition of a solution HMDS + TMCS + Pyridine (3:1:9; Sylon HTP kit; Sigma-Aldrich, MO, USA) and incubation at 80 °C for 20 min in order to produce trimethyl-silyl-glycosides. TMS glycosides were then dissolved in cyclohexane before being injected onto a Agilent 6890 N (Agilent, Palo Alto, CA, USA) gas chromatograph coupled to a Agilent 5975 MS mass spectrometer detector. Separation was performed on a polar (95% dimethylpolysiloxane) ZB-Semi-Volatiles Guardian (30 m, 0.25 mm ID, and 0.25 μm film thickness) 7HG-G027-11 GC column. The carrier gas was helium with a flow rate of 1 mL/min and the injector temperature was maintained at 280 °C in the splitless mode. The oven temperature program was maintained at 80 °C for 1 min and finally ramped at 7 °C/min to 300 °C and then held for 2 min. Mass spectral data was recorded in full scan mode (40–650 m/z) with both the ion source and quadrupole temperatures maintained at 240 °C and 150 °C respectively. The nine main monosaccharides found in plant cell walls were measured and quantified using standard sugar mixtures and myo-inositol as internal standard measured using Xcalibur software (Thermo Fisher Scientific Inc., MA, USA).

2.6. Comprehensive Microarray Polymer Profiling (CoMPP) for Polysaccharides-Proteins

Comprehensive microarray polymer profiling (CoMPP) was performed as described by Kračun et al. [42]. 10 mg of AIR was first subject to a chelating agent CDTA (diamino-cyclohexane-tetraacetic acid, 50 mM, pH 7.5) and then to an alkali extraction with NaOH (4 M + 0.1% $NaBH_4$). The AIR was extracted in 300 μL for each extract by agitating the tubes (each tube contains a glass bead) first at a frequency of 30 Hz for 2 min followed by 6 Hz for 2 h. This was performed sequentially for each extract so a total of 600 μL was collected for the CDTA (soluble pectin) and 600 μL was collected for the NaOH (soluble pectin-hemicellulose) per 10 mg of AIR. CDTA and NaOH extracts were pipetted into 384-microwell plates. Each sample was prepared as 4 dilutions (first dilution: 1:1, followed by serial five-fold dilutions of the preceding sample). From the microwell plates all samples and dilutions were then printed at 55% humidity onto nitrocellulose membranes (Whatman, pore size of

0.45 mm Whatman) using a microarray robot (Sprint, Arrayjet, Roslin, UK). Printed arrays were blocked using phosphate buffered saline PBS (140 mM NaCl, 2.7 mM KCl, 10 mM Na_2HPO4, 1.7 mM KH_2PO4, and pH 7.5) with 5% (*w*/*v*) low fat milk powder for 1 h followed by an incubation of 2 h with the various plant cell wall specific probes selected. This was followed by secondary binding in PBS and for 2 h with anti-rat, anti-mouse, or anti-His tag antibodies conjugated to alkaline phosphatase (Sigma) diluted 1:5000 (anti-rat and anti-mouse) or 1:1500 (anti-His tag). Details about the antibodies used are available in Table 2. Arrays were washed in PBS and then developed in a solution containing 5-bromo-4-chloro-3-indolylphosphate and nitro blue tetrazolium in alkaline phosphatase buffer (100 mM NaCl, 5 mM $MgCl_2$, 100 mM diethanolamine, and pH 9.5). Arrays were dried and antibodies/CBMs (Carbohydrate binding module) signal intensity was scanned at 2400 dots per inch (dpi) using a CanoScan 8800F instrument (Søborg, Denmark) and converted to TIFF image files. The pixel intensity reads representing probe signals were quantified using Array-Pro Analyzer 6.3 (Media Cybernetics, Rockville, MD, USA) software. The average of all 4 dilutions for each sample was calculated. Results data were presented in the heatmaps format with the maximal mean spot signal intensity set to 100 and other signal values normalised accordingly. A cut-off of 5 was applied as a baseline to remove the noise signal.

Table 2. List of monoclonal antibodies (mAbs) and CBMs used for the comprehensive microarray polymer profiling (CoMPP) analysis.

Homogalacturonan		low DE	JIM5	[43]
		high DE	JIM7	[44]
		Partially ME	LM18	
		Partially ME	LM19	[45]
		Partially ME	LM20	
RG-I associated		Backbone of RG-I	INRA-RU1	[46]
		D-galactan	LM5	[47]
		Feruloylated galactan	LM9	[48]
		L-arabinan	LM6	[49]
		Linearised L-arabinan	LM13	[50]
Hemicellulose		Feruloylate polymer	LM12	[51]
	Mannan	(galacto)(gluco)mannan	LM21	[52]
		D-(gluco)mannan	LM22	
	Glucan	β-D-glucan	BS-400-2	[53]
		Mixed link β-D-glucan	BS-400-3	
	Xyloglucan	Xyloglucan (XXXG motif)	LM15	[54]
		Xyloglucan	LM25	[51]
	Xylan	β-D-xylan	LM10	[55]
		β-D-xylan/arabinoxylan	LM11	
Cellulose		Cellulose (crystalline)	CBM3a	[56]
Proteins	Extensins		LM1	[57]
			JIM19	[58]
			JIM20	[59]
	AGP		JIM4	[60]
				[61]
			JIM8	[62]
			JIM13	[63]
				[61]
			LM14	[64]
		β-linked GlcA	LM2	[65]

2.7. Univariate Statistical and Multivariate Data Analysis

Twelve plants were grown for each genotype. Leaves of the same developmental stage from three different plants were pooled together, to ensure sufficient material, resulting in four different biological repeats per plant line. The biological repeats were processed and analysed individually.

The results are the average of these four biological repeats except for the GC–MS datasets where only three repeats were processed. All samples were analysed for statistical significance using Microsoft Excel 2016 and univariate statistical analyses were performed (ANOVA, with $p = 0.05$) under the guidance of the Centre for Statistical Consultation at Stellenbosch University (Prof. Martin Kidd) using Statistica 10 (StatSoft Southern Africa—Analytics, Sandton, South Africa). Py-GC–MS results were presented as variability plots after least significant difference (LSD) testing was performed. Multivariate analysis such as principal component analysis (PCA) was performed with the SIMCA 14 software package (Sartorium Stedim Biotech - Umetrics AB, Umea, Sweden).

3. Results

3.1. Lignin Compositional Analysis of Wild Type Versus Transgenic Tobacco Using Py-GC–MS

Pyrolysis gas chromatography mass spectrometry (Py-GC–MS), which allows thermogravimetric quantification, was used to determine the changes in the leaf lignin composition of transgenic tobacco plants compared to the wild type controls. Nine genotypes were tested: eight transgenic tobacco lines including four plants overexpressing the *NtCAD14* gene (these were named lines CAD4, CAD32, CAD38, and CAD42, according to the data presented in Mbewana [33] and four plants overexpressing the *VviPGIP1* gene (these were named lines PGIP24, PGIP37, PGIP45, and PGIP47; see Table 1). The *Nicotiana tabacum* cv Havana petit SR1 was used as the control line; and two sets of plants of SR1 were grown, one as controls for *NtCAD14* and one set of controls for *VviPGIP1* containing plants (see Table 1). In overview, the results from the Py-GC–MS analyses revealed that on average 80–85% of the spectra obtained from tobacco leaf AIR were made up of carbohydrates or carbohydrate related components (see Figure 1A). A further 10–14% of the spectra accounted for unknown compounds present in the AIR samples (Figure 1A). Only about 4% of the AIR recovered spectra was identified as known lignin components (Figure 1A). Little difference was observed for total lignin content and also in terms of the percentage of various lignin components identified between the different genotypes. In all the genotypes tested, p-hydroxyphenol was the most abundant monomer making up 2.1–2.6% of the total known lignin components, followed by generic phenolics (1–1.3%), guaiacyl (0.8–1%) and syringyl (0.02–0.04%). To ascertain if the enzyme activity for cinnamyl alcohol dehydrogenase (CAD) was equivalent between stems and leaves an experiment was conducted using representative samples, i.e., CAD4 for *NtCAD14* containing lines and PGIP45 for the *VviPGIP1* plants (see Figure 1B,C). Both transgenic lines displayed increased CAD activity in the stems (four to six times higher than SR1), whereas no such increased activity occurred in the leaves.

A

Genotype		C	G	S	H	P	U	O	SG	CL	L
SR1	%	80.22	0.92	0.04	2.62	1.30	0.98	13.90	0.04	16.69	4.89
	std dev	1.57	0.13	0.01	0.21	0.24	0.09	1.19	0.01	1.80	0.46
CAD 32	%	81.79	0.94	0.04	2.28	1.17	0.92	12.87	0.04	18.83	4.43
	std dev	1.70	0.08	0.01	0.39	0.13	0.10	1.45	0.01	2.41	0.50
	Fisher test	0.065	0.731	0.600	0.008	0.092	0.119	0.165	0.501	0.055	0.002
CAD 38	%	84.11	0.82	0.03	2.17	1.05	0.82	11.00	0.04	21.06	4.07
	std dev	1.45	0.07	0.01	0.30	0.13	0.12	1.07	0.01	2.55	0.46
	Fisher test	0.003	0.076	0.038	0.001	0.002	0.000	0.000	0.242	0.000	0.000
CAD 4	%	83.77	0.84	0.03	2.16	1.02	0.86	11.32	0.04	21.15	4.06
	std dev	1.44	0.06	0.01	0.22	0.09	0.08	1.20	0.01	1.61	0.31
	Fisher test	0.005	0.118	0.123	0.001	0.001	0.004	0.001	0.459	0.000	0.000
CAD 42	%	80.65	0.97	0.04	2.56	1.23	0.98	13.57	0.04	17.29	4.79
	std dev	3.10	0.12	0.01	0.32	0.19	0.15	2.38	0.01	2.89	0.61
	Fisher test	0.528	0.348	0.752	0.629	0.299	0.960	0.648	0.308	0.581	0.203
PGIP 24	%	84.64	0.79	0.02	2.25	1.05	0.86	10.39	0.03	20.77	4.11
	std dev	0.64	0.08	0.01	0.19	0.09	0.07	0.56	0.01	1.37	0.26
	Fisher test	0.002	0.039	0.000	0.005	0.002	0.004	0.000	0.000	0.001	0.000
PGIP 37	%	83.84	0.80	0.03	2.29	1.07	0.87	11.11	0.03	20.67	4.19
	std dev	2.85	0.10	0.01	0.38	0.17	0.11	2.15	0.01	3.37	0.63
	Fisher test	0.004	0.045	0.000	0.011	0.004	0.006	0.001	0.001	0.001	0.000
PGIP 45	%	81.54	0.85	0.03	2.49	1.19	0.97	12.93	0.03	17.98	4.56
	std dev	1.82	0.12	0.01	0.14	0.09	0.04	1.66	0.01	1.51	0.31
	Fisher test	0.885	0.977	0.252	0.486	0.841	0.831	0.991	0.134	0.641	0.201
PGIP 47	%	81.21	0.88	0.03	2.53	1.16	0.93	13.25	0.04	17.77	4.60
	std dev	1.42	0.12	0.01	0.23	0.11	0.07	1.26	0.01	1.43	0.33
	Fisher test	0.187	0.358	0.035	0.452	0.064	0.221	0.380	0.084	0.320	0.010

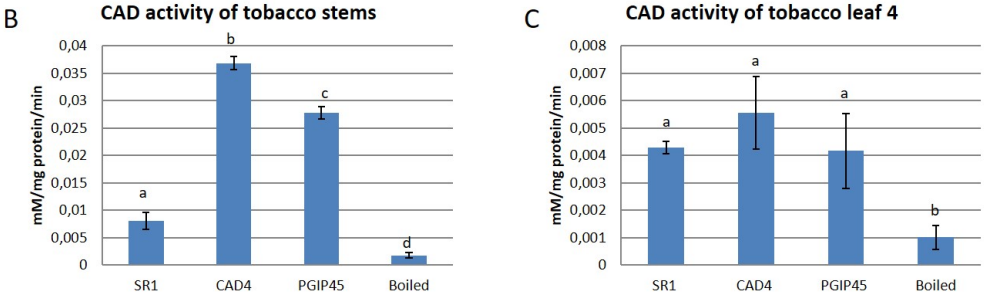

Figure 1. (**A**): Table of the lignin relative content and composition of the harvested tobacco leaves. Results are presented as the percentage of the total spectra recorded. Each percentage is the average of four biological repeats of four different leaves, showing standard deviation. A two-way ANOVA followed by a Fisher least significant difference (LSD) post-hoc test showed if the variations of the component analysed using Py-GC–MS between the different tobacco transgenic lines versus the wild type SR1 were significant with $p \leq 0.05$. C: Carbohydrate related components; G: Guaiacyl; S: Syringyl; H: p-hydroxyphenol; P: generic phenolics; U: known spectra, unknown identification; O: unknown spectra; SG: Syringyl/Guaiacyl ratio; CL: Carbohydrate related components/Lignin ratio; L: total lignin. (**B**): CAD enzyme activity assay of tobacco stems performed over a 10 min period in triplicate and expressed as mM/mg protein/min. (**C**): CAD enzyme activity assay of tobacco leaf 4 performed over a 10 min period in triplicate and expressed as mM/mg protein/min. In B and C, data were obtained from three biological repeats and boiled samples are controls where samples were boiled to inactivate proteins prior to the test. A one-way ANOVA followed by a Tukey test were performed with $p \leq 0.05$ to statistically separate the samples.

A Fisher analysis was performed as well as ANOVA multivariate tests of significance were used to evaluate the differences observed between SR1 as control and all genotypes for all leaf positions (see Figure 1A and Figure 2; see also Figure S2 for Supplementary Materials). For example, the wild type SR1 and the transgenic lines CAD42 and PGIP45 showed no significant differences for any of the compounds assayed (i.e., p-hydroxyphenol, guaiacyl, syringyl, general phenolics, carbohydrate components and the syringyl to guaiacyl ratio (S/G ratio)). However, the PGIP24 and PGIP37 lines interestingly showed a reduction in the S/G ratio compared to the control plants. The other lines showed more variable responses with many being non-significant as compared to the control plants. However, lines PGIP24 and PGIP37 had significantly lower values for all the monolignols assayed compared to the wild type plants (Figure 2), whereas the CAD32 line had significantly less p-hydroxyphenol (Figure 2A) and PGIP47 had significantly less syringyl (Figure 2C) compared with SR1 plants. Considering previous research had focused on the arabinoxyloglucan component of *VviPGIP1* transgenic tobacco and since the AIR was 80% by weight primarily polysaccharide in nature it was logical to further investigate the polysaccharide–protein network of these transgenic plants in relation to their controls.

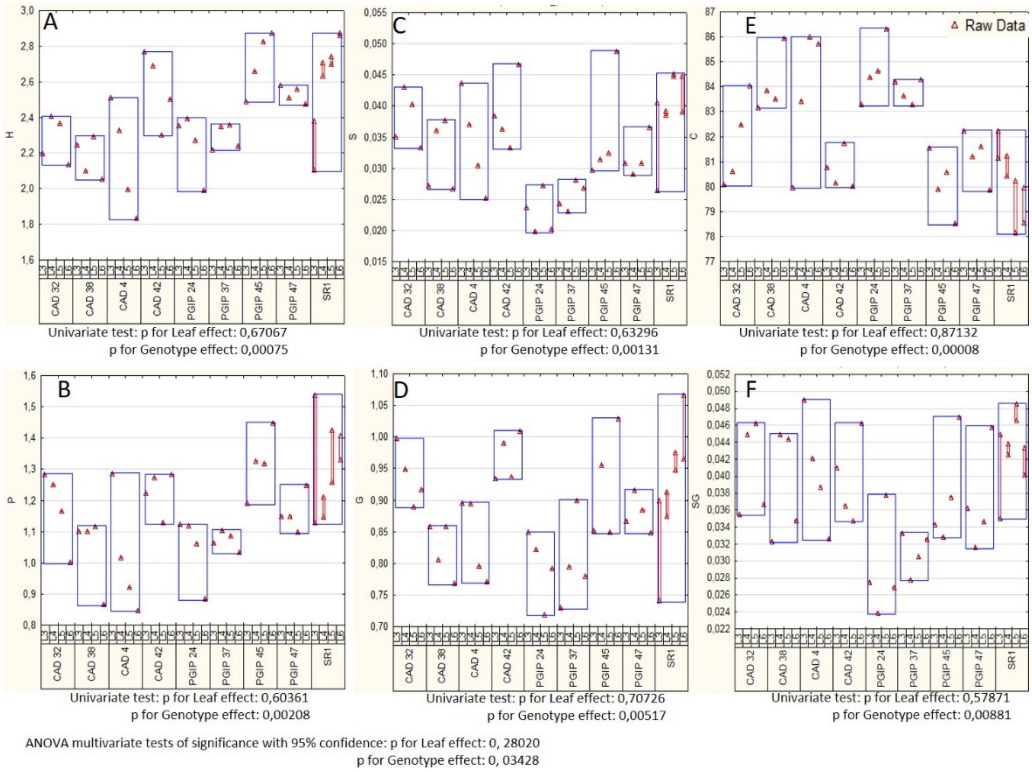

Figure 2. ANOVA box plots (multivariate tests of significance with 95% confidence intervals) of Py-GC–MS data for each analyte category SR1 vs transgenic plant lines. (**A**): p-hydroxyphenol (H); (**B**): generic phenolics (P); (**C**): syringyl (S); (**D**): guaiacyl (G); (**E**): carbohydrate related components; and (**F**): syringyl/guaiacyl ratio (SG). Data from SR1 constitute eight biological repeats whereas all other lines represent four biological repeats per transgenic plant.

3.2. Monosaccharide Composition Analysis of Wild Type Versus Transgenic Tobacco Using GC–MS

Monosaccharide analysis of tobacco AIR yielded a general profile showing; ca. 10 mol% of arabinose (Ara), ca. 10 mol% of rhamnose (Rha), ca. 1–2 mol% of fucose (Fuc), ca. 10 mol% of xylose (Xyl), ca. 2.5 mol% of mannose (Man), ca. 8–15 mol% of galactose (Gal), ca. 32–40 mol% of galacturonic acid (GalA), ca. 7–10 mol% glucose (Glc), and ca. 5 mol% glucuronic acid (GlucA; see Figure 3). Only representative lines are shown; namely CAD32, CAD42, PGIP37, and PGIP45 compared to wild type SR1 tobacco; this pattern was repeated in all lines. For the wild type plants, a standard developmental pattern was observed from leaf position 3 (L3) to leaf position 6 (L6), which showed alterations in the levels of Gal and GalA (Figure 3). The Gal decreased in a staggered manner from ca. 15 mol% for L3 to ca. 9 mol% for L6 while the GalA levels increased from ca. 32 mol% for L3 to ca. 38 mol% for L6 (the trend was visible but not statistically significant). The values between the other monosaccharides were not significantly different. A similar developmental pattern for Gal was observed with the transgenic lines PGIP37 and PGIP45 where Gal levels dropped from ca. 15 mol% for L3 or L4 to ca. 8 mol% for L6. Overall no difference in the monosaccharide profiles was observed between transgenic (both CAD and PGIP lines) and wild type SR1 tobacco.

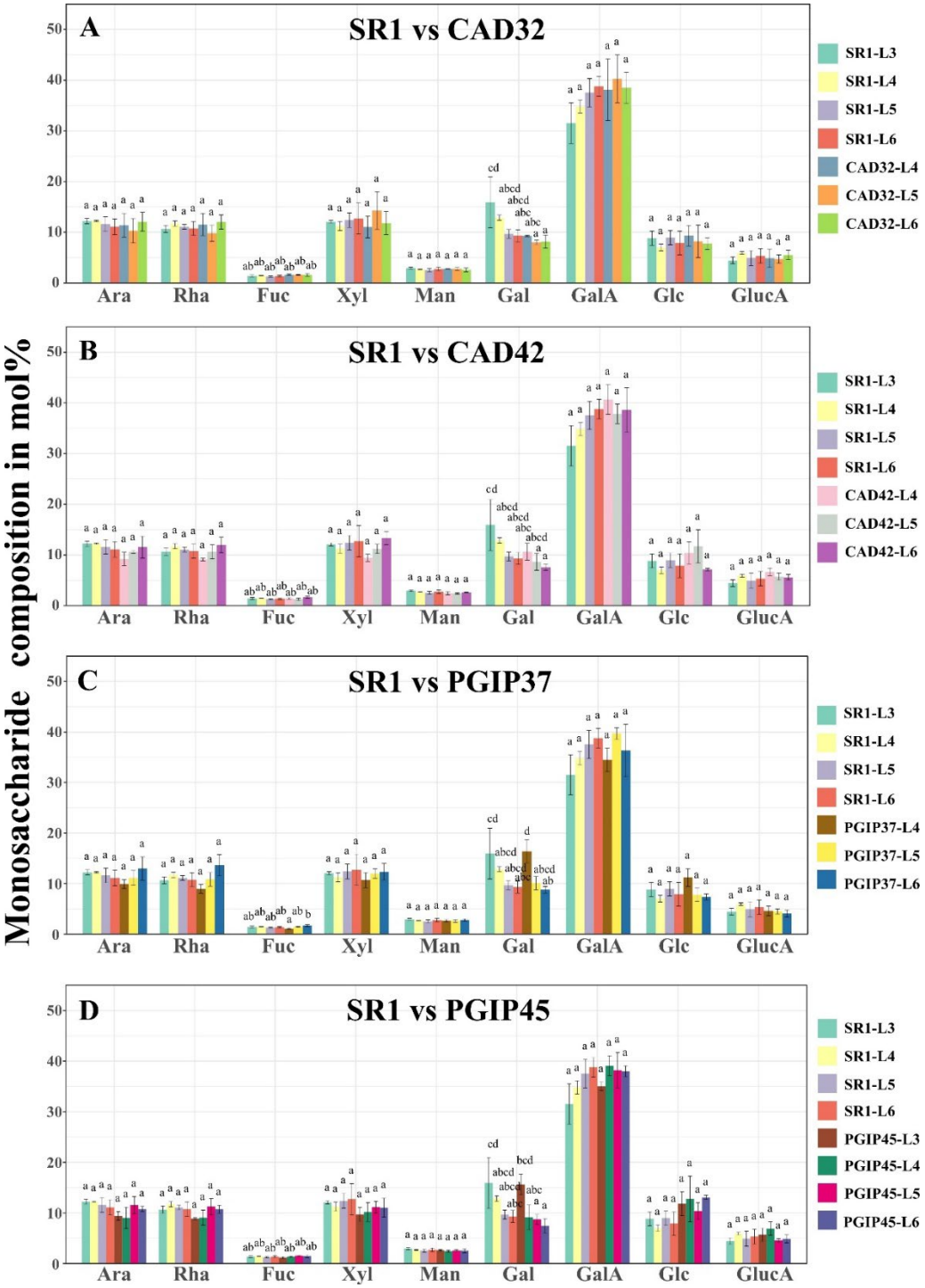

Figure 3. Monosaccharide composition of the cell wall, expressed in mol%, from the total alcohol insoluble residue (AIR) extraction of leaves from different tobacco lines. (**A**): Wild type SR1 versus CAD32. (**B**): SR1 versus CAD42. (**C**): SR1 versus PGIP37. (**D**): SR1 versus PGIP45. Ara: arabinose; Rha: rhamnose; Fuc: fucose; Xyl: xylose; Man: mannose; Gal: galactose; GalA: galacturonic acid; Glc: glucose; GlcA: glucuronic acid; L: leaf. The bars represent the average of three biological repeats. A two-way ANOVA followed by a Tukey's test were performed to statistically separate samples with $p \leq 0.05$.

3.3. Comprehensive Microarray Polymer Profiling (CoMPP) of SR1 Versus CAD Transgenic Tobacco Lines

In addition to total sugar composition analysis, an overview of the polysaccharides and glycoproteins present in the plant cell wall was obtained by performing a comprehensive microarray polymer profiling (CoMPP) analysis. A CoMPP analysis uses a range of monoclonal antibodies (mAbs) and carbohydrate binding modules (CBM) that recognise specific epitopes present on different cell wall polysaccharides. The CoMPP analysis of the CDTA extract from the CAD42 and CAD32 lines versus SR1 yielded a heatmap rich in pectins specifically in homogalacturonans (HGs) and rhamnogalacturonan I associated polymers (see Figure 4). Homogalacturonans (HG) are major pectin components. They are recognised by the monoclonal antibodies (mAbs) JIM5, JIM7, LM18, LM19, and LM20 (these bind depending on the degree and pattern of methylesterification of pectins). A leaf position (ontogenic or leaf age) pattern was observed with the wild type SR1 with an increase in signal for mAbs JIM5, JIM7, and LM19 from the youngest to the oldest leaf (Figure 4). The wild type SR1 had a stronger signal for mAbs JIM7 and LM19 than the CAD lines. Rhamnogalacturonan I (RG-I) is another major pectin polysaccharide; and the INRA-RU1 mAb binds to the RG1 backbone structure (alternating sequence of GalA and Rha monomers). Similarly to that found for HG epitopes, an increase in the INRA-RU1 signal, as a function of leaf maturation, was observed. The mAbs LM5 for galactans and mAbs LM6 for arabinans both showed a decreasing pattern of abundance and these are found as side chains of RG-1 polymers. In addition to polysaccharide binding mAbs, some probes were used that bound to cell wall glycoproteins. For the extensins, mAbs LM1, JIM19, and JIM20 were selected and for the arabinogalactan proteins (AGPs) mAbs JIM4, JIM8, JIM13, LM14, and LM2 were used. A similar decreasing signal as a function of the leaf position was notably found for mAb LM1, JIM20, JIM8, and JIM13 in all lines. However no (or very low) signals were found for mAbs JIM19, JIM4, LM14, and LM2 in the CDTA pectin fractions. It did seem however that important differences in younger leaves occurred with significantly more extensin signal (mAbs LM1 and JIM20) for the wild type compared with the CAD lines (i.e., CAD32 had higher signal than CAD42). For the AGPs it was the opposite with a much stronger signal for mAbs JIM8 and JIM13 in CAD32 than for CAD42 and SR1.

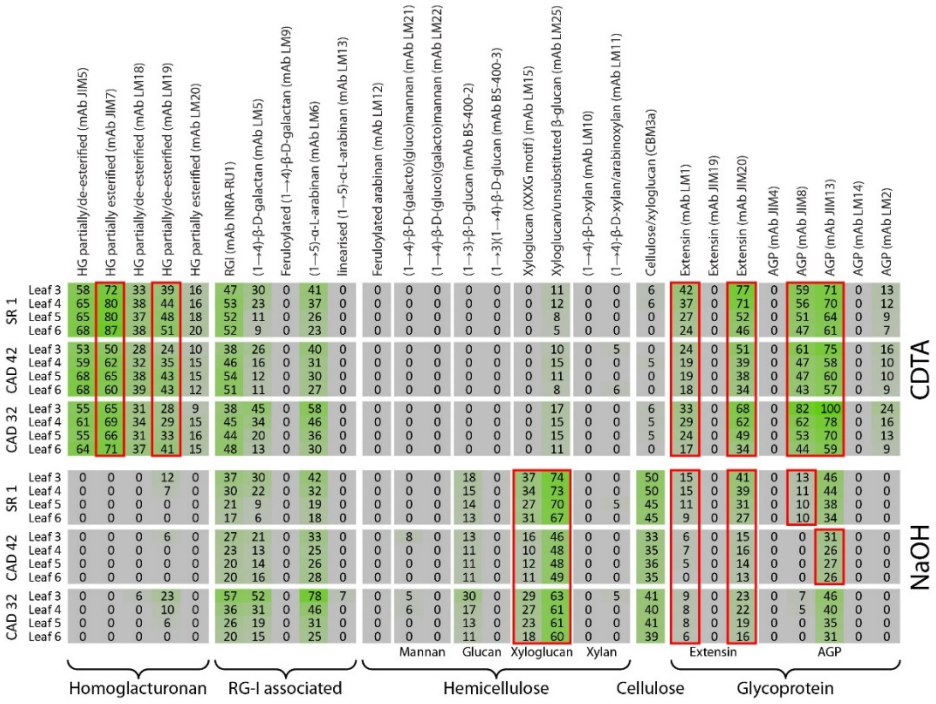

Figure 4. CoMPP (comprehensive microarray polymer profiling) of the wild type SR1, CAD42, and CAD32 tobacco leaf AIR. Heatmap showing cell wall polysaccharides and proteins relative abundance, which are from the average of four biological repeats.

CoMPP analysis of the NaOH extract from the CAD42 and CAD32 lines versus SR1 yielded a heatmap rich in RG-1 polymers, hemicelluloses such as xyloglucan and cellulose; and glycoproteins (i.e., extensins and AGPs; see Figure 4). For the INRA-RU1 mAb a decreasing signal was observed as a function of leaf maturation. The mAb LM5 galactan and LM6 arabinan chains linked to the RG-I backbones showed a decreasing signal. The RG-1 and side chain signals were similar between wild type and transgenic lines, except for leaf position 3, which showed some variability in total signals. The other main polysaccharides are the hemicelluloses and cellulose-linked epitopes. In the tobacco leaf AIR, glucan (mAb BS-400-2) and xyloglucan (mAbs LM15, LM25) binding antibodies and CBM3a displayed a signal in the NaOH fraction. The BS-400-2 mAb recognises glucans but showed no significant change in SR1 versus CAD42, whereas a very slight decrease in signal was observed as a function of leaf maturation for CAD32. For the xyloglucans, there was a slight decrease in signal for the mAb LM15 that recognises the XXXG motif (LM15) while the mAb LM25 signal remained stable. The wild type had a stronger signal for the CBM3a, a xyloglucan-cellulose binding probe than the CAD lines, and its intensity remained constant between the different leaves. The wild type had stronger signals for xyloglucan probes than CAD32, which in turn had higher signal than CAD42. The mAbs LM12, LM21, LM22, and BS-400-3, which bind mannans and some glucan motifs did not show any (or a very low) signal. For the extensin probe JIM20 the signal was higher in the wild type than the transgenic. For the AGP probe mAb JIM13 the signal pattern was very similar between the wild type and the CAD lines. However the total signal concentration did vary being lower in the transgenics for both extensins (mAb JIM20) and AGPs (mAb JIM13).

Supporting datasets for CAD4 and CAD38 are provided (see Supplementary Materials Figures S3 and S4 with CAD4, CAD38, and SR1). It was decided, in order to simplify the interpretation, to focus on one leaf position only (see Figure 5). L4 or leaf position 4 was chosen as an intermediate developmental stage; whereas L3 leaf position 3 showed quite a lot of sample variation across batches. A simplified heatmap was constructed for L4 from datasets for CDTA and NaOH (see Figure 5), effectively removing the ontogenic patterning. Compared to the CAD4, CAD42, CAD32, and CAD38 lines, the wild type had a stronger signal for homogalacturonan binding mAbs JIM5 and JIM7, which target HGs displaying both low and high degrees of methylesterification. No clear patterns between wild type and transgenic was found for the RG-1 associated epitopes (e.g., mAbs INRA-RU1, LM5, and LM6), although CAD38 and CAD32 seemed to display higher signals for mAbs LM5 and LM6 compared to the other transgenics and the wild type. The probes LM25 and CBM3a that recognise xyloglucan epitopes both had higher signal intensity in the NaOH extracts of the wild type compared to the transgenics. The most prominent differences between wild type and transgenic lines were for the extensin and some of the AGP epitopes (i.e., cell wall proteins). The data indicated that for the extensin probes mAb JIM20 and LM1, higher signal values were found for the wild type plants. Similarly for mAb JIM13 (an AGP probe) higher values were found for the wild type plants in the NaOH fraction. This is confirmed in the PCA plots for CDTA (Figure 5B) and NaOH (Figure 5C) extracts where SR1 separated from the transgenic populations due to higher signal values for cell wall proteins.

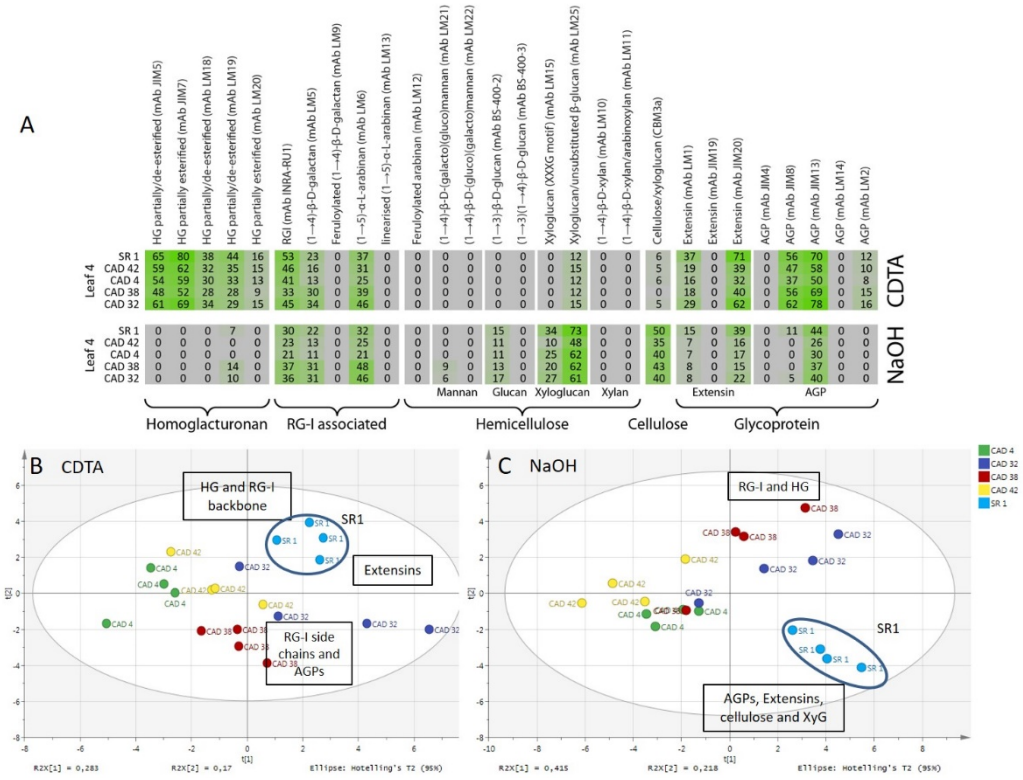

Figure 5. CoMPP of the leaf 4 AIR from SR1, CAD42, CAD4, CAD38, and CAD32 tobacco lines. (**A**): Heatmap showing cell wall polysaccharides and proteins relative abundance using antibodies signal intensity reads, presented results are the average of four biological repeats. (**B**): PCA of the pectin-rich fraction (CDTA) and (**C**): PCA of the hemicellulose-rich fraction (NaOH). On the PCA, samples are coloured according to their genotype. The wild type SR1 samples are highlighted and circled. Data obtained from four biological repeats.

3.4. Comprehensive Microarray Polymer Profiling (CoMPP) of SR1 Versus Grapevine PGIP1 Transgenic Tobacco Lines

CoMPP analysis of the SR1 control versus the four transgenic lines PGIP24, PGIP37, PGIP45, and PGIP47 yield a profile very similar to the preceding analysis on CAD transgenics although the distinction between wild type and transgenic is more subtle for the PGIP lines (see Figure 6; Figure S5). Similarly to the procedure followed for the CAD lines, PGIP24 and PGIP47 were excluded from this analysis as being very similar to PGIP37 and PGIP45 but the figures are available as supplementary data (Figures S5 and S6). The most conspicuous difference on first inspection was the significant difference between leaf 3 and the other leaf positions (Figure 6). Much higher signal intensities were found in the CDTA fraction for leaf 3 for mAbs JIM7, LM19, LM20, LM5, LM6, and LM25 compared to the other leaf positions. These probes bound to partially and highly methylated homogalacturonan, galactan, arabinan, and xyloglucan respectively. For leaf positions 4–6, signal variations were not observed except for the xyloglucan binding mAb LM25, which showed a decreasing signal with leaf maturation. In general, the mAbs showed similar signal intensities between the three lines except for mAb JIM20 (the extensin probe), which yielded a slightly stronger signal for the PGIP45 line compared to the wild type (Figure 6). The pattern was repeated for the NaOH extract where leaf position 3 separated markedly from the leaf 4–6 samples (Figure 6). This appeared to be due to stronger signals for the mAbs LM21, LM15, LM25, and CBM3a, which bind to mannan, xyloglucan, and cellulose epitopes (Figure 6).

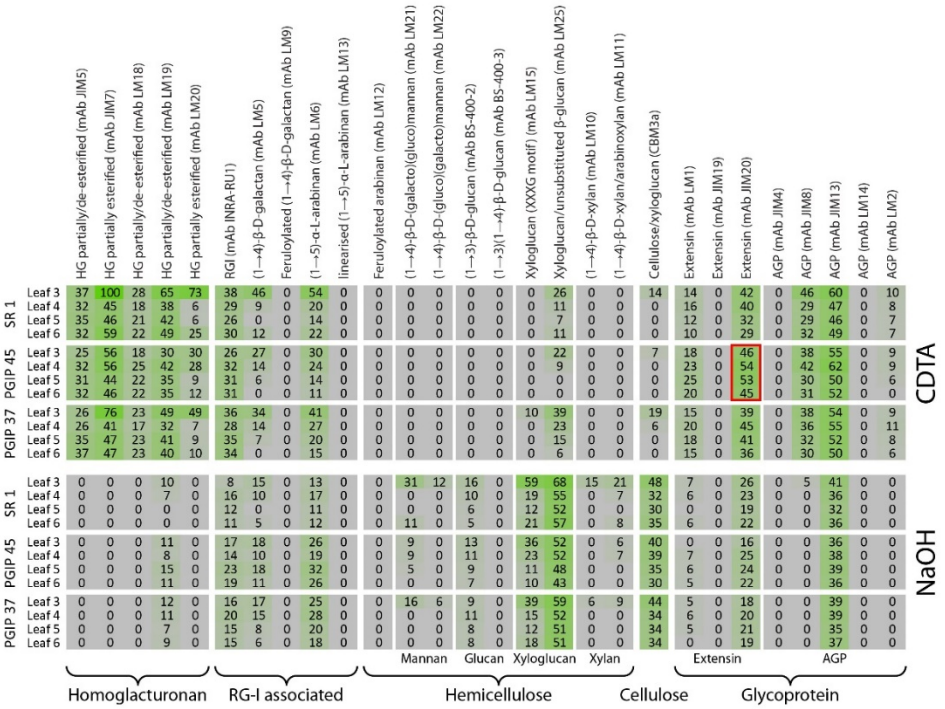

Figure 6. CoMPP of the wild type SR1, CAD42, and CAD32 tobacco leaf AIR. Heatmap showing cell wall polysaccharides and proteins relative abundance using antibodies signal intensity reads, presented results are from the average of four biological repeats.

As performed for the analysis of the CAD lines, heatmaps were constructed using only the CDTA and NaOH datasets of the leaf 4 samples from the SR1 and PGIP lines (see Figure 7). In the CDTA extracts signals for the common pectin probes mAbs JIM5, JIM7, LM18, and LM19 were found and were relatively invariant between wild type and the PGIP lines. Similarly the INRA-RU1 and LM6 probes did not show much change in the CDTA fractions. Interestingly, especially for the lines PGIP47 and PGIP45, the signal intensities for mAb LM1, JIM20, JIM8, and JIM13 (extensins and AGPs) were found to be markedly higher in the pectin CDTA fraction compared to the wild type plants. In contrast for PGIP lines 24, the pectin signals (mAbs LM19, INRA RU1, LM5, and LM6) and LM6 for PGIP line 37 were found to be higher in the transgenics for the NaOH fraction.

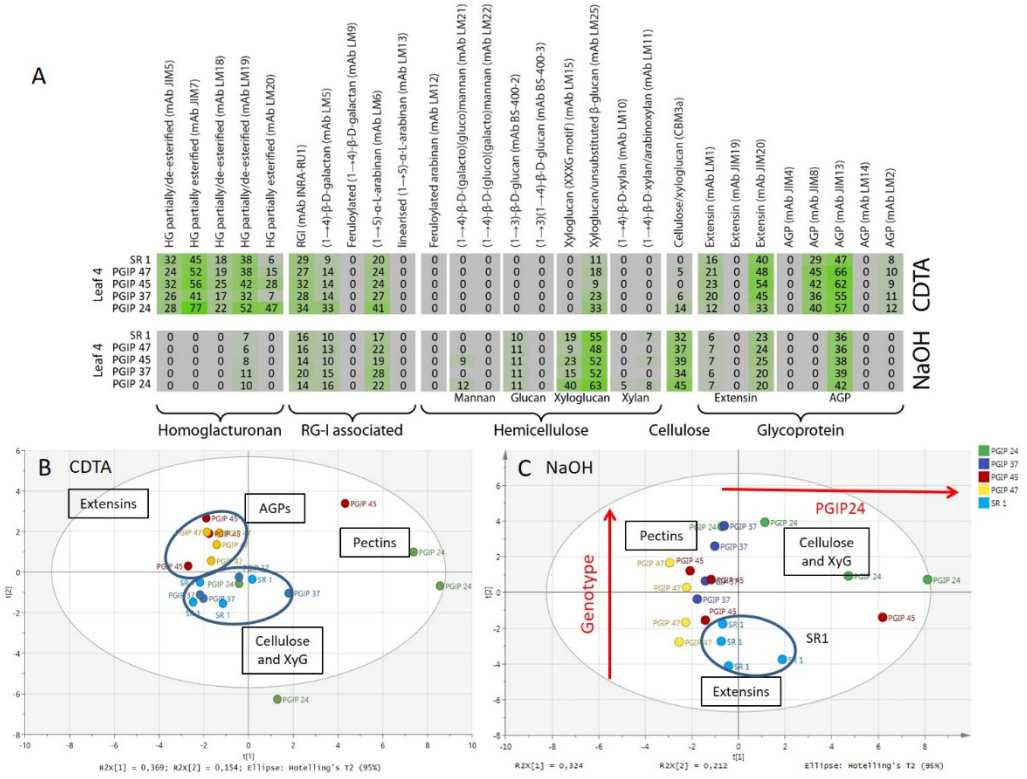

Figure 7. CoMPP of the leaf 4 AIR from SR1, CAD42, CAD4, CAD38, and CAD32 tobacco lines. (**A**): Heatmap showing cell wall polysaccharides and proteins relative abundance using antibodies signal intensity reads from the average of four biological repeats. (**B**): PCA of the pectin-rich fraction (CDTA) and (**C**): PCA of the hemicellulose-rich fraction (NaOH). On the PCA, samples are coloured according to their genotype. The wild type SR1 samples are highlighted and circled.

4. Discussion

4.1. Lignin Composition was Mostly Unaltered in Leaves of Plants Overexpressing Either CAD or the Grapevine PGIP1 Gene

The lignin analysis performed showed no significant difference in the total lignin concentration in the leaf as a function of leaf age, although ANOVA showed that significant differences did occur at the genotype level. This correlates with the results from Alexandersson et al. [18] that showed that *Vvipgip1* expression induced upregulation of CAD but that differences in the total lignin content of the leaf was not significant. Similarly, Mbewana [33] showed that tobacco plants overexpressing *CAD* had higher CAD activity in stems, but no significant differences in CAD activity were found in leaves when compared to the wild type. This indicated that overexpression of *CAD* was localised to the stem where lignin accumulation occurred with little to no effects at the leaf level. Overall, CAD activity was very low in leaves compared to the stems and this makes sense in the context of leaf function as a rapidly growing organ maximising surface area for photosynthesis. Increased levels of leaf lignification would probably be detrimental as it would impact leaf growth-expansion and therefore *CAD* expression is probably highly regulated in leaves. This argument is supported by observations of the CAD4 line, which had the highest lignin levels of all the tobacco overexpressing *CAD* lines generated, which shows a delayed and slow growing phenotype compared with other plants. This means that lignification must be tightly controlled for the plant to achieve normal growth and development [66]. The PGIP tobacco lines, similarly to the CAD lines, had an elevated CAD activity in stems but not in the leaves compared to SR1. Those results tend to confirm the model proposed by Nguema-Ona et al. [34] with spatial separation of lignification in PGIP-induced *CAD* expressing plants. CAD is a key enzyme in conversion of cinnamyl aldehydes to alcohols, which is the final step in monolignol biosynthesis before polymerisation [67]. Thus, *Vvipgip1* and *CAD* upregulation may

not necessarily affect lignin quantity, but lignin composition might well be altered. It is interesting to note that PGIP24 and PGIP37, which have the highest increase in resistance to *Botrytis cinerea* compared to the wild type [24], had significant differences in all the monolignols analysed while PGIP45 and PGIP47, which displayed lower resistance to the necrotrophic fungus, had a lignin composition much closer to SR1. The CAD4 line, which had the lowest acquired resistance to *B. cinerea* among the CAD lines tested [33], was also the one that differed the most from SR1. Since the concentration of lignin is not the determining factor, we investigated if the ratio between different monolignols could be responsible for observed resistance phenotypes. Indeed higher levels of syringyl units have been linked to higher resistance to pathogen attacks [68–70]. However, none of the lines tested had more syringyl than the wild type and the ratio of syringyl with the other monolignols (i.e., the S/G ratio) have not in all cases been correlated with an increased resistance to biotic stress [68]. This is in line with our results where PGIP24 and PGIP37, the less susceptible lines to *B. cinerea*, had the lowest S/G ratio. These data alone were insufficient to support the hypothesis that lignin changes prior to the infection are responsible for the increased resistance phenotype to *B. cinerea* infection. It is necessary to also look at the polysaccharide and protein components of the leaf cell walls to search for cell wall architectural changes linked to resistance priming against pathogenic fungi.

4.2. Pectin Organisation Varied between the SR1 and the Transgenic CAD and PGIP Lines

The CoMPP analysis performed on both CAD and *Vvi*PGIP1 transgenic plants showed differences in polysaccharide availability due to the leaf maturation stage and age. Large variations within the leaf 3 sample repeats were found as compared to other the leaf positions 4–6. Leaf 3 leaves are still growing and have not fully matured. Size variations, due to non-perfectly synchronised plants, might have brought about these observable differences. To assess this potential problem, we analysed leaves separately and characterised the ontogenic effect. The ontogenic effects linked to the leaf maturation process include a reduction in the galactan and arabinan side chains associated with RG-I as the leaf matures. Such changes associated with RG-1 side chains have been well described in the literature [71,72] and involve cell elongation and cell wall tightening events. These pectin side chains have been shown to be linked to cellulose microfibrils [73,74] and support the xyloglucan/cellulose network [75]. The decreasing xyloglucan probe signals found for many of the leaf CDTA fractions, which is probably linked to the arabinan and galactan side chains helping form pectin-xyloglucan linkages, supports this. In addition to its role in the lignin biosynthesis pathway, *CAD* seems to be directly and/or indirectly involved in cell wall polysaccharide reorganisation. In datasets from the CAD lines it seemed that xyloglucan and cellulose had become less accessible as compared to the SR1 lines suggesting biosynthetic alterations and/or architectural reorganisation. A role for xyloglucan changes has already been well established in PGIP lines. The downregulation of *XTH*/*XET* gene expression in *Vvi*PGIP1 plants [18] was further confirmed by Nguema-Ona et al. [34] who proposed a model where the cellulose/xyloglucan network was strengthened or 'primed' against pathogen attack in PGIP lines. A role for xyloglucan in functioning as the damage associated molecular pattern (DAMP) in plant–pathogen interactions supports this [35]. How *CAD* is able to directly influence *XTH*/*XET* gene expression remains unclear. Therefore, by lowering accessibility to the xyloglucan and cellulose network [2,76–78], the accessibility of the matrix to cellulases and other CWDEs would be substantially diminished.

A range of homogalacturonan binding mAbs were used, which displayed specificity to a variety methylesterified states or motifs. SR1 appeared to have the highest level of highly methylesterified HG. Although differences between SR1, CAD, and PGIP were slight and subtle; it would seem that PGIP lines seemed to maintain a stable degree of methylesterification of their leaf pectins. Pectin methylesterification protects pectin against the action of CWDEs and pectinases such as ePGs more specifically. The action of ePGs is essential for necrotrophic fungi such as *Botrytis* spp. to breach the cell wall barrier and penetrate plant tissues [10,11]. Methylesterification of the galacturonic acid residues from homogalacturonan can protect the plant against fungal pathogen as shown by Volpi et al. [79] in wheat by the overexpression of a pectin-methyl-esterase inhibitor (PMEI) from kiwifruit

(see also the review from Lionetti et al. [80]). Homogalacturonan is synthesised in the methylesterified state and only demethylesterified in the cell wall by pectin-methyl-esterases (PMEs) [81,82]. During de-esterification they form homogalacturonan Ca^{2+} ion egg-box structures [83,84]. De-esterification of the transgenic lines HG polymers could facilitate the easier release of oligogalacturonides (OGs) into the apoplast during infection. Oligogalacturonides have been studied for their role as defence elicitors or DAMPs [29]. OG DAMPs would trigger other plant defence mechanisms, which could act as defence primers [26–28,30,31]. It is tempting to speculate that PGIP expression can modulate pectin esterification levels through signalling pathways so as to 'prime' the wall to be able to release OG DAMPs upon infection by a fungal pathogen allowing the plant to respond in a faster and stronger manner.

4.3. Extensin and AGP Epitope Distribution Varies between Wild Type and Transgenic Lines Suggesting a Role in Cell Wall Resistance

Vvipgip1 overexpression seemed to elevate the level of extensins and AGPs in some of the lines. Extensins as proteins from the HRGP family have been more extensively studied in defence [85] and their role as cell wall strengthening agents is well documented [86]. Interestingly, Boudart et al. [87] showed that ePG action was able to induce extensin accumulation via a mechanism of OG elicitation. That process could also be involved with *Vvipgip*1 overexpression datasets presented. This could suggest that one of the priming defence mechanisms associated with *Vvipgip*1 overexpression is an elevated level of extensins. Cell wall proteins have been linked with a number of biotic (pathogen linked) or abiotic stress studies in plants [85,88,89]. AGPs have known roles in plant growth and development [89,90]. Mareri et al. [91] recently reviewed a role for AGPs in plant defence against biotic and abiotic stress. The authors reported AGP accumulation and up/downregulation of AGP encoding genes in plants have been observed during a range of abiotic stresses such as temperature stress, drought, flooding, hypoxia, salinity stress, mineral deficiency, and mineral toxicity. Additional findings have shown an accumulation of AGPs in root border cells have suggested they play an important role in recognition within the rhizosphere microbiome [92]. A more direct argument for an AGP role against biotic stress was found in pea roots where it was shown that in vitro, AGPs attract zoospores, inhibit cyst germination, and further mycelium development of *Aphanomyces euteiches* [93].

5. Conclusions

The overexpression of CAD and PGIP1 tobacco plants led to modifications of their cell wall structure in uninfected plants. Previous research has confirmed a role for arabinoxyloglucan modification of transgenic tobacco leaves, which could lead to a tightened cell wall matrix and the release of xyloglucan oligomers during infection, which could in turn act as DAMPs. The lignin composition in the PGIP lines (the S/G ratio specifically) did seem to correlate with resistance susceptibility however direct causality is lacking. At the level of pectin methylesterification the differences between transgenic lines and wild type was slight. Clearly, a more detailed picture of pectin methylesterification levels and patterning, by performing a more advanced analysis of pectins, is needed and could provide valuable new information on how the accessibility of HGs to ePGs in these transgenic lines is altered. Finally, cell wall proteins such as extensins and AGPs were modified by expression of both *NtCAD14* and *VviPGIP1* in tobacco plants. Further research should be focused on investigating what are the changes at the cell wall level in PGIP transgenic lines during an actual infection process with a necrotrophic pathogen such as *Botrytis cinerea*. Understanding the *in planta* functions of PGIP is a high priority area and this study has shed some valuable light in this respect; as well as in the area of 'priming' the plant cell wall for pathogen defence.

Supplementary Materials: The following are available online at www.mdpi.com/2076-393X/8/3/388/s1. Figure S1: A photograph of an SR1 tobacco plant used in this study in order to indicate leaf positions harvested (indicated by the numbered boxes). Out of the eight leaves present on the plant at the time of the experiment, leaf 2 was the youngest of those harvested, closest to the apical meristem and leaves 4-6 are fully expanded leaves.

Figure S2: ANOVA box plots (multivariate tests of significance with 95% confidence intervals) of Py-GC-MS data for each analyte category SR1 vs transgenic plant lines. A: known spectra, unknown identification (U); B: unknown spectra (O); C: total lignin (L); D: Carbohydrate related components/Lignin ratio (CL). Each percentage is the average of four biological repeats of four different leaves, showing standard deviation. Figure S3: CoMPP of the CDTA fraction of the wild type SR1, CAD4 and CAD38 tobacco leaf AIR. Heatmap showing cell wall polysaccharides and proteins relative abundance using antibodies signal intensity reads which are the average of four biological repeats. Figure S4: CoMPP of the NaOH fraction of the wild type SR1, CAD4 and CAD38 tobacco leaf AIR. Heatmap showing cell wall polysaccharides and proteins relative abundance using antibodies signal intensity reads which are the average of four biological repeats. Figure S5: CoMPP of the CDTA fraction of the wild type SR1, PGIP24 and PGIP47 tobacco leaf AIR. A: Heatmap showing cell wall polysaccharides and proteins relative abundance using antibodies signal intensity reads which are the average of four biological repeats. B: PCA of the pectin-rich fraction (CDTA) C: Loading plot showing the separation by variables. On the PCA, samples are coloured according to their leaf position, each genotype is represented with a different symbol, and SR1 is circled. Figure S6: CoMPP of the NaOH fraction of the wild type SR1, PGIP24 and PGIP47 tobacco leaf AIR. A: Heatmap showing cell wall polysaccharides and proteins relative abundance using antibodies signal intensity reads which are the average of four biological repeats. B: PCA of the pectin-rich fraction (NaOH) C: Loading plot of the previous PCA showing the separation of the variable. On the PCA, samples are coloured according to their leaf position, each genotype is represented with a different symbol, and SR1 circled.

Author Contributions: F.W. conducted experiments, performed analyses. F.W. and J.P.M. drafted the initial manuscript. F.W., A.D., M.AV. and J.P.M. designed and planned the study. J.P.M., M.AV. and A.D. secured funding support. L.G. performed the PyGC–MS analysis. J.T. assisted with multivariate data analysis. J.U.F. and W.G.T.W. performed the CoMPP analysis. All authors have read and agreed to the published version of the manuscript.

Funding: This research was funded by the Wine Industry Network of Expertise and Technology of South Africa (Winetech; Grant Nos. IWBT-P 09/01 and IWBT P14/03), Technology and Human Resources for Industry Programme (THRIP; Grant No. TP 13081327560), Stellenbosch University and the National Research Foundation of South Africa (NRF; Grant No. 92290). Thanks are also due to the University of Rouen, the GRR-Végétal-Agronomie- Sols-Innovation of Haute Normandie, Le Fonds Européen de Développement Regional (FEDER) for financial support to Azeddine Driouich. The funders were not involved in the design of the study; in the collection, analysis and interpretation of data; in the writing of the report; or in the decision to submit the article for publication.

Acknowledgments: The Central Analytical Facility (CAF) of Stellenbosch University (Lucky Mokwena) is thanked technical support with GC–MS analyses. Eric Nguema-Ona and Varsha Premsagar are thanked for their help in plant growth and tissue processing. Yu Gao is thanked for performing the CAD enzyme assays. Martin Kidd is thanked for his support and advice with the statistical data analysis.

Conflicts of Interest: The authors declare that the submitted work was carried out without any personal, professional or financial relationships that could potentially be construed as a conflict of interest.

References

1. Albersheim, P.; Darvill, A.G.; Roberts, K.; Sederoff, R.; Staehelin, A. Cell Walls and Plant Anatomy. In *Plant Cell Walls*; Garland Science: New York, NY, USA; 2011; pp. 1–42. ISBN 9780815319962.
2. Carpita, N.C.; Gibeaut, D.M. Structural models of primary cell walls in flowering plants: Consistency of molecular structure with the physical properties of the walls during growth. *Plant J.* **1993**, *3*, 1–30, doi:10.1111/j.1365-313X.1993.tb00007.x.
3. Bacete, L.; Mélida, H.; Miedes, E.; Molina, A. Plant cell wall-mediated immunity: Cell wall changes trigger disease resistance responses. *Plant J.* **2018**, *93*, 614–636, doi:10.1111/tpj.13807.
4. Petrasch, S.; Silva, C.J.; Mesquida-Pesci, S.D.; Gallegos, K.; van den Abeele, C.; Papin, V.; Fernandez-Acero, F.J.; Knapp, S.J.; Blanco-Ulate, B. Infection strategies deployed by *Botrytis cinerea*, *Fusarium acuminatum*, and *Rhizopus stolonifer* as a function of tomato fruit ripening stage. *Front. Plant Sci.* **2019**, *10*, 1–17, doi:10.3389/fpls.2019.00223.
5. Castilleux, R.; Plancot, B.; Ropitaux, M.; Carreras, A.; Leprince, J.; Boulogne, I.; Follet-Gueye, M.-L.; Popper, Z.A.; Driouich, A.; Vicré-Gibouin, M. Cell wall extensins in root–microbe interactions and root secretions. *J. Exp. Bot.* **2018**, *69*, 4235–4247, doi:10.1093/jxb/ery238.

6. Castilleux, R.; Plancot, B.; Gügi, B.; Attard, A.; Loutelier-Bourhis, C.; Lefranc, B.; Nguema-Ona, E.; Arkoun, M.; Yvin, J.-C.; Driouich, A.; et al. Extensin arabinosylation is involved in root response to elicitors and limits oomycete colonization. *Ann. Bot.* **2019**, *22*, 1–13, doi:10.1093/aob/mcz068.
7. Ryder, L.S.; Talbot, N.J. Regulation of appressorium development in pathogenic fungi. *Curr. Opin. Plant Biol.* **2015**, *26*, 8–13, doi:10.1016/J.PBI.2015.05.013.
8. Prins, T.W.; Tudzynski, P.; von Tiedemann, A.; Tudzynski, B.; Ten Have, A.; Hansen, M.E.; Tenberge, K.; van Kan, J.A.L. Infection strategies of *Botrytis cinerea* and related necrotrophic pathogens. In *Fungal Pathology*; Springer: Dordrecht, The Netherlands, 2000; pp. 33–64.
9. ten Have, A. The Botrytis Cinerea Endopolygalacturonase Gene Family; PhD Thesis, Wageningen University, Wageningen, the Netherlands; 2000.
10. Esquerré-Tugayé, M.T.; Boudart, G.; Dumas, B. Cell wall degrading enzymes, inhibitory proteins, and oligosaccharides participate in the molecular dialogue between plants and pathogens. *Plant Physiol.* **2000**, *38*, 157–163.
11. Kars, I.; Krooshof, G.H.; Wagemakers, L.; Joosten, R.; Benen, J.A.E.; Van Kan, J.A.L. Necrotizing activity of five *Botrytis cinerea* endopolygalacturonases produced in Pichia pastoris. *Plant J.* **2005**, *43*, 213–225, doi:10.1111/j.1365-313X.2005.02436.x.
12. Kühnel, S. Characterization of Cell Wall Degrading Enzymes from Chrysosporium Lucknowense C1 and Their Use to Degrade Sugar Beet Pulp; PhD Thesis, Wageningen University, Wageningen, the Netherlands; 2011.
13. Tudzynski, P.; Kokkelink, L. *Botrytis cinerea*: molecular aspects of a necrotrophic life style. *Style DeKalb IL* **2009**, *5*, 29–50, doi:10.1007/978-3-540-87407-2_2.
14. Barnes, W.J.; Anderson, C.T. Release, recycle, rebuild: cell-wall remodeling, autodegradation, and sugar salvage for new wall biosynthesis during plant development. *Mol. Plant* **2018**, *11*, 31–46, doi:10.1016/J.MOLP.2017.08.011.
15. De Lorenzo, G.; Ferrari, S. Polygalacturonase-inhibiting proteins in defense against phytopathogenic fungi. *Curr. Opin. Plant Biol.* **2002**, *5*, 295–299, doi:10.1016/S1369-5266(02)00271-6.
16. Gomathi, V.; Gnanamanickam, S.S. Polygalacturonase-inhibiting proteins in plant defence. *Current* **2004**, *87*, 1211–1217.
17. Kalunke, R.M.; Tundo, S.; Benedetti, M.; Cervone, F.; De Lorenzo, G.; D'Ovidio, R. An update on polygalacturonase-inhibiting protein (PGIP), a leucine-rich repeat protein that protects crop plants against pathogens. *Front. Plant Sci.* **2015**, *6*, 146, doi:10.3389/fpls.2015.00146.
18. Alexandersson, E.; Becker, J.V.W.; Jacobson, D.; Nguema-Ona, E.; Steyn, C.; Denby, K.J.; Vivier, M.A. Constitutive expression of a grapevine polygalacturonase-inhibiting protein affects gene expression and cell wall properties in uninfected tobacco. *BMC Res. Notes* **2011**, *4*, 493, doi:10.1186/1756-0500-4-493.
19. Joubert, D.A.; Kars, I.; Wagemakers, L.; Bergmann, C.; Kemp, G.; Vivier, M.A.; Van Kan, J.A.L. A polygalacturonase-inhibiting protein from grapevine reduces the symptoms of the endopolygalacturonase BcPG2 from *Botrytis cinerea* in *Nicotiana benthamiana* leaves without any evidence for in vitro interaction. *Mol. Plant-Microbe Interact.* **2007**, *20*, 392–402, doi:10.1094/MPMI-20-4-0392.
20. Federici, L.; Caprari, C.; Mattei, B.; Savino, C.; Di Matteo, A.; De Lorenzo, G.; Cervone, F.; Tsernoglou, D.; Staskawicz, B.J. Structural requirements of endopolygalacturonase for the interaction with PGIP (polygalacturonase- inhibiting protein). *Proc. Natl. Acad. Sci. USA* **2001**, *98*, 13425–13430, doi:10.1073/pnas.231473698.
21. Sicilia, F.; Fernandez-Recio, J.; Caprari, C.; De Lorenzo, G.; Tsernoglou, D.; Cervone, F.; Federici, L. The Polygalacturonase-inhibiting protein pgip2 of *Phaseolus vulgaris* has evolved a mixed mode of inhibition of endopolygalacturonase pg1 of *Botrytis cinerea* 1. *Plant Physiol.* **2005**, *139*, 1380–1388, doi:10.1104/pp.105.067546.
22. Liu, N.; Zhang, X.; Sun, Y.; Wang, P.; Li, X.; Pei, Y.; Li, F.; Hou, Y. Molecular evidence for the involvement of a polygalacturonase-inhibiting protein, GhPGIP1, in enhanced resistance to Verticillium and Fusarium wilts in cotton. *Sci. Rep.* **2017**, *7*, 39840, doi:10.1038/srep39840.
23. Liu, N.; Ma, X.; Zhou, S.; Wang, P.; Sun, Y.; Li, X.; Hou, Y. Molecular and functional characterization of a polygalacturonase-inhibiting protein from *Cynanchum komarovii* that confers fungal resistance in Arabidopsis. *PLoS ONE* **2016**, *11*, e0146959, doi:10.1371/journal.pone.0146959.
24. Joubert, D.A.; Slaughter, A.R.; Kemp, G.; Becker, J.V.W.; Krooshof, G.H.; Bergmann, C.; Benen, J.; Pretorius, I.S.; Vivier, M.A. The grapevine polygalacturonase-inhibiting protein (VvPGIP1) reduces *Botrytis cinerea*

susceptibility in transgenic tobacco and differentially inhibits fungal polygalacturonases. *Transgenic Res.* **2006**, *15*, 687–702, doi:10.1007/s11248-006-9019-1.

25. Spadoni, S.; Zabotina, O.; Di Matteo, A.; Dalgaard Mikkelsen, J.; Cervone, F.; De Lorenzo, G.; Mattei, B.; Bellincampi, D. Polygalacturonase-inhibiting protein interacts with pectin through a binding site formed by four clustered residues of arginine and lysine 1. *Plant Physiol.* **2006**, doi:10.1104/pp.106.076950.
26. D'Ovidio, R.; Mattei, B.; Roberti, S.; Bellincampi, D. Polygalacturonases, polygalacturonase-inhibiting proteins and pectic oligomers in plant-pathogen interactions. *Biochim. Biophys. Acta Proteins Proteom.* **2004**, *1696*, 237–244, doi:10.1016/j.bbapap.2003.08.012.
27. Davidsson, P.; Broberg, M.; Kariola, T.; Sipari, N.; Pirhonen, M.; Palva, E.T. Short oligogalacturonides induce pathogen resistance-associated gene expression in *Arabidopsis thaliana*. *BMC Plant Biol.* **2017**, *17*, 19, doi:10.1186/s12870-016-0959-1.
28. Benedetti, M.; Pontiggia, D.; Raggi, S.; Cheng, Z.; Scaloni, F.; Ferrari, S.; Ausubel, F.M.; Cervone, F.; De Lorenzo, G. Plant immunity triggered by engineered in vivo release of oligogalacturonides, damage-associated molecular patterns. *Proc. Natl. Acad. Sci. USA* **2015**, *112*, 5533–5538, doi:10.1073/pnas.1504154112.
29. Ferrari, S.; Savatin, D.V.; Sicilia, F.; Gramegna, G.; Cervone, F.; Lorenzo, G. De Oligogalacturonides: Plant damage-associated molecular patterns and regulators of growth and development. *Front. Plant Sci.* **2013**, *4*, 49, doi:10.3389/fpls.2013.00049.
30. Vorwerk, S.; Somerville, S.; Somerville, C. The role of plant cell wall polysaccharide composition in disease resistance. *Trends Plant Sci.* **2004**, *9*, 203–209, doi:10.1016/j.tplants.2004.02.005.
31. Voxeur, A.; Habrylo, O.; Guénin, S.; Miart, F.; Soulié, M.-C.; Rihouey, C.; Pau-Roblot, C.; Domon, J.-M.; Gutierrez, L.; Pelloux, J.; et al. Oligogalacturonide production upon *Arabidopsis thaliana-Botrytis cinerea* interaction. *Proc. Natl. Acad. Sci. USA* **2019**, *116*, 19743–19752, doi:10.1073/pnas.1900317116.
32. Joubert, D.A.; de Lorenzo, G.; Vivier, M.A. Regulation of the grapevine polygalacturonase-inhibiting protein encoding gene: Expression pattern, induction profile and promoter analysis. *J. Plant Res.* **2013**, *126*, 267–281, doi:10.1007/s10265-012-0515-5.
33. Mbewana, S. Functional Analysis of a lignin biosynthetic gene in transgenic tobacco. Master's Thesis, University of Stellenbosch, Stellenbosch, South Africa, 2010.
34. Nguema-Ona, E.; Moore, J.P.; Fagerström, A.D.; Fangel, J.U.; Willats, W.G.T.; Hugo, A.; Vivier, M.A. Overexpression of the grapevine PGIP1 in tobacco results in compositional changes in the leaf arabinoxyloglucan network in the absence of fungal infection. *BMC Plant Biol.* **2013**, *13*, 46, doi:10.1186/1471-2229-13-46.
35. Claverie, J.; Balacey, S.; Lemaître-Guillier, C.; Brulé, D.; Chiltz, A.; Granet, L.; Noirot, E.; Daire, X.; Darblade, B.; Héloir, M.-C.; et al. The cell wall-derived xyloglucan is a new damp triggering plant immunity in *Vitis vinifera* and *Arabidopsis thaliana*. *Front. Plant Sci.* **2018**, *9*, 1725, doi:10.3389/fpls.2018.01725.
36. Basson, C.E. Transcriptomic analysis of disease resistance responses using a tobacco-*Botrytis cinerea* pathosystem. Ph.D. Thesis, Stellenbosch University, Stellenbosch, South Africa, 2017.
37. Clough, S.J.; Bent, A.F. Floral dip: A simplified method for Agrobacterium-mediated transformation of *Arabidopsis thaliana*. *Plant J.* **1998**, *16*, 735–743.
38. Murashige, T.; Skoog, F. A revised medium for rapid growth and bio assays with tobacco tissue cultures. *Physiol. Plant.* **1962**, *15*, 473–497, doi:10.1111/j.1399-3054.1962.tb08052.x.
39. Nguema-Ona, E.; Moore, J.P.; Fagerström, A.; Fangel, J.U.; Willats, W.G.T.; Hugo, A.; Vivier, M.A. Profiling the main cell wall polysaccharides of tobacco leaves using high-throughput and fractionation techniques. *Carbohydr. Polym.* **2012**, *88*, 939–949, doi:10.1016/j.carbpol.2012.01.044.
40. Gerber, L.; Eliasson, M.; Trygg, J.; Moritz, T.; Sundberg, B. Multivariate curve resolution provides a high-throughput data processing pipeline for pyrolysis-gas chromatography/mass spectrometry. *J. Anal. Appl. Pyrolysis* **2012**, *95*, 95–100, doi:10.1016/j.jaap.2012.01.011.
41. York, W.S.; Darvill, A.G.; McNeil, M.; Stevenson, T.T.; Albersheim, P. Isolation and characterization of plant cell walls and cell wall components. *Methods Enzymol.* **1986**, *118*, 3–40.
42. Kračun, S.K.; Fangel, J.U.; Rydahl, M.G.; Pedersen, H.L.; Vidal-Melgosa, S.; Willats, W.G.T. Carbohydrate microarray technology applied to high-throughput mapping of plant cell wall glycans using comprehensive microarray polymer profiling (CoMPP). *Methods Mol. Biol. (Clifton NJ)* **2017**, *1503*, 147–165.
43. Knox, J.P.; Linstead, P.; King, J.; Cooper, C.; Roberts, K. Pectin esterification is spatially regulated both within cell walls and between developing tissues of root apices. *Planta* **1990**, *181*, 512–521, doi:10.1007/BF00193004.

44. Clausen, M.H.; Willats, W.G.T.; Knox, J.P. Synthetic methyl hexagalacturonate hapten inhibitors of anti-homogalacturonan monoclonal antibodies LM7, JIM5 and JIM7. *Carbohydr. Res.* **2003**, *338*, 1797–1800, doi:10.1016/S0008-6215(03)00272-6.
45. Verhertbruggen, Y.; Marcus, S.E.; Haeger, A.; Ordaz-Ortiz, J.J.; Knox, J.P. An extended set of monoclonal antibodies to pectic homogalacturonan. *Carbohydr. Res.* **2009**, *344*, 1858–1862, doi:10.1016/j.carres.2008.11.010.
46. Ralet, M.-C.; Tranquet, O.; Poulain, D.; Moïse, A.; Guillon, F. Monoclonal antibodies to rhamnogalacturonan I backbone. *Planta* **2010**, *231*, 1373–1383, doi:10.1007/s00425-010-1116-y.
47. Jones, L.; Seymour, G.B.; Knox, J.P. Localization of pectic galactan in tomato cell walls using a monoclonal antibody specific to (1→4)-[beta]-D-galactan. *Plant Physiol.* **1997**, *113*, 1405–1412, doi:10.1104/PP.113.4.1405.
48. Clausen, M.H.; Ralet, M.-C.; Willats, W.G.T.; McCartney, L.; Marcus, S.E.; Thibault, J.-F.; Knox, J.P. A monoclonal antibody to feruloylated-(1→4)-β-d-galactan. *Planta* **2004**, *219*, 1036–1041, doi:10.1007/s00425-004-1309-3.
49. Willats, W.G.T.; Marcus, S.E.; Knox, J.P. Generation of a monoclonal antibody specific to (1→5)-α-l-arabinan. *Carbohydr. Res.* **1998**, *308*, 149–152, doi:10.1016/S0008-6215(98)00070-6.
50. Verhertbruggen, Y.; Marcus, S.E.; Haeger, A.; Verhoef, R.; Schols, H.A.; McCleary, B.V.; McKee, L.; Gilbert, H.J.; Knox, J.P. Developmental complexity of arabinan polysaccharides and their processing in plant cell walls. *Plant J.* **2009**, *59*, 413–425, doi:10.1111/j.1365-313X.2009.03876.x.
51. Pedersen, H.L.; Fangel, J.U.; McCleary, B.; Ruzanski, C.; Rydahl, M.G.; Ralet, M.-C.; Farkas, V.; von Schantz, L.; Marcus, S.E.; Andersen, M.C.F.; et al. Versatile high resolution oligosaccharide microarrays for plant glycobiology and cell wall research. *J. Biol. Chem.* **2012**, *287*, 39429–39438, doi:10.1074/jbc.M112.396598.
52. Marcus, S.E.; Blake, A.W.; Benians, T.A.S.; Lee, K.J.D.; Poyser, C.; Donaldson, L.; Leroux, O.; Rogowski, A.; Petersen, H.L.; Boraston, A.; et al. Restricted access of proteins to mannan polysaccharides in intact plant cell walls. *Plant J.* **2010**, *64*, 191–203, doi:10.1111/j.1365-313X.2010.04319.x.
53. Meikle, P.J.; Bonig, I.; Hoogenraad, N.J.; Clarke, A.E.; Stone, B.A. The location of (1→3)-β-glucans in the walls of pollen tubes of *Nicotiana alata* using a (1→3)-β-glucan-specific monoclonal antibody. *Planta* **1991**, *185*, 1–8, doi:10.1007/BF00194507.
54. Marcus, S.E.; Verhertbruggen, Y.; Hervé, C.; Ordaz-Ortiz, J.J.; Farkas, V.; Pedersen, H.L.; Willats, W.G.T.; Knox, J.P. Pectic homogalacturonan masks abundant sets of xyloglucan epitopes in plant cell walls. *BMC Plant Biol.* **2008**, *8*, 60, doi:10.1186/1471-2229-8-60.
55. McCartney, L.; Marcus, S.E.; Knox, J.P. Monoclonal antibodies to plant cell wall xylans and arabinoxylans. *J. Histochem. Cytochem.* **2005**, *53*, 543–546, doi:10.1369/jhc.4B6578.2005.
56. Tormo, J.; Lamed, R.; Chirino, A.J.; Morag, E.; Bayer, E.A.; Shoham, Y.; Steitz, T.A. Crystal structure of a bacterial family-III cellulose-binding domain: A general mechanism for attachment to cellulose. *EMBO J.* **1996**, *15*, 5739–5751, doi:10.1002/j.1460-2075.1996.tb00960.x.
57. Smallwood, M.; Martin, H.; Knox, J.P. An epitope of rice threonine- and hydroxyproline-rich glycoprotein is common to cell wall and hydrophobic plasma-membrane glycoproteins. *Planta* **1995**, *196*, 510–522, doi:10.1007/BF00203651.
58. Smallwood, M.; Beven, A.; Donovan, N.; Neill, S.J.; Peart, J.; Roberts, K.; Knox, J.P. Localization of cell wall proteins in relation to the developmental anatomy of the carrot root apex. *Plant J.* **1994**, *5*, 237–246, doi:10.1046/j.1365-313X.1994.05020237.x.
59. Knox, J.P.; Peart, J.; Neill, S. Identification of novel cell surface epitopes using a leaf epidermal-strip assay system. *Planta* **1995**, *196*, doi:10.1007/BF00201383.
60. Knox, J.P.; Day, S.; Roberts, K. A set of cell surface glycoproteins forms an early position, but not cell type, in the root apical carota L. *Development* **1989**, *106*.
61. Yates, E.A.; Valdor, J.-F.; Haslam, S.M.; Morris, H.R.; Dell, A.; Mackie, W.; Knox, J.P. Characterization of carbohydrate structural features recognized by anti-arabinogalactan-protein monoclonal antibodies. *Glycobiology* **1996**, *6*, 131–139, doi:10.1093/glycob/6.2.131.
62. McCabe, P.F.; Valentine, T.A.; Forsberg, L.S.; Pennell, R.I. Soluble signals from cells identified at the cell wall establish a developmental pathway in carrot. *Plant Cell* **1997**, *9*, 2225–2241, doi:10.1105/tpc.9.12.2225.
63. Knox, J.P.; Linstead, P..; Cooper, J.P.C.; Roberts, K. Developmentally regulated epitopes of cell surface arabinogalactan proteins and their relation to root tissue pattern formation. *Plant J.* **1991**, *1*, 317–326, doi:10.1046/j.1365-313X.1991.t01-9-00999.x.

64. Moller, I.; Marcus, S.E.; Haeger, A.; Verhertbruggen, Y.; Verhoef, R.; Schols, H.; Ulvskov, P.; Mikkelsen, J.D.; Knox, J.P.; Willats, W. High-throughput screening of monoclonal antibodies against plant cell wall glycans by hierarchical clustering of their carbohydrate microarray binding profiles. *Glycoconj. J.* **2008**, *25*, 37–48, doi:10.1007/s10719-007-9059-7.
65. Smallwood, M.; Yates, E.A.; Willats, W.G.T.; Martin, H.; Knox, J.P. Immunochemical comparison of membrane-associated and secreted arabinogalactan-proteins in rice and carrot. *Planta* **1996**, *198*, 452–459, doi:10.1007/BF00620063.
66. Yoon, J.; Choi, H.; An, G. Roles of lignin biosynthesis and regulatory genes in plant development. *J. Integr. Plant Biol.* **2015**, *57*, 902–912, doi:10.1111/jipb.12422.
67. Ma, Q.-H. Functional analysis of a cinnamyl alcohol dehydrogenase involved in lignin biosynthesis in wheat. *J. Exp. Bot.* **2010**, *61*, 2735–2744, doi:10.1093/jxb/erq107.
68. Ma, Q.-H.; Zhu, H.-H.; Qiao, M.-Y. Contribution of both lignin content and sinapyl monomer to disease resistance in tobacco. *Plant Pathol.* **2018**, *67*, 642–650, doi:10.1111/ppa.12767.
69. Menden, B.; Kohlhoff, M.; Moerschbacher, B.M. Wheat cells accumulate a syringyl-rich lignin during the hypersensitive resistance response. *Phytochemistry* **2007**, *68*, 513–520, doi:10.1016/J.PHYTOCHEM.2006.11.011.
70. Cesarino, I. Structural features and regulation of lignin deposited upon biotic and abiotic stresses. *Curr. Opin. Biotechnol.* **2019**, *56*, 209–214, doi:10.1016/J.COPBIO.2018.12.012.
71. Brummell, D.A. Cell wall disassembly in ripening fruit. *Funct. Plant Biol.* **2006**, *33*, 103, doi:10.1071/FP05234.
72. Willats, W.G.T.; Steele-King, C.G.; Marcus, S.E.; Knox, J.P. Side chains of pectic polysaccharides are regulated in relation to cell proliferation and cell differentiation. *Plant J.* **1999**, *20*, 619–628, doi:10.1046/j.1365-313X.1999.00629.x.
73. Zykwinska, A.W.; Ralet, M.-C.J.; Garnier, C.D.; Thibault, J.-F. Evidence for *in vitro* binding of pectin side chains to cellulose. *Plant Physiol.* **2005**, *139*, 397–407, doi:10.1104/pp.105.065912.
74. Zykwinska, A.; Thibault, J.-F.; Ralet, M.-C. Organization of pectic arabinan and galactan side chains in association with cellulose microfibrils in primary cell walls and related models envisaged. *J. Exp. Bot.* **2007**, *58*, 1795–1802, doi:10.1093/jxb/erm037.
75. Park, Y.B.; Cosgrove, D.J. Xyloglucan and its interactions with other components of the growing cell wall. *Plant Cell Physiol.* **2015**, *56*, 180–194, doi:10.1093/pcp/pcu204.
76. Cosgrove, D.J.; Jarvis, M.C. Comparative structure and biomechanics of plant primary and secondary cell walls. *Front. Plant Sci.* **2012**, *3*, 204, doi:10.3389/fpls.2012.00204.
77. Nishitani, K.; Demura, T. Editorial: An emerging view of plant cell walls as an apoplastic intelligent system. *Plant Cell Physiol.* **2015**, *56*, 177–179, doi:10.1093/pcp/pcv001.
78. Park, Y.B.; Cosgrove, D.J. A revised architecture of primary cell walls based on biomechanical changes induced by substrate-specific endoglucanases. *Plant Physiol.* **2012**, *158*, 1933–1943, doi:10.1104/pp.111.192880.
79. Volpi, C.; Janni, M.; Lionetti, V.; Bellincampi, D.; Favaron, F.; D'Ovidio, R. The ectopic expression of a pectin methyl esterase inhibitor increases pectin methyl esterification and limits fungal diseases in wheat. *Mol. Plant. Microbe. Interact.* **2011**, *24*, 1012–1019, doi:10.1094/MPMI-01-11-0021.
80. Lionetti, V.; Cervone, F.; Bellincampi, D. Methyl esterification of pectin plays a role during plant-pathogen interactions and affects plant resistance to diseases. *J. Plant Physiol.* **2012**, *169*, 1623–1630, doi:10.1016/j.jplph.2012.05.006.
81. Micheli, F. Pectin methylesterases: cell wall enzymes with important roles in plant physiology. *Trends Plant Sci.* **2001**, *6*, 414–419, doi:10.1016/S1360-1385(01)02045-3.
82. Pelloux, J.; Rustérucci, C.; Mellerowicz, E.J. New insights into pectin methylesterase structure and function. *Trends Plant Sci.* **2007**, *12*, 267–277, doi:10.1016/j.tplants.2007.04.001.
83. Cabrera, J.C.; Boland, A.; Messiaen, J.; Cambier, P.; Van Cutsem, P. Egg box conformation of oligogalacturonides: The time-dependent stabilization of the elicitor-active conformation increases its biological activity. *Glycobiology* **2008**, *18*, 473–482, doi:10.1093/glycob/cwn027.
84. Hocq, L.; Pelloux, J.; Lefebvre, V. Connecting homogalacturonan-type pectin remodeling to acid growth. *Trends Plant Sci.* **2017**, *22*, 20–29, doi:10.1016/j.tplants.2016.10.009.
85. Deepak, S.; Shailasree, S.; Kini, R.K.; Muck, A.; Mithöfer, A.; Shetty, S.H. Hydroxyproline-rich glycoproteins and plant defence. *J. Phytopathol.* **2010**, *158*, 585–593, doi:10.1111/j.1439-0434.2010.01669.x.

86. Showalter, A.M. Structure and function of plant cell wall proteins. *Plant Cell* **1993**, *5*, 9–23, doi:10.1105/tpc.5.1.9.
87. Boudart, G.; Dechamp-Guillaume, G.; Lafitte, C.; Ricart, G.; Barthe, J.-P.; Mazau, D.; Esquerré-Tugayé, M.T. Elicitors and suppressors of hydroxyproline-rich glycoprotein accumulation are solubilized from plant cell walls by endopolygalacturonase. *Eur. J. Biochem.* **1995**, *232*, 449–457, doi:10.1111/j.1432-1033.1995.449zz.x.
88. Cassab, G.I. Plant cell wall proteins. *Annu. Rev. Plant Physiol. Plant Mol. Biol.* **1998**, *49*, 281–309, doi:10.1146/annurev.arplant.49.1.281.
89. Showalter, A.M. Arabinogalactan-proteins: structure, expression and function. *Cell. Mol. Life Sci.* **2001**, *58*, 1399–1417, doi:1420-682X/01/101399-19.
90. Ellis, M.; Egelund, J.; Schultz, C.J.; Bacic, A. Arabinogalactan-proteins: key regulators at the cell surface? *Plant Physiol.* **2010**, *153*, 403–419, doi:10.1104/pp.110.156000.
91. Mareri, L.; Romi, M.; Cai, G. Arabinogalactan proteins: actors or spectators during abiotic and biotic stress in plants? *Plant Biosyst.* **2018**, 1–13, doi:10.1080/11263504.2018.1473525.
92. Nguema-Ona, E.; Vicré-Gibouin, M.; Cannesan, M.A.; Driouich, A. Arabinogalactan proteins in root-microbe interactions. *Trends Plant Sci.* **2013**, *18*, 1360–1385, doi:10.1016/j.tplants.2013.03.006.
93. Cannesan, M.A.; Durand, C.; Burel, C.; Gangneux, C.; Lerouge, P.; Ishii, T.; Laval, K.; Follet-Gueye, M.-L.; Driouich, A.; Vicré-Gibouin, M. Effect of arabinogalactan proteins from the root caps of pea and *Brassica napus* on *Aphanomyces euteiches* zoospore chemotaxis and germination. *Plant Physiol.* **2012**, *159*, 1658–1670, doi:10.1104/pp.112.198507.

Chapter 4

Research chapter 2

VviPGIP1 transgenic tobacco leaves infected by *Botrytis cinerea* results in localised pectin degradation as well as AGP and extensin reorganisation at the lesion site

Chapter 4

VviPGIP1 transgenic tobacco leaves infected by *Botrytis cinerea* results in localised pectin degradation as well as AGP and extensin reorganisation at the lesion site

Florent Weiller [1,4], Jonatan U. Fangel [2#], William G.T. Willats [3], Azeddine Driouich [4], Melané A. Vivier [1], John P. Moore [1*]

[1] *South African Grape and Wine Research Institute, Department of Viticulture and Oenology, Stellenbosch University, South Africa*; FW: florent@sun.ac.za; MAV: mav@sun.ac.za; JPM: moorejp@sun.ac.za

[2] *Department of Plant and Environmental Sciences, University of Copenhagen, Copenhagen, Denmark*; JUF: jonatanfangel@gmail.com

[3] *School of Agriculture, Food and Rural Development, Newcastle University, Newcastle-upon-Tyne, United Kingdom*; WW: william.willats@newcastle.ac.uk

[4] *Université de ROUEN Normandie, Laboratoire de Glycobiologie et Matrice Extracellulaire Végétale, UPRES-EA 4358, Fédération de Recherche « Normandie-Végétal » - FED 4277, F-76821 Mont-Saint-Aignan, France;* AD : Azeddine.Driouich@univ-rouen.fr

#Present Address: Novozymes, Copenhagen, Denmark

*Correspondence: moorejp@sun.ac.za ; +27 21 808 2733

Simple Summary:

Polygalacturonase inhibiting proteins (PGIP) have been shown to be involved in plant resistance to pathogens. When grapevine PGIP1 is overexpressed in tobacco, an increased resistance phenotype against *Botrytis cinerea* is evident. By analysing the transgenic plant cell wall composition during fungal infection, possible cell wall changes involved in the acquired resistance phenotype were evaluated. The expected de-pectination due to fungal enzymes was confirmed, but modification in the cell wall glycoprotein fraction, with increased availability of extensins and arabinogalactan protein (AGPs) compared to the wild-type control confirmed cell wall changes as part of the resistance phenotype of the *VviPGIP1* expressing transgenic lines.

1. Abstract

The necrotrophic fungus *Botrytis cinerea* macerates host tissues with a range of secreted enzymes and is responsible for disease damage on a wide variety of fruit crop species. Expressing the *Vitis vinifera* polygalacturonase inhibiting protein 1 (VviPGIP1) in *Nicotiana tabacum* has been linked to reduced susceptibility to *B. cinerea.* Uninfected VviPGIP1 transgenic tobacco display cell wall modifications in advance of any infection. These cell wall changes include; altered stem lignin

content, reorganisation of leaf xyloglucan composition, pectin methylesterification modifications, as well as extensin and arabinogalactan protein (AGP) changes. These results suggested that cell wall changes may prime the plant in preparation for defence. The aim of this study was to extend the previous studies of pre-infection cell wall analysis and now track cell wall changes using comprehensive microarray polymer profiling (CoMPP) in wild type and VviPGIP1 transgenic lines both undergoing infection with inoculated *B. cinerea.* The analyses focused on the first 72 hours post infection (hpi) time frame, since it is known to be critical for *Botrytis* infection initiation and plant response. In addition to CoMPP, monosaccharide analysis using Gas chromatography – Mass spectometry (GC-MS) was performed. Visual inspection of lesions was supplemented with scanning electron microscopy (SEM) to describe the infection progression. Cell wall analysis was performed on tissue from the lesion site (local response), but also in adjacent tissues and uninfected leaves (distal/systemic responses). During *B. cinerea* infection, all lines showed tissue maceration with fungal enzymes breaking-down the homogalacturonan (HG) layers, exposing the rhamnogalacturonan I (RG-I) backbones of the leaf pectins in all lines. A common pattern revealing an increase in extensins and AGPs was observed in tissues from the lesion site (local response) as well as from systemic leaves at 72 hpi in the transgenic lines compared to the control SR1 plants, consistent with a primed state.

Keywords:

cell wall, *Botrytis cinerea*, pectin, extensin, arabinogalactan protein, PGIP1, tobacco

2. Introduction

The cell wall is an essential structure in plant growth and development as it provides mechanical strength for support and forms an effective physico-chemical barrier to stop pathogen penetration (Malinovsky *et al.* 2014; Höfte and Voxeur 2017). Indeed, plants are constantly challenged by a wide range of pathogens. Many plant cell wall properties and defence mechanisms have been investigated by generating transgenic plants that either silence or over-express cell wall related genes; see review by Bacete *et al.* (2018) with a focus on *Arabidopsis thaliana*. These genetic studies have investigated the role of cell wall alterations during pathogen infection as well as defence

stimulation by elicitors. Use of screening systems by measuring plant hormone levels, callose deposition, lignin and other biochemical markers is common. Such an approach was performed by Van der Does *et al.* (2017) where the authors showed that the *A. thaliana* leucine-rich repeat receptor kinase MIK2 was involved in sensing biotic and abiotic stressors and in so doing activating stress response pathways. Immunofluorescence staining has also been used to compare cell wall compositional changes during infection with root-knot nematodes, focusing on changes in cell wall polysaccharides observed for *Arabidopsis*, maize and Azuki bean plants (Bozbuga *et al.* 2018). A range of transcriptomic, proteomic and metabolomic approaches have also been employed to decipher plant-pathogen interactions and identify pathogen and/or plant effectors that are essential for virulence (Plett and Martin 2018). From a molecular perspective identifying the regulatory network is important; as an example, the transcription factor WRKY33 was shown to be important in activating defence pathways against *B. cinerea* in *A. thaliana* (Sham *et al.* 2017).

B. cinerea (grey rot) is one of the most serious plant pathogens, as it occurs worldwide and can infect more than 1000 different species of host plants (Elad *et al.* 2015). Recent studies suggest that *B. cinerea* might be fairly ubiquitous, but asymptomatic in many organisms, or during most of the hosts life cycle, waiting for favourable conditions in the form of an endophyte (Sowley *et al.* 2009; van Kan *et al.* 2014). In addition to its necrotrophic nature, *B. cinerea* seems to have a short-lived biotrophic stage during early infection on hosts (roughly the first 36 hours post infection (hpi), before lesion spread occurs, as described by Eizner et al. (2017)) (Veloso and van Kan 2018).

The capacity of *B. cinerea* to infect the host organism depends on the molecular dialogue between pathogen and plant. For example, a knockout mutant for the BcExo70 subunit of the exocyst complex, greatly impacted fungal development and pathogenicity (Guan *et al.* 2019). *B. cinerea* also secretes numerous secondary metabolites involved in pathogenicity such as terpenes, abscisic acid, carotenoids and polyketides, including botrydial and botcinic acid which have been recently highlighted (Collado and Viaud 2016). Some *Botrytis* species do display a narrow host range (Valero-Jiménez *et al.* 2019), but *B. cinerea* is a very wide ranging adaptive pathogen. Comparative studies on wild and domesticated tomato using 97 different *B. cinerea* isolates (genetically different) showed the fungal capacity to develop a wide variety of infection strategies, with a highly polygenic virulence

response, shown with single-nucleotide polymorphisms analysis, which suggested that the fungal isolates customise their virulence level depending on the host (Breeze 2019; Soltis *et al.* 2019).

Fungal pathogens have developed a range of strategies to breach the plant cell wall. Many fungi are opportunistic and penetrate host plants through stomata and/or wounds. Some develop an appressorium which creates physical pressure differentials in order to breach the cell wall (Howard and Valent 1996; Mendgen and Hahn 2002; Ryder and Talbot 2015). Necrotrophic fungi develop an appressorium-like structure that further secretes cell wall degrading enzymes (CWDEs) into the plant cell wall regions. These CWDEs break down the cell wall polysaccharides in order to penetrate and colonise their host plant (Prins *et al.* 2000; van Kan 2006). In the apoplast, fungal effectors can have a dual action, for example, fungal enzymes perform their primary enzymatic functions, but have also been shown to trigger plant defence responses such as apoptosis as is the case for BcXYG1, a xyloglucanase (Zhu *et al.* 2017). In order to degrade cell walls and form necrotic lesions, *B. cinerea* secretes a wide range of pectinolytic enzymes, including endo-polygalacturonases (ePGs), pectate lyases and pectin methyl esterases (Tudzynski and Kokkelink 2009). The ePGs, in particular, have been shown to be essential for *B. cinerea* virulence (ten Have *et al.* 1998, 2002; Wubben *et al.* 2000; Ten Have *et al.* 2001; Kars *et al.* 2005). They hydrolyse the de-esterified polygalacturonic acid (PGA) stretches of the homogalacturonan (HG) network, one of the major pectin components of the cell wall (Jayani *et al.* 2005). The pectinolytic fungal enzyme action that degrades the host plant cell wall has been shown to release oligogalacturonides (OG) of various lengths into the apoplast. Oligogalacturonides participate in the plant pathogen dialogue, they are perceived as Damage-Associated Molecular Patterns (DAMPs) that trigger the stimulation of defence response mechanisms including the hypersensitive response (HR) with the secretion of reactive oxygen species (ROS) or the production of pathogenesis-related proteins (Esquerré-Tugayé *et al.* 2000; Vorwerk *et al.* 2004; Ferrari *et al.* 2013; Benedetti *et al.* 2015). The HR is an efficient response against biotrophic fungi as it kills plant cells around the infection area to limit fungal development, but the same response benefits the necrotrophic fungi which have been shown to trigger or enhance it (Govrin and Levine 2000; Rossi *et al.* 2017). Necrotrophic pathogens, such as *B. cinerea*, are able to feed and develop on dead tissue and so are not impeded, but rather aided by the HR during infection.

Early detection of the pathogen so as to trigger the plant defence system has been shown to be crucial for effective resistance responses. Recognition of Microbe-Associated Molecular Patterns (MAMPs), conserved molecules from the pathogen and DAMPs, degradation products endogenous to the plant (Gust *et al.* 2017; Saijo *et al.* 2018; Harris *et al.* 2020), are recognised by pattern recognition receptors (PRRs) and lead to the activation of the MAMP-triggered immunity (MTI) (Heil and Land 2014; De Lorenzo *et al.* 2018; Saijo and Loo 2020). Most PRRs are receptor kinases, plasma membranes proteins with an extracellular receptor domain and a cytoplasmic kinase domain which induce a signal phosphorylation cascade, that leads to activation of plant defence genes (Trdá *et al.* 2015; Li *et al.* 2016; Wolf 2017). In contrast, MTI, is a non-specific defence response, commonly associated with callose deposition, lignification and production of ROS (Toruño *et al.* 2016). There is also effector-triggered immunity which involves intracellular receptors that recognise pathogen effectors and then triggers a strong response (e.g. HR) at the infection zone area and then systemically spread to other parts of the plant (Cui *et al.* 2015; Peng *et al.* 2018). Much of the plant-pathogen communication at the infection site is mediated by hormones such as jasmonic acid and salicylic acid which leads to differential gene expression pathways in the host and fungal systems respectively (Zhang *et al.* 2017).

To protect the plant against CWDEs, plants can reorganise their cell wall matrix to make it more resistant to degradation. As an example, inactivation of the *reduced wall acetylation2* gene in *A. thaliana* lead to ca. 20% decrease in cell wall polysaccharide acetylation compared to the wild type with the mutant plant showing an increased resistance to *B. cinerea* (Manabe *et al.* 2011). In contrast, mutation of the endogenous *A. thaliana* PME inhibitor (PMEi) genes *pmei10*, *pmei11*, and *pmei12* which encode proteins that regulate pectin methylesterification have been linked to increased susceptibility to pathogenic fungi (Lionetti *et al.* 2017). To inhibit fungal ePGs, some plants produce polygalacturonases-inhibiting proteins (PGIPs) (De Lorenzo and Ferrari 2002; Gomathi and Gnanamanickam 2004). These PGIPs are conserved leucine rich repeat proteins (Di Matteo *et al.* 2003, 2006) that are able to inhibit fungal ePG activity (Joubert *et al.* 2007; Liu *et al.* 2017). Site directed mutagenesis studies (Federici *et al.* 2001; Benedetti *et al.* 2013) and work on PGIP2 from *Phaseolus vulgaris* against polygalacturonase 1 (PG1) from *Fusarium moniliform* (Sicilia *et al.* 2005) showed a mixed mode of inhibition occurring. Furthermore, a PGIP from *P. vulgaris* displayed the

ability to bind to pectin and limit ePG access (Spadoni *et al.* 2006). PGIPs have also been shown to stimulate the production of OGs that can then act as DAMPs triggering plant defence responses downstream (D'Ovidio *et al.* 2004; Benedetti *et al.* 2015; Davidsson *et al.* 2017).

Characterisation of the *VviPGIP1* gene isolated from grapevine (*Vitis vinifera*) has indicated multiple functions and molecular roles in disease resistance. Expression of the grapevine PGIP1 in tobacco plants results in enhanced resistance against *B. cinerea* infection (Joubert *et al.* 2006). Transgenic PGIP1 tobacco plants display altered hormonal levels compared to wild type plants, particularly in jasmonic acid levels (Alexandersson *et al.* 2011; Basson 2017). Even in the absence of infection, the PGIP1 plants also displayed upregulated cinnamyl alcohol dehydrogenase (CAD) activity with increased lignin staining of stems and downregulation of xyloglucan endotransglucosylase (XET) /xyloglucan endotransglucosylase/hydrolase (XTH) enzyme levels in leaves (Alexandersson *et al.* 2011; Joubert *et al.* 2013). The VviPGIP1 transgenic plants most notably have an altered arabinoxyloglucan content which is correlated with a tighter, more resistant leaf cell wall composition (Nguema-Ona, Moore, *et al.* 2013). Current knowledge is very scarce on plant cell wall polysaccharides and matrix modifications during necrotrophic fungi attacks. The VViPGIP1 plants, known to have enhanced resistance to Botrytis infection will serve as a model pathosystem to describe and compare plant cell wall degradation and/or reorganisation during fungal infection with the susceptible controls.

In this study two VviPGIP1 tobacco lines were subjected to whole plant infections with *B. cinerea* (a hypervirulent grape strain) and followed over a 72 hour time course. In addition to visual inspection, scanning electron microscopy (SEM) was used to characterise the infection progression, comparing wild type to transgenic lines. Furthermore, leaf cell wall composition was also performed using comprehensive microarray polymer profiling (CoMPP) and monosaccharide profiles using Gas chromatography – Mass spectometry (GC-MS). This was performed on local lesion sites as well as on adjacent tissue (to the lesion) of the infected leaf as well as on systemic uninfected leaves on each of the experimental plants. This surveying approach appeared most suitable to 'track' the changes in polymer abundance and turnover during the *B. cinerea* infection progression.

3. Materials and Methods

3.1. Plant material and growth conditions

Plant material consisted of the control tobacco (wild type *Nicotiana tabacum cv Havana Petit* SR1) and two VviPGIP1 transgenic lines, namely 37 and 45 (see Joubert et al, 2006 for more details). Seeds were germinated on Murashige and Skoog media (Murashige and Skoog 1962) with (transgenic) and without (SR1) kanamycin selection. Seedlings were first grown in peat plugs (Jiffy Products International AS, Norway) and then transferred to pots with a final mixture of soil, peat moss and vermiculite. Growth room temperature was kept at 25 °C, under artificial lights with a 16 hour light to 8 hour dark photoperiod. Organic fertilizer (Nitrosol, Fleuron (Pty) Ltd, South Africa) was added during watering once every two weeks. Plant infection experiments were conducted on plants with six fully expanded leaves. The youngest leaf, L1, being the smallest, close to the shoot apical meristem and the L6 being the oldest fully expanded leaf (see Figure 4.1A for a representative plant).

3.2. *Botrytis cinerea* sporulation and culturing

B. cinerea spores previously isolated from a South African vineyard and the strain described as hypervirulent in Joubert *et al.* (2006) and more extensively characterised by Atwell *et al.* (2015) were used for infection experiments. *B. cinerea* stock cultures were grown on sterile apricot halves (Naturlite, Tiger Food Brands Limited, South Africa) kept in the dark for two weeks at 23 °C to induce sporulation. Spores were harvested with sterile water and filtered through glass wool filled tips to remove the hyphae and other cell debris. Prior to infection, the spores were hydrated overnight in water at 4 °C and their concentration calculated with a haemocytometer. Spore viability was assessed by placing a few drops of spore mixtures on 1 % (w/v) water agar plate and calculating the percentage germination after 12 h at 23 °C.

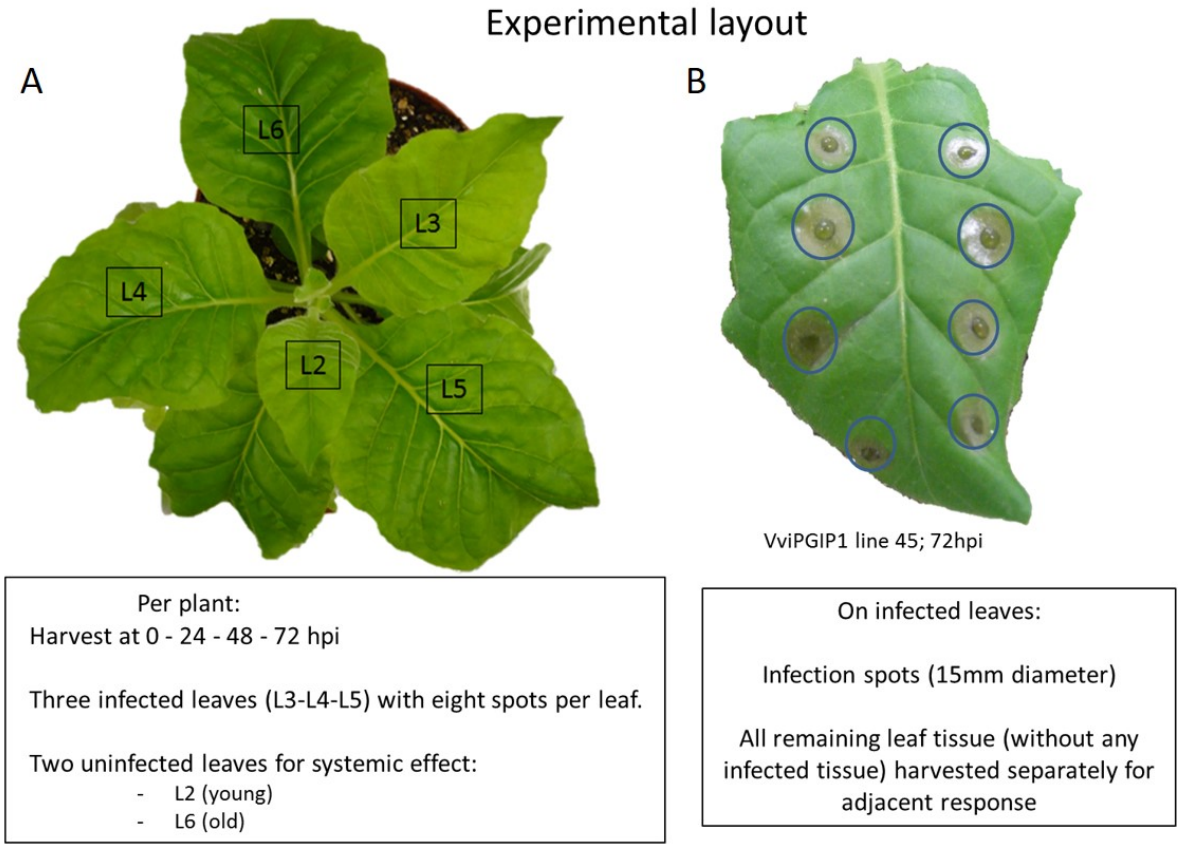

Figure 4.1: A: Photograph of a typical tobacco plant used for the study to indicate leaf positions harvested (indicated in the black boxes). Out of the eight leaves on the plant at the time of the experiment, leaf 2 was the youngest harvested one, close to the apical meristem and leaves 4 – 6 fully expanded leaves. Leaves one, seven and eight were not harvested. **B**: Photograph of an infected leave 72 hpi. For analysis, tissue inside the blue circles (15 mm diameter) represent the lesions and are harvested separately from the rest of the leaf that represent adjacent tissue.

3.3. Plant infection experiments and sampling during the infection process

Fully expanded tobacco plants were transferred to infection chambers 24 h before the start of the infection to acclimate them (as before 25 °C, under artificial lights with a 16 hour light to 8 hour dark period were used). However, the chamber was kept at 100 % humidity. The day before an infection experiment, spores were harvested as described previously and re-suspended in filtered 50 % grape juice solution (Liqui-Fruit Red Grape Juice) at a 1 x 10^6 spores/mL concentration. Eight spots of 5 µL (equivalent to a total of 5000 spores) were deposited on the adaxial side of each L3, L4 and L5 tobacco leaf, (see Figure 4.1).

To follow the plant infection process, a time course experiment was established and samples were harvested at different times: 0, 24, 48 and 72 hpi. To track local lesion development, samples

were generated from leaves L3, L4 and L5. Leaf disks of 15 mm in diameter around the infection spots were isolated using a cork borer and processed separately from the remaining leaf tissue. The remaining infected L3, L4 and L5 leaf tissue were labelled and processed as the 'adjacent response' tissue. The uninfected leaves (L)2 and (L)6 were also harvested to track distal (systemic) response to the fungus infection. For each line and time point, samples from four individual plants (biological repeats) were harvested and their respective disks and leaves pooled together according to their leaf position. Four plants (per line/control) were mock inoculated (using water and grape juice) and harvested at 72 hpi in addition to uninfected plants. The whole infection experiment was performed three times and showed consistent results.

3.4. Scanning electron microscopy

Infection progression was tracked using a Leo® 1430VP Scanning Electron Microscope (Central Analytical Facility, Stellenbosch University). Images were taken at 24, 48, 72 and 96 hpi with *B. cinerea* spore suspension. Prior to imaging; leaf tissue was cut and carefully mounted on aluminium stubs, centring on the infection spots, using double sided carbon tape for adherence. Beam conditions during imaging were 7 kV at approximately 1.5 nA resolution. For each time point, two lesions and a healthy area from a single leaf were observed for each cultivar.

3.5. Cell wall isolation protocol

Alcohol insoluble residue (AIR) was prepared from tobacco leaves as outlined in Nguema-Ona et al. (2012). Leaf material was frozen using liquid nitrogen and ground to a powder with a Retsch Mixer Mill (Retsch, Haan, Germany) set at 30 rounds per minute for 60 seconds. Powder was boiled in 80 % aqueous ethanol for 20 min. Insoluble material was washed with methanol for two hours on a rotating wheel. The pellets were sequentially washed twice with a (1:1) methanol/chloroform solution for 2 h then rinsed with acetone for another 2 h and air dried. The extracted material was re-suspended in water and freeze-dried to obtain cell wall AIR which was used as material for all further analytical experiments. All solvents used were from (Sigma-Aldrich, MO, USA) at reagent grade.

3.6. Gas chromatography – mass spectrometry for monosaccharides

Monosaccharide analysis using GC-MS was performed according to York et al. (1986) (York *et al.* 1986) with some modifications. Hydrolysis of AIR was performed using 2 M Trifluoroacetic acid (TFA) incubated at 110°C for 2 h. Sequential derivatization was performed first; 80°C for 16 h using 1 M methanolic HCl; and thereafter; 20 min with a Hexamethyldisilazane (HMDS) + Trimethylsilyl chloride (TMCS) + Pyridine (3:1:9) (Sylon HTP) kit (Sigma-Aldrich, MO, USA). Silylation was performed at 80 °C. Trimethyl-silyl-glycosides were then dissolved in cyclohexane prior to injection into the GC-MS system. A gas chromatograph Agilent 6890 N (Agilent, Palo Alto, CA) coupled to an Agilent 5975 MS mass spectrometer detector was used for analysis. A polar (95 % dimethylpolysiloxane) ZB-Semivolatiles Guardian (30 m, 0.25 mm ID, 0.25 µm film thickness) part number 7HG-G027-11 GC column was used. Arabinose (Ara), rhamnose (Rha), fucose (Fuc), xylose (Xyl), mannose (Man), galacturonic acid (GalA), galactose (Gal), glucose (Glc) and glucuronic acid (GlcA) were quantified using standards (from Sigma-Aldrich, MO, USA). The software Xcalibur (Thermo Fisher Scientific Inc., MA, USA) was used for integration and quantitation. Results are expressed in mg/g of AIR and statistical significance was calculated with an ANOVA (P=0.05).

3.7. Comprehensive microarray polymer profiling for polysaccharides-proteins

Comprehensive microarray polymer profiling (see (Moller *et al.* 2007)) on tobacco AIR was performed as described in Nguema-Ona et al. (2012) (Nguema-Ona *et al.* 2012). 300 µL of cyclohexane diamine tetra acetic acid (CDTA) which mainly extracts pectins was added to 10 mg of AIR and shaken 2 h at 60°C. 300 µl NaOH (4 M + 0.1 % $NaBH_4$), which mainly extracts hemicelluloses, was added to the pellet and shaken another 2 h. CDTA and NaOH fractions were printed onto nitrocellulose membranes (Whatman, pore size 0.45 mm Whatman) using a microarray printer (Sprint, Arrayjet, Roslin, UK), with two replicates and four dilution each per sample. A set of monoclonal antibodies (mAbs) and carbohydrate binding modules (CBMs) were used to probe the printed arrays (see Table 4.1 for the detailed list of antibodies and associated references). Arrays were developed and quantified using a flatbed scanner and results presented as semi-quantitative heatmaps. The highest value was set at 100 and all other values normalised accordingly. A cut off of 5 was applied at the lower end.

3.8. Statistical and multivariate data analysis

Each sample represented four leaves at the same developmental stage, taken from different plants and pooled together before processing. Thus for all experiments, at least 12 plants were tested for each genotype. The changes observed in the data obtained from the various analysis were analysed for statistical significance using univariate statistical analysis software tools (Statistica 10, Statsoft Southern Africa Analytics, Sandton, South Africa). Multivariate analysis such as principal component analysis (PCA) was performed with the SIMCA 14 software package (Sartorium Stedim Biotech - Umetrics AB, Umea, Sweden).

Table 4.1: List of mAbs and CBMs used for the CoMPP analysis. DE: Degree of esterification; ME: Methylesterification.

Homogalacturonan		low DE	JIM5	Knox *et al.* 1990; Clausen *et al.* 2003
		high DE	JIM7	
		Partially ME	LM18	Verhertbruggen *et al.* 2009a
		Partially ME	LM19	
		Partially ME	LM20	
		HG in “egg-box” motif	2F4	Liners *et al.* 1989
		Xylogalacturonan	LM8	Willats *et al.* 2004
RG-I associated		Backbone of RG-I	INRA-RU1	
		Backbone of RG-I	INRA-RU2	Ralet *et al.* 2010
		D-galactan	LM5	Jones *et al.* 1997
		L-arabinan	LM6	Willats *et al.* 1998
		Linearised L-arabinan	LM13	Verhertbruggen *et al.* 2009b
	Mannan	(galacto)(gluco)mannan	LM21	Marcus *et al.* 2010
		D-(gluco)mannan	LM22	
	Glucan	β-D-glucan	BS-400-2	Meikle *et al.* 1991
	Xyloglucan	Xyloglucan backbone (XXXG motif)	LM15	Marcus *et al.* 2008
		Xyloglucan	LM25	Pedersen *et al.* 2012
	Xylan	β-D-xylan	LM10	McCartney *et al.* 2005
		β-D-xylan/arabinoxylan	LM11	
Cellulose		Cellulose (crystalline)	CBM3a	Tormo *et al.* 1996
Proteins	Extensins		LM1	Smallwood *et al.* 1995
			JIM11	Smallwood *et al.* 1994
			JIM20	Knox *et al.* 1995
	AGP		JIM8	McCabe *et al.* 1997
			JIM13	Knox *et al.* 1991; Yates *et al.* 1996
			LM14	Moller *et al.* 2008
		β-linked GlcA	LM2	Smallwood *et al.* 1996

4. Results

4.1. *Botrytis cinerea* infection and lesion development of wild type versus VviPGIP1 tobacco

Infections were carried out using the *B. cinerea* (grape strain) spores placed on plant lines, under conditions that would favour pathogen success, and assessed visually for lesion development. A lesion index developed by Carstens *et al.* (2003) was used as a baseline comparative reference. The wild type tobacco *Nicotiana tabacum* cv Havana Petit (SR1) was selected as control with two transgenic tobacco lines (lines 37 and 45). The results obtained replicated observations described in Joubert *et al.* (2006) showing a resistance phenotype for the transgenic tobacco expressing VviPGIP1, clearly visible from 72-96 hpi onwards (Figure 4.2).

At the 24 hpi stage, the tissue beneath the infection droplet spot retained a healthy appearance although the first signs of light browning and primary lesion development was also evident (Figures 4.2A, B, C). At 48 hpi the primary lesion had begun to spread away from the infection spore-filled droplet and signs of tissue maceration, indicative of type 2 and/or type 3 lesions (Figures 4.2D, E, F) were present with no obvious visible difference between genotypes observed. After 72 hpi, the lesions had enlarged with two different zones visible; an inner dark, wet and macerated zone where the spore drop was placed, surrounded by a light brown and dry ring (Figures 4.2G, H, I). For some of the infected tissues, a thin darker ring was visible at the interface with non-infected leaf area. Chlorosis was also visible on the "healthy" leaf tissue around the infection area. Still, at this stage no difference was evident between wild type and transgenic leaves with regards to symptom progression. At 96 hpi, differences started to become noticeable between PGIP lines and the SR1 plants. At 96 hpi in SR1, the lesion had spread beyond the second ring, forming a third ring of macerated tissue, looking similar to the primary infection area and characterised as a type 6 lesion (Figure 4.2J). However, for the PGIP transgenic lines 37 and 45 the infection spread had ceased (Figures 4.2K, L) and remained similar to the lesions present at 72 hpi showing evidence of infection 'containment' (Figure 4.2H, L). At 192 hpi or five days later, infected SR1 tobacco displayed lesions that had spread throughout the leaf and tissue maceration was widespread (see Figure 4.2 M). Leaf shedding in heavily infected plants was also observed (F. Weiller, personal observation). In contrast for PGIP transgenic lines 37 and 45, a reduced and limited area remained infected (see Figures 4.2N, O) on the leaves. For the PGIP lines, the primary lesions around the infection spot were clearly

visible with macerated tissue. Two infection rings were present; one clear and dry, of two to three millimetres in diameter; and the second, darker, of about one millimetre in diameter, dry and of a consistency close to non-infected tissue (not yet macerated). Based on a lesion index from Carstens *et al.* (2003), these correspond to type 3 lesions. Chlorosis was also observed as a whitening of the tissue surrounding the infected area (Figure 4.2O). Less damage, i.e. lesion size and colour, was observed for PGIP transgenic line 37 compared to 45, suggesting a slightly enhanced resistance phenotype, as previously observed by Joubert *et al.* (2006).

Scanning electron microscopy was used to track infection progression under high magnification levels. The infected tobacco leaves from the different lines were observed at 24 hpi and 72 hpi (Figure 4.3). As PGIP lines 37 and 45 produced similar images, only line 37 are shown here in comparison to SR1 tobacco. Non-infected regions of the SR1 leaf surface shows evidence of undamaged cells, stomata and leaf hairs (trichomes) (Figure 4.3A). At a lower magnification, non-infected PGIP line 37 (Figure 4.3E) shows similar undamaged tissue with dark circles indicative of micro droplets of water present at the leaf surface. Images of a 24 hpi lesion at two different magnification levels for SR1 (see Figures 4.3 B, C) and for PGIP line 37 (Figures 4.3 F, G) are shown. The entire lesion after 24 hpi in SR1 is presented in Figure 4.3B, with subsequent imaging at the centre (Figure 4.3C) revealing the presence of multiple holes indicative of tissue maceration. The centre zone would be where the *B. cinerea* spores were deposited. In the same way for PGIP line 37, the lesion after 24 hpi is presented in Figure 4.3F; interestingly here evidence of collapsed leaf hairs beyond the lesion zone was noted. Figure 4.3E reveals high magnified images of the lesion centre where again multiple holes are present revealing tissue maceration and collapse. After 72 hpi (Figures 4.3D, H), fungal structures were visible at the leaf surface with a network of hyphae on the necrotised tissue for both wild type and PGIP line.

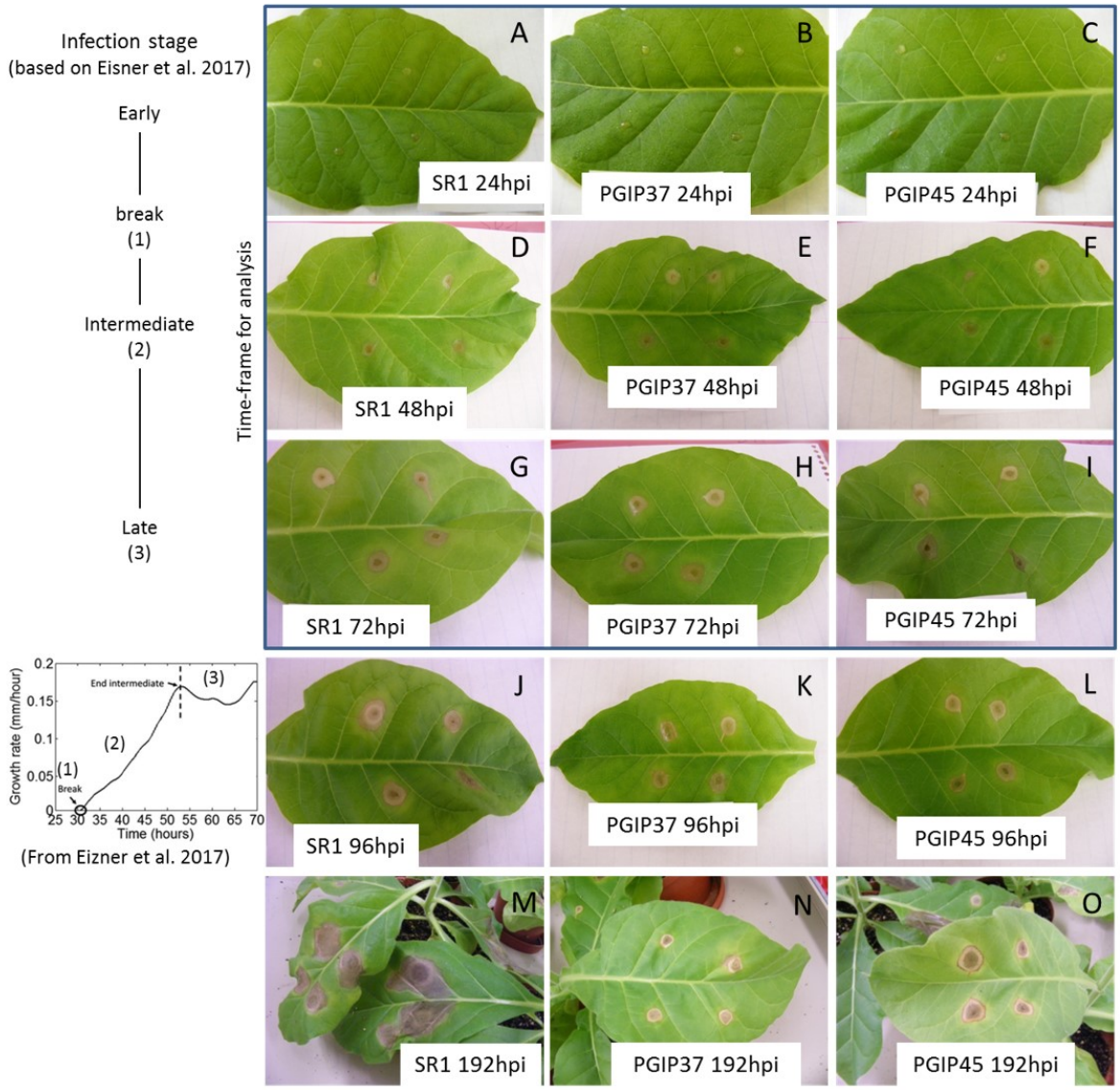

Figure 4.2: Photographs of representative infected leaves of the wild-type SR1 and the transgenic lines VviPGIP1 line 37 and line 45 infected with *B. cinerea* over time. The blue frame represent the time-points selected for biochemical analysis based on the infection stages described in Eizner *et al.* (2017) (Eizner *et al.* 2017) as shown on the left side. hpi: hours post infection

In general, no difference was noted in lesion ultrastructure between the wild type and the transgenic lines PGIP lines 37 and 45 in the first 72 hpi. Non-infected leaf tissue of the three lines was also observed with a transmission electron microscope, but no difference could be seen between any of the lines (data not shown).

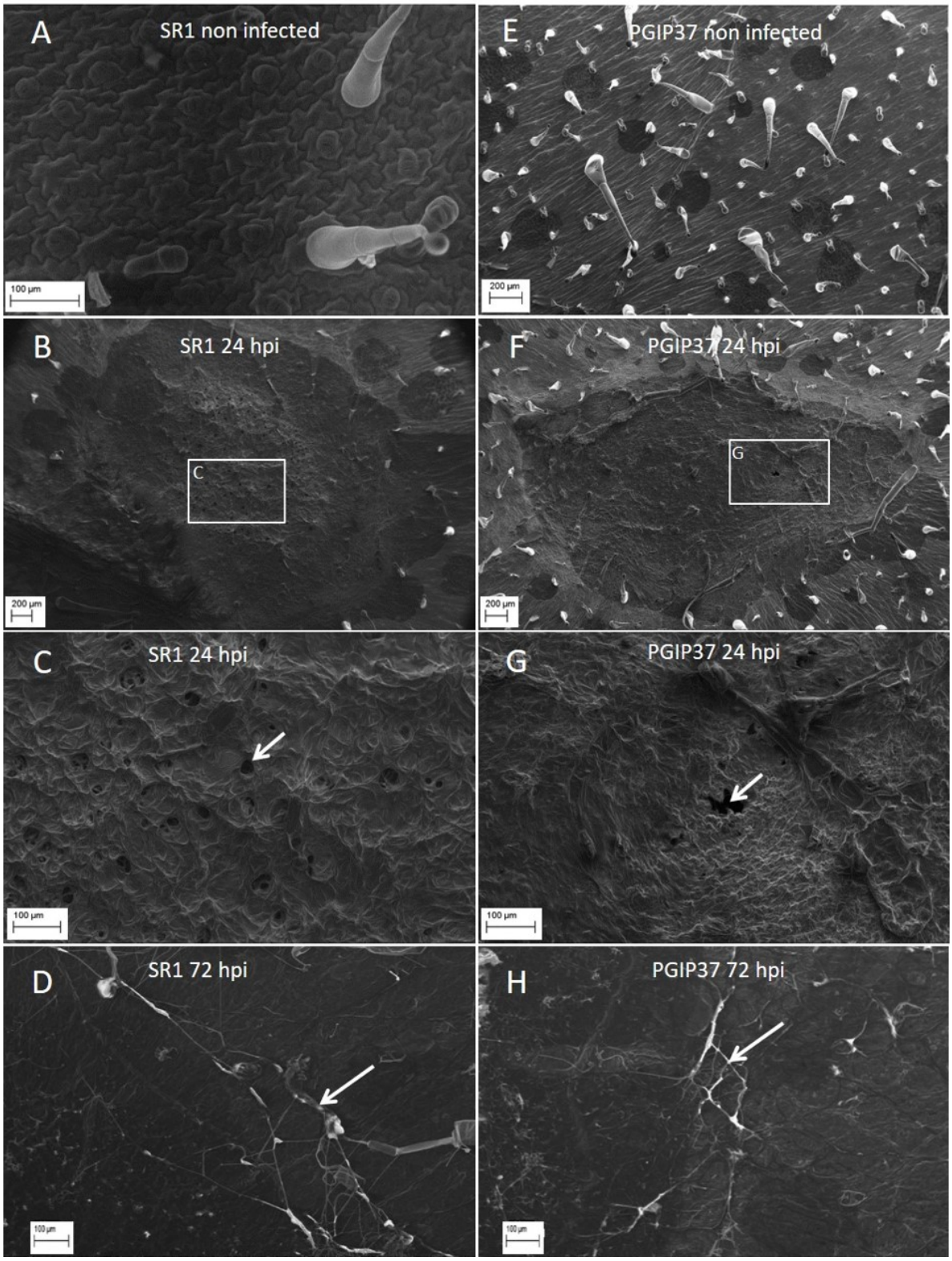

Figure 4.3: Representative micrographs of the surface of infected tobacco leaves observed with a scanning electron microscope (SEM). A, B, C, D: SR1; E, F, G, H: VviPGIP1 line 37; The arrows show tissue degradation on C and G and fungal hyphae on D and H; A, E: non-infected SR1 and VvPGIP1 plant leaf surface used as a control. hpi: hours post infection

4.2. Monosaccharide compositional analysis using GC-MS of lesions and adjacent tissue

To evaluate broad changes in cell wall composition during the first 72 hpi, AIR samples from lesions as well as the adjacent leaf tissue were hydrolysed and their monosaccharide components analysed using GC-MS (see Table 4.2 and Table 4.3). The monosaccharide profiles of the three genotypes were very similar. An increase of GalA level with leaf age (position) was observed for both wild type and transgenic plants (Weiller *et al.* 2020). A marked and significant decrease in GalA from 0 hpi to 72 hpi was mirrored by an inverse increase in Glc for all three genotypes at the lesion site (Table 4.2) and represents a characteristic feature of Botrytis infection.

For the lesion tissue, a decrease for Xyl and Gal was observed in the first 24 hpi and a slight increase in Man at 48 hpi for both wild type and transgenic plants (Table 4.2). Less markedly than at the lesion site, GalA levels decreased significantly for adjacent tissue with Glc levels increasing at 48 hpi and thereafter for all three genotypes (Table 4.3). Ara, Rha, Fuc, Xyl, Man, Gal and GlucA levels remained relatively unchanged in AIR from adjacent tissue (Table 4.3).

Table 4.2: Monosaccharide composition of cell wall, expressed in mg/g of the wild-type SR1, PGIP37 and PGIP45 tobacco leave AIR of Botrytis cinerea infected tissue (lesion). The standard deviation represents the average of 3 biological repeats. Ara: arabinose; Rha: rhamnose; Fuc: fucose; Xyl: xylose; Man: mannose; Gal: galactose; GalA: galacturonic acid; Glc: glucose; GlcA: glucuronic acid. The std dev rows also display the significant letters showing the different statistical groups after an ANOVA (P=0.05). Different colours were used to quickly visualise different statistical groups between time points for each sugar.

	Time	Data	Ara	Rham	Fuc	Xyl	Man	Gal	GalA	Glc	GlucA
SR1											
	T0	mg/g	13.45	12.51	2.55	17.31	6.05	24.16	88.41	41.02	5.09
		std dev	0.8 ab	0.73 a	0.84 a	0.52 c	0.92 abcd	0.73 c	0.53 c	10.38 a	0.7 ab
	T24	mg/g	10.9	11.8	2.57	9.68	4.66	13.91	43.99	47.85	4.19
		std dev	1.47 a	0.83 a	0.36 a	1.42 a	0.97 a	1.87 a	8.29 a	6.97 a	0.46 a
	T48	mg/g	16.41	12.35	2.45	10.87	6.62	15.59	32.09	37.11	6.3
		std dev	2.41 ab	1.83 a	0.12 a	1.63 ab	1.55 abcd	2.19 ab	7.61 a	37.24 a	1.25 b
	T72	mg/g	17.69	13.05	2.24	11.45	10.03	16.38	45.79	48.48	5.92
		std dev	1.11 b	0.85 a	0.11 a	0.68 ab	2.06 d	0.91 ab	22.25 ab	30.35 a	0.36 ab
PGIP45											
	T0	mg/g	10.2	11.28	2.19	14.17	5.13	19.96	80.42	19.54	4.55
		std dev	1.53 a	1.68 a	0.24 a	1.97 bc	0.59 abc	2.69 bc	13.06 bc	6.23 a	0.69 ab
	T24	mg/g	11.87	12.42	2.22	9.76	3.41	14.07	45	32.62	4.4
		std dev	2.25 ab	2.06 a	0.16 a	2.27 a	1.47 a	3.05 a	14.25 ab	5.29 a	0.13 ab
	T48	mg/g	15.62	12.48	2.69	10.42	6.76	14.92	42.96	46.56	4.71
		std dev	2.24 ab	0.25 a	1.12 a	0.29 ab	0.55 abcd	0.42 ab	5.73 a	5.02 a	0.45 ab
	T72	mg/g	15.54	12.42	2.01	10.71	9.42	15.39	29.99	68.19	5.23
		std dev	0.3 ab	1.24 a	0.09 a	0.72 ab	1.13 bcd	0.98 ab	5.02 a	2.58 a	0.4 ab
PGIP37											
	T0	mg/g	12.77	13	2.38	16.97	5.35	23.74	64.79	20.23	4.34
		std dev	2.93 a	0.55 a	0.78 a	0.7 a	1.03 a	0.95 a	15.47 ab	8 ab	0.55 a
	T24	mg/g	12.32	12.84	1.9	15.44	5.29	21.7	70.91	20.65	4.67
		std dev	1.94 a	0.65 a	0.32 a	2.19 a	0.79 a	2.9 a	5.1 ab	7.11 ab	0.11 a
	T48	mg/g	10.75	12.23	2.25	15.5	5.71	21.76	60.68	42.51	4.21
		std dev	0.75 a	0.15 a	0.61 a	0.76 a	0.72 a	1.04 a	6.49 ab	10.88 ab	0.12 a
	T72	mg/g	11.66	11.34	3.33	14.4	4.93	20.24	50.63	35.51	4.38
		std dev	2.3 a	1.35 a	0.37 a	2.75 a	1.14 a	3.72 a	4.79 a	15.54 ab	0.4 a

Table 4.3 Monosaccharide composition of cell walls from tobacco leave AIR, expressed in mg/g of the wild-type SR1, PGIP37 and PGIP45 of tissues adjacent to the infection spots of Botrytis cinerea. The standard deviation represents the average of 3 biological repeats. Ara: arabinose; Rha: rhamnose; Fuc: fucose; Xyl: xylose; Man: mannose; Gal: galactose; GalA: galacturonic acid; Glc: glucose; GlucA: glucuronic acid. The std dev rows also display the significant letters showing the different statistical groups after an ANOVA (P=0.05). The colours sort the time points for each sugar in different statistical groups.

	Time	Data	Ara	Rham	Fuc	Xyl	Man	Gal	GalA	Glc	GlucA
SR1											
	T0	mg/g	13.45	12.51	2.55	17.31	6.05	24.16	88.41	41.02	5.09
		std dev	0.8 a	0.73 a	0.84 a	0.52 a	0.92 a	0.73 a	0.53 b	10.38 ab	0.7 a
	T24	mg/g	11.53	12.12	2.02	14.94	5.32	20.97	66.94	12.17	4.36
		std dev	1.48 a	1.05 a	0.95 a	1.01 a	0.66 a	1.31 a	11.88 ab	13.49 a	0.25 a
	T48	mg/g	13.27	12.07	2.04	16.17	5.75	22.65	56.81	67.45	4.49
		std dev	2.23 a	0.34 a	0.17 a	1.28 a	0.76 a	1.74 a	2.9 a	50.57 b	0.55 a
	T72	mg/g	13.1	12.71	1.97	16.82	5.71	23.52	54.83	43.11	5.1
		std dev	0.29 a	0.2 a	0.06 a	1.49 a	1.05 a	2.01 a	9.33 a	18.1 ab	0.37 a
PGIP45											
	T0	mg/g	10.2	11.28	2.19	14.17	5.13	19.96	80.42	19.54	4.55
		std dev	1.53 a	1.68 a	0.24 a	1.97 a	0.59 a	2.69 a	13.06 ab	6.23 ab	0.69 a
	T24	mg/g	11.86	12.9	1.64	14.39	4.81	20.32	60.2	12.74	4.09
		std dev	0.73 a	0.98 a	0.02 a	0.63 a	0.22 a	0.86 a	12.36 ab	4 a	0.35 a
	T48	mg/g	13.54	13.07	2.48	18.19	6.03	25.33	70.57	30.1	4.64
		std dev	1.02 a	0.87 a	0.97 a	1.09 a	0.44 a	1.45 a	5.76 ab	16.86 ab	0.11 a
	T72	mg/g	12.22	11.81	2.3	17.46	5.41	24.38	53.04	40.33	4.69
		std dev	2.48 a	1.58 a	0.44 a	7.79 a	1.27 a	10.41 a	20.74 a	10.02 ab	0.42 a
PGIP37											
	T0	mg/g	12.77	13	2.38	16.97	5.35	23.74	64.79	20.23	4.34
		std dev	2.93 a	0.55 a	0.78 a	0.7 a	1.03 a	0.95 a	15.47 ab	8 ab	0.55 a
	T24	mg/g	12.32	12.84	1.9	15.44	5.29	21.7	70.91	20.65	4.67
		std dev	1.94 a	0.65 a	0.32 a	2.19 a	0.79 a	2.9 a	5.1 ab	7.11 ab	0.11 a
	T48	mg/g	10.75	12.23	2.25	15.5	5.71	21.76	60.68	42.51	4.21
		std dev	0.75 a	0.15 a	0.61 a	0.76 a	0.72 a	1.04 a	6.49 ab	10.88 ab	0.12 a
	T72	mg/g	11.66	11.34	3.33	14.4	4.93	20.24	50.63	35.51	4.38
		std dev	2.3 a	1.35 a	0.37 a	2.75 a	1.14 a	3.72 a	4.79 a	15.54 ab	0.4 a

4.3. Comprehensive microarray polymer profiling of wild type tobacco (SR1) infected with *Botrytis cinerea*: a time course analysis at the lesion sites, adjacent tissues and distal leaves and taking into consideration ontogenic responses

Comprehensive microarray polymer profiling analysis uses a wide variety of mAbs and CBMs which bind to various pectin, hemicellulose and cell wall protein epitopes. Successive extractions with first CDTA and then NaOH leads to the exposure of hemicelluloses and is represented separately on heatmaps. The outcomes of a *B. cinerea* infection progression on SR1 tobacco plants are presented in Figure 4.4, combining data from all leaf positions (ontogenic responses), data at the lesions, the surrounding tissues, as well as from uninfected leaves distal to the infections (leaves 2 and 6). Leaf developmental patterns for cell wall probes were evident in the CoMPP dataset (see Figure 4.4). A general increase in signal for mAbs binding to HG with leaf age was evident in the datasets for adjacent and distal tissue of the CDTA fraction (Figure 4.4). In addition, the mAb that binds to calcium ion egg box motifs present in pectins, 2F4, followed this increasing trend with leaf age. A decreasing signal for mAbs LM5 and LM6 (galactans and arabinans) that form part of rhamnogalacturonan I (RG-I) side chains was observed. mAbs INRA-RU1 and INRA-RU2 which bind the RG-I backbone showed a relatively invariant signal pattern. Probes also recognised extensin (mAbs LM1, JIM11, JIM20) and AGP (mAbs JIM8, JIM13, LM2) epitopes in the leaf tissue. Differences in adjacent and distal tissue to the infection were slight and the overall patterning was similar to the ontogenic leaf age effect (see Figure 4.4). A PCA based on the CoMPP raw data of adjacent and distal tissue (see supplementary Figure S4.1) was performed. This unsupervised PCA confirmed the previously described results and the ontogenic effect as the main driver of separation while infection also separated nicely the samples on the second dimension.

At the lesion site (see Figure 4.4) however, major changes in epitope abundance for HG, RG-I, AGP and extensin epitopes were noticed in the CDTA but mainly in the NaOH fraction in a time-course dependent manner. From 0 hpi to 24 hpi there was an increase in signal for mAbs LM5 and LM6 (arabinans and galactans) in the CDTA fraction. Thereafter the signals decreased, suggesting de-pectination/degradation of the epitopes in the CDTA component. This would support pectin degradation occurring due to pathogen infection. HG epitopes (mAbs JIM5, JIM7, LM18, LM19) and RG-I backbone (INRA-RU1, INRA-RU2) signals decreased at 72 hpi supporting evidence of signal

degradation. In the CDTA fraction of the lesions; epitopes associated with AGPs (mAbs JIM11, JIM20) and extensins (mAbs JIM8, JIM13) remained relatively unchanged. In the NaOH fraction of the lesion; marked changes were evident at 24 hpi and 72 hpi. INRA-RU1, INRA-RU2, LM5 and LM6 all increased after 24 hpi suggesting pectin exposure of underlying RG-I networks of the cell wall. LM22 glucomannan increased at 24 hpi then decreased 72 hpi in the NaOH fraction. Glucans (recognised by BS-400-2) increased stepwise at 24 hpi and 72 hpi in the alkali extract. Xyloglucans recognised by mAbs LM15 and LM25 followed a decreasing or increasing, then decreasing signal in the datasets. Interestingly, the LM8 probe, which binds to xylogalacturonan (XGA) was detected at 72 hpi in the NaOH soluble material. AGP and extensin probes JIM11, JIM20, JIM8 and JIM13 all increased markedly at 24 hpi and 72 hpi in the lesion tissue. A PCA run on CoMPP lesion data showed a clear separation according to the infection times (Figure S4.2), while the ontogenic effect was not visible anymore.

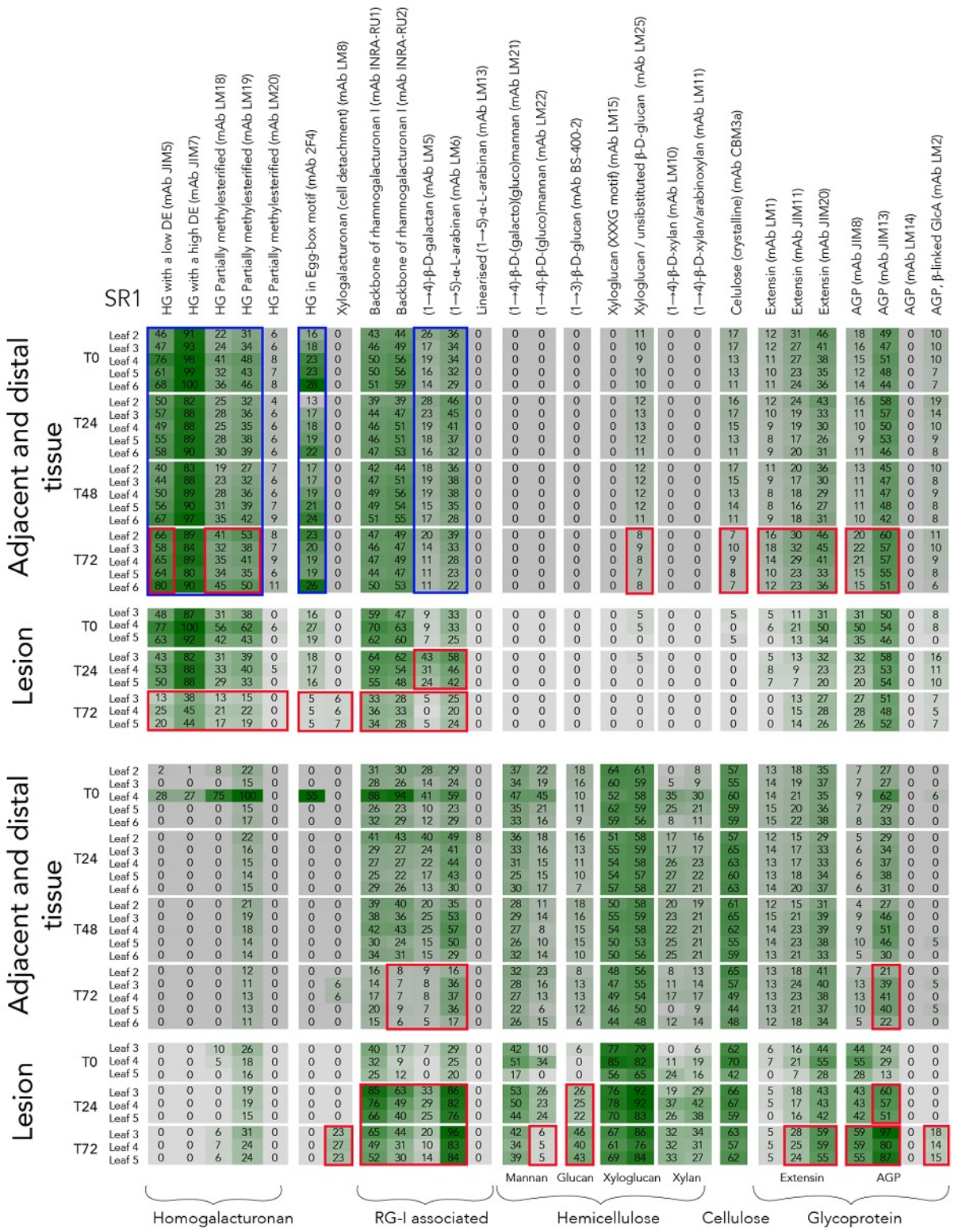

Figure 4.4: Comprehensive microarray polymer profiling (CoMPP) analysis of the wild-type SR1, tobacco leave AIR infected by *B. cinerea*. Results are presented as heatmaps of both CDTA and NaOH extractions, showing the relative abundance of cell wall associated epitopes and separated between non-infected tissue (adjacent and distal to the infection) and infected tissue (lesion). Detailed list of the antibody used is available in Table 4.1. Red boxes indicate variations due to the infection. Blue boxes indicate variations due to ontogenic effect. AGP: arabinogalactan protein, HG: homogalacturonan, mAbs: monoclonal antibody, T: time point (in hours)

4.4. Comprehensive microarray polymer profiling of infection spots and surrounding tissue from *Vvi*PGIP1 lines 37 and 45 infected with *Botrytis cinerea*, in comparison with those of SR1.

To evaluate the possible links between cell wall modifications and the VviPGIP1-related *B. cinerea* resistance phenotypes recorded in the transgenic lines, a CoMPP analysis of the lesions and adjacent tissues over a 72 h time-course was conducted. Based on the strong ontogenic responses confirmed in both uninfected tobacco (Weiller *et al.* 2020), as well as during infection (Figure 4.4), data for leaf position 4 was the focus for this analysis (Figure 4.5). Data for leaves 3 and leaf 5 are available as supplementary datasets (see Figures S4.1 to S4.6).

At the lesion site, evidence of pectin degradation were present following the 0 hpi, 24 hpi and 72 hpi time points for all three genotypes (see Figure 4.5). HG associated mAbs JIM5, JIM7, LM18, LM19 and 2F4 all decreased from 0 hpi to 72 hpi in the CDTA extracts. Similarly, for RG-I associated mAbs INRA-RU1, INRA-RU2, LM5 and LM6 the probe signals decreased from 24 hpi. The extensin probes JIM11 and JIM20; and the AGP probes JIM8 and JIM13 decreased at 24 hpi. No major differences between wild type and transgenic material were present. In the case of the NaOH extract RG-I probes (INRA-RU1, INRA-RU2, LM5 and LM6), increased at 24 hpi and remained high at 72 hpi. Mannans (LM21 and LM22) decreased with infection progression. Xyloglucans detected by mAbs LM15 and LM25 as well as CBM3a followed a decreasing trend in the datasets. Extensins (JIM11 and JIM20) and AGPs (JIM8 and JIM13) showed a general trend of increasing in abundance through 24 hpi to 72 hpi. The AGP LM2 epitope was detectable at 72 hpi and LM8 probe for xylogalacturonan was present at 72 hpi for all lines. Again, no major differences were observed between SR1 and the PGIP1 expressing lines.

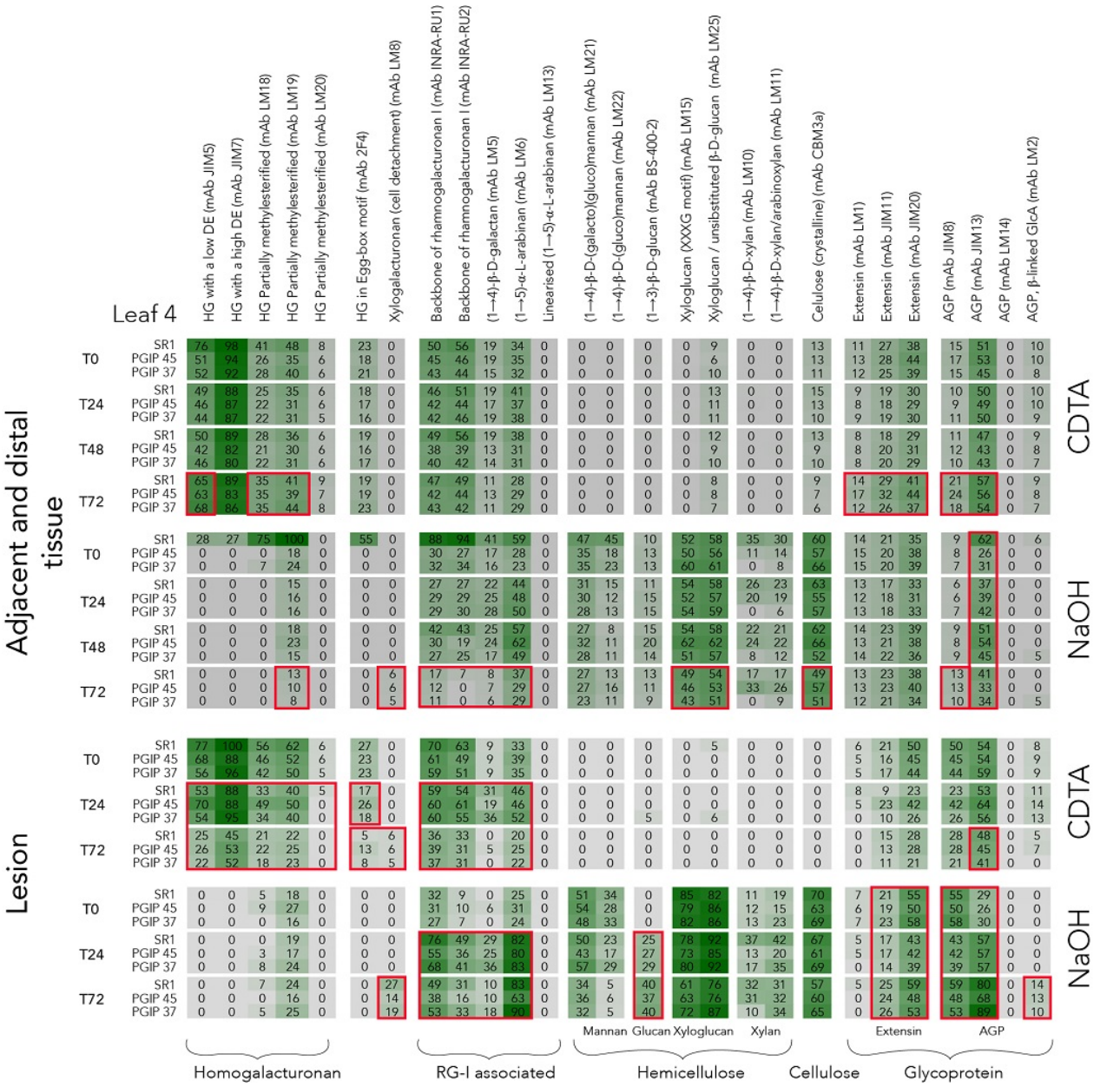

Figure 4.5: Comprehensive microarray polymer profiling (CoMPP) analysis of the wild-type SR1, PGIP37 and PGIP45 AIR of the leaf 4 lesion and adjacent tissue to the lesion. Results are presented as heatmaps showing the relative abundance of cell wall associated epitopes (see material and methods for more information). Detailed list of the antibody used is available in Table 4.1. Red boxes indicate variations due to the infection. AGP: arabinogalactan protein, HG: homogalacturonan, mAbs: monoclonal antibody, T: time point (in hours)

Adjacent and distal tissue were also evaluated using CoMPP arrays (see Figure 4.5, supplementary datasets Figures S4.3 to S4.6). For adjacent tissue the major patterns in the CDTA datasets show JIM5, JIM7, LM18, LM19 and 2F4 as the major signals along with RG-I backbones (INRA-RU1 and INRA-RU2) and side chains (LM5 and LM6) (Figure 4.5). Extensins (LM1, JIM11 and JIM20) and AGPs (JIM8 and JIM13) also present in CDTA extracts increased in abundance in all lines at 72 hpi.

For the NaOH extracts the major RG-I backbones (INRA-RU1 and INRA-RU2) and side chains (LM5 and LM6) showed a decreasing signal especially for PGIP line 37 for all time points. Interestingly LM21 and LM22 which bind to mannans showed an increasing trend for PGIP line 37 and 45. LM15, LM25 and CBM3a signals from xyloglucans were present and these increased markedly for PGIP line 37 at 72 hpi compared to wild type. NaOH soluble extensin (mAbs LM1, JIM11, JIM20) and AGP (mAbs JIM8 and JIM13) epitopes remained relatively unchanged over time. For distal (systemic) tissue analysis was conducted on L2 – youngest leaf – and L6 – oldest leaf. The CDTA extract of L2 and L6 showed signals for HG (mAbs JIM5, JIM7, LM18, LM19), RG-I (mAbs INRA-RU1, INRA-RU2, LM5, LM6), extensins (mAbs LM1, JIM11, JIM20) and AGPs (JIM8, JIM13, LM2). A maturation pattern between L2 and L6 can be seen, as LM5 (galactans), LM6 (arabinans) and LM2 (AGPs) decrease from L2 to L6; whereas pectin egg-boxes increase (mAb 2F4), however no clear differences between SR1 and transgenic PGIP1 line 37 and 45 were evident. For the NaOH extract, the major signals were for RG-I (mAbs INRA-RU1, INRA-RU2, LM5, LM6), mannans (mAb LM21, LM22), xyloglucan (mAbs LM15, LM25, CBM3a), extensins (LM1, JIM11 and JIM20) and AGPs (JIM8 and JIM13). Here differences for mannans (mAb LM21, LM22), xyloglucan (mAbs LM15, LM25, CBM3a) and xylans (mAbs LM10, LM11) between wild type and transgenic lines were observed.

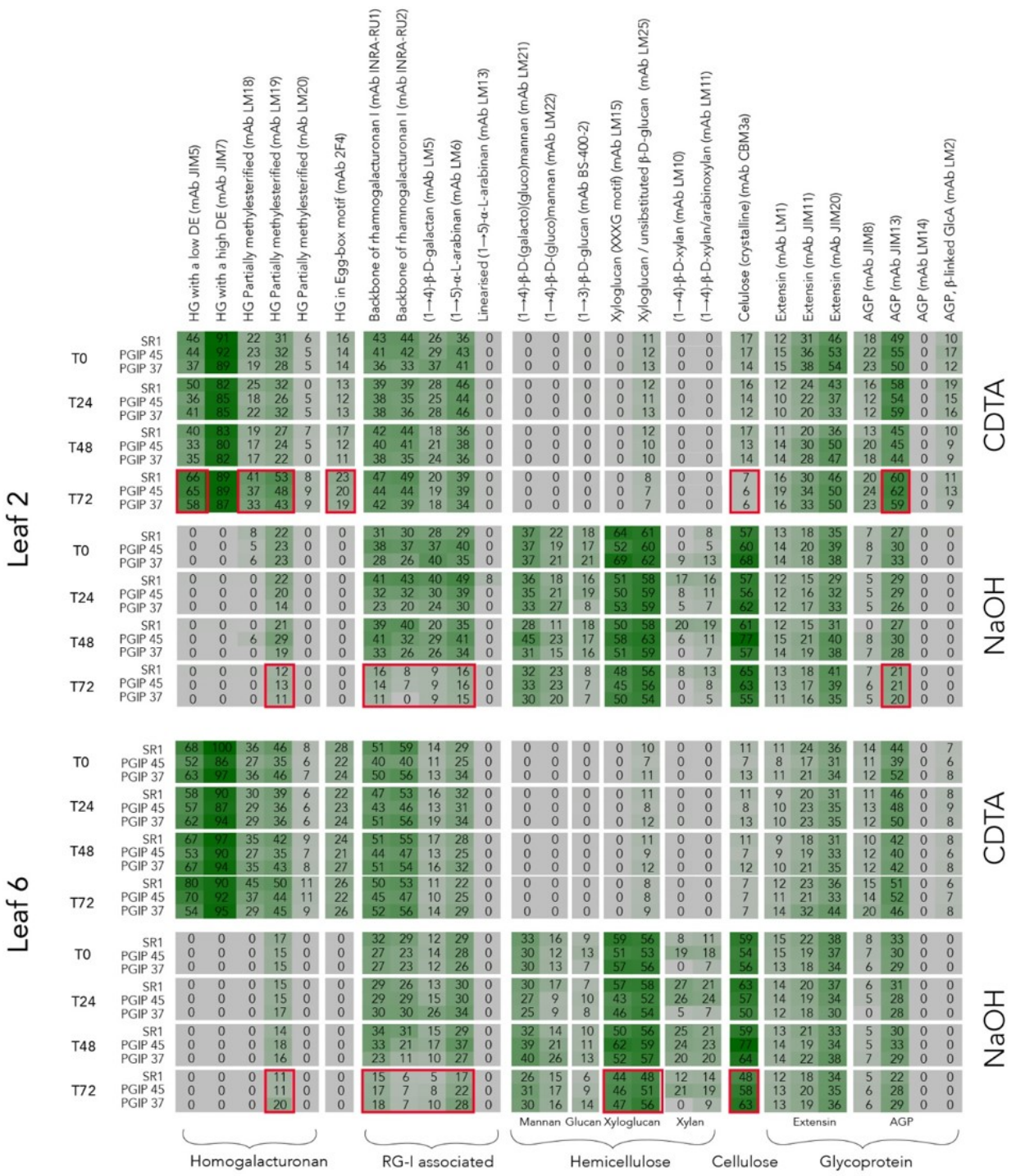

Figure 4.6: Comprehensive microarray polymer profiling (CoMPP) analysis of the wild-type SR1, PGIP37 and PGIP45 tobacco leave AIR of distal tissue to the infection (non-infected leaves 2 and 6). Results are presented as heatmaps showing the relative abundance of cell wall associated epitopes from the CDTA and NaOH extractions for both L2 and L6 leaves (see material and methods for more information). Detailed list of the antibody used is available in Table 4.1. Red boxes indicate variations due to the infection. AGP: arabinogalactan protein, HG: homogalacturonan, mAbs: monoclonal antibody, T: time point (in hours)

5. Discussion

5.1. *Botrytis cinerea* infects tobacco leaves and develop lesions with macerated tissue in the first 72 hpi

N. tabacum cv. Petit Havana is not an easily susceptible host to the necrotrophic fungus *B. cinerea* as it accumulates numerous alkaloids such as scopoletin, essential oils and lipids, phenylpropanoids and pathogenesis-related proteins in response to fungal infection (El Oirdi *et al.* 2010). Infection can be promoted with a high concentration of spores under favourable conditions of temperature and humidity (Hain *et al.* 1993; Joubert *et al.* 2006). When Botrytis infects tobacco, spreading lesions from 72 h onwards occurred, characteristic of a susceptible interaction.

B. cinerea first penetrates into the leaf tissue which corresponds with the multiple holes visible in the lesion visible during the early stages of infection. After tissue penetration, it grows into a mycelium network beneath the epidermis and starts to degrade the tissue inducing necrosis. In the first 72h of infection, cell wall profiling confirmed that tissue maceration through extensive depectination occurs at the infection spots, as expected for Botrytis, via degradation of the HGs with a strong decrease of signal for mAbs such as JIM7 and a drop in GalA levels. GalA is found in the cell wall as PGA chains forming the HG pectin backbone. At 72 and 96 hpi, we observed external (ectopic) mycelium formation on the necrotised tissue close to the border of the infection, similar to what was described previously in tomato by Prins et al. (2000). Electron microscopic observations on tomato and broad beans showed that the *B. cinerea* spores germinated and grew an appressorium like structure that enzymatically breaks through the cuticle and cell wall layers (Rijkenberg *et al.* 1980; Mansfield and Richardson 1981). *B. cinerea* often enters a quiescent stage, after penetration into the host, producing a symptomless infection at early stages (Prins *et al.* 2000; Emmanuel *et al.* 2018; Veloso and van Kan 2018) and later develops an expanding lesion with tissue maceration (Elad 1988; Prins *et al.* 2000; van Kan 2005). That was not the case in this study where all inoculation spots developed into a lesion, except in the cases where the initial droplet had evaporated before the formation of the lesion. *B. cinerea* can develop a variety of different kinds of local lesions (Carstens *et al.* 2003). Our results showed that the initial lesion type is often indicative of the susceptibility or future resistance of the plant to the fungus.

Moreover, the cell wall profiling showed ontogenic patterns, characterised by an increase of HG availability, a modifications of their methylesterification levels, more HG in egg-box conformation and less RG-I arabinan and galactan side chains available with leaf maturation, even though the lesion development on the different leaves was not discernibly different. These slight ontogenic differences therefore do not change the outcome of the infection, specifically in this assay where the conditions would favour the pathogen (high spore loads and ideal conditions in terms of humidity and temperature).

5.2. *Botrytis cinerea* degrades pectin-rich leaf cell walls and AGP-extensin proteins are deposited in response to the infection

Comparing the cell walls at the lesion sites, the surrounding tissue, or in uninfected distal leaves, differences could be observed with the cell wall profiling. The major differences between the lesions and the non-infected tissues were the previously mentioned massive depectination and an increase of glycoproteins signal at the lesion. From 48 hpi, glucose levels increased at the lesion suggesting callose deposition. In the non-infected tissues, subtle differences were observed from 72 hpi. Adjacent tissue had elevated levels of HGs and different methylesterification profiles. Distal leaves interestingly displayed a different response to the infection depending on their developmental stage, with younger leaves having higher HG values (with various methylesterification levels as observed in fruit; see (Kelloniemi *et al.* 2015)), while older leaves displayed elevated xyloglucan/cellulose. Considering the variations of the cell wall matrix during leaf maturation (described more extensively in Weiller *et al.* (2020)), plants seem to adapt their response to the infection accordingly. All tissues (lesion, adjacent, distal) showed an increased signal for extensins and even more for AGPs at 72 hpi, with particular high levels at the lesion site.

B. cinerea life cycle and infection process have been widely described and numerous virulence factors have been characterised (van Kan 2005, 2006; Williamson *et al.* 2007; Shah *et al.* 2012). The CWDEs have been shown to be crucial for *B. cinerea* virulence and aid in its capacity to breach the plant cuticle and cell wall layers (ten Have *et al.* 1998, 2002; Tudzynski and Kokkelink 2009).

Facing numerous ePGs, HG was observed as the weak element allowing matrix disorganisation and maceration progression. Indeed, RG-I polymers appeared much more resistant to fungal

degradation than HG epitopes. *B. cinerea* appears to be more limited in releasing RG-I targeting enzymes; only RG acetyl-esterase for example has been reported (Blanco-Ulate *et al.* 2014). RG-I cross-links with xyloglucan and xylan (Popper and Fry 2005, 2008; Ralet *et al.* 2016; Broxterman and Schols 2018), as well as xyloglucan-cellulose (Zykwinska *et al.* 2007; Park and Cosgrove 2015) polymers in plant cell walls limiting their ease of degradation as reported in our results added with the limited hemicellulose degradation during our experiment's timeframe.

Cell wall proteins have established roles in plant defence described and reviewed by Showalter (1993), Cassab (1998) and Deepak *et al.* (2010). Hydroxy-proline-rich glycoproteins (HRGP) are a family of cell wall proteins which function in plant defence in addition to multiple other functions that are being characterised (Deepak *et al.* 2010; Rashid 2016). Extensin gene expression is induced in *A. thaliana* during infection with *Xanthomonas campestris* and *Pseudomonas syringae* (Merkouropoulos and Shirsat 2003; Wei and Shirsat 2006). In roots, extensin epitopes have been linked to infection by *Fusarium oxysporum* of banana (Wu *et al.* 2017). Similarly, extensin upregulation is found in *Solanum tuberosum* when infected by *Pectobacterium atrosepticum* (Koroney *et al.* 2016). In addition, *A. thaliana* mutants impaired in extensin arabinosylation were found to have increase susceptibility to *Phytophthora parasitica* (Castilleux *et al.* 2020). The role of extensins in plant pathosystems was recently reviewed in Castilleux *et al.* (2018). In a similar manner to extensins; AGPs are HRGPs with multiple functions in plant growth and development (Showalter 2001). AGPs have roles in plant defence against biotic and abiotic stressors; *in vitro* studies have shown their capacity to attract zoospores and inhibit *Aphanomyces euteiches* growth and development (Cannesan *et al.* 2012). In roots, they have been shown to be very important for rhizobium interactions (reviewed by Nguema-Ona *et al.* 2013b). In bananas, AGP expression and distribution is stimulated by *F. oxysporum* infection (Wu *et al.* 2017). In *Oriza sativa*, infection with *Magnaporthe oryzae* induces increased expression of AGPs; suggesting a role in plant-pathogen signalling (Liang *et al.* 2018). *N. alata*, *Na*AGP4 expression was found to be modulated by *B. cinerea* presence (Gilson *et al.* 2001). In apple, (*Malus x domestica*), *Penicillium spinulosum* induced AGP accumulation around the injection area and AGP deactivation led to increased symptoms (Leszczuk *et al.* 2019). Additional roles for AGPs in pathogen interactions have been summarised in *Mareri et al.* (2018).

5.3. Cell wall degradation leads to production of DAMPs

The approach used in this study is useful, because the profiling results show that the cell wall degradation activities would generate a number of DAMPs (starting after 24 hpi and the beginning of tissue maceration). HG degradation is mediated by CWDEs which also releases mono-sugars which can be used for fungal growth (Blanco-Ulate *et al.* 2015). PGA degradation, for example, has been shown to be essential for *Aspergillus niger* growth as shown in Alazi *et al.* (2016). Short PGAs termed OGs are essential for plant protection as they act as DAMPs to signal infection and trigger plant immune responses (Boutrot and Zipfel 2017; Bacete *et al.* 2018). It is also known that OGs length influence the strength and duration of the defence response (Davidsson *et al.* 2017; Hou *et al.* 2019). Our analysis also confirmed a strong decrease of mannan (LM22 epitope) at the lesion. Mannan was recently identified as DAMP molecules that trigger typical Mitogen-activated protein kinase signalling pathways and increasing resistance to *Xanthomonas oryzae* and *Phytophthora nicotianae* in rice and tobacco (Zang *et al.* 2019). However, in this study, the wild-type tobacco host was clearly not capable of mounting an effective resistance response, leading to severe infection.

5.4. VviPGIP1 plants contain *Botrytis cinerea* infection with limited cell wall modifications

The tobacco lines overexpressing the *VviPGIP1* gene could mount an effective resistance response, although the initial symptom development was identical to that of the wild-type plants over the first 72 hours. Previous analysis already confirmed that the transgenic lines had altered cell walls, hormone levels and enzyme activities (Alexandersson *et al.* 2011; Nguema-Ona, Moore, *et al.* 2013). Transcriptional profiling during infection confirmed an altered timing of disease responses and supported a quick response in limiting ROS and systemic activation in the first 72h after infection (Basson 2017). Our experiments have shown that the first 72 hpi appear crucial for effective plant resistance to be mounted. The infection progression slowed down and was contained after 72 hpi in the transgenic plants compared to wild type plants. Shlezinger *et al.* (2011) have shown that the first 48 hpi are crucial for *B. cinerea.* It was also shown in transgenic tobacco expressing a grapevine phytoalexin, resveratrol, that its rapid accumulation at the local lesion site in the first 48 hpi was correlated with enhanced plant resistance to pathogenic fungi (Hain *et al.* 1993). Veloso and van

Kan (2018) showed that the ability of *B. cinerea* to successfully infect plants depended on its capacity to shut down plant autophagy early in favour of apoptosis. Linked to our observations, this suggests that resistant plants are able to quickly create a buffer zone surrounding the macerated tissue and confine the fungi in order to stop its expansion. In the transgenic plants, a thin dark and dry ring was formed between healthy and macerated tissue between 72 and 96 hpi and the lesion didn't spread further.

Polygalacturonase inhibiting proteins possess well documented anti-ePG activity (Esquerré-Tugayé *et al.* 2000; D'Ovidio *et al.* 2004; Sicilia *et al.* 2005; Di Matteo *et al.* 2006; Joubert *et al.* 2007; Kalunke *et al.* 2015; Li and Smigocki 2018) in addition to its capacity to bind pectin and prevent HG degradation (Spadoni *et al.* 2006). PGIPs have also been shown to promote the production of OGs (Benedetti *et al.* 2015) possibly inducing a stronger response to pectin degradation when overexpressed. Here, cell wall profiling was conducted showing that PGIP1 plants displayed a distinct response with increased levels of xyloglucan/cellulose in adjacent tissue. This stronger signal observed for xyloglucan in the transgenic plants is probably linked to the downregulation of XET/XTH observed in the non-infected plants (Alexandersson *et al.* 2011).

6. Conclusion

This study followed cell wall modifications during an infection by *B. cinerea*, between sensitive and resistant plants to the fungus. It was conducted using a combination of microscopy and monosaccharide quantification completed with the recently developed glycan CoMPP.

The overexpression of VviPGIP1 has been shown to induce cell wall modifications in tobacco leaves prior to infection and this work is, to our knowledge, the first report to present an overview of the cell wall transformations during fungal infection of PGIP1 tobacco lines. The most notable effect observed was the depectination with HG degradation and RG-I exposure. During the time-frame of our experiment, hemicellulose including the xyloglucan/cellulose network showed limited degradation, especially in the PGIP plants. A differential response was observed between the lesion, adjacent and distal tissue with an accumulation of glycoproteins at and around the infection site. This is interesting as the role of glycoproteins, namely extensins and AGPs, in plant defence is not fully understood. Extensins have been described as defence proteins but their mode of action is only

starting to be deciphered in roots. As for AGP, the topic is very new and direct evidence of their protective role are still lacking.

The compositional role of the cell wall in plant immunity is also suggested with the accumulation of polysaccharides and proteins at the lesion site. These changes were not limited to the infection area but started to be detectable in distal tissue and non-infected leaves, signs of a systemic response to the fungal attack. Despite a clear susceptibility difference to *B. cinerea*, the transgenic and control plants showed small cell wall compositional variations. More than just compositional changes it might be the timing of response that matters.

Together these results show that the response to *B. cinerea* infection is multifactorial and includes various mechanisms such as the strengthening of the cell wall and the production and accumulation of defence proteins. The VviPGIP1 tobacco – *B. cinerea* is a valuable pathosystem highlighting new functional aspects of PGIP1 functioning in plant immunity. The use of the CoMPP analysis allowed us to screen the cell wall composition at different infection stages leading to a better understanding of cell wall mediated infection process. This work provides a foundation for the understanding of PGIP1 during an active infection and of the role of cell wall modifications under necrotrophic fungi infection. It would benefit from combining immunomicroscopy techniques with a selection of specific cell wall probes, targeting extensins and AGPs for example, in future studies.

7. References

Alazi E, Niu J, Kowalczyk JE, *et al.* 2016. The transcriptional activator GaaR of *Aspergillus niger* is required for release and utilization of d-galacturonic acid from pectin. *FEBS Letters* **590**: 1804–1815.

Alexandersson E, Becker JVW, Jacobson D, *et al.* 2011. Constitutive expression of a grapevine polygalacturonase-inhibiting protein affects gene expression and cell wall properties in uninfected tobacco. *BMC Research Notes* **4**: 493.

Atwell S, Corwin JA, Soltis NE, Subedy A, Denby KJ, Kliebenstein DJ. 2015. Whole genome resequencing of *Botrytis cinerea* isolates identifies high levels of standing diversity. *Frontiers in Microbiology* **6**: 996.

Bacete L, Mélida H, Miedes E, Molina A. 2018. Plant cell wall-mediated immunity: cell wall changes trigger disease resistance responses. *Plant Journal* **93**: 614–636.

Basson CE. 2017. Transcriptomic analysis of disease resistance responses using a tobacco-*Botrytis cinerea* pathosystem. *PhD thesis, Stellenbosch University, South Africa*.

Benedetti M, Andreani F, Leggio C, *et al.* 2013. A single amino-acid substitution allows endo-polygalacturonase of *Fusarium verticillioides* to acquire recognition by PGIP2 from *Phaseolus vulgaris*. *PloS one* **8**: e80610.

Benedetti M, Pontiggia D, Raggi S, *et al.* 2015. Plant immunity triggered by engineered *in vivo* release of oligogalacturonides, damage-associated molecular patterns. *Proceedings of the National Academy of Sciences of the United States of America* **112**: 5533–5538.

Blanco-Ulate B, Labavitch JM, Vincenti E, Powell ALT, Cantu D. 2015. Hitting the wall: Plant cell walls during *Botrytis cinerea* infections In: *Botrytis – the Fungus, the Pathogen and its Management in Agricultural Systems*. Cham: Springer International Publishing, Switzerland, 361–386.

Blanco-Ulate B, Morales-Cruz A, Amrine KCH, Labavitch JM, Powell ALT, Cantu D. 2014. Genome-wide transcriptional profiling of *Botrytis cinerea* genes targeting plant cell walls during infections of different hosts. *Frontiers in Plant Science* **5**.

Boutrot F, Zipfel C. 2017. Function, discovery, and exploitation of plant pattern recognition receptors for broad-spectrum disease resistance. *Annual Review of Phytopathology* **55**: 257–286.

Bozbuga R, Lilley CJ, Knox JP, Urwin PE. 2018. Host-specific signatures of the cell wall changes induced by the plant parasitic nematode, Meloidogyne incognita. *Scientific Reports* **8**: 17302.

Breeze E. 2019. 97 Shades of gray: genetic interactions of the gray mold, *Botrytis cinerea*, with wild and domesticated tomato. *The Plant Cell* **31**: 280–281.

Broxterman SE, Schols HA. 2018. Characterisation of pectin-xylan complexes in tomato primary plant cell walls. *Carbohydrate Polymers* **197**: 269–276.

Cannesan MA, Durand C, Burel C, *et al.* 2012. Effect of arabinogalactan proteins from the root caps of pea and *Brassica napus* on *Aphanomyces euteiches* zoospore chemotaxis and germination. *Plant Physiology* **159**: 1658–1670.

Carstens M, Vivier MA, Pretorius IS. 2003. The *Saccharomyces cerevisiae* chitinase, encoded by the *CTS1-2* gene, confers antifungal activity against *Botrytis cinerea* to transgenic tobacco. *Transgenic Research* **12**: 497–508.

Castilleux R, Plancot B, Gügi B, *et al.* 2020. Extensin arabinosylation is involved in root response to elicitors and limits oomycete colonization. *Annals of Botany* **125**: 751–763.

Castilleux R, Plancot B, Ropitaux M, *et al.* 2018. Cell wall extensins in root–microbe interactions and root secretions. *Journal of Experimental Botany* **69**: 4235–4247.

Clausen MH, Willats WGT, Knox JP. **2003**. Synthetic methyl hexagalacturonate hapten inhibitors of anti-homogalacturonan monoclonal antibodies LM7, JIM5 and JIM7. *Carbohydrate Research* **338**: 1797–1800.

Collado IG, Viaud M. **2016**. Secondary metabolism in *Botrytis cinerea*: combining genomic and metabolomic approaches In: *Botrytis – the Fungus, the Pathogen and its Management in Agricultural Systems*. Cham: Springer International Publishing, 291–313.

Cui H, Tsuda K, Parker JE. **2015**. Effector-triggered immunity: From pathogen perception to robust defense. *Annual Review of Plant Biology* **66**: 487–511.

D'Ovidio R, Mattei B, Roberti S, Bellincampi D. **2004**. Polygalacturonases, polygalacturonase-inhibiting proteins and pectic oligomers in plant-pathogen interactions. *Biochimica et Biophysica Acta - Proteins and Proteomics* **1696**: 237–244.

Davidsson P, Broberg M, Kariola T, Sipari N, Pirhonen M, Palva ET. **2017**. Short oligogalacturonides induce pathogen resistance-associated gene expression in *Arabidopsis thaliana*. *BMC Plant Biology* **17**: 19.

Deepak S, Shailasree S, Kini RK, Muck A, Mithöfer A, Shetty SH. **2010**. Hydroxyproline-rich glycoproteins and plant defence. *Journal of Phytopathology* **158**: 585–593.

Van der Does D, Boutrot F, Engelsdorf T, *et al.* 2017. The Arabidopsis leucine-rich repeat receptor kinase MIK2/LRR-KISS connects cell wall integrity sensing, root growth and response to abiotic and biotic stresses. *PLoS Genetics* **13**: e1006832.

Eizner E, Ronen M, Gur Y, Gavish A, Zhu W, Sharon A. **2017**. Characterization of *Botrytis*-plant interactions using PathTrack © - an automated system for dynamic analysis of disease development. *Molecular Plant Pathology* **18**: 503–512.

Elad Y. **1988**. Scanning electron microscopy of parasitism of *Botrytis cinerea* on flowers and fruits of cucumber. *Transactions of the British Mycological Society* **91**: 185–190.

Elad Y, Pertot I, Cotes Prado AM, Stewart A. **2015**. Plant hosts of *Botrytis* spp. In: *Botrytis - The Fungus, the Pathogen and its Management in Agricultural Systems*. Cham: Springer International Publishing, 413–486.

Emmanuel CJ, van Kan JAL, Shaw MW. **2018**. Differences in the gene transcription state of *Botrytis cinerea* between necrotic and symptomless infections of lettuce and *Arabidopsis thaliana*. *Plant Pathology*: 1–9.

Esquerré-Tugayé MT, Boudart G, Dumas B. **2000**. Cell wall degrading enzymes, inhibitory proteins, and oligosaccharides participate in the molecular dialogue between plants and pathogens. *Plant Physiology and Biochemistry* **38**: 157–163.

Federici L, Caprari C, Mattei B, *et al.* 2001. Structural requirements of endopolygalacturonase for the interaction with PGIP (polygalacturonase- inhibiting protein). *Proceedings of the National Academy of Sciences* **98**: 13425–13430.

Ferrari S, Savatin D V, Sicilia F, Gramegna G, Cervone F, Lorenzo G De. **2013**. Oligogalacturonides: plant damage-associated molecular patterns and regulators of growth and development. *Frontiers in Plant Science* **4**: 49.

Gilson P, Gaspar YM, Oxley D, Youl JJ, Bacic A. **2001**. NaAGP4 is an arabinogalactan protein whose expression is suppressed by wounding and fungal infection in *Nicotiana alata*. *Protoplasma* **215**: 128–139.

Gomathi V, Gnanamanickam SS. **2004**. Polygalacturonase-inhibiting proteins in plant defence. *Current* **87**: 1211–1217.

Govrin EM, Levine A. **2000**. The hypersensitive response facilitates plant infection by the necrotrophic pathogen *Botrytis cinerea*. *Current Biology* **10**: 751–757.

Guan W, Feng J, Wang R, *et al.* 2019. Functional analysis of the exocyst subunit BcExo70 in Botrytis cinerea. *Current Genetics* **66**: 85–95(2020).

Gust AA, Pruitt R, Nürnberger T. **2017**. Sensing danger: key to activating plant immunity. *Trends in Plant Science* **22**: 779–791.

Hain R, Reif H-J, Krause E, *et al.* 1993. Disease resistance results from foreign phytoalexin expression in a novel plant. *Nature* **361**: 153–156.

Harris JM, Balint-Kurti P, Bede JC, *et al.* 2020. What are the Top 10 Unanswered Questions in Molecular Plant-Microbe Interactions? *Molecular Plant-Microbe Interactions®* **33**: 1354–1365.

Ten Have A, Breuil WO, Wubben JP, Visser J, Van Kan JAL. **2001**. *Botrytis cinerea* endopolygalacturonase genes are differentially expressed in various plant tissues. *Fungal Genetics and Biology* **33**: 97–105.

ten Have A, Mulder W, Visser J, Van Kan JAL. **1998**. The endopolygalacturonase gene *Bcpg1* is required to full virulence of *Botrytis cinerea*. *Molecular Plant-Microbe Interactions* **11**: 1009–1016.

ten Have A, Tenberge K, Benen JAE, Tudzynski P, Visser J, van Kan JAL. **2002**. The contribution of cell wall degrading enzymes to pathogenesis of fungal plant pathogens In: *Kempken F. (eds) Agricultural Applications. The Mycota (A Comprehensive Treatise on Fungi as Experimental Systems for Basic and Applied Research)*. Berlin, Heidelberg: Springer Berlin Heidelberg, 341–358.

Heil M, Land WG. **2014**. Danger signals - damaged-self recognition across the tree of life. *Frontiers in Plant Science* **5**: 578.

Höfte H, Voxeur A. **2017**. Plant cell walls. *Current biology* **27**: 865–870.

Hou S, Liu Z, Shen H, Wu D. **2019**. Damage-associated molecular pattern-triggered immunity in plants. *Frontiers in Plant Science* **10**: 646.

Howard RJ, Valent B. **1996**. Breaking and entering: Host penetration by the fungal rice blast pathogen *Magnaporthe grisea*. *Annual Review of Microbiology* **50**: 491–512.

Jayani RS, Saxena S, Gupta R. **2005**. Microbial pectinolytic enzymes: A review. *Process Biochemistry* **40**: 2931–2944.

Jones L, Seymour GB, Knox JP. **1997**. Localization of pectic galactan in tomato cell walls using a monoclonal antibody specific to (1→4)-β-D-galactan. *Plant Physiology* **113**: 1405–1412.

Joubert DA, Kars I, Wagemakers L, *et al.* 2007. A polygalacturonase-inhibiting protein from grapevine reduces the symptoms of the endopolygalacturonase BcPG2 from *Botrytis cinerea* in *Nicotiana benthamiana* leaves without any evidence for in vitro interaction. *Molecular Plant-Microbe Interactions* **20**: 392–402.

Joubert DA, de Lorenzo G, Vivier MA. **2013**. Regulation of the grapevine polygalacturonase-inhibiting protein encoding gene: expression pattern, induction profile and promoter analysis. *Journal of plant research* **126**: 267–81.

Joubert DA, Slaughter AR, Kemp G, *et al.* 2006. The grapevine polygalacturonase-inhibiting protein (*Vv*PGIP1) reduces *Botrytis cinerea* susceptibility in transgenic tobacco and differentially inhibits fungal polygalacturonases. *Transgenic research* **15**: 687–702.

Kalunke RM, Tundo S, Benedetti M, Cervone F, De Lorenzo G, D'Ovidio R. **2015**. An update on polygalacturonase-inhibiting protein (PGIP), a leucine-rich repeat protein that protects crop plants against pathogens. *Frontiers in Plant Science* **6**: 146.

van Kan JAL. **2005**. Infection strategies of *Botrytis cinerea*. *Acta Horticulturae* **669**: 77–90.

van Kan JAL. **2006**. Licensed to kill: the lifestyle of a necrotrophic plant pathogen. *Trends in plant science* **11**: 247–53.

van Kan JAL, Shaw MW, Grant-downton RT. **2014**. *Botrytis species* : relentless necrotrophic thugs or endophytes gone rogue? *Molecular Plant Pathology* **15**: 957–961.

Kars I, Krooshof GH, Wagemakers L, Joosten R, Benen JAE, Van Kan JAL. **2005**. Necrotizing activity of five *Botrytis cinerea* endopolygalacturonases produced in *Pichia pastoris*. *The Plant Journal* **43**: 213–225.

Kelloniemi J, Trouvelot S, Héloir M-C, *et al.* 2015. Analysis of the molecular dialogue between gray mold (*Botrytis cinerea*) and grapevine (*Vitis vinifera*) reveals a clear shift in defense mechanisms during berry ripening. *Molecular Plant-Microbe Interactions* **28**: 1167–1180.

Knox JP, Linstead P., Cooper JPC, Roberts K. **1991**. Developmentally regulated epitopes of cell surface arabinogalactan proteins and their relation to root tissue pattern formation. *The Plant Journal* **1**: 317–326.

Knox JP, Linstead P, King J, Cooper C, Roberts K. **1990**. Pectin esterification is spatially regulated both within cell walls and between developing tissues of root apices. *Planta* **181**: 512–521.

Koroney AS, Plasson C, Pawlak B, *et al.* 2016. Root exudate of *Solanum tuberosum* is enriched in galactose-containing molecules and impacts the growth of *Pectobacterium atrosepticum*. *Annals of Botany* **118**: 797–808.

Leszczuk A, Pieczywek PM, Gryta A, Frąc M, Zdunek A. **2019**. Immunocytochemical studies on the distribution of arabinogalactan proteins (AGPs) as a response to fungal infection in *Malus x domestica* fruit. *Scientific Reports* **9**: 1–15.

Li H, Smigocki AC. **2018**. Sugar beet polygalacturonase-inhibiting proteins with 11 LRRs confer *Rhizoctonia*, *Fusarium* and *Botrytis* resistance in *Nicotiana* plants. *Physiological and Molecular Plant Pathology* **102**: 200–208.

Li L, Yu Y, Zhou Z, Zhou JM. **2016**. Plant pattern-recognition receptors controlling innate immunity. *Science China Life Sciences* **59**: 878–888.

Liang Y, Zhao J, Wang C, Jing Y, Chengyun L, Baldwin TC. **2018**. Infection with blast fungus (*Magnaporthe orzyae*) leads to increased expression of an arabinogalactan-protein epitope in both susceptible and resistant rice cultivars. *Physiological and Molecular Plant Pathology* **102**: 136–143.

Liners F, Letesson J-J, Didembourg C, Van Cutsem P. **1989**. Monoclonal antibodies against pectin. *Plant Physiology* **91**: 1419–1424.

Lionetti V, Fabri E, De Caroli M, *et al.* 2017. Three pectin methylesterase inhibitors protect cell wall integrity for arabidopsis immunity to *Botrytis*. *Plant Physiology* **173**: 1844–1863.

Liu N, Zhang X, Sun Y, *et al.* 2017. Molecular evidence for the involvement of a polygalacturonase-inhibiting protein, GhPGIP1, in enhanced resistance to *Verticillium* and *Fusarium* wilts in cotton. *Scientific Reports* **7**: 39840.

De Lorenzo G, Ferrari S. **2002**. Polygalacturonase-inhibiting proteins in defense against phytopathogenic fungi. *Current Opinion in Plant Biology* **5**: 295–299.

De Lorenzo G, Ferrari S, Cervone F, Okun E. **2018**. Extracellular DAMPs in plants and mammals: immunity, tissue damage and repair. *Trends in Immunology* **39**: 937–950.

Malinovsky FG, Fangel JU, Willats WGT. **2014**. The role of the cell wall in plant immunity. *Frontiers in Plant Science* **5**: 178.

Manabe Y, Nafisi M, Verhertbruggen Y, *et al.* 2011. Loss-of-function mutation of *REDUCED WALL ACETYLATION2* in Arabidopsis leads to reduced cell wall acetylation and increased resistance to *Botrytis cinerea*. *Plant Physiology* **155**: 1068–1078.

Mansfield JW, Richardson A. 1981. The ultrastructure of interactions between *Botrytis* species and broad bean leaves. *Physiological Plant Pathology* **19**: 41-IN23.

Marcus SE, Blake AW, Benians TAS, *et al.* 2010. Restricted access of proteins to mannan polysaccharides in intact plant cell walls. *The Plant Journal* **64**: 191–203.

Marcus SE, Verhertbruggen Y, Hervé C, *et al.* 2008. Pectic homogalacturonan masks abundant sets of xyloglucan epitopes in plant cell walls. *BMC Plant Biology* **8**: 60.

Mareri L, Romi M, Cai G. 2019. Arabinogalactan proteins: actors or spectators during abiotic and biotic stress in plants? *Plant Biosystems* **153**: 173–185.

Di Matteo A, Bonivento D, Tsernoglou D, Federici L, Cervone F. 2006. Polygalacturonase-inhibiting protein (PGIP) in plant defence: a structural view. *Phytochemistry* **67**: 528–33.

Di Matteo A, Federici L, Mattei B, *et al.* 2003. The crystal structure of polygalacturonase-inhibiting protein (PGIP), a leucine-rich repeat protein involved in plant defense. *Proceedings of the National Academy of Sciences of the United States of America* **100**: 10124–8.

McCabe PF, Valentine TA, Forsberg LS, Pennell RI. 1997. Soluble signals from cells identified at the cell wall establish a developmental pathway in carrot. *Plant Cell* **9**: 2225–2241.

McCartney L, Marcus SE, Knox JP. 2005. Monoclonal antibodies to plant cell wall xylans and arabinoxylans. *Journal of Histochemistry and Cytochemistry* **53**: 543–546.

Meikle PJ, Bonig I, Hoogenraad NJ, Clarke AE, Stone BA. 1991. The location of (1→3)-β-glucans in the walls of pollen tubes of *Nicotiana alata* using a (1→3)-β-glucan-specific monoclonal antibody. *Planta* **185**: 1–8.

Mendgen K, Hahn M. 2002. Plant infection and the establishment of fungal biotrophy. *Trends in Plant Science* **7**: 352–356.

Merkouropoulos G, Shirsat AH. 2003. The unusual *Arabidopsis* extensin gene *atExt1* is expressed throughout plant development and is induced by a variety of biotic and abiotic stresses. *Planta* **217**: 356–366.

Moller I, Marcus SE, Haeger A, *et al.* 2008. High-throughput screening of monoclonal antibodies against plant cell wall glycans by hierarchical clustering of their carbohydrate microarray binding profiles. *Glycoconjugate Journal* **25**: 37–48.

Moller I, Sørensen I, Bernal AJ, *et al.* 2007. High-throughput mapping of cell-wall polymers within and between plants using novel microarrays. *The Plant Journal* **50**: 1118–28.

Murashige T, Skoog F. 1962. A revised medium for rapid growth and bio assays with tobacco tissue cultures. *Physiologia Plantarum* **15**: 473–497.

Nguema-Ona E, Moore JP, Fagerström A, *et al.* 2012. Profiling the main cell wall polysaccharides of tobacco leaves using high-throughput and fractionation techniques. *Carbohydrate Polymers* **88**: 939–949.

Nguema-Ona E, Moore JP, Fagerström AD, *et al.* 2013. Overexpression of the grapevine PGIP1 in tobacco results in compositional changes in the leaf arabinoxyloglucan network in the absence of fungal infection. *BMC Plant Biology* **13**: 46.

Nguema-Ona E, Vicré-Gibouin M, Cannesan MA, Driouich A. 2013. Arabinogalactan proteins in root-microbe interactions. *Trends in Plant Science* **18**: 1360–1385.

El Oirdi M, Trapani A, Bouarab K. 2010. The nature of tobacco resistance against *Botrytis cinerea* depends on the infection structures of the pathogen. *Environmental Microbiology* **12**: 239–253.

Park YB, Cosgrove DJ. **2015**. Xyloglucan and its interactions with other components of the growing cell wall. *Plant & Cell Physiology* **56**: 180–94.

Paul Knox J, Peart J, Neill SJ. **1995**. Identification of novel cell surface epitopes using a leaf epidermal-strip assay system. *Planta* **196**: 266–270.

Pedersen HL, Fangel JU, McCleary B, *et al.* 2012. Versatile high resolution oligosaccharide microarrays for plant glycobiology and cell wall research. *Journal of Biological Chemistry* **287**: 39429–39438.

Peng Y, van Wersch R, Zhang Y. **2018**. Convergent and divergent signaling in PAMP-triggered immunity and effector-triggered immunity. *Molecular Plant-Microbe Interactions* **31**: 403–409.

Plett JM, Martin FM. **2018**. Know your enemy, embrace your friend: using omics to understand how plants respond differently to pathogenic and mutualistic microorganisms. *The Plant Journal* **93**: 729–746.

Popper ZA, Fry SC. **2005**. Widespread occurrence of a covalent linkage between xyloglucan and acidic polysaccharides in suspension-cultured angiosperm cells. *Annals of Botany* **96**: 91–99.

Popper ZA, Fry SC. **2008**. Xyloglucan−pectin linkages are formed intra-protoplasmically, contribute to wall-assembly, and remain stable in the cell wall. *Planta* **227**: 781–794.

Prins TW, Tudzynski P, von Tiedemann A, *et al.* 2000. Infection strategies of *Botrytis cinerea* and related necrotrophic pathogens In: *Kronstad J.W. (eds) Fungal Pathology*. Dordrecht: Springer, Dordrecht, The Netherlands, 33–64.

Ralet MC, Crépeau MJ, Vigouroux J, *et al.* 2016. Xylans provide the structural driving force for mucilage adhesion to the Arabidopsis seed coat. *Plant Physiology* **171**: 165–178.

Ralet M-C, Tranquet O, Poulain D, Moïse A, Guillon F. **2010**. Monoclonal antibodies to rhamnogalacturonan I backbone. *Planta* **231**: 1373–1383.

Rashid A. **2016**. Defense responses of plant cell wall non-catalytic proteins against pathogens. *Physiological and Molecular Plant Pathology* **94**: 38–46.

Rijkenberg FHJ, Leeuw GTN De, Verhoeff K. **1980**. Light and electron microscopy studies on the infection of tomato fruits by *Botrytis cinerea*. *Canadian Journal of Botany* **58**: 1394–1404.

Rossi FR, Krapp AR, Bisaro F, Maiale SJ, Pieckenstain FL, Carrillo N. **2017**. Reactive oxygen species generated in chloroplasts contribute to tobacco leaf infection by the necrotrophic fungus *Botrytis cinerea*. *The Plant Journal* **92**: 761–773.

Ryder LS, Talbot NJ. **2015**. Regulation of appressorium development in pathogenic fungi. *Current Opinion in Plant Biology* **26**: 8–13.

Saijo Y, Loo EP. **2020**. Plant immunity in signal integration between biotic and abiotic stress responses. *New Phytologist* **225**: 87–104.

Saijo Y, Loo EP iian, Yasuda S. **2018**. Pattern recognition receptors and signaling in plant–microbe interactions. *Plant Journal* **93**: 592–613.

Shah P, Powell ALTT, Orlando R, Bergmann C, Gutierrez-Sanchez G. **2012**. Proteomic analysis of ripening tomato fruit infected by *Botrytis cinerea*. *Journal of Proteome Research* **11**: 2178–92.

Sham A, Moustafa K, Al-Shamisi S, Alyan S, Iratni R, AbuQamar S. **2017**. Microarray analysis of Arabidopsis WRKY33 mutants in response to the necrotrophic fungus *Botrytis cinerea*. *PLoS ONE* **12**.

Shlezinger N, Minz A, Gur Y, *et al.* 2011. Anti-apoptotic machinery protects the necrotrophic fungus *Botrytis cinerea* from host-induced apoptotic-like cell death during plant infection. *PLoS Pathogens* **7**: e1002185.

Showalter AM. **2001**. Arabinogalactan-proteins: structure, expression and function. *Cellular and Molecular Life Sciences* **58**: 1399–1417.

Sicilia F, Fernandez-Recio J, Caprari C, *et al.* 2005. The polygalacturonase-inhibiting protein PGIP2 of *Phaseolus vulgaris* has evolved a mixed mode of inhibition of endopolygalacturonase PG1 of *Botrytis cinerea*. *Plant Physiology* **Vol. 139**: 1380–1388.

Smallwood M, Beven A, Donovan N, *et al.* 1994. Localization of cell wall proteins in relation to the developmental anatomy of the carrot root apex. *The Plant Journal* **5**: 237–246.

Smallwood M, Martin H, Knox JP. **1995**. An epitope of rice threonine- and hydroxyproline-rich glycoprotein is common to cell wall and hydrophobic plasma-membrane glycoproteins. *Planta* **196**: 510–522.

Smallwood M, Yates EA, Willats WGT, Martin H, Knox JP. **1996**. Immunochemical comparison of membrane-associated and secreted arabinogalactan-proteins in rice and carrot. *Planta* **198**: 452–459.

Soltis NE, Atwell S, Shi G, *et al.* 2019. Interactions of tomato and *Botrytis cinerea* genetic diversity: Parsing the contributions of host differentiation, domestication, and pathogen variation. *Plant Cell* **31**: 502–519.

Sowley ENKK, Shaw MW, Dewey FM, Shaw MW. **2009**. Persistent, symptomless, systemic, and seed-borne infection of lettuce by *Botrytis cinerea*. *European Journal of Plant Pathology* **126**: 61–71.

Spadoni S, Zabotina O, Di Matteo A, *et al.* 2006. Polygalacturonase-inhibiting protein interacts with pectin through a binding site formed by four clustered residues of arginine and lysine. *Plant Physiology*.

Tormo J, Lamed R, Chirino AJ, *et al.* 1996. Crystal structure of a bacterial family-III cellulose-binding domain: a general mechanism for attachment to cellulose. *The EMBO Journal* **15**: 5739–5751.

Toruño TY, Stergiopoulos I, Coaker G. **2016**. Plant-pathogen effectors: cellular probes interfering with plant defenses in spatial and temporal manners. *Annual Review of Phytopathology* **54**: 419–441.

Trdá L, Boutrot F, Claverie J, Brulé D, Dorey S, Poinssot B. **2015**. Perception of pathogenic or beneficial bacteria and their evasion of host immunity: pattern recognition receptors in the frontline. *Frontiers in Plant Science* **6**: 219.

Tudzynski P, Kokkelink L. **2009**. *Botrytis cinerea*: Molecular aspects of a necrotrophic life style In: Deising HB, ed. *Deising H.B. (eds) Plant Relationships. The Mycota (A Comprehensive Treatise on Fungi as Experimental Systems for Basic and Applied Research),*. Springer, Berlin, Heidelberg, 29–50.

Valero-Jiménez CA, Veloso J, Staats M, Van Kan JAL. **2019**. Comparative genomics of plant pathogenic *Botrytis* species with distinct host specificity. *BMC Genomics* **20**: 1–12.

Veloso J, van Kan JAL. **2018**. Many shades of grey in *Botrytis*–Host plant interactions. *Trends in Plant Science* **23**: 613–622.

Verhertbruggen Y, Marcus SE, Haeger A, Verhoef R, *et al.* 2009. Developmental complexity of arabinan polysaccharides and their processing in plant cell walls. *The Plant Journal* **59**: 413–425.

Verhertbruggen Y, Marcus SE, Haeger A, Ordaz-Ortiz JJ, Knox JP. **2009**. An extended set of monoclonal antibodies to pectic homogalacturonan. *Carbohydrate Research* **344**: 1858–1862.

Vorwerk S, Somerville S, Somerville C. **2004**. The role of plant cell wall polysaccharide composition in disease resistance. *Trends in Plant Science* **9**: 203–209.

Wei G, Shirsat AH. **2006**. Extensin over-expression in *Arabidopsis* limits pathogen invasiveness. *Molecular Plant Pathology* **7**: 579–592.

Weiller F, Gerber L, Trygg J, *et al.* 2020. Overexpression of VviPGIP1 and NtCAD14 in tobacco screened using glycan microarrays reveals cell wall reorganisation in the absence of fungal infection. *Vaccines* **8**: 388.

Willats WGT, Marcus SE, Knox JP. **1998**. Generation of a monoclonal antibody specific to (1→5)-α-l-arabinan. *Carbohydrate Research* **308**: 149–152.

Willats WGT, McCartney L, Steele-King CG, *et al.* 2004. A xylogalacturonan epitope is specifically associated with plant cell detachment. *Planta* **218**: 673–681.

Williamson B, Tudzynski B, Tudzynski P, van Kan JAL. **2007**. *Botrytis cinerea*: the cause of grey mould disease. *Molecular Plant Pathology* **8**: 561–580.

Wolf S. **2017**. Plant cell wall signalling and receptor-like kinases. *Biochemical Journal* **474**: 471–492.

Wu Y, Fan W, Li X, *et al.* 2017. Expression and distribution of extensins and AGPs in susceptible and resistant banana cultivars in response to wounding and *Fusarium oxysporum*. *Scientific Reports* **7**: 42400.

Wubben JP, Ten Have A, Van Kan JAL, Visser J. **2000**. Regulation of endopolygalacturonase gene expression in *Botrytis cinerea* by galacturonic acid, ambient pH and carbon catabolite repression. *Current Genetics* **37**: 152–157.

Yates EA, Valdor J-F, Haslam SM, *et al.* 1996. Characterization of carbohydrate structural features recognized by anti-arabinogalactan-protein monoclonal antibodies. *Glycobiology* **6**: 131–139.

York WS, Darvill AG, McNeil M, Stevenson TT, Albersheim P. **1986**. Isolation and characterization of plant cell walls and cell wall components. *Methods in Enzymology* **118**: 3–40.

Zang H, Xie S, Zhu B, *et al.* 2019. Mannan oligosaccharides trigger multiple defence responses in rice and tobacco as a novel danger-associated molecular pattern. *Molecular Plant Pathology* **20**: 1067–1079.

Zhang W, Corwinand JA, Copeland D, *et al.* 2017. Plastic transcriptomes stabilize immunity to pathogen diversity: The jasmonic acid and salicylic acid networks within the *Arabidopsis/Botrytis* pathosystem open. *Plant Cell* **29**: 2727–2752.

Zhu W, Ronen M, Gur Y, *et al.* 2017. BcXYG1, a secreted xyloglucanase from *Botrytis cinerea*, triggers both cell death and plant immune responses. *Plant Physiology* **175**: 438–456.

Zykwinska AW, Thibault J-F, Ralet M-C. **2007**. Organization of pectic arabinan and galactan side chains in association with cellulose microfibrils in primary cell walls and related models envisaged. *Journal of Experimental Botany* **58**: 1795–1802.

Chapter 5

Research chapter 3

Tracking cell wall changes in wine and table grapes undergoing *Botrytis cinerea* infection using glycan microarrays

This chapter was submitted for publication in **Annals of Botany** and has been formatted according to their guideline rules

Tracking cell wall changes in wine and table grapes undergoing *Botrytis cinerea* infection using glycan microarrays

Florent Weiller [1], Julia Schückel [2#], William G.T. Willats [3], Azeddine Driouich [4], Melané A. Vivier [1], John P. Moore [1*]

[1] *South African Grape and Wine Research Institute, Department of Viticulture and Oenology, Stellenbosch University, South Africa*

[2] *Department of Plant and Environmental Sciences, University of Copenhagen, Copenhagen, Denmark*

[3] *School of Agriculture, Food and Rural Development, Newcastle University, Newcastle-upon-Tyne, United Kingdom*

[4] *Université de ROUEN Normandie, Laboratoire de Glycobiologie et Matrice Extracellulaire Végétale, UPRES-EA 4358, Fédération de Recherche « Normandie-Végétal » - FED 4277, F-76821 Mont-Saint-Aignan, France*

#Present Address: DKMS Life Science Lab, Germany

***For correspondence:** moorejp@sun.ac.za

Abstract

Background and Aims: The necrotrophic fungus *Botrytis cinerea* infects a broad range of fruit crops including domesticated grapevine *Vitis vinifera* cultivars. Damage caused by this pathogen is severely detrimental to the table and wine grape industries and results in substantial crop losses worldwide. The apoplast and cell wall interface is an important setting where many plant-pathogen interactions take place and where some defence related messenger molecules are generated. Limited studies have investigated changes in grape cell wall composition upon infection with *Botrytis cinerea* with much being inferred from studies on other fruit crops.

Methods: In this study, comprehensive microarray polymer profiling in combination with monosaccharide compositional analysis was applied for the first time to investigate cell wall compositional changes in the berries of wine (Sauvignon Blanc and Cabernet Sauvignon) and table (Dauphine and Barlinka) grape cultivars during *Botrytis* infection and tissue maceration. This was used in conjunction with scanning electron microscopy (SEM) and X-ray computed tomography (CT) to characterise infection progression.

Key Results: At véraison, infected grapes did not develop visible infection symptoms, whereas grapes inoculated at the post-véraison and ripe stages showed evidence of significant tissue degradation. The latter was characterised by a reduction in signals for pectin epitopes in the berry cell walls, implying the degradation of pectin polymers. The table grape cultivars showed more severe infection symptoms, and corresponding pectin depolymerisation, compared to wine grape cultivars. In both grape types, hemicellulose layers were largely unaffected, as were the arabinogalactan protein content, whereas in moderate to severely infected table grape cultivars, evidence of extensin epitope deposition was present.

Conclusions: Specific changes in grape cell wall compositional profiles appear to correlate with fungal disease susceptibility. Cell wall factors important in influencing resistance may include pectin methylesterification profiles, as well as altered hemicellulose and extensin reorganisation.

Key words: *Vitis vinifera*, *Botrytis cinerea*, grey rot, grapes, cell wall, pectin

INTRODUCTION

Grapes (*Vitis vinifera* and associated spp.) are arguably the world's most important fruit crop, grown globally for table grape and raisin production, with wine grape cultivars converted into products such as wine, vinegar and grape seed oil. In 2018, over 7.4 million hectares of vineyards have been cultivated globally yielding 77.8 million tonnes of fresh grapes and a further 292 million hectolitres of wine produced (OIV; International Organisation of Vine and Wine, http://www.oiv.int/). However, grape yields are severely curtailed by disease pressure both before harvest and during post-harvest storage and transport (Wilcox *et al.* 2015; Sonker *et al.* 2016). Most grape producers and wineries invest in pesticide and fungicide spraying programmes to control disease spread and limit damage during the season and after harvest. However, chemical fungicides are often not environmentally friendly and display unwanted toxicity to humans and animals. There is a strong movement to limit or eliminate the use of toxic chemicals in vineyard management strategies, but finding suitable replacement practises are challenging for various reasons.

One approach, which is becoming more mainstream, is to develop products which act by enhancing the plant's own innate immunity to disease causing organisms such as fungi. Many of these molecules have dual roles as either having direct anti-fungal roles or as elicitors, thereby triggering defence responses in plants. For example, peptides identified and cloned from grapevine such as VviAMP1 display antifungal properties against *Fusarium oxysporum* and *Verticillium dahlia* whereas VviAMP2 shows strong action against *Botrytis*

cinerea (De Beer and Vivier 2008; Nanni *et al.* 2014). Three *V. vinifera* endo-β-1,3-glucanases, pathogenesis-related (PR) proteins have recently been identified as belonging to the PR-2 family, and have been shown to have antimicrobial activity, tested *in vitro* against *Plasmopara viticola*, the oomycete responsible for downey mildew (Mestre *et al.* 2017). In addition to peptides and proteins; plant phenolics such as resveratrol, a stilbene phytoalexin which possesses anti-cancer, anti-diabetes and anti-aging properties also functions in grapevine pathogen defence pathways (Pasinetti *et al.* 2015; Singh *et al.* 2015).

B. cinerea is a "probably ubiquitous" necrotrophic fungus responsible for grey mould disease (van Kan *et al.* 2014). It colonises a broad range of hosts including grapevine with severe impacts worldwide with respect to crop losses (Elad *et al.* 2015). Numerous distinct Botrytis species and *B. cinerea* strains have been isolated from fruit crops and shown to display variation in host specificity, as well as infection strategies dependent on the host immune system response (Valero-Jiménez *et al.* 2019; Zhang *et al.* 2019; Soltis *et al.* 2019). Botrytis is also capable to remain dormant or to colonise tissue, such as flowers, asymptomatically and thereafter exit this quiescent phase when conditions become more favourable, such as during fruit ripening (Pezet *et al.* 2003; Mehari *et al.* 2017; Emmanuel *et al.* 2018; Petrasch *et al.* 2019).

B. cinerea early infection is coincident with a short biotrophic phase where the fungus inhibits plant immune responses using small RNAs in order to first develop its biomass (Weiberg *et al.* 2013; Veloso and van Kan 2018). When the fungal biomass reaches a critical point, Botrytis can switch to a necrotrophic 'lifestyle'. Its infection strategies usually involve secretion of numerous pectinolytic enzymes in order to breach plant cell walls and cause tissue maceration (Tudzynski and Kokkelink 2009; Blanco-Ulate *et al.* 2014). In addition, secondary metabolites are secreted which will trigger the hypersensitive plant immune response resulting in apoptosis ultimately aiding the necrotrophic invasion (van Kan 2006). Necrotrophic fungi, such as Botrytis, secrete cell wall degrading enzymes, proteases, reactive oxygen species (ROS) and ROS scavengers, phytotoxic components, secondary metabolites and membrane transporters (Kelloniemi *et al.* 2015).

During noble rot infection, *B. cinerea* has been shown to downregulate some oxidative stress genes and pathways leading to Botrydial and Botcinic acid production, two phytotoxins essential for virulence (Lovato *et al.* 2019). In the case of véraison stage grapes versus ripe mature berries, Botrytis shows variable infection success with generally lower levels of infection at the véraison phase. This is however genotype dependent, since some cultivars are susceptible at this developmental stage, while others display some relative resistance (Kelloniemi *et al.* 2015; Paňitrur-De La Fuente *et al.* 2018).

From the plant's perspective, grapevine is able to mount a resistance response upon challenge with a pathogen (i.e. Botrytis) or elicitor substance. Upon elicitation with *B. cinerea* generated oligogalacturonides, Cabernet Sauvignon plants were shown to accumulate defence related mRNA transcripts in conjunction with increased resistance to downy and powdery mildew (Saigne-Soulard *et al.* 2015). Upon Botrytis infection, green and véraison berries from Trincadeira were shown to reprogram their lipid and carbohydrate metabolism leading to increased secondary metabolite production (Agudelo-Romero *et al.* 2015). These changes were linked to ethylene and jasmonic acid mediated pathways (Agudelo-Romero *et al.* 2015). The jasmonic pathway was also activated during noble rot with the accumulation of secondary metabolites (Blanco-Ulate, Amrine, *et al.* 2015), showcasing the importance of phytohormone pathways in plant-pathogen interactions and specificity (Nafisi *et al.* 2015; Molina *et al.* 2020). Phytohormones are also essential in fruits ripening and mediate fruit softening through upstream plant enzymes regulation, like with polygalacturonases leading to pectin depolymerisation. This process is also crucial during plant-pathogen interaction as extensively described in tomato fruits (Blanco-Ulate *et al.* 2016). In grapes, a non-climacteric fruit, salicylic acid, jasmonates and indole-3-acetic acid are involved in ripening and *B. cinerea* infections responses (Coelho *et al.* 2019). If *B. cinerea* is able to hijack these pathways to its advantage, products of degradation of its numerous cell wall degrading enzymes are perceived by the plants and can lead to the activation of specific responses (Blanco-Ulate, Labavitch, *et al.* 2015; Engelsdorf *et al.* 2018).

However, little is known about how the grape berry cell wall composition changes before, during and after *B. cinerea* infection. This study 'tracked' two wine (Cabernet Sauvignon and Sauvignon Blanc) and two table (Barlinka and Dauphine) grape cultivars following deliberate *B. cinerea* infection under controlled conditions. Glycan microarray technology was used to assess véraison, post-véraison and ripe fruit cell wall composition by virtue of a selection of key epitopes recognised by a variety of probes. Patterns of de-pectination, leading to hemicellulose uncovering, and glycoprotein deposition or reorganisation varied between stages of infection, fruit maturity and the cultivars in question.

MATERIALS AND METHODS

Plant material and sampling

Grapes (*Vitis vinifera*) were harvested and sourced from four commercial cultivars, namely; the wine grapes Cabernet Sauvignon and Sauvignon Blanc, and the table grapes Dauphine and Barlinka. Cabernet Sauvignon grapes were sourced from the Welgevallen Experimental Farm of the Department of Viticulture and Oenology at Stellenbosch University situated at

33°56′42″S, 18°51′44″E. Sauvignon Blanc grapes were sourced from a vineyard located at 34°9′52.19″S; 19°0′57.48″E in the Elgin region (Western Cape, South Africa). The table grape cultivars Dauphine and Barlinka were sourced from the De Doorns Experimental Farm in the Hex River Valley (Western Cape, South Africa). Grapes were harvested at three different stages of sugar ripeness; namely at véraison (when grapes start to colour and soften), at post-véraison and at ripe stage (ready for winemaking or consumption). To determine these stages, the colour, firmness and sugar levels (°B) of the grapes were regularly assessed, as well as classified according to the modified Eichhorn and Lorenz (EL) growth scale (Coombe 1995). Wine grapes at 15-16 °B, corresponding to the EL-35 stage , were considered to be at véraison, while at 18-20 °B (EL-36) they were classed as post-véraison and at 22-25 °B (EL-38) they were considered ripe (ready for harvest). Table grapes at 14 °B (EL-35) were classed at véraison, at 18 °B (EL-36) as post-véraison and above 21 °B (EL-38) as harvest ripe. All grape bunches were randomly handpicked in the fields after verifying the absence of disease or mechanical damage.

Botrytis cinerea spore cultivation

B. cinerea spores previously isolated from a South African vineyard, described in Joubert et al. (2006) as the grape strain and characterised by Rowe and Kliebenstein (2008) were used for infection experiments. The BO.5.10 strain, genome sequenced model isolate, was also used for certain experiments (Van Kan *et al.* 2017). The spores, stored at -80 °C as 50 % (v/v) glycerol stocks, were transferred onto sterile apricot halves (Naturlite, Tiger Food Brands Limited, South Africa) that were placed on petri dishes and treated with UV irradiation for 30 min in lamina flow hoods. The petri plates were sealed using adhesive tape and placed in the dark for two weeks at 23 °C to induce sporulation for the grape strain and placed under artificial light for BO.5.10. Spores were harvested with sterile water and filtered through glass wool filled tips to remove fungal hyphae and debris. Spores were re-suspended twice in sterile water after brief centrifugation. Spore viability was assessed on a 0.8 % (w/v) water agar plate by calculating percentage germination after 12 h at 23 °C.

Botrytis cinerea infection of grapes

Grapes were individually separated from an intact bunch (cluster) by cutting the rachis with a scalpel to leave a short pedicel still attached to each grape berry. 16 visibly healthy and undamaged grape berries from the same bunch were pooled together to represent one sample, and surface sterilised with 70 % ethanol (reagent grade) for 30 seconds, then with 0.5 % sodium hypochlorite solution for 3 minutes and finally rinsed three times (5 minutes

each) with autoclaved MilliQ water. The grapes were then dried on sterile tissue paper in a laminar flow hood. Thereafter the grapes were placed on 24 well ELISA plates in sterile Tupperware lunch boxes with wetted tissue-paper in order to create a humid atmosphere. The Tupperware boxes were placed in a plant infection room (16 h photoperiod at 23 °C) two hours before the start of the infection. *B. cinerea* spores harvested the day before were inoculated as a 2 µL droplet containing 2000 spores onto each grape berry (without creating a wound). Mock controls were inoculated using droplets of distilled water. For each time point, one mock and seven samples were harvested per cultivar (i.e. 128 berries). For the ripe table grapes, positive (infection) controls were produced by dipping grapes in chloroform to remove the protective waxy layer before infection.

Sampling from the infections proceeded as follows: For the ripe grape infection, grape samples (i.e. 16 berries from the same bunch) were sampled at T0 and then every 72 hours post infection (hpi) or 3 days until day 12. For the post-véraison infection, considering the limited number of infected grapes, grapes were not sampled according to time but were sorted according to infection severity (divided into four groups) after the end of the experiment (12 days post infection). These groups were no-infection (Ni), light infection (Li) when fungal mycelia were covering the top of the grapes around the infection spot, mild or moderate infection (Mi) when the mycelium was covering more than 30 % of the grape surface and high infection (Hi) when the mycelium was covering more than 50 % of the grape surface (also see supplementary file Figure S1).

Cell wall isolation protocol

Grapes uninfected, infected or mock infected were sampled and processed to yield alcohol insoluble residues (AIR) as outlined in Moore et al. (2014). Grapes were flash frozen using liquid nitrogen and ground to a fine powder using a Retsch Mixer Mill (30 rounds per minute, 60 seconds, Retsch, Haan, Germany). Ground tissue was boiled for 20 min in 80 % v/v aqueous ethanol to deactivate any endogenous enzymes. After centrifugation, the insoluble residue or pellet was subjected to a series of solvent washes using methanol (twice); (1:1) methanol/chloroform solution (twice) followed by acetone and then partial air-drying of the pellet. The pellet was re-suspended in water and freeze-dried to obtain cell wall AIR. All solvents used were of reagent grade (Sigma-Aldricht, MO, USA). A flow diagram showing the different experiments conducted after obtaining AIR is available as supplementary material (Figure S2).

Gas Chromatography – Mass Spectrometry for monosaccharide composition

Monosaccharide composition of the grape berry AIR was determined using *Gas Chromatography – Mass Spectrometry* (GC-MS) according to York et al., (1986) with some modifications. Five mg of AIR was hydrolysed with 2M trifluoroacetic acid (TFA) at 110 °C for 2 h. The free monosaccharides were derivatised and converted to methoxy sugars using 1 M methanolic HCl at 80 °C for 16 h. Thereafter, silylation was performed at 80 °C for 20 min with the Sylon HTP (Hexamethyldisilazane (HMDS) + Trimethylsilyl chloride (TMCS) + Pyridine (3:1:9)) kit (Sigma-Aldrich, MO, USA) to produce trimethyl-silyl-glycosides which were dissolved in cyclohexane. A gas chromatograph Agilent 6890 N (Agilent, Palo Alto, CA) using a polar (95 % dimethylpolysiloxane) 7HG-G027-11 GC column coupled to an Agilent 5975 MS mass spectrometer detector was used for analysis. Helium was used as carrier gas with a flow rate of 1 ml/min. The injector temperature was maintained at 280 °C in a splitless mode. Mass spectral data were recorded on a Mass Selective Detector operated in full scan mode (40-650 m/z). Nine common cell wall monosaccharides were measured: arabinose (Ara), rhamnose (Rha), fucose (Fuc), xylose (Xyl), mannose (Man), galacturonic acid (GalA), galactose (Gal), glucose (Glc) and glucuronic acid (GlcA). Myo-inositol was used as internal standard. The software Xcalibur (Thermo Fisher Scientific Inc., MA, USA) was used for peaks integration and quantification and results were expressed in molar percentage. Samples were run as triplicates and separated into different statistical groups with an ANOVA followed by a Tukey's test with $p \leq 0,05$.

Comprehensive microarray polymer profiling for polysaccharides and proteins

Comprehensive microarray polymer profiling (CoMPP) of grape berry AIR was performed as described in Kračun et al., (2017). Ten mg of AIR per sample was extracted first using a cyclohexane diamine tetra acetic acid (CDTA) solution for pectins and thereafter a NaOH solution which mainly liberates hemicellulose polymers. These CDTA and NaOH extracts are then spotted on nitrocellulose membranes and probed with a selection of monoclonal antibodies (mAbs) and carbohydrate binding modules (CBMs) (presented in Table 1). These mAbs and CBMs target different classes of cell wall polysaccharides (e.g. pectins, xyloglucans, xylans) and proteins (e.g. arabinogalactan proteins and extensins) epitopes. Datasets are presented as heatmaps with a range varying from 100 to 5 where the highest value is set at 100 and the other values adjusted accordingly with a cut-off value of 5 imposed at the lower end. Véraison and post-véraison data represent the average of two samples, whereas an average of six samples was used for the ripe grape datasets. Measurements were also imported into multivariate data analysis software SIMCA 14

(Umetrics, Sartorius Stedim Biotech, Germany) for principal component analysis (PCA) of the raw datasets conducted in an unsupervised manner and looking at the first four dimensions generated.

Scanning electron microscopy of the grape surface

Scanning electron microscope micrograph images were acquired using a Zeiss (LEO) 1450VP SEM equipped with Lanthanum Hexaboride (LaB_6) Filaments, an Energy Dispersive X-ray Spectrometer and a Backscattered Electron Detector. A cryo-chamber is mounted on the system with a Fisons transfer unit. Prior to observation, the samples were gold-coated. Observations were made using type I secondary electron signals at 10.0 kV.

X-ray computed tomography (CT)

X-ray computed tomography scans (CT scanning) were conducted with a microCT instrument, (General Electric Sensing and Inspection Technologies/Phoenix X-ray, Wunstorff, Germany). Each sample was recorded with a voltage of 50 kV and a current of 350 µA. 2400 images were acquired in 750 ms with a 360° rotation of each sample. Further information on the methodology is outlined in du Plessis et al. (2016). The images obtained from the scans were processed using VGSTUDIO MAX 3.0 software (Volume Graphics, Heidelberg, Germany). An infected ripe grape from Cabernet Sauvignon, Sauvignon Blanc, Dauphine and Barlinka cultivars were scanned at 36, 72 and 108 hpi.

Univariate statistical and multivariate data analysis

Sample statistical significance was assessed using the univariate statistical analysis software Statistica 10 (Statsoft Analytics, Sandton, South Africa) with a two-way ANOVA followed by a Tukey's test conducted on the GC-MS results after confirming that samples follow a normal distribution, with $P \leq 0.05$. Multivariate analysis was performed using the SIMCA 14 software package (Umetrics, Sartorius Stedim Biotech, Germany).

RESULTS

Visual observations of infection progression of Botrytis cinerea on grapes

Infection experiments were conducted on the white wine grape Sauvignon Blanc and the black wine grape Cabernet Sauvignon (see Figure 1), both commercially important cultivars in the global wine industry. In addition, experiments were also conducted on the white table grape Dauphine and the black table grape Barlinka (see Figure 2), both important cultivars in the South African table grape industry. All four grape cultivars tested were sensitive to *B.*

cinerea. Infection experiments using the *B. cinerea* BO.5.10, the first genome sequenced strain, and a hypervirulent grape strain (see Joubert et al., 2006) were conducted on grapes at different developmental stages in the ripening period (i.e. véraison, post-véraison, and ripe). The first experiment was conducted on grapes at the onset of ripening at the véraison stage, but very little to no infections developed successfully (see supplementary Figure S3 for a representative box of véraison infected Barlinka grapes showing the absence of successful infection development). Post-véraison grapes, between 18-20 °B (or EL-36/37), also showed very little infection 'take' with only few grapes developing symptoms when challenged with *B. cinerea* (see supplementary Figure S1). The final set of infection experiments were performed on harvest ripe grapes (see Figure 1 and Figure 2, and Supplementary Table 1) which developed clear infections, which were then monitored over a period of 216 to 288 hpi.

For the ripe Sauvignon Blanc and Cabernet Sauvignon grapes, the 24 hpi time-point did not show any visible evidence of infection compared to the mock infection controls (Figure 1, Table S1). At 48 hpi, Sauvignon Blanc displayed some grapes where infection had begun to set in, as seen by visible mycelia, whereas Cabernet Sauvignon did not show any infection symptoms. At 72 hpi, about 20 % of the Sauvignon Blanc grapes showed signs of infection with white hyphae developing around the inoculation point, described as lightly infected (the supplementary Table S1 includes percentage of the grape infection levels per time point for the four grape cultivars).

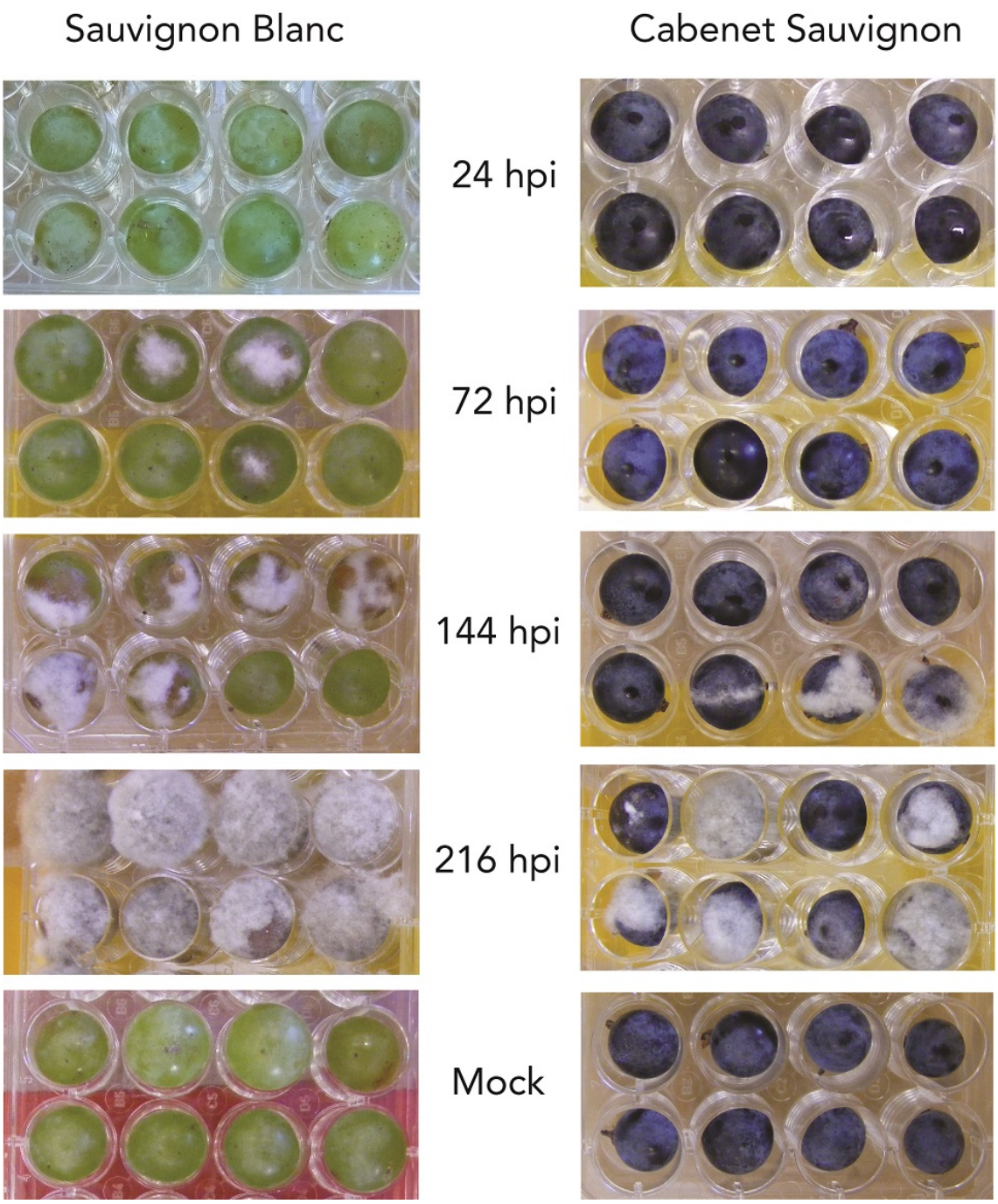

Figure 1: Photographs of representative Sauvignon Blanc and Cabernet Sauvignon ripe grapes (EL-38) infected by *B. cinerea* over time.

Cabernet Sauvignon still did not show any infectious symptoms at 72 hpi but by 144 hpi it had almost reached the number of Sauvignon Blanc infected grapes with 30 % of infected grapes, albeit with lighter severity. At 144 hpi, the infected Sauvignon Blanc grapes became brown and necrotised under the hyphal network that covered the berry surfaces (moderately infected). The Cabernet Sauvignon grapes seemed to take longer to develop infections than the Sauvignon Blanc grapes and had around 18 % of grapes becoming highly infected at 216 hpi while 48 % of Sauvignon Blanc grapes already had most of their surface covered

with mycelium (highly/severely infected). At 288 hpi (not shown) Sauvignon Blanc and Cabernet Sauvignon grapes showed similar infection level and *Botrytis* had developed a white mycelium over the grapes, indicating a full-blown grey rot infection. In both cultivars, it was observed that about 20 % of the grapes remained uninfected even after 288 hpi.

The table grapes Dauphine and Barlinka similarly (to the wine grapes) did not show symptoms after 24 hpi (Figure 2 and Table S1). The first signs of infection on individual grapes appeared at 48 and 72 hpi as limited hyphae from the top of the inoculation point (lightly infected). From 72 hpi the infections began taking over more of the grapes so that almost a third of the grapes displayed signs of infection, particularly evidence of white mycelium over the grape surface was visible. Evidence of tissue browning in the Dauphine cultivar was present beneath the white mycelium. From 144 hpi more than 35 % of the grapes were moderately to highly infected for both cultivars. At 216 hpi, more than 60 % of Dauphine and Barlinka grapes showed signs of infection with some grapes completely covered in white mycelium representing 36 % (Dauphine) to 48 % (Barlinka) of grapes being highly infected. The development of white mycelium was asynchronous for both Dauphine and Barlinka, and even after 216 hpi some grapes did not seem to have developed an infection. No difference between the BO.5.10 and the grape strains in term of symptom severity or cell wall compositional difference were observed (see supplementary Figure S4 for a CoMPP analysis showing the absence of strain cell wall compositional differences).

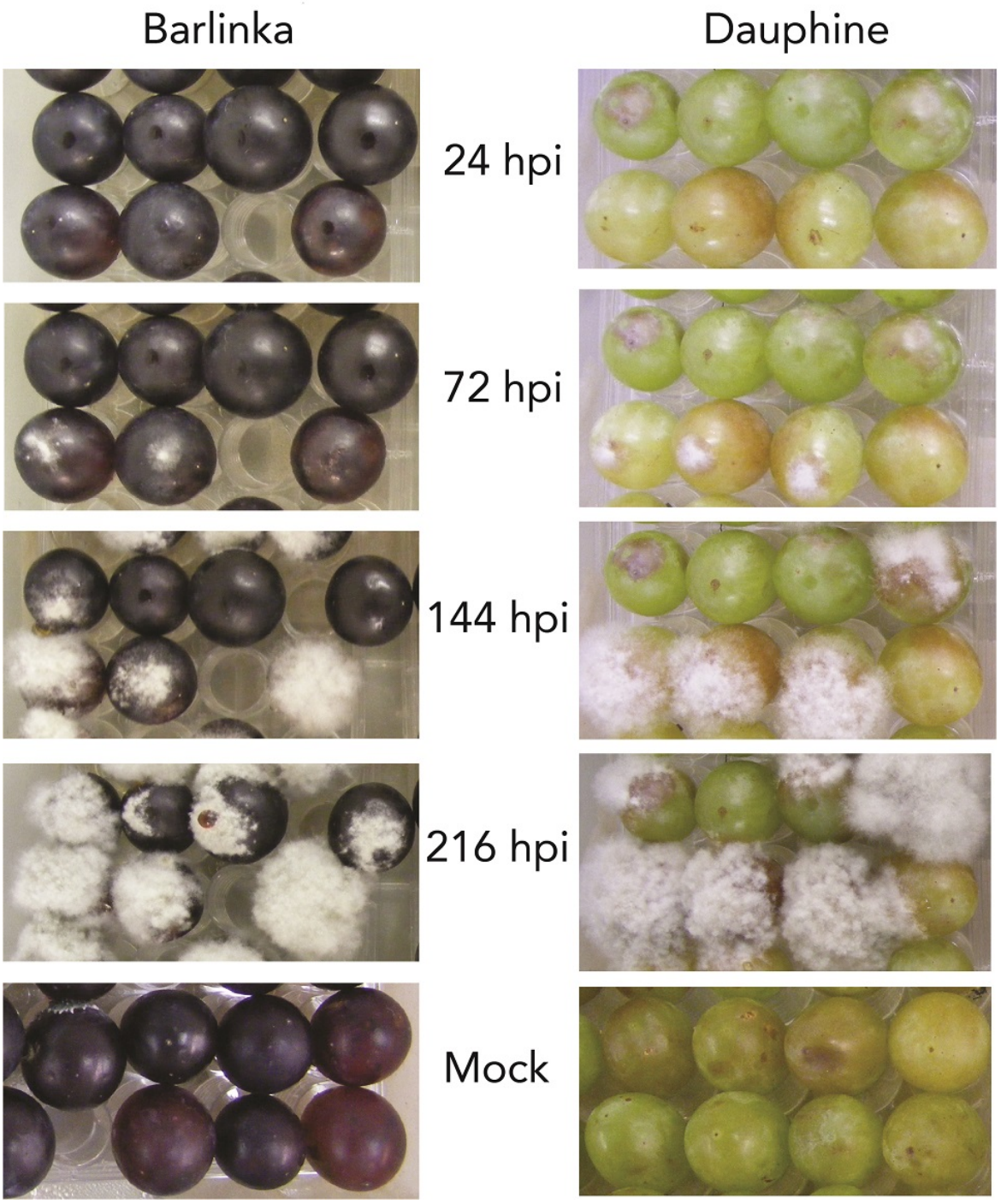

Figure 2: Photographs of representative Barlinka and Dauphine ripe grapes (EL-38) infected by *B. cinerea* over infection progression.

Higher magnification images were taken with a binocular microscope at the beginning of the infection (at 48 hpi for Sauvignon Blanc, Dauphine and Barlinka grapes and at 216 hpi for Cabernet Sauvignon – see Figure 3). Infection symptoms consisted of a hyphal network developing on the surface of the grapes, usually starting from the spore inoculation point. For the white grape cultivars Sauvignon Blanc and Dauphine, brown tissue under the inoculation point and the fungal structures revealed evidence of a necrotic lesion present.

For Sauvignon Blanc and Cabernet Sauvignon grapes, a droplet of juice was notably present having been released presumably where the fungus had breached the grape surface and was accompanied by a white mycelium. For Dauphine and Barlinka, as compared to the wine grapes, the infection seemed to be more localised at the infection droplet and then enlarged from there.

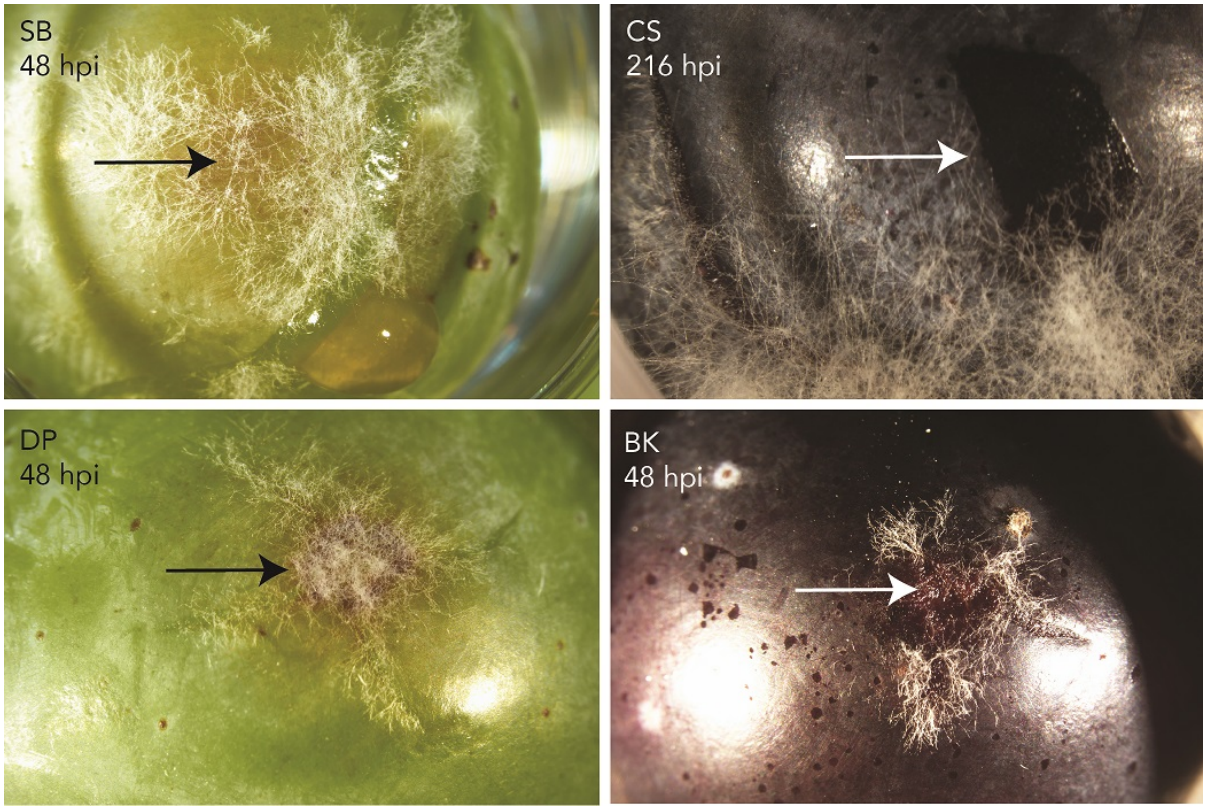

Figure 3: Micrographs of *B. cinerea* infection at the surface of Sauvignon Blanc (SB), Cabernet Sauvignon (CS), Dauphine (DP) and Barlinka (BK) grapes observed under binocular microscope. SB, DP and BK were observed at 48 hpi, whereas, CS was observed 216 hpi to have lesions at a comparable stage.

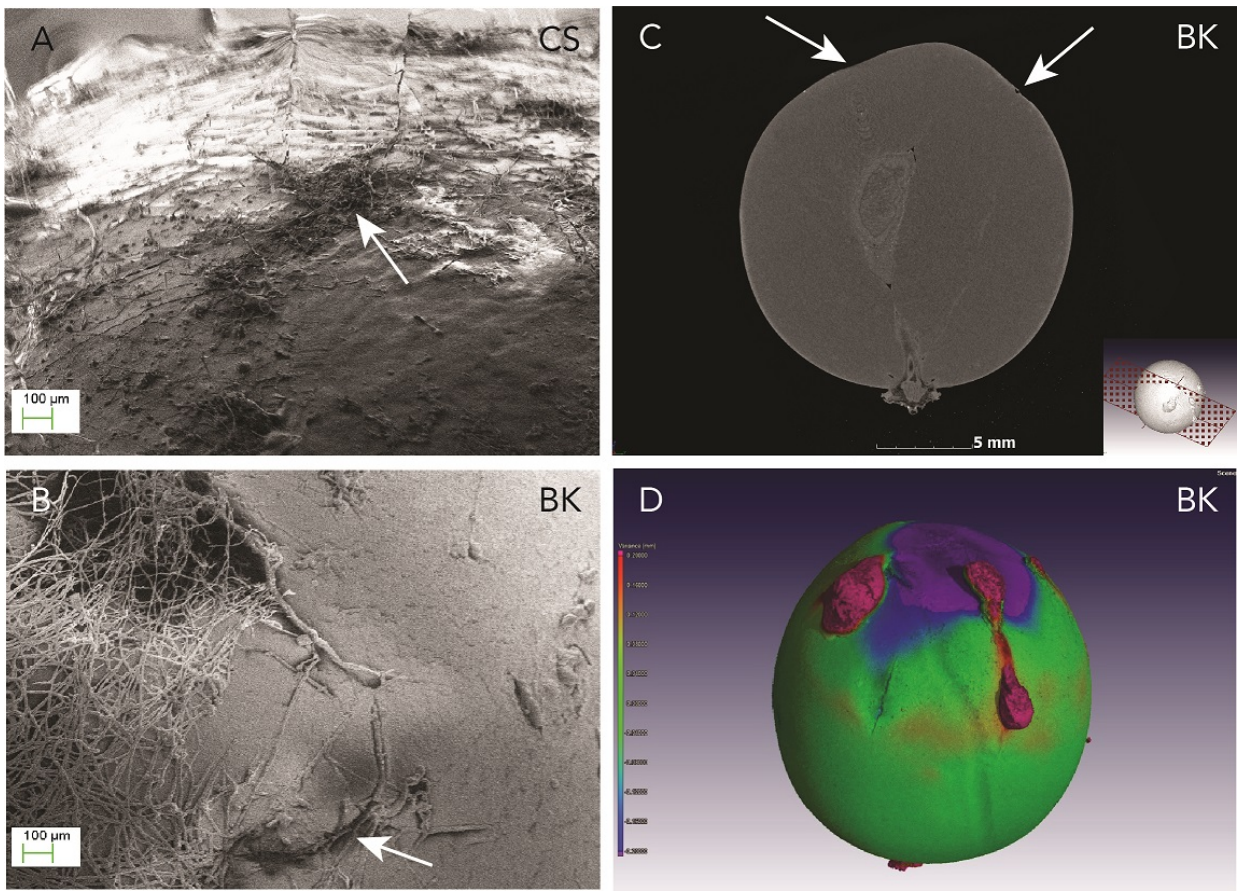

Figure 4: Scanning electron micrographs of infected grape berries (A, B), or with a CT scanner (C,D). A: Cabernet Sauvignon (CB) 96 hpi; B: Barlinka (BK) 72 hpi; C: Barlinka grape 108 hpi. Arrows indicate areas degraded by *B. cinerea* and the hyphal network; D: An overlay of two 3D reconstruction CT-scans of the same infected Barlinka grape taken at 36 hpi and at 108 hpi. It shows the impact of *B.* cinerea infection on the grape integrity. The colour scale highlights the morphology variations between the two observations. The violet and blue colours show areas degraded by the fungus. The pink corresponds to grape juice that burst out of the grape when its skin was breached.

Scanning electron microscopy was used to investigate the surface of Cabernet Sauvignon and Barlinka grapes at 96 hpi with *B. cinerea* when the hyphal network started to develop away from the infection point on both selected grapes (see Figure 4). Evidence of a dense hyphal network present as patches across the grape surfaces were visible for Cabernet Sauvignon (Figure 4A). In contrast, a single large network of hyphae was evident for Barlinka (Figure 4B). Tears or breaches in the grape surface could be seen for both Cabernet Sauvignon and Barlinka, which presumably facilitated fungal entry into the fruit. X-ray CT scanning was used to image the inside of an inoculated Barlinka grape (see Figure 4) to gain insights into the infection process. This technology allows the user to create density profiles of an object. This could help indicate where tissues have been broken down during an infection process. The interior structures of the grape were visible with the pedicel, vascular strands and seeds as high density contrasted with the flesh and area around the seed as low density (Figure 4C). To observe the variations of the grape shape over time,

images of the same grape were taken at 36 and 108 hpi and overlapped digitally (Figure 4D). In this compound image areas that are green have not changed from 36 hpi to 108 hpi; whereas areas that are blue and violet indicate a depletion of density over time (Figure 4D). This could be due to *B. cinerea* degradation and berry shrinking with the production of a droplet of juice (coloured violet) running down the berry from the infection zone (Figure 4D).

Cell wall monosaccharide composition analysis of uninfected (control) grapes versus those infected with Botrytis cinerea using Gas Chromatography – Mass Spectrometry

Grapes from all four cultivars were classified as mock or Ni, Li where only small amount of white mycelium was present, Mi where half of the grape was covered with mycelium or Hi where the whole grape was engulfed in fungal hyphae. These grapes were obtained after inoculation at either véraison, post-véraison, and ripe stages of development. Control and infected grapes were sampled at the various degrees of infection (Li, Mi and Hi) and processed to AIR for monosaccharide analysis by gas chromatography (see Figure 5). Taking T0 V (véraison) as the initial comparison point, all nine monosaccharides were detected. These showed values of ca. 15 mol% Ara, ca. 4 mol% Rha, ca. 1.5 mol% Fuc, ca. 9 mol% Xyl, ca. 2.5 mol% Man, ca. 8 mol% Gal, ca. 45 to 55 mol% GalA, ca. 4 mol% Glc and ca. 4 mol% GlcA. This would indicate a pectin-rich fruit with over half the sugar composition due to GalA. Variations between cultivars were very small; wine grapes had a slightly higher proportion of Ara (~3 %) but less GalA (~5-10 %) than the table grapes. Between véraison and the ripe stages, only a small increase of Ara was observed (~1 to 6 %) for all cultivars whereas Barlinka showed a decrease for GalA. During the infection process from none to highly infected, the GalA content decreased by 30 mol% in some cases, indicating pectin degradation. At the same time the amount of Glc increased substantially by 30 mol% in some instances which is likely due to the accumulation of glucans that constitute the fungal hyphae and from callose production.

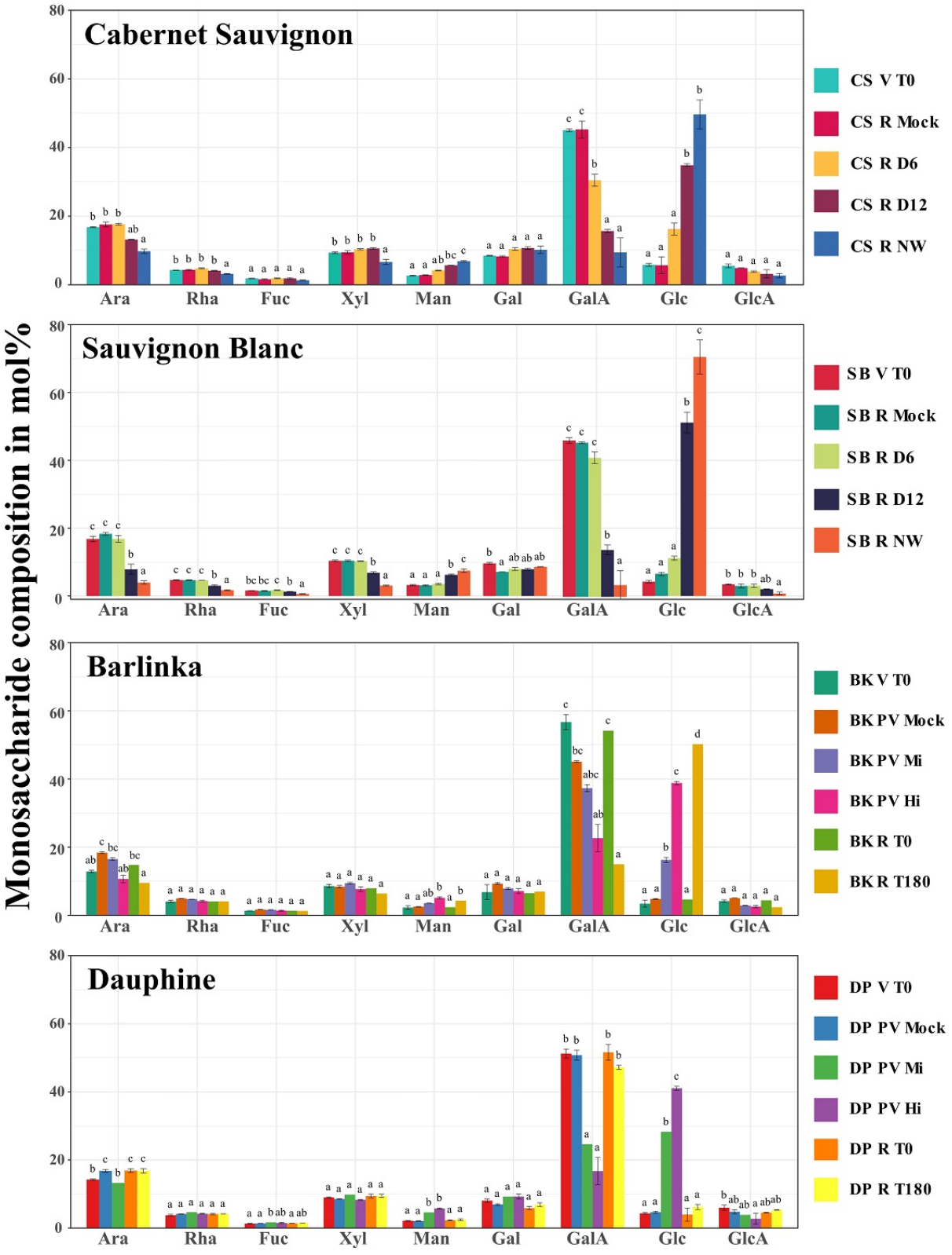

Figure 5: Monosaccharide analysis of cell wall, expressed in %mol of Barlinka, Dauphine, Cabernet Sauvignon and Sauvignon blanc grapes. The standard deviation represents the average of minimum 3 biological repeats. A two-way ANOVA followed by a Tukey's test were performed to statistically separate samples with P ≤0.05. V: Veraison, PV: post-veraison; R: ripe; Mi: mild infection; Hi: high infection; NW: no wax treatment; Ara: arabinose; Rha: rhamnose; Fuc: fucose; Xyl: xylose; Man: mannose; Gal: galactose; GalA: galacturonic acid; Glc: glucose; GlcA: glucuronic acid.

Cell wall analysis using Comprehensive Microarray Polymer Profiling of uninfected (control) grapes versus those infected with Botrytis cinerea

Cell walls from Sauvignon Blanc and Cabernet Sauvignon displayed very similar CoMPP profiles to each other for both the CDTA and NaOH extracts when looking at the ripe grape stages (see Figure 6A). The CDTA extracts showed strong signals for mAbs JIM5, JIM7, LM18, LM19 and LM20 which recognise homogalacturonan (HG) stretches of various degrees of methylesterification. mAbs INRA-RU1, INRA-RU2 and LM6 also display strong signals indicative of rhamnogalacturonan 1 (RG-1) and arabinan side chains. Weaker signals for mAbs JIM11 and JIM20 representing extensins and mAbs JIM8, JIM13 and LM2 representing arabinogalactan proteins were also evident. Both Sauvignon Blanc and Cabernet Sauvignon grapes showed a decrease in HG signals (e.g. JIM5, JIM7 and LM20 in particular) and RG-1 epitopes (e.g. INRA-RU1) suggesting de-pectination having taken place from 0 hpi to 288 hpi. A positive infection control was established where grapes were de-waxed in solvent prior to infection,resulting in substantial hyphal growth and rot on the grapes. This ‘no wax’ treatment revealed substantial degradation of signals for HG and RG-1 epitopes in the CoMPP heatmaps (Figure 6). Looking at the NaOH heatmaps, the major signals were similar again for both Sauvignon Blanc and Cabernet Sauvignon grapes. The NaOH extract displayed strong signals for RG-1 (e.g. mAbs INRA-RU1, LM6), mannans (mAb LM21) and xyloglucan (mAbs LM15, LM25 and CBM3a). Weaker signals for mAbs LM1, JIM11 and JIM20 representing extensins, as well as for mAbs JIM8, JIM13 and LM2 representing arabinogalactan proteins were also present. The major change in the NaOH extract during infection from 0 hpi to 288 hpi was that glucan epitopes increased (recognised by BS-400-2) likely due to fungal glucan presence and that extensins (mAbs LM1, JIM11 and JIM 20) were progressively masked or degraded during infection.

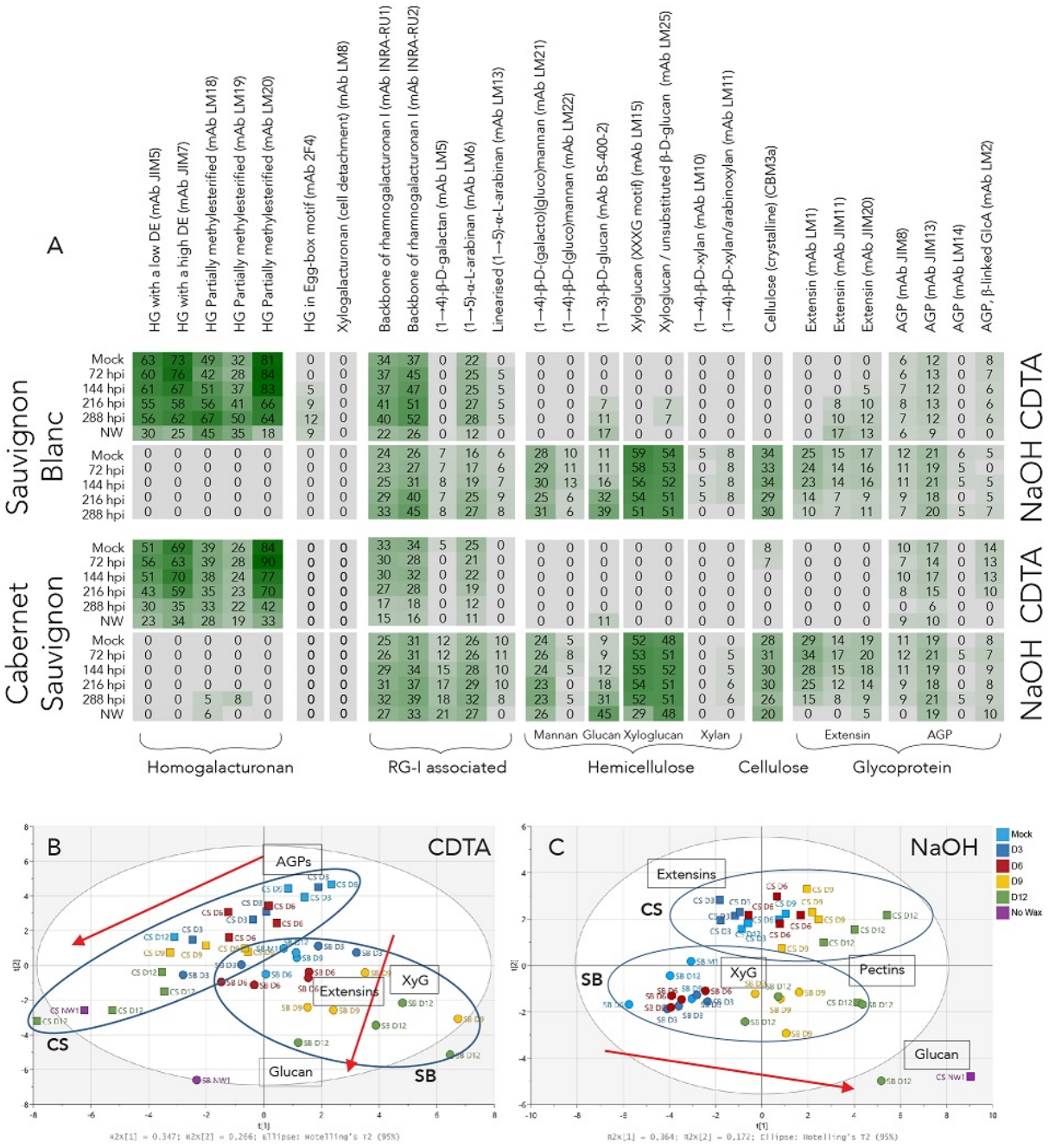

Figure 6: CoMPP analysis of Sauvignon blanc (SB) and Cabernet Sauvignon (CS) grapes infected by *B. cinerea* at ripe stage. **A**: Heatmap showing the relative abundance of cell wall associated epitopes (see material and methods for more information). **B**: PCA of the pectin-rich fraction (CDTA). **C**: PCA of the hemicellulose-rich fraction (NaOH). Samples are coloured according to infection progression. Red arrows show the infection progression. Interesting groupings of antibodies observed on the loading plots are reported on each PCA by their target name. The loading plots associated to each PCA are available as supplementary material. Detailed list of the antibody used is available in Table 1.
D: days post infection, NW: no wax (wax removal treatment to maximise infection), XyG: xyloglucan

The raw CoMPP datasets were also processed using multivariate data analysis software (SIMCA) to generate PCA plots for the CDTA and NaOH extracts of the wine grapes. Control (mock and not-infected) grapes were compared with those harvested at the different times of sample collection. The PCA allowed us to visualise sample separation and the main drivers of separation. With the wine grapes (Figure 6B, C), Cabernet Sauvignon and

Sauvignon Blanc ripe samples were separated according to the infection progression which was mostly explained by the first dimension principal component (PC1) and accounted for 34 % (CDTA fraction Figure 6B) and 36 % (NaOH fraction Figure 6C) of the separation. The separation was mostly driven by the most infected samples while the non-infected and early stage samples were more closely grouped. The second dimension PC2 could be explained by the cultivar difference and represented 26 % of the separation for the CDTA fraction. The cultivar separation was similar for the NaOH fraction (17 % of the separation). The separation was consistently driven by BS-400-2 and 2F4 mAbs that bind respectively to the β-1,3-glucan epitope (BS-400-2 recognises plant glucan, it is assumed that it also recognises some fungal glucan, not including chitin, that would suggest the signal is from fungal origin; it can alternatively be due to callose deposition) and to HG forming egg-box motifs on the highly infected samples side, followed by the LM18 and LM19, HG binding mAbs (see supplementary Figure S5 for complete loadings). Xyloglucan epitopes were driving samples in the opposite direction (no infection or symptoms) while glycoproteins signals had different effects between CDTA and NaOH fractions being respectively at intermediate levels or grouping with xyloglucan epitopes. A PCA showing individual cultivars (available as supplementary data, Figure S6) confirmed these results and highlighted the high similarity between the two wine grape cultivars epitope variations during the infection.

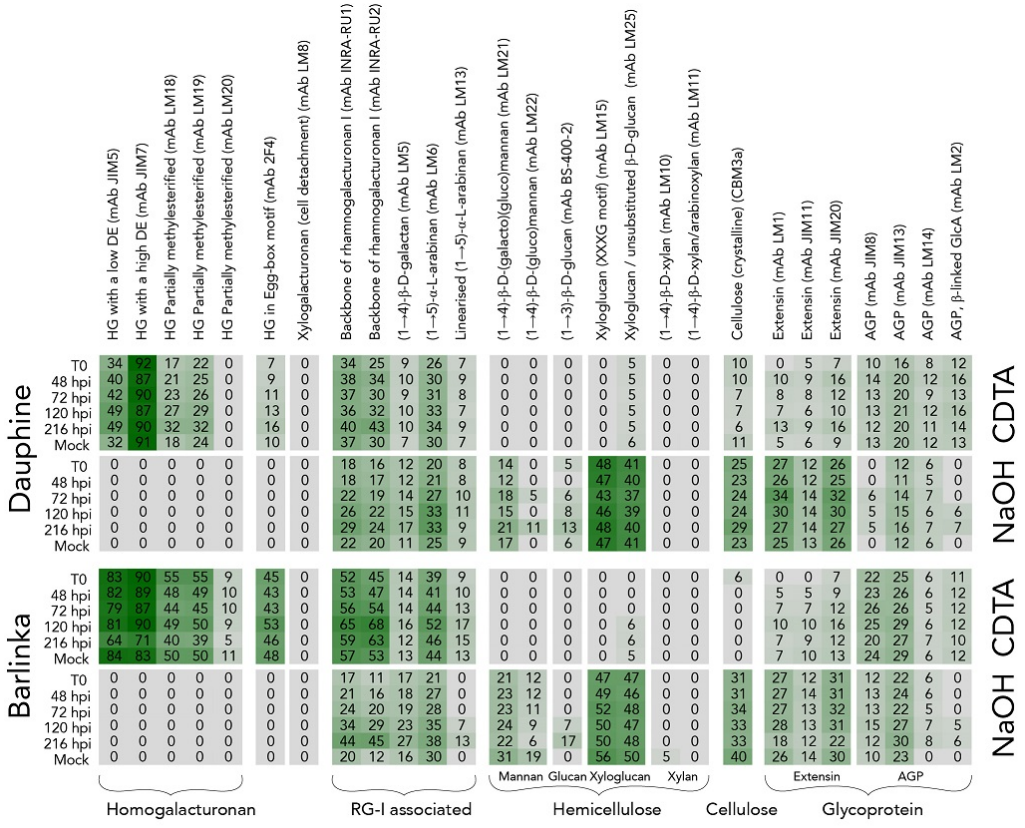

Figure 7: CoMPP analysis of Dauphine (DP) and Barlinka (BK) grapes infected by *B. cinerea* at ripe stage. Results are presented as heatmap showing the relative abundance of cell wall associated epitopes (see

material and methods for more information). Detailed list of the antibody used is available in Table 1.

For the table grapes Dauphine and Barlinka the CoMPP profiles obtained from both the CDTA and NaOH extracts were similar to each other (see Figure 7). Signals for HG, RG-1 and arabinan side chains were evident in the CDTA fraction as strong signals for mAbs JIM5, JIM7, LM18, LM19 and LM20 as well as INRA-RU1, INRA-RU2 and LM6 were obtained. The signals for glycoproteins, namely extensins (mAbs LM1, JIM11 and JIM20) and arabinogalactan proteins (mAbs JIM8, JIM13 and LM2) were stronger than those obtained for the wine grapes suggesting a higher proportion of these components in table grape AIR. However, for tracking the infection progression from 0 hpi to 216 hpi, little in the way of epitope abundance differences were evident in the datasets for these two table grapes as compared to the wine grapes. In the case of the NaOH fraction the main signals observed were for RG-1 (mAbs INRA-RU1, INRA-RU2, LM6), mannans (mAb LM21 and LM22) and xyloglucan (mAbs LM15, LM25, CBM3a). Extensin (mAbs LM1, JIM11 and JIM20) and arabinogalactan protein (mAbs JIM8, JIM13 and LM14) signals also showed up in the NaOH extracts. Considering the infection progression from 0 hpi to 216 hpi the RG-1 side chains (mAbs INRA-RU1, INRA-RU2, LM6) and the extensins (mAbs LM1 and JIM20) showed slightly increasing signal intensity. The BS-400-2 signal only marginally increased in the two table grapes suggesting much less production of fungal glucans or grape callose in these samples. At the end of the previously mentioned post-véraison infection attempt on table grapes, the few grapes showing infection symptoms were separated and analysed according to infection severity, as scored on ripe grapes. CoMPP analysis (Figure 8A) showed very similar results as for ripe grapes but with a more marked signal increase for the 2F4 (HG egg-box motif) and extensin epitopes.

A similar PCA was produced with the table grapes at post-véraison (Figure 8B, C). On both CDTA and NaOH fraction, the PC1 explaining respectively 56 % and 41 % of sample separation was dispersing samples according to infection severity. The second dimension was showing the separation between Barlinka and Dauphine grapes and represented 17 % (CDTA) and 20 % (NaOH) of the sample separation. Similarly to the wine grapes, the more infected the grapes were, the further they separated from the other groups. The separation was mostly driven by glucan, glycoproteins and RG-1 epitopes being higher in infected samples and more cellulose in the non-infected samples. Notably, the 2F4 epitope didn’t drive separation as with the wine grape cultivars.

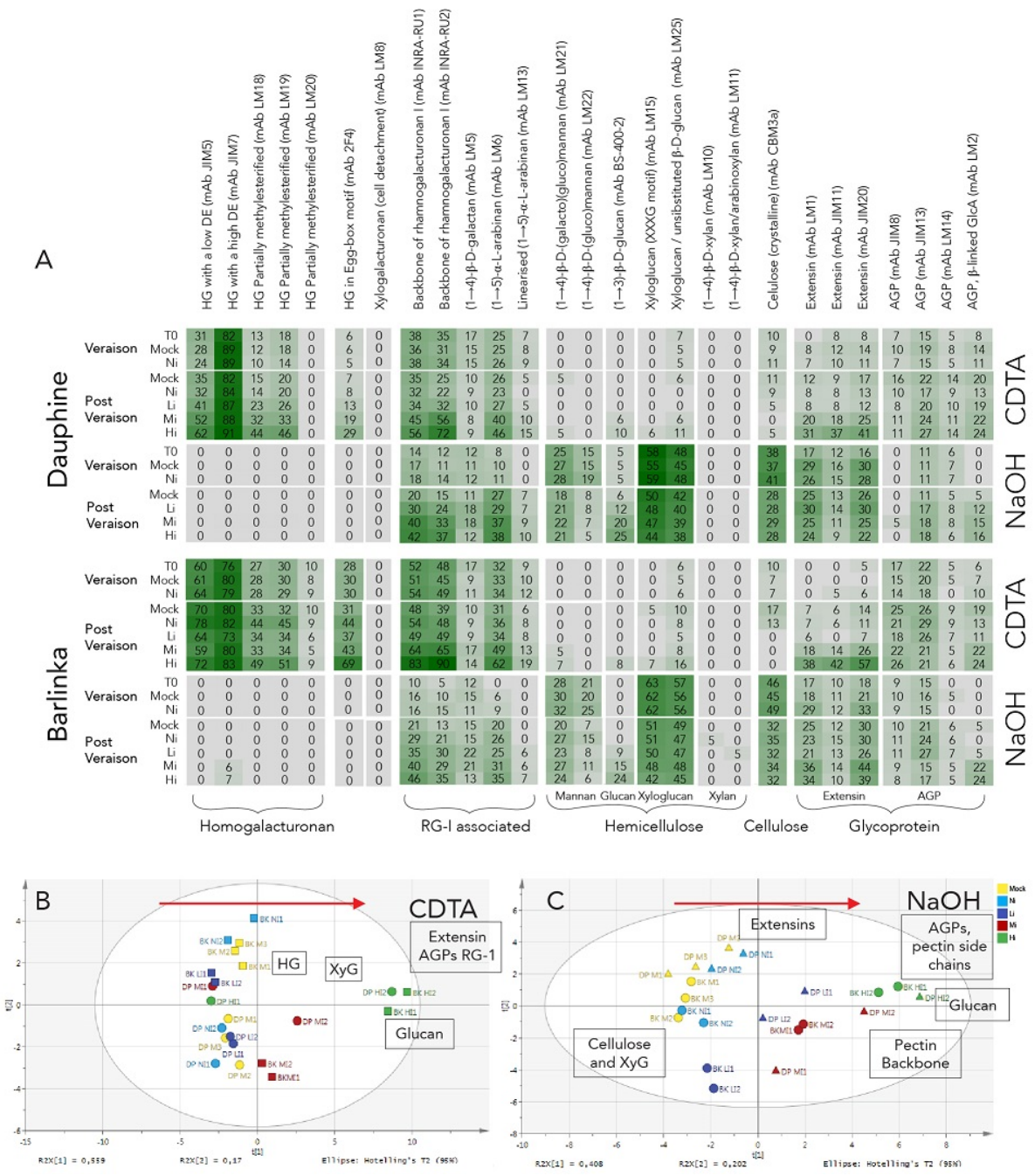

Figure 8: CoMPP analysis of Dauphine (DP) and Barlinka (BK) grapes infected by *B.* cinerea at véraison and post-véraison stages. **A**: heatmap showing the relative abundance of cell wall associated epitopes (see material and methods for more information

A: PCA of the pectin-rich fraction **(**CDTA). **B**: PCA of the hemicellulose-rich fraction (NaOH). Samples are coloured according to infection progression. Red arrows show the infection progression. Interesting groupings of antibodies observed on the loading plots are reported on each PCA by their target name. The loading plots associated to each PCA are available as supplementary material. Detailed list of the antibody used is available in Table 1.

M: mock; Ni: no-infection; Li: light infection; Mi: mild infection; Hi: high infection. See supplementary Figure S1 for visual description of these stages.

DISCUSSION

Wine and table grape cultivars display differential susceptibility to Botrytis cinerea

Grape susceptibility is not uniformly reported on in the literature and differences in infection parameters (e.g. laboratory versus field assays, detached grapes versus bunches, pathogen drop deposits versus spray treatments) complicates progress in this area. A recent comparative study of wine cultivars and their susceptibility to *B. cinerea* was conducted in France and Chile over three years (Paňitrur-De La Fuente *et al.* 2018). They suggest Cabernet Sauvignon is relatively less susceptible to fungal pathogen infection compared with other *vinifera* cultivars (Paňitrur-De La Fuente *et al.* 2018). Of course, in comparison to non-*vinifera* species such as *V. aestivalis*-derived 'Norton' grapes, Cabernet Sauvignon would be classified as a relatively susceptible cultivar in the larger view of grape species and sub-species comparisons. In our controlled environment analyses, and compared to Dauphine and Barlinka, the wine grape cultivars Sauvignon Blanc and Cabernet Sauvignon appeared less susceptible to *B. cinerea.* Plausible reasons for this could be the waxy cuticle and the thicker skins present in the wine grapes, which act as physical barriers to infection. For Cabernet Sauvignon, the least susceptible cultivar from this study, the skin composition is most likely the key as Botrytis started to develop under the skin rather than at the grape surface as was observed with the other cultivars. It was also noted that grape maturity influenced infection severity with véraison and post-véraison grapes not showing much tissue maceration of the cultivars tested, whereas harvest ripe grapes were much more susceptible to *B. cinerea.* Variations in grape cell wall composition during ripening has been reported (Moore *et al.* 2014; Tian *et al.* 2019) and, in agreement with the presented results, could partially explain the difference in grape susceptibility to *B. cinerea* between véraison and ripe stages.

Botrytis cinerea causes pectin degradation in both wine and table grape cultivars

Comparing the four cultivars tested, the two wine grape cultivars Sauvignon Blanc and Cabernet Sauvignon showed clear evidence of pectin degradation using both monosaccharide composition as well as CoMPP analysis. For the cultivars Dauphine and Barlinka the results from the monosaccharide analysis suggested degradation (a decrease in GalA levels), but this was not as definitive from the CoMPP profiling. This could be due to the ratio of skin to pulp in the AIR that differed between the wine and table grape cultivars, as pulp tissue generally yields much less AIR for analysis. Composition variations between the epidermis and hypodermis of Corvina grapes have been shown, highlighting cell wall localisation specificity and plasticity (Fasoli *et al.* 2016). Variations in and between skin and

pulp composition have also been reported between wine grape cultivars (Ortega-Regules *et al.* 2008) so it shouldn't be surprising between wine and table grape varieties. For both Sauvignon Blanc and Cabernet Sauvignon the HG epitopes mAb JIM5, JIM7 and LM20 levels decreased strongly whereas the mAb LM18 and LM19 signals increased slightly. This would indicate that the methylesterified epitope stretches recognised by these probes were less susceptible (resistant) to fungal enzymes released by *B. cinerea* during infection. As these probes recognise methylesterification patterns, it would be interesting to understand the reason for the pectin probe signals obtained. Fungi such as *B. cinerea* are able to modify, disrupt and degrade pectin networks of berry fruit through the action of fungal polygalacturonases as well as fungal pectin methylesterases (PMEs) (L'Enfant et al. 2015). Pectin methylesterase inhibiting proteins (PMEIs) vary from one plant species to another and their sequences are not highly conserved across organisms (Rocchi *et al.* 2012; Wang *et al.* 2013). PMEIs from wheat and *Arabidopsis thaliana* were found to increase resistance to fungi (Volpi *et al.* 2011; Lionetti *et al.* 2017). PMEIs, as well as secondary metabolites are able to inhibit fungal PME activity. L'Enfant et al. (2015) showed that BcPME1 was not sensitive to chemical inhibition (over 3600 compounds tested) nor to some plant PMEIs but that high concentration of polyphenols could inhibit this fungal enzyme.

Cellulose-hemicellulose network is exposed after pectin degradation

Botrytis virulence is highly associated with its pectin degrading enzyme activity and information on its hemicellulolytic enzyme complex remains limited (Kars and Van Kan 2007; Blanco-Ulate *et al.* 2014; Valero-Jiménez *et al.* 2019). The xylanases BcXyl1 and Xyn11A were shown to be important virulence factors by promoting plant necrosis rather than through their enzymatic activity (Noda *et al.* 2010; Yang *et al.* 2018). The endo-arabinanase BcAra1 was shown to be important for secondary lesion formation against *Arabidopsis* but not against *Nicotiana benthamiana*, (Nafisi *et al.* 2014). Hence, most hemicellulose enzymes seem to be functioning indirectly of their enzyme action as immunomodulatory factors in plant defence (Blanco-Ulate *et al.* 2014). From the hemicellulose perspective following grape infection by Botrytis the data presented in this paper suggest that the glucan level increase could be due to exposure of cellulose-hemicellulose layers in macerated cell walls. Such an idea is supported by work on grape pomace characterisation following fermentation and pectinase treatment reported on in Zietsman *et al.* (2017) and Gao *et al.* (2019).

Botrytis cinerea results in glucan production and extensin glycoprotein degradation/deposition

The cell wall of Botrytis, the ubiquitous necrotrophic fungal pathogen, is composed of around 90 mol % of glucose (Cantu *et al.* 2009) which naturally suggests that an increase in glucose composition of AIR material from infected materials is probably a sign of fungal biomass growth. An increase of glucose was observed when analysing the cell walls in a time-course following *B. cinerea* infection. The increase in glucose coincided with a reduction in GalA levels (i.e. pectin degradation), with the former most likely due to *B. cinerea* metabolism and mobilisation of free sugar metabolites (e.g. GalA from pectin degradation) into its growing mycelium (Veillet *et al.* 2017). In addition to glucan production, the CoMPP datasets confirmed extensin degradation/deposition in both the CDTA and the NaOH fractions of the cell wall matrices. Importantly, the results of extensin turnover varied between wine and table grapes. For ripe wine grapes Cabernet Sauvignon and Sauvignon Blanc, the extensin signals for LM1, JIM11 and JIM20 were strongest in the NaOH fraction and decreased markedly as infection proceeded suggesting degradation had taken place. Alternatively, reorganisation or crosslinking of extensins could also decrease the signal for these glycoproteins, possibly suggesting its interaction with either another cell wall or fungal component. For the table grapes Barlinka and Dauphine the signals for ripe wine grapes were unchanged, however for véraison and post-véraison table grapes the extensin signal for LM1, JIM11 and JIM20 increased dramatically in the CDTA fraction and somewhat in the NaOH extracts. This suggests a possible role for this class of glycoproteins in response to the infection as reviewed recently by Castilleux et al., (2018) and commented on by Tan and Mort (2020). Castilleux *et al.* (2020) recently provided strong evidence for extensins in limiting root colonisation by oomycete pathogens in a *A. thaliana* mutant analysis. The role for extensins, proteins from the hydroxyproline-rich glycoprotein family, in plant defence are now only starting to be uncovered (Wei and Shirsat 2006; Koroney *et al.* 2016; Wu *et al.* 2017) and warrants further investigation.

CONCLUSION

This study is, to our knowledge, the first to profile the berry cell wall of different grape cultivars during *B. cinerea* infection. Information on four commercial, commonly grown grape cultivars are presented. Under the controlled conditions during the infections, differences in grape susceptibility to the fungus were observed, as well as in the infection symptoms between Cabernet Sauvignon, Sauvignon blanc, Barlinka and Dauphine, and the influence of grape maturity on infection occurrence. The present results have highlighted some

common changes in grape cell wall during *B. cinerea* infection like variations of homogalacturonan methyl-esterification pattern, glucan deposition or extensin deposition or degradation. These results were obtained with the CoMPP technique using specific probes against cell wall epitopes. The mAbs LM18 and LM20 are complementary and allow to follow variations of homogalacturonan methylesterification patterns, BS-400-2 to track glucan deposition or LM1, JIM11, JIM20 and JIM8, JIM13, LM2 for respectively extensin and arabinogalactan proteins (AGPs) reorganisation. While this study provides information within the grape–*B. cinerea* pathosystem, the precise locations of the observed variations remain unknown. A future study using immunofluorescence, or electron microscopy with some of the previously named antibodies would complement this study and ascertain what cell wall variations occur at the lesion and its surroundings.

FUNDING

This research was supported by the Wine Industry Network of Expertise and Technology of South Africa (Winetech; Grant Nos. IWBT-P 09/01, IWBT P14/03 and IWBT P14/04), Technology and Human Resources for Industry Programme (THRIP; Grant No. TP 13081327560), Stellenbosch University and the National Research Foundation of South Africa (NRF; Grant No. 92290). Thanks are also due to the University of Rouen, the GRR-Végétal-Agronomie- Sols-Innovation of Haute Normandie, Le Fonds Européen de Développement Regional (FEDER) for financial support to Professor Azeddine Driouich.

ACKNOWLEDGMENTS

The Central Analytical Facility (CAF) of Stellenbosch University (Mr Lucky Mokwena) is thanked for technical support with GC-MS analyses. Eunice and Jan Avenant are thanked for their help in providing the table grapes.

AUTHOR CONTRIBUTIONS

FW conducted experiments, performed analyses. FW drafted the initial manuscript with JM support. FW, AD, MV and JM designed and planned the study. JM, MV and AD secured funding support. JS and WGTW performed the CoMPP analysis. All authors read and approved the final manuscript.

LITERATURE CITED

Agudelo-Romero P, Erban A, Rego C, *et al.* 2015. Transcriptome and metabolome reprogramming in *Vitis vinifera* cv. Trincadeira berries upon infection with *Botrytis cinerea*. *Journal of Experimental Botany* **66**: 1769–1785.

De Beer A, Vivier MA. **2008**. Vv-AMP1, a ripening induced peptide from *Vitis vinifera* shows strong antifungal activity. *BMC Plant Biology* **8**: 1–16.

Blanco-Ulate B, Amrine KCH, Collins TS, *et al.* 2015. Developmental and metabolic plasticity of white-skinned grape berries in response to *Botrytis cinerea* during noble rot. *Plant Physiology* **169**: 2422–2443.

Blanco-Ulate B, Labavitch JM, Vincenti E, Powell ALT, Cantu D. **2015**. Hitting the wall: Plant cell walls during *Botrytis cinerea* infections In: *Botrytis – the Fungus, the Pathogen and its Management in Agricultural Systems*. Cham: Springer International Publishing, Switzerland, 361–386.

Blanco-Ulate B, Morales-Cruz A, Amrine KCH, Labavitch JM, Powell ALT, Cantu D. **2014**. Genome-wide transcriptional profiling of *Botrytis cinerea* genes targeting plant cell walls during infections of different hosts. *Frontiers in Plant Science* **5**.

Blanco-Ulate B, Vincenti E, Cantu D, Powell ALT. **2016**. Ripening of tomato fruit and susceptibility to *Botrytis cinerea* In: *Botrytis – the Fungus, the Pathogen and its Management in Agricultural Systems*. Cham: Springer International Publishing, 387–412.

Cantu D, Carl Greve L, Labavitch JM, Powell ALT. **2009**. Characterization of the cell wall of the ubiquitous plant pathogen *Botrytis cinerea*. *Mycological Research* **113**: 1396–1403.

Castilleux R, Plancot B, Gügi B, *et al.* 2020. Extensin arabinosylation is involved in root response to elicitors and limits oomycete colonization. *Annals of Botany* **125**: 751–763.

Castilleux R, Plancot B, Ropitaux M, *et al.* 2018. Cell wall extensins in root–microbe interactions and root secretions. *Journal of Experimental Botany* **69**: 4235–4247.

Clausen MH, Willats WGT, Knox JP. **2003**. Synthetic methyl hexagalacturonate hapten inhibitors of anti-homogalacturonan monoclonal antibodies LM7, JIM5 and JIM7. *Carbohydrate Research* **338**: 1797–1800.

Coelho J, Almeida-Trapp M, Pimentel D, *et al.* 2019. The study of hormonal metabolism of Trincadeira and Syrah cultivars indicates new roles of salicylic acid, jasmonates, ABA and IAA during grape ripening and upon infection with *Botrytis cinerea*. *Plant Science* **283**: 266–277.

Coombe BG. **1995**. Growth Stages of the Grapevine: Adoption of a system for identifying grapevine growth stages. *Australian Journal of Grape and Wine Research* **1**: 104–110.

Elad Y, Pertot I, Cotes Prado AM, Stewart A. **2015**. Plant hosts of *Botrytis* spp. In: *Botrytis - The Fungus, the Pathogen and its Management in Agricultural Systems*. Cham: Springer International Publishing, 413–486.

Emmanuel CJ, van Kan JAL, Shaw MW. **2018**. Differences in the gene transcription state of *Botrytis cinerea* between necrotic and symptomless infections of lettuce and *Arabidopsis thaliana*. *Plant Pathology*: 1–9.

Engelsdorf T, Gigli-Bisceglia N, Veerabagu M, *et al.* 2018. The plant cell wall integrity maintenance and immune signaling systems cooperate to control stress responses in *Arabidopsis thaliana*. *Science Signaling* **11**: eaao3070.

Fasoli M, Dell'Anna R, Dal Santo S, *et al.* 2016. Pectins, hemicelluloses and celluloses show specific dynamics in the internal and external surfaces of grape berry skin during ripening. *Plant and Cell Physiology* **57**: 1332–1349.

Jones L, Seymour GB, Knox JP. **1997**. Localization of pectic galactan in tomato cell walls using a monoclonal antibody specific to (1→4)-β-D-galactan. *Plant Physiology* **113**: 1405–1412.

Joubert DA, Slaughter AR, Kemp G, *et al.* 2006. The grapevine polygalacturonase-inhibiting protein (*Vv*PGIP1) reduces *Botrytis cinerea* susceptibility in transgenic tobacco and differentially inhibits fungal polygalacturonases. *Transgenic research* **15**: 687–702.

van Kan JAL. **2006**. Licensed to kill: the lifestyle of a necrotrophic plant pathogen. *Trends in plant science* **11**:

247–53.

van Kan JAL, Shaw MW, Grant-downton RT. **2014**. *Botrytis species* : relentless necrotrophic thugs or endophytes gone rogue? *Molecular Plant Pathology* **15**: 957–961.

Van Kan JAL, Stassen JHM, Mosbach A, *et al.* 2017. A gapless genome sequence of the fungus *Botrytis cinerea*. *Molecular Plant Pathology* **18**: 75–89.

Kars I, Van Kan JAL. **2007**. Extracellular enzymes and metabolites involved in pathogenesis of *Botrytis* In: *Botrytis: Biology, Pathology and Control*. Dordrecht: Springer Netherlands, 99–118.

Kelloniemi J, Trouvelot S, Héloir M-C, *et al.* 2015. Analysis of the molecular dialogue between gray mold (*Botrytis cinerea*) and grapevine (*Vitis vinifera*) reveals a clear shift in defense mechanisms during berry ripening. *Molecular Plant-Microbe Interactions* **28**: 1167–1180.

Knox JP, Linstead P., Cooper JPC, Roberts K. **1991**. Developmentally regulated epitopes of cell surface arabinogalactan proteins and their relation to root tissue pattern formation. *The Plant Journal* **1**: 317–326.

Knox JP, Linstead P, King J, Cooper C, Roberts K. **1990**. Pectin esterification is spatially regulated both within cell walls and between developing tissues of root apices. *Planta* **181**: 512–521.

Koroney AS, Plasson C, Pawlak B, *et al.* 2016. Root exudate of *Solanum tuberosum* is enriched in galactose-containing molecules and impacts the growth of *Pectobacterium atrosepticum*. *Annals of Botany* **118**: 797–808.

L'Enfant M, Domon JM, Rayon C, *et al.* 2015. Substrate specificity of plant and fungi pectin methylesterases: Identification of novel inhibitors of PMEs. *International Journal of Biological Macromolecules* **81**: 681–691.

Liners F, Letesson J-J, Didembourg C, Van Cutsem P. **1989**. Monoclonal antibodies against pectin. *Plant Physiology* **91**: 1419–1424.

Lionetti V, Fabri E, De Caroli M, *et al.* 2017. Three pectin methylesterase inhibitors protect cell wall integrity for arabidopsis immunity to *Botrytis*. *Plant Physiology* **173**: 1844–1863.

Lovato A, Zenoni S, Tornielli GB, Colombo T, Vandelle E, Polverari A. **2019**. Specific molecular interactions between *Vitis vinifera* and *Botrytis cinerea* are required for noble rot development in grape berries. *Postharvest Biology and Technology* **156**: 110924.

Marcus SE, Blake AW, Benians TAS, *et al.* 2010. Restricted access of proteins to mannan polysaccharides in intact plant cell walls. *The Plant Journal* **64**: 191–203.

Marcus SE, Verhertbruggen Y, Hervé C, *et al.* 2008. Pectic homogalacturonan masks abundant sets of xyloglucan epitopes in plant cell walls. *BMC Plant Biology* **8**: 60.

McCabe PF, Valentine TA, Forsberg LS, Pennell RI. **1997**. Soluble signals from cells identified at the cell wall establish a developmental pathway in carrot. *Plant Cell* **9**: 2225–2241.

McCartney L, Marcus SE, Knox JP. **2005**. Monoclonal antibodies to plant cell wall xylans and arabinoxylans. *Journal of Histochemistry and Cytochemistry* **53**: 543–546.

Mehari ZH, Pilati S, Sonego P, *et al.* 2017. Molecular analysis of the early interaction between the grapevine flower and *Botrytis cinerea* reveals that prompt activation of specific host pathways leads to fungus quiescence. *Plant Cell and Environment* **40**: 1409–1428.

Meikle PJ, Bonig I, Hoogenraad NJ, Clarke AE, Stone BA. **1991**. The location of (1→3)-β-glucans in the walls of pollen tubes of *Nicotiana alata* using a (1→3)-β-glucan-specific monoclonal antibody. *Planta* **185**: 1–8.

Mestre P, Arista G, Piron M-CC, *et al.* 2017. Identification of a *Vitis vinifera* endo-β-1,3-glucanase with antimicrobial activity against *Plasmopara viticola*. *Molecular Plant Pathology* **18**: 708–719.

Moller I, Marcus SE, Haeger A, *et al.* 2008. High-throughput screening of monoclonal antibodies against plant cell wall glycans by hierarchical clustering of their carbohydrate microarray binding profiles. *Glycoconjugate Journal* **25**: 37–48.

Moller I, Sørensen I, Bernal AJ, *et al.* 2007. High-throughput mapping of cell-wall polymers within and between plants using novel microarrays. *The Plant Journal* **50**: 1118–28.

Moore JP, Fangel JU, Willats WGT, Vivier MA. **2014**. Pectic-β(1,4)-galactan, extensin and arabinogalactan–protein epitopes differentiate ripening stages in wine and table grape cell walls. *Annals of Botany* **114**: 1279–1294.

Nafisi M, Fimognari L, Sakuragi Y. **2015**. Interplays between the cell wall and phytohormones in interaction between plants and necrotrophic pathogens. *Phytochemistry* **112**: 63–71.

Nafisi M, Stranne M, Zhang L, Van Kan JAL, Sakuragi Y. **2014**. The endo-arabinanase BcAra1 is a novel host-specific virulence factor of the necrotic fungal phytopathogen *Botrytis cinerea*. *Molecular Plant-Microbe Interactions* **27**: 781–792.

Nanni V, Schumacher J, Giacomelli L, *et al.* 2014. VvAMP2, a grapevine flower-specific defensin capable of inhibiting *Botrytis cinerea* growth: insights into its mode of action. *Plant Pathology* **63**: 899–910.

Noda J, Brito N, González C. **2010**. The *Botrytis cinerea* xylanase Xyn11A contributes to virulence with its necrotizing activity, not with its catalytic activity. *BMC Plant Biology* **10**: 1–15.

Ortega-Regules A, Ros-García JM, Bautista-Ortín AB, López-Roca JM, Gómez-Plaza E. **2008**. Differences in morphology and composition of skin and pulp cell walls from grapes (*Vitis vinifera* L.): Technological implications. *European Food Research and Technology* **227**: 223–231.

Paňitrur-De La Fuente C, Valdés-Gómez H, Roudet J, *et al.* 2018. Classification of winegrape cultivars in Chile and France according to their susceptibility to *Botrytis cinerea* related to fruit maturity. *Australian Journal of Grape and Wine Research* **24**: 145–157.

Pasinetti GM, Wang J, Ho L, Zhao W, Dubner L. **2015**. Roles of resveratrol and other grape-derived polyphenols in Alzheimer's disease prevention and treatment. *Biochimica et Biophysica Acta (BBA) - Molecular Basis of Disease* **1852**: 1202–1208.

Paul Knox J, Peart J, Neill SJ. **1995**. Identification of novel cell surface epitopes using a leaf epidermal-strip assay system. *Planta: An International Journal of Plant Biology* **196**: 266–270.

Pedersen HL, Fangel JU, McCleary B, *et al.* 2012. Versatile high resolution oligosaccharide microarrays for plant glycobiology and cell wall research. *The Journal of biological chemistry* **287**: 39429–38.

Petrasch S, Knapp SJ, van Kan JAL, Blanco-Ulate B. **2019**. Grey mould of strawberry, a devastating disease caused by the ubiquitous necrotrophic fungal pathogen *Botrytis cinerea*. *Molecular Plant Pathology* **20**: 877–892.

Pezet R, Viret O, Perret C, Tabacchi R. **2003**. Latency of *Botrytis cinerea* Pers.: Fr. and biochemical studies during growth and ripening of two grape berry cultivars, respectively susceptible and resistant to grey mould. *Journal of Phytopathology* **151**: 208–214.

du Plessis A, le Roux SG, Guelpa A. **2016**. The CT Scanner Facility at Stellenbosch University: An open access X-ray computed tomography laboratory. *Nuclear Instruments and Methods in Physics Research Section B: Beam Interactions with Materials and Atoms* **384**: 42–49.

Ralet M-C, Tranquet O, Poulain D, Moïse A, Guillon F. **2010**. Monoclonal antibodies to rhamnogalacturonan I backbone. *Planta* **231**: 1373–1383.

Rocchi V, Janni M, Bellincampi D, Giardina T, D'Ovidio R. **2012**. Intron retention regulates the expression of pectin methyl esterase inhibitor (*Pmei*) genes during wheat growth and development. *Plant Biology* **14**: 365–373.

Rowe HC, Kliebenstein DJ. **2008**. Complex genetics control natural variation in *Arabidopsis thaliana* resistance to *Botrytis cinerea*. *Genetics* **180**: 2237–2250.

Saigne-Soulard C, Abdelli-Belhadj A, Télef-Micouleau M, *et al.* 2015. Oligosaccharides from *Botrytis cinerea* and elicitation of Grapevine defense In: *Polysaccharides*. Cham: Springer International Publishing, 939–958.

Singh CK, Liu X, Ahmad N. **2015**. Resveratrol, in its natural combination in whole grape, for health promotion and disease management. *Annals of the New York Academy of Sciences* **1348**: 150–60.

Smallwood M, Beven A, Donovan N, *et al.* 1994. Localization of cell wall proteins in relation to the developmental anatomy of the carrot root apex. *The Plant Journal* **5**: 237–246.

Smallwood M, Martin H, Knox JP. **1995**. An epitope of rice threonine- and hydroxyproline-rich glycoprotein is common to cell wall and hydrophobic plasma-membrane glycoproteins. *Planta* **196**: 510–522.

Smallwood M, Yates EA, Willats WGT, Martin H, Knox JP. **1996**. Immunochemical comparison of membrane-associated and secreted arabinogalactan-proteins in rice and carrot. *Planta* **198**: 452–459.

Soltis NE, Atwell S, Shi G, *et al.* 2019. Interactions of tomato and *Botrytis cinerea* genetic diversity: Parsing the contributions of host differentiation, domestication, and pathogen variation. *Plant Cell* **31**: 502–519.

Sonker N, Pandey AK, Singh P. **2016**. Strategies to control post-harvest diseases of table grape: a review.

Journal of Wine Research **27**: 105–122.

Tan L, Mort A. **2020**. Extensins at the front line of plant defence. A commentary on: 'Extensin arabinosylation is involved in root response to elicitors and limits oomycete colonization.' *Annals of Botany* **125**: vii–viii.

Tian B, Harrison R, Morton J, Jaspers M. **2019**. Changes in pathogenesis-related proteins and phenolics in *Vitis vinifera* L. cv. 'Sauvignon Blanc' grape skin and pulp during ripening. *Scientia Horticulturae* **243**: 78–83.

Tormo J, Lamed R, Chirino AJ, *et al.* 1996. Crystal structure of a bacterial family-III cellulose-binding domain: a general mechanism for attachment to cellulose. *The EMBO Journal* **15**: 5739–5751.

Tudzynski P, Kokkelink L. **2009**. *Botrytis cinerea*: Molecular aspects of a necrotrophic life style In: Deising HB, ed. *Deising H.B. (eds) Plant Relationships. The Mycota (A Comprehensive Treatise on Fungi as Experimental Systems for Basic and Applied Research),*. Springer, Berlin, Heidelberg, 29–50.

Valero-Jiménez CA, Veloso J, Staats M, Van Kan JAL. **2019**. Comparative genomics of plant pathogenic *Botrytis* species with distinct host specificity. *BMC Genomics* **20**: 1–12.

Veillet F, Gaillard C, Lemonnier P, Coutos-Thévenot P, La Camera S. **2017**. The molecular dialogue between *Arabidopsis thaliana* and the necrotrophic fungus *Botrytis cinerea* leads to major changes in host carbon metabolism. *Scientific Reports* **7**: 1–13.

Veloso J, van Kan JAL. **2018**. Many shades of grey in *Botrytis*–Host plant interactions. *Trends in Plant Science* **23**: 613–622.

Verhertbruggen Y, Marcus SE, Haeger A, Verhoef R, *et al.* 2009. Developmental complexity of arabinan polysaccharides and their processing in plant cell walls. *The Plant Journal* **59**: 413–425.

Verhertbruggen Y, Marcus SE, Haeger A, Ordaz-Ortiz JJ, Knox JP. **2009**. An extended set of monoclonal antibodies to pectic homogalacturonan. *Carbohydrate Research* **344**: 1858–1862.

Volpi C, Janni M, Lionetti V, Bellincampi D, Favaron F, D'Ovidio R. **2011**. The ectopic expression of a pectin methyl esterase inhibitor increases pectin methyl esterification and limits fungal diseases in wheat. *Molecular plant-microbe interactions : MPMI* **24**: 1012–1019.

Wang M, Yuan D, Gao W, Li Y, Tan J, Zhang X. **2013**. A comparative genome analysis of PME and PMEI families reveals the evolution of pectin metabolism in plant cell walls (OA Zabotina, Ed.). *PLoS ONE* **8**: e72082.

Wei G, Shirsat AH. **2006**. Extensin over-expression in *Arabidopsis* limits pathogen invasiveness. *Molecular Plant Pathology* **7**: 579–592.

Weiberg A, Wang M, Lin F-M, *et al.* 2013. Fungal small RNAs suppress plant immunity by hijacking host RNA interference pathways. *Science (New York, N.Y.)* **342**: 118–23.

Wilcox WF, Gubler WD, Uyemoto JK. **2015**. *Compendium of grape diseases, disorders, and pests*. APS Press, St. Paul.

Willats WGT, Marcus SE, Knox JP. **1998**. Generation of a monoclonal antibody specific to (1→5)-α-l-arabinan. *Carbohydrate Research* **308**: 149–152.

Willats WGT, McCartney L, Steele-King CG, *et al.* 2004. A xylogalacturonan epitope is specifically associated with plant cell detachment. *Planta* **218**: 673–681.

Wu Y, Fan W, Li X, *et al.* 2017. Expression and distribution of extensins and AGPs in susceptible and resistant banana cultivars in response to wounding and *Fusarium oxysporum*. *Scientific Reports* **7**: 42400.

Yang Y, Yang X, Dong Y, Qiu D. **2018**. The *Botrytis cinerea* xylanase BcXyl1 modulates plant immunity. *Frontiers in Microbiology* **9**: 2535.

Yates EA, Valdor J-F, Haslam SM, *et al.* 1996. Characterization of carbohydrate structural features recognized by anti-arabinogalactan-protein monoclonal antibodies. *Glycobiology* **6**: 131–139.

York WS, Darvill AG, McNeil M, Stevenson TT, Albersheim P. **1986**. Isolation and characterization of plant cell walls and cell wall components. *Methods in Enzymology* **118**: 3–40.

Zhang W, Corwin JA, Copeland DH, *et al.* 2019. Plant–necrotroph co-transcriptome networks illuminate a metabolic battlefield. *eLife* **8**: 1–32.

Table 1: List of mAbs and CBMs used for the CoMPP analysis. DE: Degree of esterification; ME: Methylesterification.

Homogalacturonan		low DE	JIM5	Knox *et al.* 1990; Clausen *et al.* 2003
		high DE	JIM7	
		Partially ME	LM18	Verhertbruggen *et al.* 2009a
		Partially ME	LM19	
		Partially ME	LM20	
		HG in “egg-box” motif	2F4	Liners *et al.* 1989
		Xylogalacturonan	LM8	Willats *et al.* 2004
RG-I associated		Backbone of RG-I	INRA-RU1	
		Backbone of RG-I	INRA-RU2	Ralet *et al.* 2010
		D-galactan	LM5	Jones *et al.* 1997
		L-arabinan	LM6	Willats *et al.* 1998
		Linearised L-arabinan	LM13	Verhertbruggen *et al.* 2009b
	Mannan	(galacto)(gluco)mannan	LM21	Marcus *et al.* 2010
		D-(gluco)mannan	LM22	
	Glucan	β-D-glucan	BS-400-2	Meikle *et al.* 1991
	Xyloglucan	Xyloglucan backbone (XXXG motif)	LM15	Marcus *et al.* 2008
		Xyloglucan	LM25	Pedersen *et al.* 2012
	Xylan	β-D-xylan	LM10	McCartney *et al.* 2005
		β-D-xylan/arabinoxylan	LM11	
Cellulose		Cellulose (crystalline)	CBM3a	Tormo *et al.* 1996
Proteins	Extensins		LM1	Smallwood *et al.* 1995
			JIM11	Smallwood *et al.* 1994
			JIM20	Knox *et al.* 1995
	AGP		JIM8	McCabe *et al.* 1997
			JIM13	Knox *et al.* 1991; Yates *et al.* 1996
			LM14	Moller *et al.* 2008
		β-linked GlcA	LM2	Smallwood *et al.* 1996

SUPPLEMENTARY DATA

Table S1

Levels of grape infection severity on four *Vitis vinifera* cultivars, following a time-course *Botrytis cinerea* infection experiment on ripe grapes. Barlinka and Dauphine were only scored until 216 hours post infection (hpi) The data are expressed as percentages, based on the scoring of the infection experiments where Ni, indicates no infection; Li, low infection; Mi, mild infection; and .Hi, high infections. In total, this experiment was conducted on 816 Cabernet Sauvignon grapes, 912 Sauvignon Blanc grapes, 592 Dauphine grapes and 540 Barlinka grapes. For each time point, a portion of the total number was sampled for analysis.

		Cabernet Sauvignon	Sauvignon blanc	Dauphine	Barlinka
24 hpi	Ni	100,0	100,0	100,0	100,0
	Li	0,0	0,0	0,0	0,0
	Mi	0,0	0,0	0,0	0,0
	Hi	0,0	0,0	0,0	0,0
	Total % Infected	0,0	**0,0**	**0,0**	**0,0**
72 hpi	Ni	98,8	79,2	68,9	73,0
	Li	1,3	20,8	26,2	17,5
	Mi	0,0	0,0	4,9	9,5
	Hi	0,0	0,0	0,0	0,0
	Total % Infected	**1,3**	**20,8**	**31,1**	**27,0**
144 hpi	Ni	69,8	64,4	63,1	50,7
	Li	16,7	16,2	0,8	11,0
	Mi	7,8	19,4	11,5	15,5
	Hi	5,7	0,0	24,6	22,8
	Total % Infected	**30,2**	**35,6**	**36,9**	**49,3**
216 hpi	Ni	45,9	40,0	38,5	31,6
	Li	17,7	5,0	11,5	7,5
	Mi	18,2	6,9	13,9	12,8
	Hi	18,2	48,1	36,1	48,1
	Total % Infected	**54,2**	**60,0**	**61,5**	**68,4**
288 hpi	Ni	22,4	23,7		
	Li	7,8	5,4		
	Mi	13,5	10,8		
	Hi	56,3	60,1		
	Total % Infected	**77,6**	**76,4**		

The supplementary figures listed below are available in this thesis appendix

Figure S1

Barlinka and Dauphine grapes at the end of the post-véraison infection experiment showing the four infection levels. From the least to the most infected: Ni: no-infection; Li: light infection; Mi: mild or moderate infection; Hi: high infection

Figure S2

Flow diagram showing the experimental procedure employed in the present study.

Figure S3

Picture showing a representative box of Barlinka grapes at the end of the véraison infection experiment. It highlights the absence of successful infection at véraison with our experimental setup.

Figure S4

CoMPP analysis of Dauphine (DP) grapes infected by two *B. cinerea* strains, the grape strain and BO.5.10, at ripe stage. Results are presented as heatmap showing the relative abundance of cell wall associated epitopes (see material and methods for more information). Detailed list of the antibody used is available in Table 1.

Figure S5

Loading plot showing the separation by variables of previously shown PCA analysis of grapes infected by *B. cinerea*. **A**: Loading of the CDTA fraction of CS and SB grapes (Fig. 6B); **B**: Loading of the NaOH fraction of CS and SB grapes (Fig. 6C); Loading of the CDTA fraction of BK and DP grapes (Fig. 8B); **B**: Loading of the NaOH fraction of BK and DP grapes (Fig. 8C). Interesting groupings of antibodies are annotated and circled in blue.

Figure S6:

PCA of CoMPP results of AIR from Barlinka (**A**, **B**, **C**, **D)** and Dauphine (**E**, **F**, **G**, **H**) ripe grapes infected by *B. cinerea*. **A**, **C**, **E**, **G**: PCA showing sample separation for the CDTA (**A**, **E**) and NaOH (**C**, **G**) extractions. Samples are coloured according to infection progression. **B**, **D**, **F**, **H**: Loading plots of the respective PCA showing the epitopes that drive sample separation. Red arrows show the infection progression. Detailed list of the antibody used is available in Table 1.

Chapter 6

General discussion and conclusion

General discussion and conclusion

6.1. General discussion / scope of the study

The plant cell wall, due to its central role in defence against pathogen attack, biofuel production and plant support/signalling is at the centre of many research areas. This study looked at cell wall changes correlated with overexpression of *Vvi*PGIP1, a polygalacturonase-inhibiting protein involved in plant defence against fungal pathogens. Secondly, to follow cell wall changes in leaves of *VviPGIP1* tobacco plants infected with *B. cinerea* in comparison to wild type controls. Thirdly, to compare the cell wall composition of Cabernet Sauvignon, Sauvignon Blanc, Dauphine and Barlinka grape berries before and during *B. cinerea* infection.

The first part of this study screened the cell wall composition of different tobacco lines overexpressing either *VviPGIP1* or *NtCAD14* genes which are linked to enhanced resistance to *B. cinerea*. *VviPGIP1* has been shown to have additional effects than its classical PG inhibiting activity on the cell wall matrix organisation via a proposed defence signalling role (Alexandersson *et al.* 2013; Nguema-Ona *et al.* 2013). *Vvi*PGIP1 tobacco plants were shown to upregulate CAD enzyme activity and result in increased stem lignification. To evaluate the role of CAD activity in the resistance phenotype observed, tobacco lines overexpressing *Nt*CAD14 were previously generated (Mbewana 2010). By focusing on the cell wall analysis of different lines of these constructs in the absence of pathogens, we evaluated if a cell wall priming effect was at play. CoMPP methodology was used which combines a wide range of antibodies and carbohydrate binding modules targeting the main cell wall polysaccharide epitopes in a high-throughput format (Kračun *et al.* 2017). In addition, monosaccharide quantification was performed using GC-MS and Py-GC-MS analysis was conducted to obtain total lignin and monolignol composition datasets. All analyses were conducted on leaf tissue harvested from healthy plants grown in an environmentally controlled greenhouse. The overall cell wall composition based on monosaccharide content and CoMPP analysis was very similar between the control plants (SR1) and the various *Vvi*PGIP1 and *Nt*CAD14 lines tested. HG methylesterification patterns were altered and AGPs and extensin were more abundant in the overexpressing lines. Lignin levels have been linked with increased resistance to biotic and abiotic stress (Sattler and Funnell-Harris 2013). We showed that leaves from the transgenic plants had low lignin levels which did not differ significantly from wild type plants. CAD activity was higher in the stems compared to the leaves and given the higher amount of vascular tissue in the stem this is understandable. HG methylesterification patterning has been associated with enhanced resistance to fungal pathogens by blocking pectinolytic enzyme action (Lionetti *et al.* 2012, 2017; Levesque-Tremblay *et al.* 2015). A greater abundance of extensins and AGPs were observed in *Vvi*PGIP1 and *Nt*CAD14 transgenic lines compared to wild type controls. Interestingly, recent work on roots have

shown a role of AGPs and extensins involvement in protection against *Aphanomyces euteiches* and *Phytophthora parasitica* respectively (Cannesan *et al.* 2012; Castilleux *et al.* 2020). Cell wall composition differences were also observed between leaves of different developmental stages. Some aspects of this ontogenic effect have been described previously such as degradation of RG-I arabinan and galactan side chains (Caffall and Mohnen 2009). It would be interesting to combine the cell wall analyses with RNAseq transcriptomic datasets to correlate gene expression with changes in polymer abundance.

In the second part of this work, the aim was to follow and characterise cell wall changes during *B. cinerea* infection of PGIP1 overexpressing tobacco lines compared to wild type controls. Two *Vvi*PGIP1 lines (line 37 and line 45) that showed the best resistance phenotypes against *B. cinerea* were chosen. The first 72 hpi, where no difference in lesion development are visible, are critical for the outcome of the infection. Variations in lesion development between the transgenic plants and the wild type started to be seen between 72 and 96 hpi. This time frame (0 to 72 hpi) was chosen based on our preliminary infection results and on results from Eizner *et al.* (2017) who separated the infection progression chart into different infection stages based on lesion growth-rates. *B. cinerea*, is a hemibiotroph and starts its infection with a short biotrophic phase before switching to necrotrophic growth (Veloso and van Kan 2018). This highlights the importance of the first few days of the infection in determining if the fungus can overcome the plant defences or not. During this time frame, our observations did not show any visible differences at the plant surface on and around the lesions between the control (SR1) and transgenic plants (*Vvi*PGIP1 lines). CoMPP analysis were performed on tissue harvested at regular times during the infection; this is to our knowledge, the first time that the CoMPP approach was used to follow/track an infection progression in a comparative study between sensitive (SR1) and resistant plants (VviPGIP1 lines). The CoMPP results were complemented with monosaccharide analysis. The analysis of leaf tissue adjacent to the infection and of non-infected leaves (distal) also allowed us to identify cell wall modifications that might be the result of a systemic response to the fungus. *B. cinerea* possesses a wide range of cell wall degrading enzymes including rhamnogalacturonases, hemicellulases and PGs (Blanco-Ulate *et al.* 2015). However, at the lesion site, HG polymers were degraded whereas RG-I and hemicelluloses became exposed. HG methylesterification did not vary between wild type and VviPGIP1 lines during the infection process. Glycoproteins, and particularly AGPs, seemed to accumulate, however their role during infection remains unclear. Cannesan *et al.* (2012) showed that AGPs are involved in *Aphanomyces euteiches* zoospore attraction in roots. A colocalization study using AGP and Botrytis targeting probes observed under immunofluorescence would bring more insight into their possible interactions. The cellulose/xyloglucan network showed limited degradation during our infection experiments. In agreement with the model proposed by Nguema-Ona *et al.* (2013) on *Vvi*PGIP1 mode of action in cell wall priming.

The last part of this work aimed to broaden the scope of this study by conducting similar infection experiments on different varieties of grapes. The four cultivars selected, namely Cabernet Sauvignon, Sauvignon Blanc, Barlinka and Dauphine, were chosen because of their widespread commercial use and that they represented both wine and table grape cultivars as well as white and black varieties. Cabernet Sauvignon was the least sensitive cultivar selected and its infection process was different from the other three cultivars with the Botrytis infection first developing under its skin rather than on the infection spot. These results showcase again the adaptability of necrotrophic fungi such as Botrytis to its host as described by Soltis *et al.* (2019). Cabernet Sauvignon and Sauvignon Blanc showed similar profiles in terms of pectin methylesterification patterning but this differed for Barkinka and Dauphine. These differences probably partly explain the difference in susceptibility to Botrytis. This highlights the importance of comprehensive characterisation of grape cultivars in respect of pathogen susceptibility this was partly carried out by Paňitrur-De La Fuente *et al.* (2018)) who wine grape classified cultivars according to their sensitivity to Botrytis. Infection experiments were conducted on single grape berries at three developmental stages: véraison, post-véraison and ripe. At both véraison and post-véraison, the number of inoculated grapes which developed symptoms of infection was very low. These results are in agreement with common observations on fruit ripening and disease susceptibility (Blanco-Ulate *et al.* 2016) but contrast with recent findings describing Botrytis susceptibility in Trincadeira green stage berries (Agudelo-Romero *et al.* 2015). At the ripe stage, the majority of the grape samples developed a symptomatic infection. Our results showed that during infection, HG methylesterification patterning and the extensin epitopes were modified, in addition to glucan deposition being observed.

6.2. Concluding remarks and perspectives

CoMPP technology was used as the main analysis tool in this study. The use of a wide variety of mAbs and CBMs targeting a wide range of epitopes makes it a very versatile although currently underused tool. It is no surprise that some research groups are working to combine the CoMPP approach with datasets obtained from genome wide association mapping, transcriptomic or proteomic studies (Wood *et al.* 2017; Salmeán *et al.* 2018). However, CoMPP is only considered as semi-quantitative and requires the support of additional analysis such as GC-MS for quantification information (as was done in the results reported in this study).

This research thesis has provided a better understanding of the *in planta* actions of the defence protein *Vvi*PGIP1 by providing a comprehensive picture of cell wall remodelling and its role in plant resistance against *B. cinerea*. We also characterised the cell wall composition of both tobacco leaves and Cabernet Sauvignon, Sauvignon Blanc, Barlinka and Dauphine berries during *B. cinerea* infection. The response to pathogens such as *B. cinerea*, from the cell wall perspective,

seemed multifactorial and involve both polysaccharide and glycoprotein reorganisation. Understanding the action of each polymeric component during an infection inside the cell wall matrix and in relation to one another is quite valuable to develop comprehensive models of plant cell wall changes/responses during plant – pathogen interactions. Some differences in plant cell wall degradation were observed between tobacco and the grape cultivars during *B. cinerea* infection. It would be interesting to investigate if these traits could be classified as markers of susceptibility or resistance to infection.

However, this study also raises a number of questions. This study showed reorganisation of the leaf cell wall matrix due to the overexpression of the defence related protein VviPGIP1 before and during *B. cinerea* infection. It would be extremely valuable to compare our results to transcriptomic datasets obtained under the same infection conditions (Basson 2017) to link some of the cell wall modifications observed (degradation and reorganisation) with changes in gene expression. It would also be interesting to obtain more detailed information on the pectin components, including HG methylesterification patterns and localisation, using analytical tools such as HILIC-MS and ESI-MS in a cell wall enzyme-MS fingerprinting approach.

This study has shown that *B. cinerea* infection induces cell wall degradation and matrix rearrangement of tobacco leaves and *V. vinifera* grape berries. However, the exact cellular location of these matrix modifications remains unknown. It would be very valuable to observe a tobacco lesion or infected grapes using an immunofluorescence microscopy approach with selected cell wall targeting probes. A microscopy study could further confirm the hypothesis that AGPs and extensins accumulate at the lesion site.

6.3. References

Agudelo-Romero P, Erban A, Rego C, *et al.* 2015. Transcriptome and metabolome reprogramming in *Vitis vinifera* cv. Trincadeira berries upon infection with *Botrytis cinerea*. *Journal of Experimental Botany* **66**: 1769–1785.

Alexandersson E, Ali A, Resjö S, Andreasson E. 2013. Plant secretome proteomics. *Frontiers in plant science* **4**: 9.

Basson CE. 2017. Transcriptomic analysis of disease resistance responses using a tobacco-*Botrytis cinerea* pathosystem. *PhD thesis, Stellenbosch University, South Africa*.

Blanco-Ulate B, Labavitch JM, Vincenti E, Powell ALT, Cantu D. 2015. Hitting the wall: Plant cell walls during *Botrytis cinerea* infections In: *Botrytis – the Fungus, the Pathogen and its Management in Agricultural Systems*. Cham: Springer International Publishing, Switzerland, 361–386.

Cannesan MA, Durand C, Burel C, *et al.* 2012. Effect of arabinogalactan proteins from the root caps of pea and *Brassica napus* on *Aphanomyces euteiches* zoospore chemotaxis and germination. *Plant Physiology* **159**: 1658–1670.

Castilleux R, Plancot B, Gügi B, *et al.* 2020. Extensin arabinosylation is involved in root response to elicitors and limits oomycete colonization. *Annals of Botany* **125**: 751–763.

Eizner E, Ronen M, Gur Y, Gavish A, Zhu W, Sharon A. **2017**. Characterization of *Botrytis*-plant interactions using PathTrack © - an automated system for dynamic analysis of disease development. *Molecular Plant Pathology* **18**: 503–512.

Joubert DA, Slaughter AR, Kemp G, *et al.* 2006. The grapevine polygalacturonase-inhibiting protein (*Vv*PGIP1) reduces *Botrytis cinerea* susceptibility in transgenic tobacco and differentially inhibits fungal polygalacturonases. *Transgenic research* **15**: 687–702.

Kračun SK, Fangel JU, Rydahl MG, Pedersen HL, Vidal-Melgosa S, Willats WGTGT. **2017**. Carbohydrate microarray technology applied to high-throughput mapping of plant cell wall glycans using comprehensive microarray polymer profiling (CoMPP) In: *Lauc G., Wuhrer M. (eds) High-Throughput Glycomics and Glycoproteomics. Methods in Molecular Biology*. Humana Press, New York, NY, 147–165.

Levesque-Tremblay G, Pelloux J, Braybrook SA, Müller K. **2015**. Tuning of pectin methylesterification: consequences for cell wall biomechanics and development. *Planta* **242**: 791–811.

Lionetti V, Cervone F, Bellincampi D. **2012**. Methyl esterification of pectin plays a role during plant-pathogen interactions and affects plant resistance to diseases. *Journal of Plant Physiology* **169**: 1623–30.

Lionetti V, Fabri E, De Caroli M, *et al.* 2017. Three pectin methylesterase inhibitors protect cell wall integrity for arabidopsis immunity to *Botrytis*. *Plant Physiology* **173**: 1844–1863.

Mbewana S. **2010**. Functional analysis of a lignin biosynthetic gene in transgenic tobacco. *MSc thesis, Stellenbosch University, South Africa,*.

Nguema-Ona E, Moore JP, Fagerström AD, *et al.* 2013. Overexpression of the grapevine PGIP1 in tobacco results in compositional changes in the leaf arabinoxyloglucan network in the absence of fungal infection. *BMC Plant Biology* **13**: 46.

Paňitrur-De La Fuente C, Valdés-Gómez H, Roudet J, *et al.* 2018. Classification of winegrape cultivars in Chile and France according to their susceptibility to *Botrytis cinerea* related to fruit maturity. *Australian Journal of Grape and Wine Research* **24**: 145–157.

Salmeán AA, Guillouzo A, Duffieux D, *et al.* 2018. Double blind microarray-based polysaccharide profiling enables parallel identification of uncharacterized polysaccharides and carbohydrate-binding proteins with unknown specificities. *Scientific Reports* **8**: 1–11.

Sattler SE, Funnell-Harris DL. **2013**. Modifying lignin to improve bioenergy feedstocks: Strengthening the barrier against pathogens? *Frontiers in Plant Science* **4**: 1–8.

Soltis NE, Atwell S, Shi G, *et al.* 2019. Interactions of tomato and *Botrytis cinerea* genetic diversity: Parsing the contributions of host differentiation, domestication, and pathogen variation. *Plant Cell* **31**: 502–519.

Veloso J, van Kan JAL. **2018**. Many shades of grey in *Botrytis*–Host plant interactions. *Trends in Plant Science* **23**: 613–622.

Wood IP, Pearson BM, Garcia-Gutierrez E, *et al.* 2017. Carbohydrate microarrays and their use for the identification of molecular markers for plant cell wall composition. *Proceedings of the National Academy of Sciences of the United States of America* **114**: 6860–6865.

Zykwinska AW, Thibault J-F, Ralet M-C. **2007**. Organization of pectic arabinan and galactan side chains in association with cellulose microfibrils in primary cell walls and related models envisaged. *Journal of Experimental Botany* **58**: 1795–1802.

Appendix

Appendix chapter 3

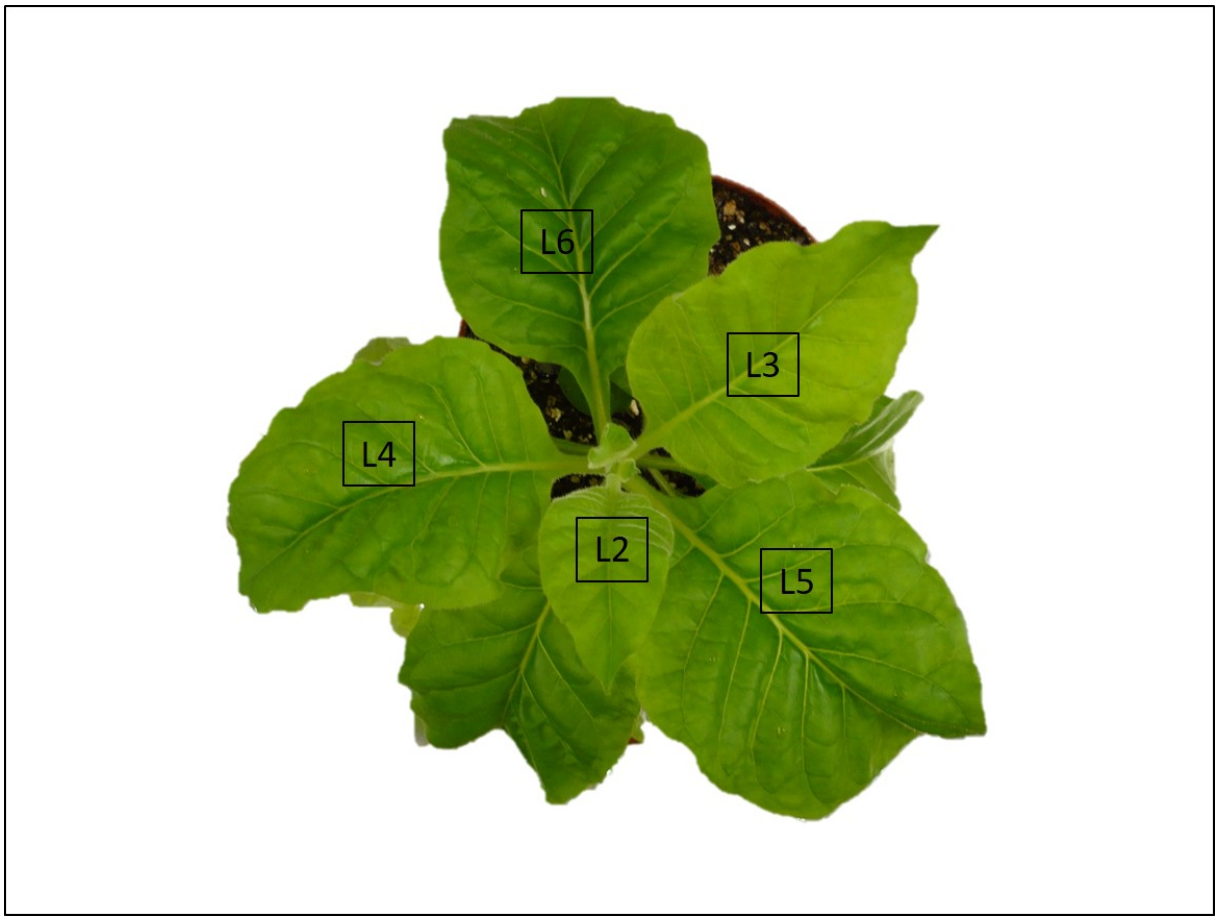

Figure S3.1: A photograph of an SR1 tobacco plant used in this study in order to indicate leaf positions harvested (indicated by the numbered boxes). Out of the eight leaves present on the plant at the time of the experiment, leaf 2 was the youngest of those harvested, closest to the apical meristem and leaves 4-6 are fully expanded leaves.

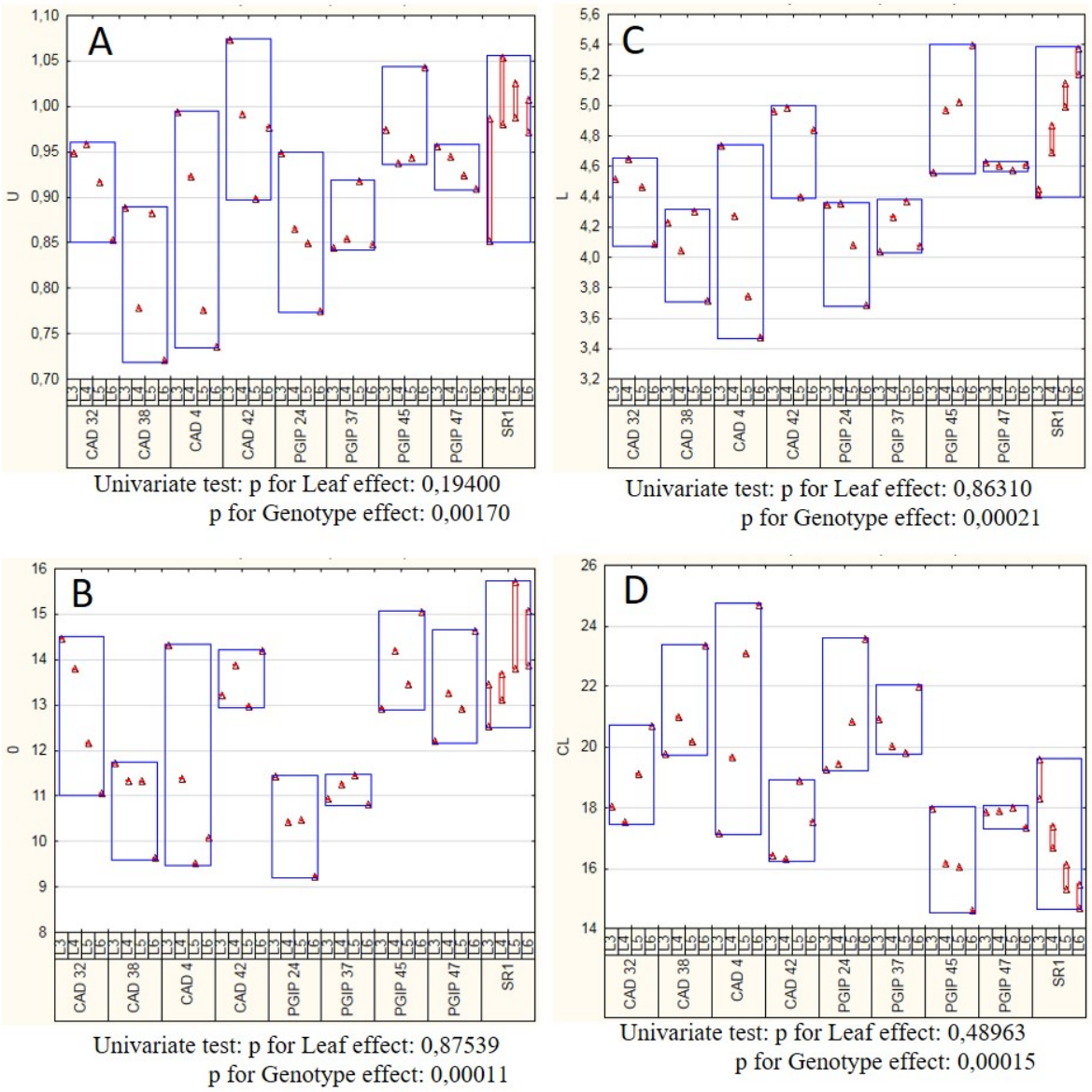

Figure S3.2: ANOVA box plots (multivariate tests of significance with 95% confidence intervals) of Py-GC-MS data for each analyte category SR1 vs transgenic plant lines. **A**: known spectra, unknown identification (U); **B**: unknown spectra (O); **C**: total lignin (L); **D**: Carbohydrate related components/Lignin ratio (CL). Each percentage is the average of four biological repeats of four different leaves, showing standard deviation.

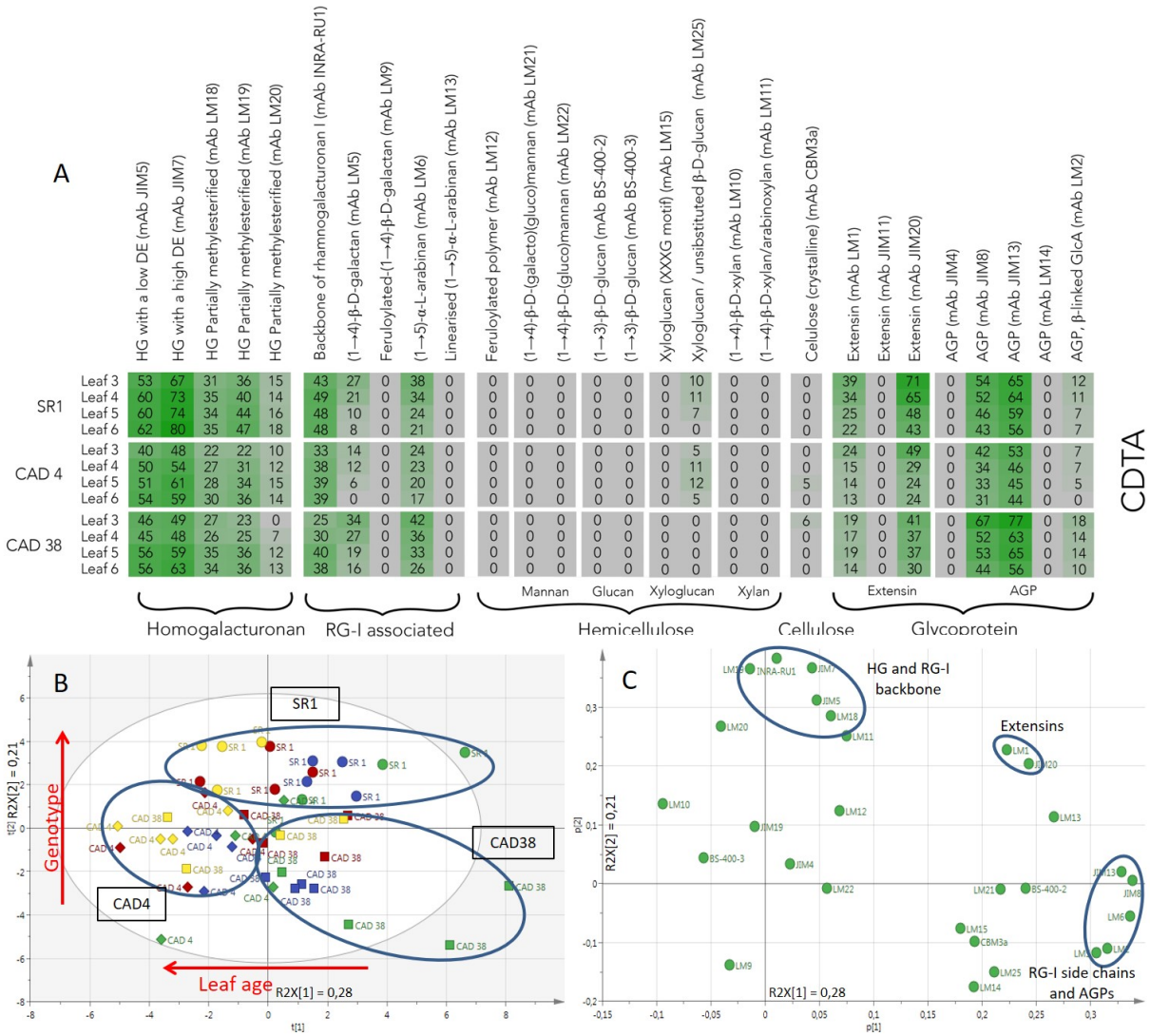

Figure S3.3: CoMPP of the CDTA fraction of the wild type SR1, CAD4 and CAD38 tobacco leaf AIR. Heatmap showing cell wall polysaccharides and proteins relative abundance using antibodies signal intensity reads which are the average of four biological repeats.

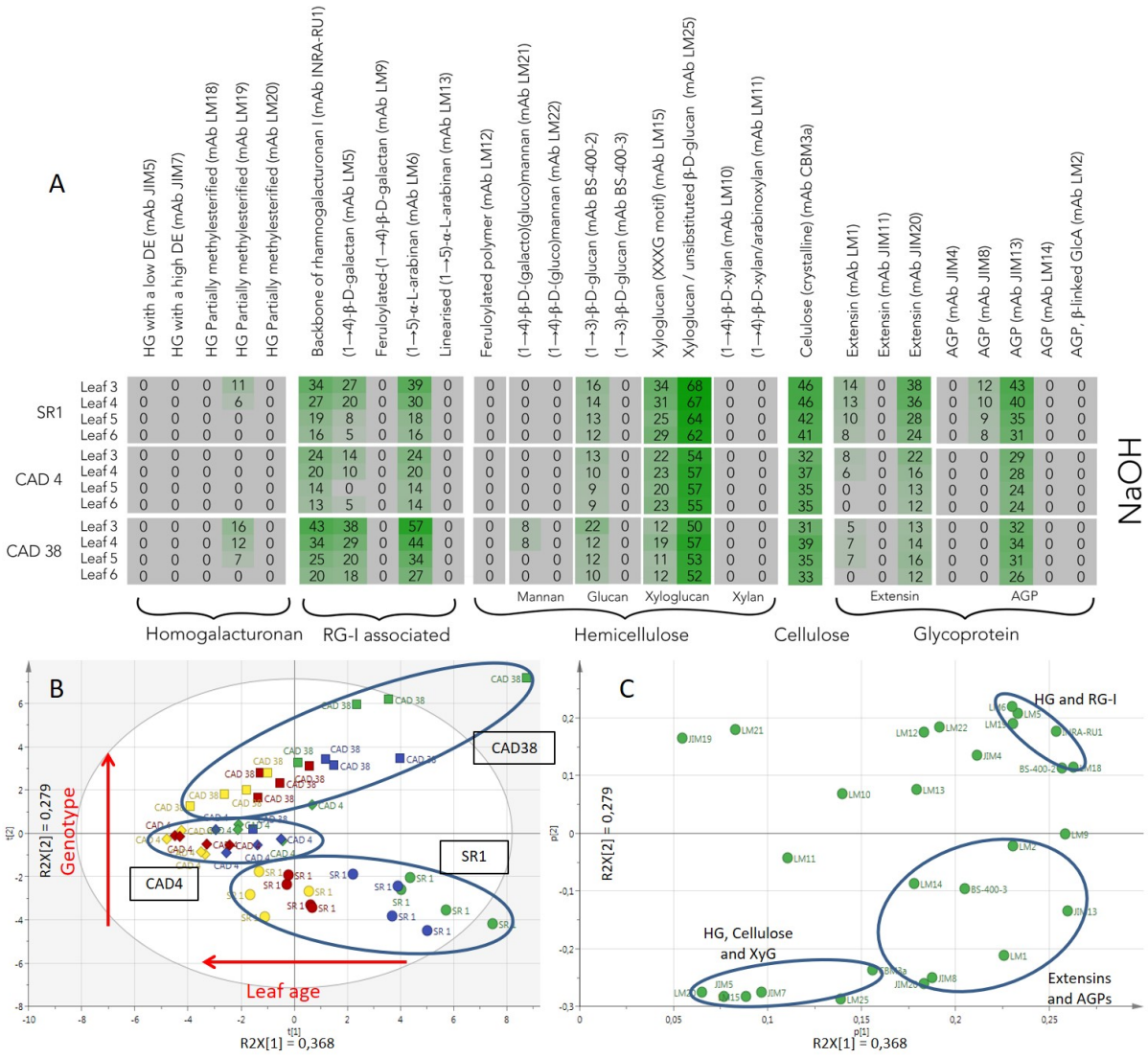

Figure S3.4: CoMPP of the NaOH fraction of the wild type SR1, CAD4 and CAD38 tobacco leaf AIR. Heatmap showing cell wall polysaccharides and proteins relative abundance using antibodies signal intensity reads which are the average of four biological repeats.

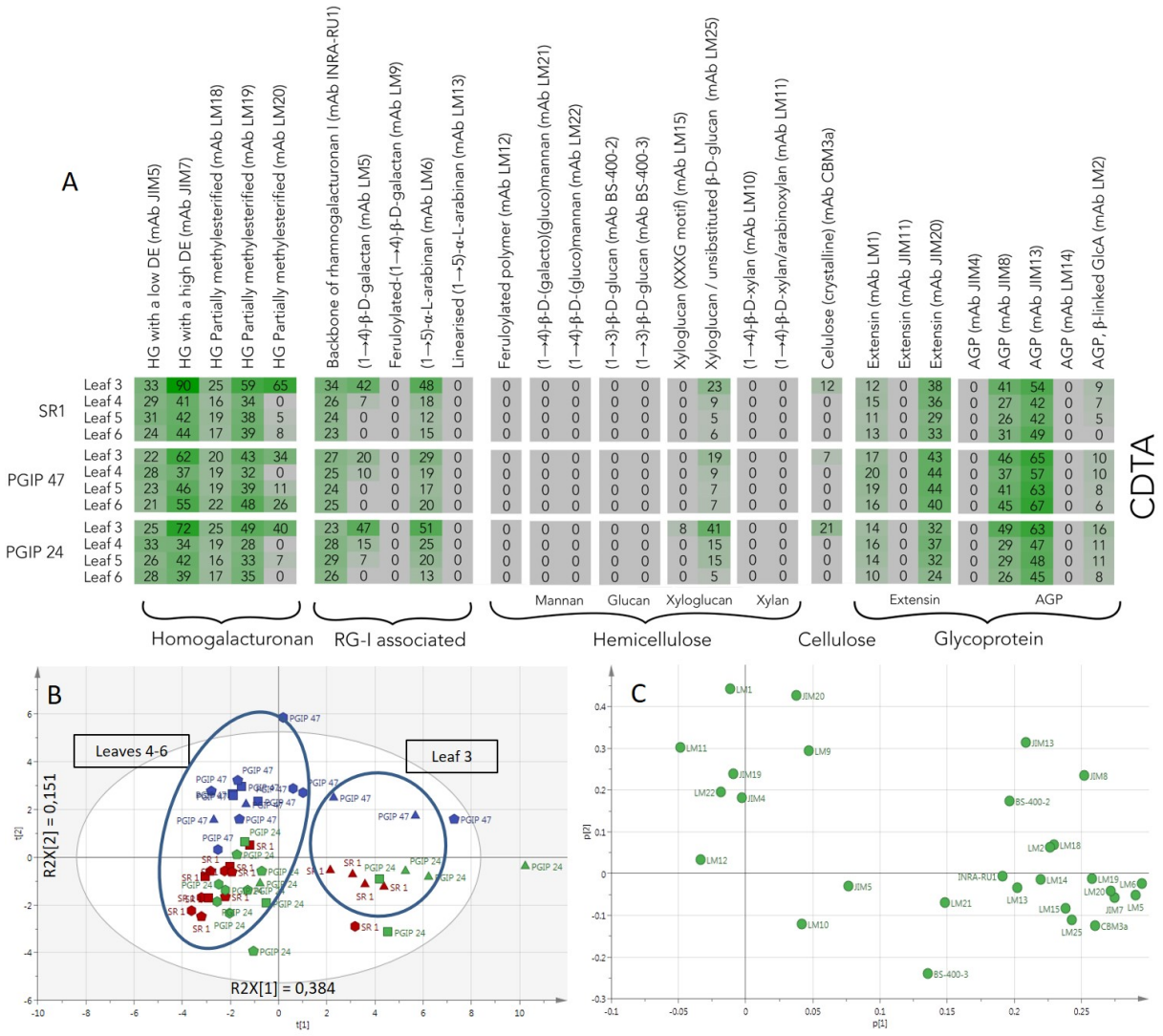

Figure S3.5: CoMPP of the CDTA fraction of the wild type SR1, PGIP24 and PGIP47 tobacco leaf AIR. **A**: Heatmap showing cell wall polysaccharides and proteins relative abundance using antibodies signal intensity reads which are the average of four biological repeats. **B**: PCA of the pectin-rich fraction (CDTA) **C**: Loading plot showing the separation by variables. On the PCA, samples are coloured according to their leaf position, each genotype is represented with a different symbol, and SR1 is circled.

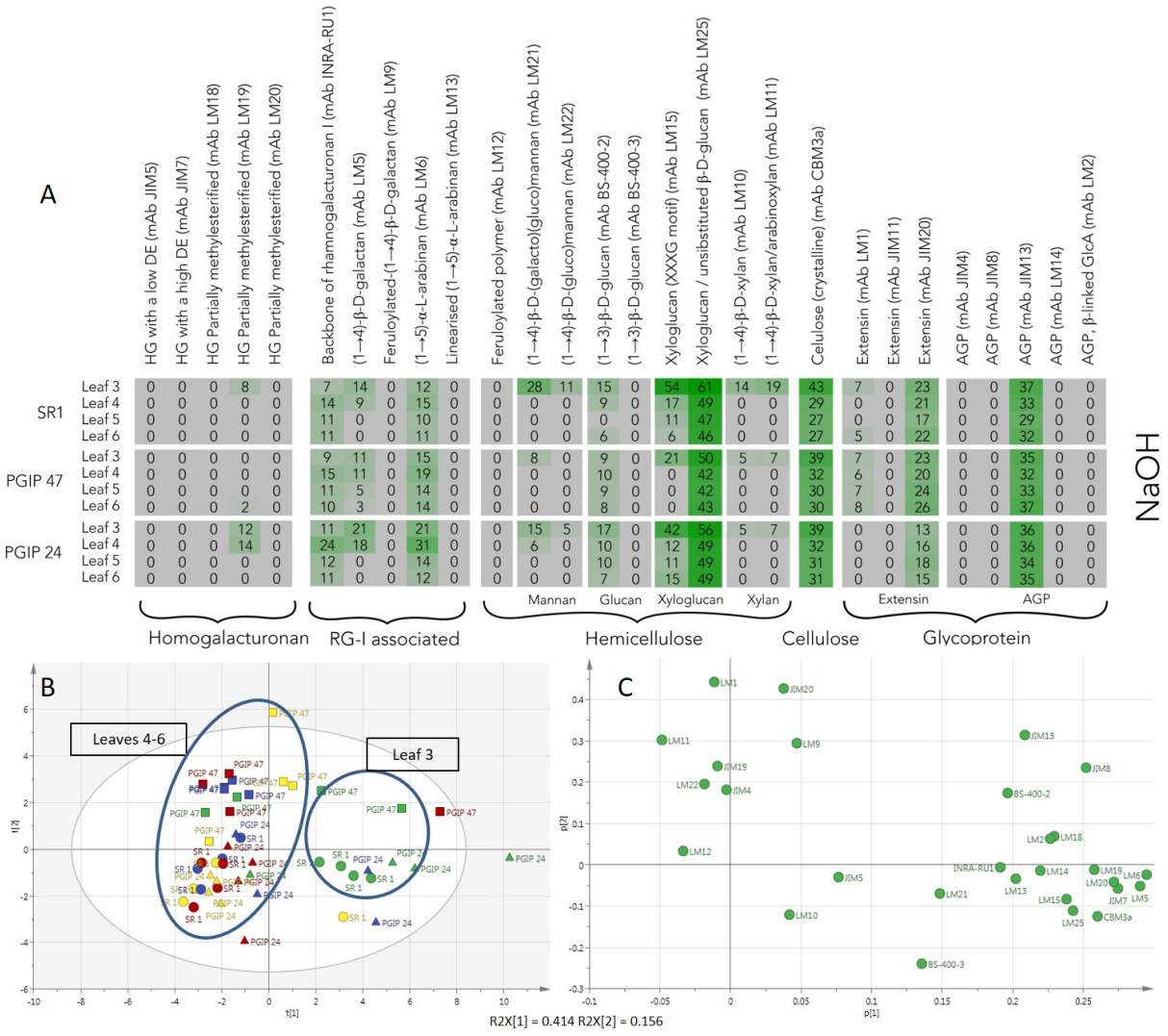

Figure S3.6: CoMPP of the NaOH fraction of the wild type SR1, PGIP24 and PGIP47 tobacco leaf AIR. **A**: Heatmap showing cell wall polysaccharides and proteins relative abundance using antibodies signal intensity reads which are the average of four biological repeats. **B**: PCA of the pectin-rich fraction (NaOH) **C**: Loading plot of the previous PCA showing the separation of the variable. On the PCA, samples are coloured according to their leaf position, each genotype is represented with a different symbol, and SR1 circled.

Appendix chapter 4

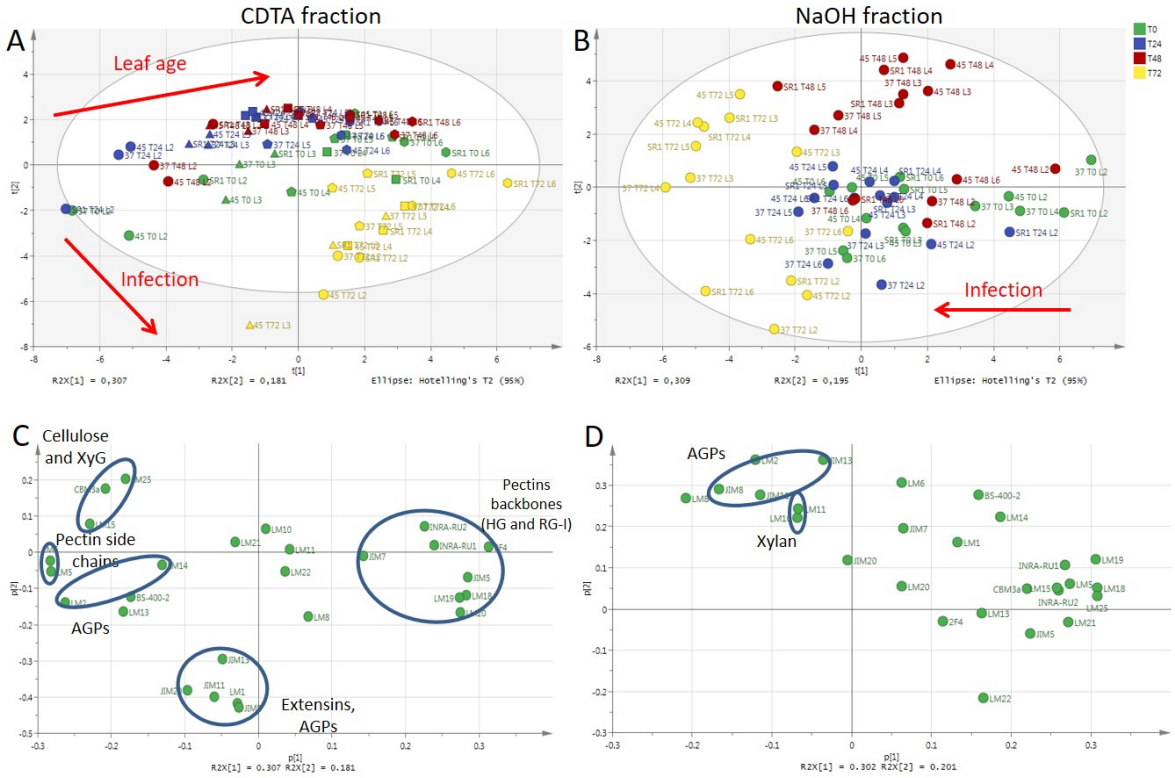

Figure S4.1: PCA of CoMPP results of the wild type SR1, VviPGIP37 and VviPGIP45 tobacco leaf AIR from tissue adjacent and distal to the infection by *B. cinerea*. (**A**, **C)** CDTA fraction and (**B, D**) NaOH fraction **A**, **B**: PCA showing sample separation. Samples are coloured according to infection progression. **C**, **D**: Loading plots of the respective PCA showing the epitopes that drive sample separation. Red arrows show the infection progression and leaf age effect. Detailed list of the antibody used is available in Table 4.1.

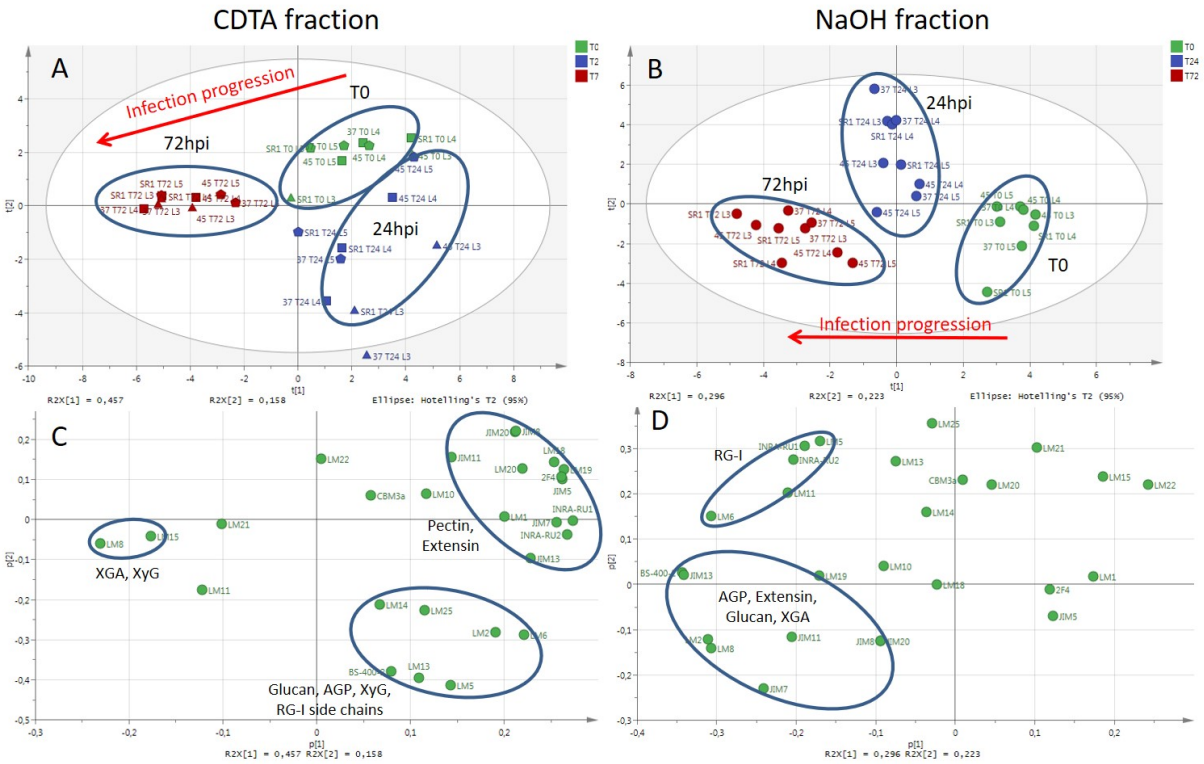

Figure S4.2: PCA of CoMPP results of the wild type SR1, VviPGIP37 and VviPGIP45 tobacco leaf AIR showing lesion tissue from the infection by *B. cinerea*. (**A**, **C)** CDTA fraction and (**B, D**) NaOH fraction **A**, **B**: PCA showing sample separation. Samples are coloured according to infection progression. **C**, **D**: Loading plots of the respective PCA showing the epitopes that drive sample separation. Red arrows show the infection progression and leaf age effect. Detailed list of the antibody used is available in Table 4.1.

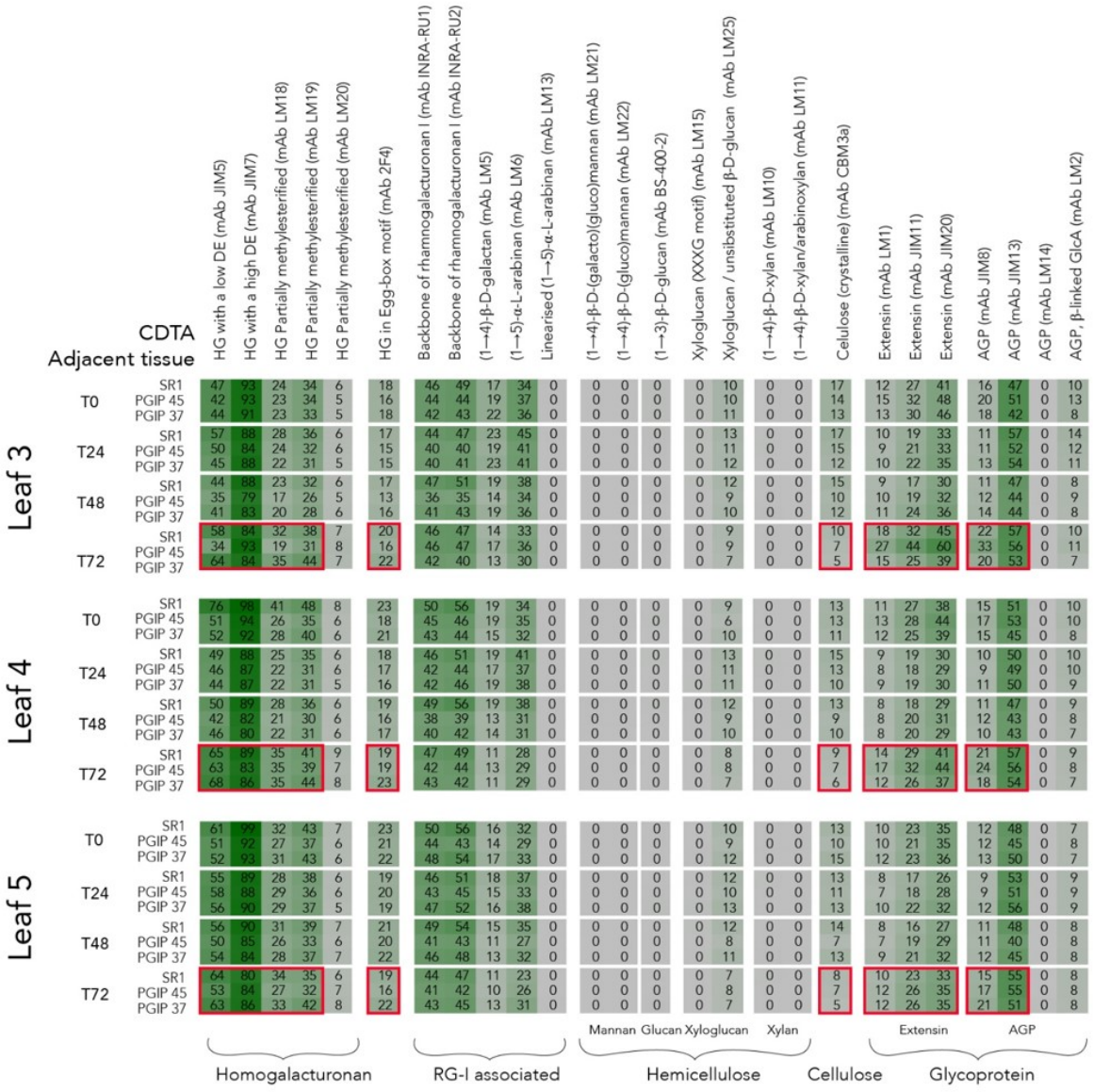

Figure S4.3: Comprehensive microarray polymer profiling (CoMPP) analysis of the wild-type SR1, PGIP37 and PGIP45 tobacco leave AIR of adjacent tissue to the lesion infected by *B. cinerea*. Results are presented as heatmaps of the CDTA extraction, showing the relative abundance of cell wall associated epitopes and separated between infected leaves. Detailed list of the antibody used is available in Table 4.1. Red boxes indicate variations due to the infection. AGP: arabinogalactan protein, HG: homogalacturonan, mAbs: monoclonal antibody, T: time point (in hours)

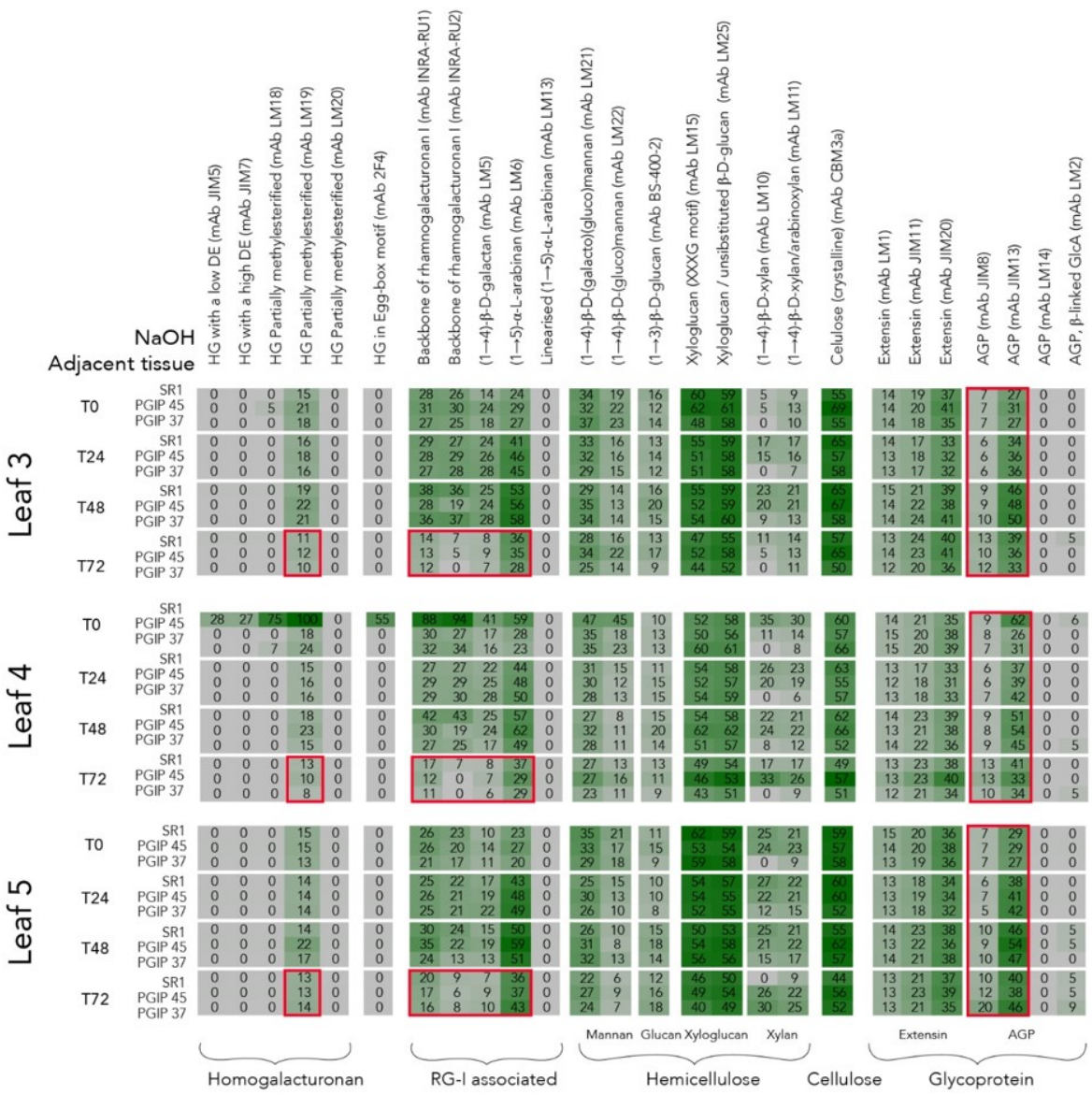

Figure S4.4: Comprehensive microarray polymer profiling (CoMPP) analysis of the wild-type SR1, PGIP37 and PGIP45 tobacco leave AIR of adjacent tissue to the lesion infected by *B. cinerea*. Results are presented as heatmaps of the NaOH extraction, showing the relative abundance of cell wall associated epitopes and separated between infected leaves. Detailed list of the antibody used is available in Table 4.1. Red boxes indicate variations due to the infection. AGP: arabinogalactan protein, HG: homogalacturonan, mAbs: monoclonal antibody, T: time point (in hours)

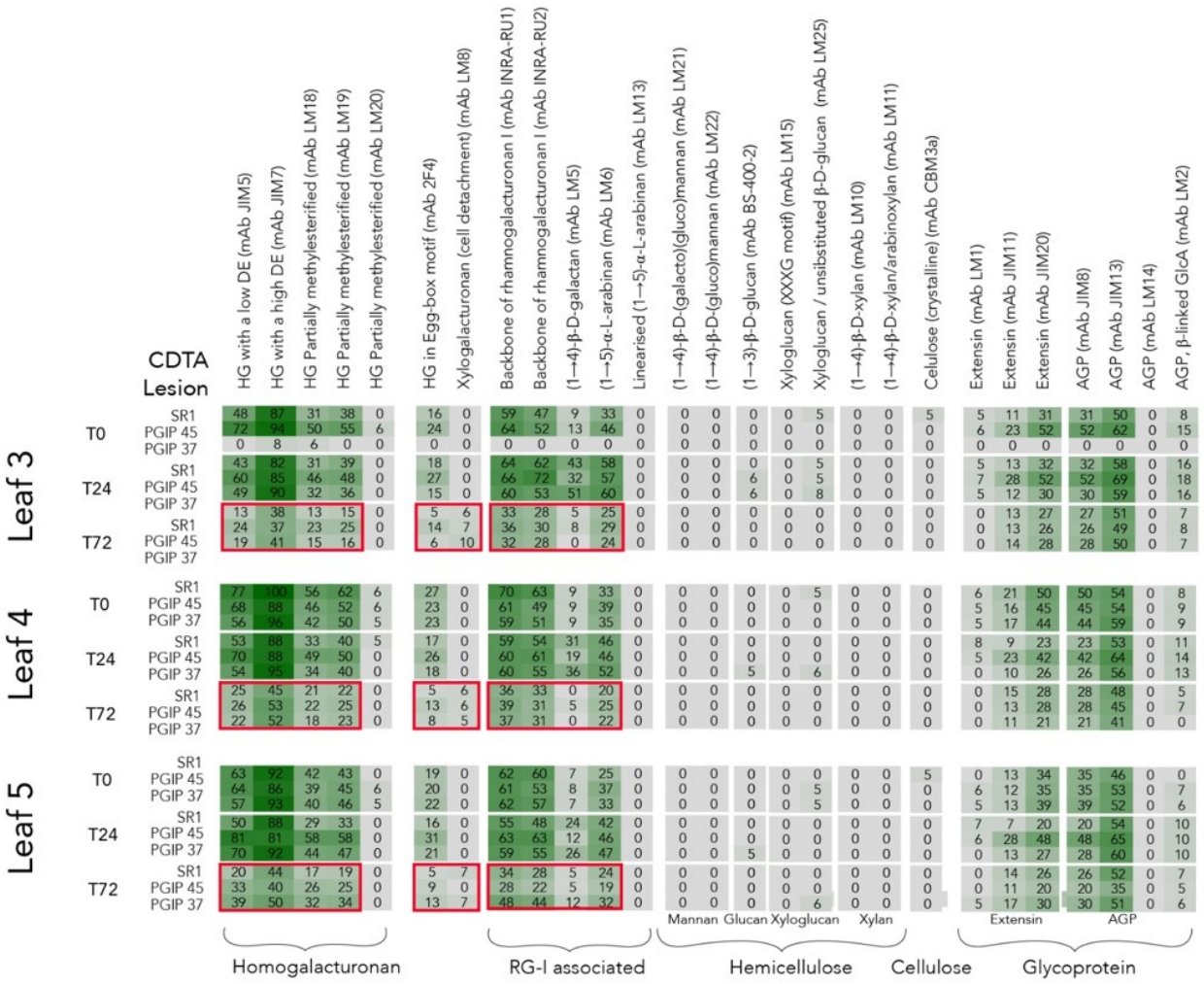

Figure S4.5: Comprehensive microarray polymer profiling (CoMPP) analysis of the wild-type SR1, PGIP37 and PGIP45 tobacco leave AIR of lesion tissue infected by *B. cinerea*. Results are presented as heatmaps of the CDTA extraction, showing the relative abundance of cell wall associated epitopes and separated between infected leaves. Detailed list of the antibody used is available in Table 4.1. Red boxes indicate variations due to the infection. AGP: arabinogalactan protein, HG: homogalacturonan, mAbs: monoclonal antibody, T: time point (in hours)

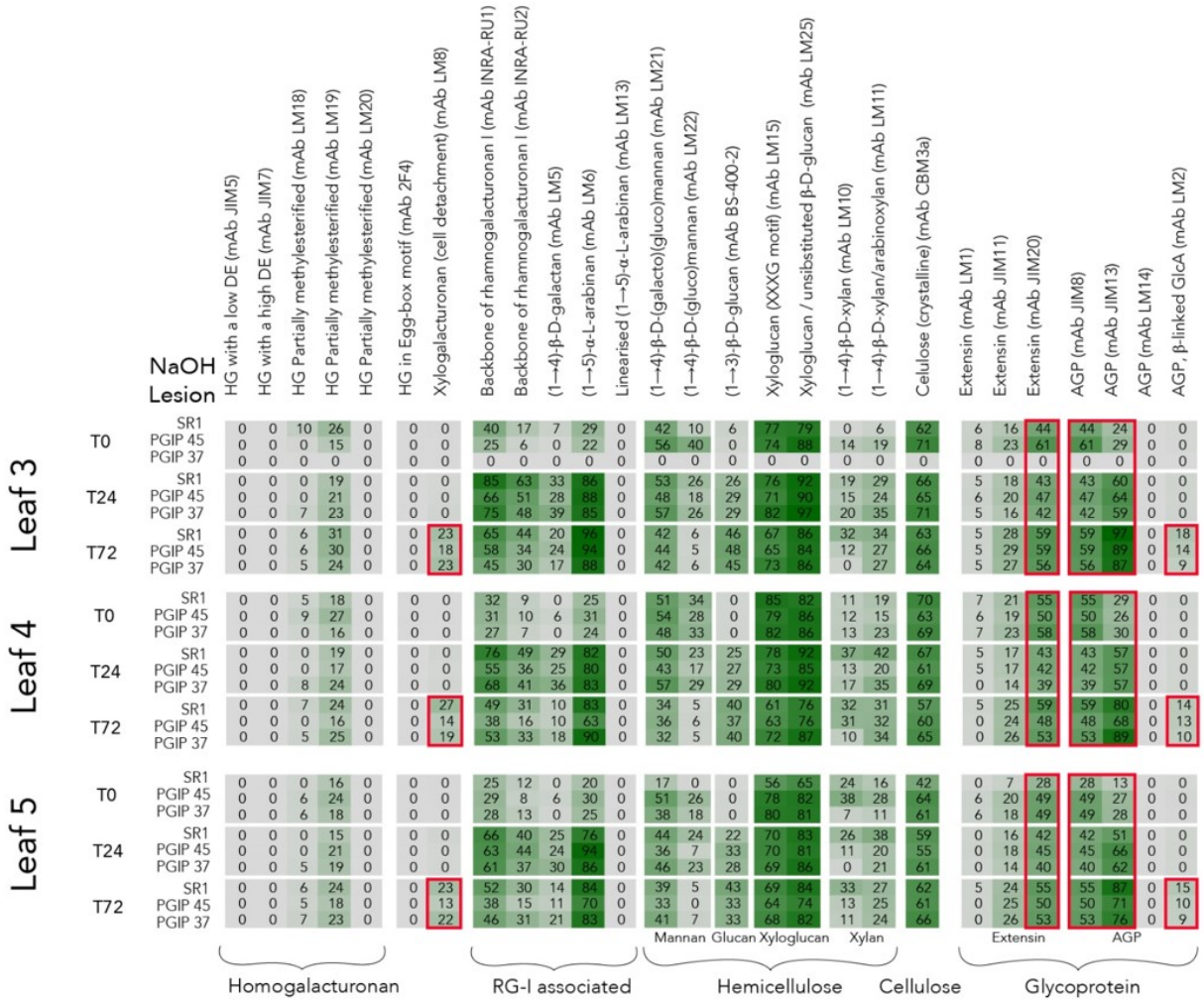

Figure S4.6: Comprehensive microarray polymer profiling (CoMPP) analysis of the wild-type SR1, PGIP37 and PGIP45 tobacco leave AIR of lesion tissue infected by *B. cinerea*. Results are presented as heatmaps of the NaOH extraction, showing the relative abundance of cell wall associated epitopes and separated between infected leaves. Detailed list of the antibody used is available in Table 4.1. Red boxes indicate variations due to the infection. AGP: arabinogalactan protein, HG: homogalacturonan, mAbs: monoclonal antibody, T: time point (in hours)

Appendix Chapter 5

Table S1: Levels of grape infection severity on four *Vitis vinifera* cultivars, following a time-course *Botrytis cinerea* infection experiment on ripe grapes. Barlinka and Dauphine were only scored until 216 hours post infection (hpi) The data is expressed as percentages, based on the scoring of the infection experiments where Ni, indicates no infection; Li, low infection; Mi, mild infection; and .Hi, high infections. In total, this experiment was conducted on 816 Cabernet Sauvignon grapes, 912 Sauvignon Blanc grapes, 592 Dauphine grapes and 540 Barlinka grapes. For each time point, a portion of the total number was sampled for analysis.

		Cabernet Sauvignon	Sauvignon blanc	Dauphine	Barlinka
24 hpi	Ni	100,0	100,0	100,0	100,0
	Li	0,0	0,0	0,0	0,0
	Mi	0,0	0,0	0,0	0,0
	Hi	0,0	0,0	0,0	0,0
	Total % Infected	0,0	**0,0**	**0,0**	**0,0**
72 hpi	Ni	98,8	79,2	68,9	73,0
	Li	1,3	20,8	26,2	17,5
	Mi	0,0	0,0	4,9	9,5
	Hi	0,0	0,0	0,0	0,0
	Total % Infected	**1,3**	**20,8**	**31,1**	**27,0**
144 hpi	Ni	69,8	64,4	63,1	50,7
	Li	16,7	16,2	0,8	11,0
	Mi	7,8	19,4	11,5	15,5
	Hi	5,7	0,0	24,6	22,8
	Total % Infected	**30,2**	**35,6**	**36,9**	**49,3**
216 hpi	Ni	45,9	40,0	38,5	31,6
	Li	17,7	5,0	11,5	7,5
	Mi	18,2	6,9	13,9	12,8
	Hi	18,2	48,1	36,1	48,1
	Total % Infected	**54,2**	**60,0**	**61,5**	**68,4**
288 hpi	Ni	22,4	23,7		
	Li	7,8	5,4		
	Mi	13,5	10,8		
	Hi	56,3	60,1		
	Total % Infected	**77,6**	**76,4**		

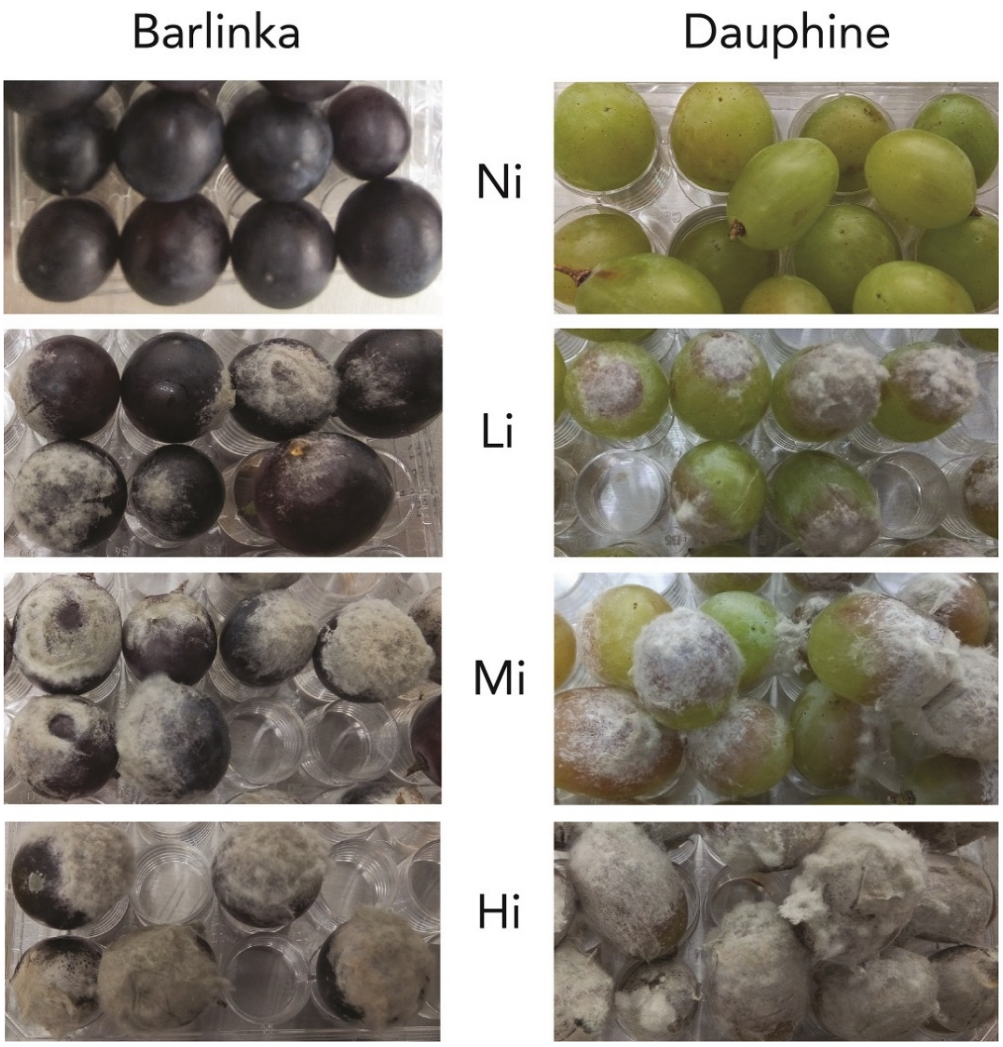

Figure S5.1: Barlinka and Dauphine grapes at the end of the post-véraison infection experiment showing the four infection levels. From the least to the most infected: Ni: no-infection; Li: light infection; Mi: mild or moderate infection; Hi: high infection

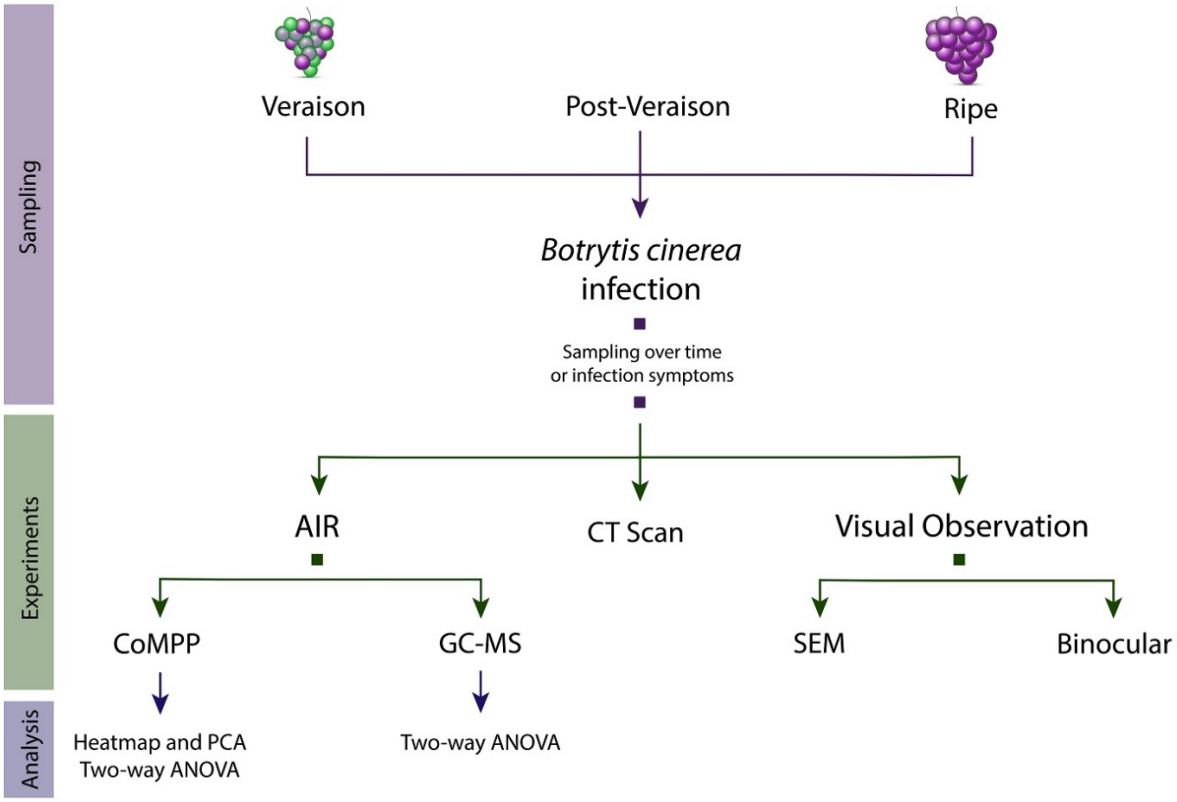

Figure S5.2: Flow diagram showing the experimental procedure employed in the present study.

Figure S5.3: Picture showing a representative box of Barlinka grapes at the end of the véraison infection experiment. It highlights the absence of successful infection at véraison with our experimental setup.

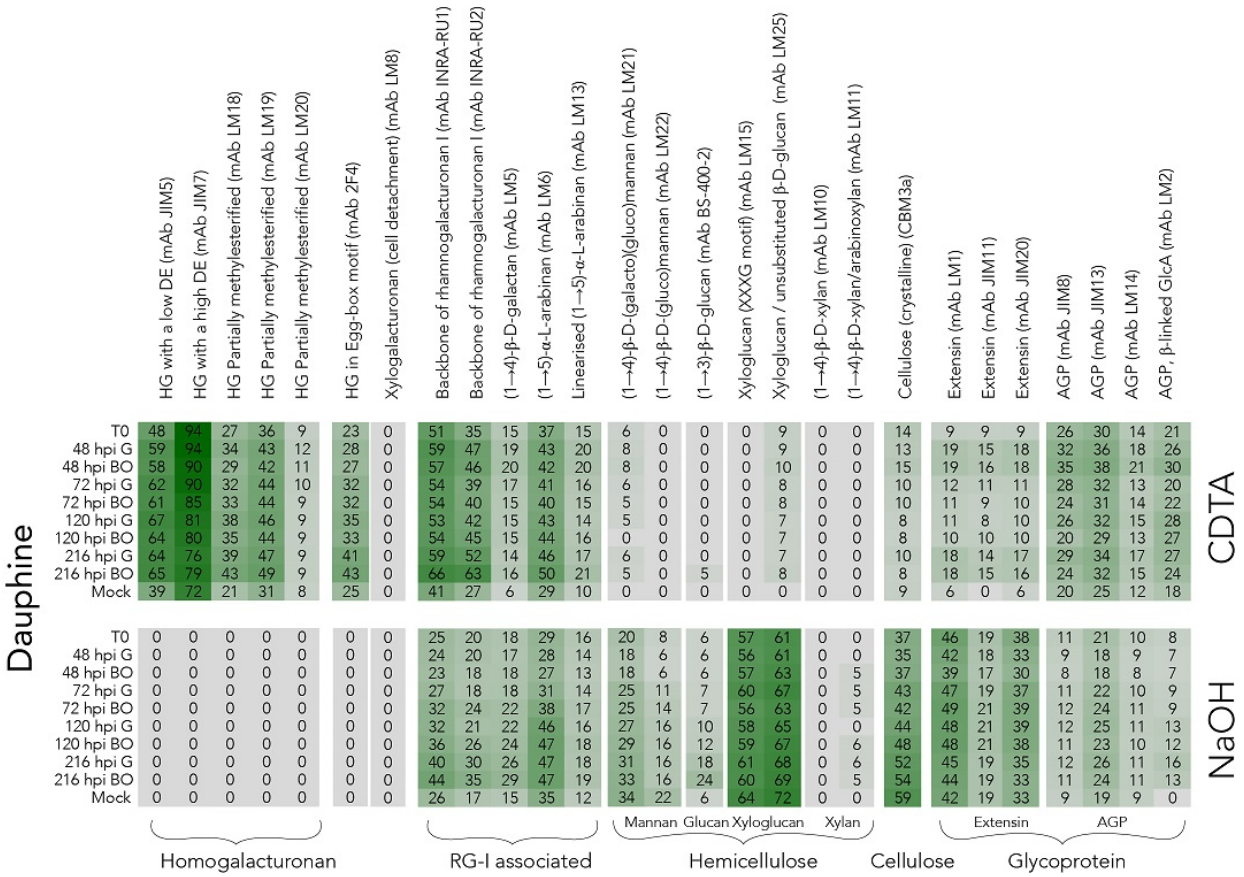

Figure S5.4: CoMPP analysis of Dauphine (DP) grapes infected by two *B. cinerea* strains, the grape strain and BO.5.10, at ripe stage. Results are presented as heatmap showing the relative abundance of cell wall associated epitopes (see material and methods for more information). Detailed list of the antibody used is available in Table 1.

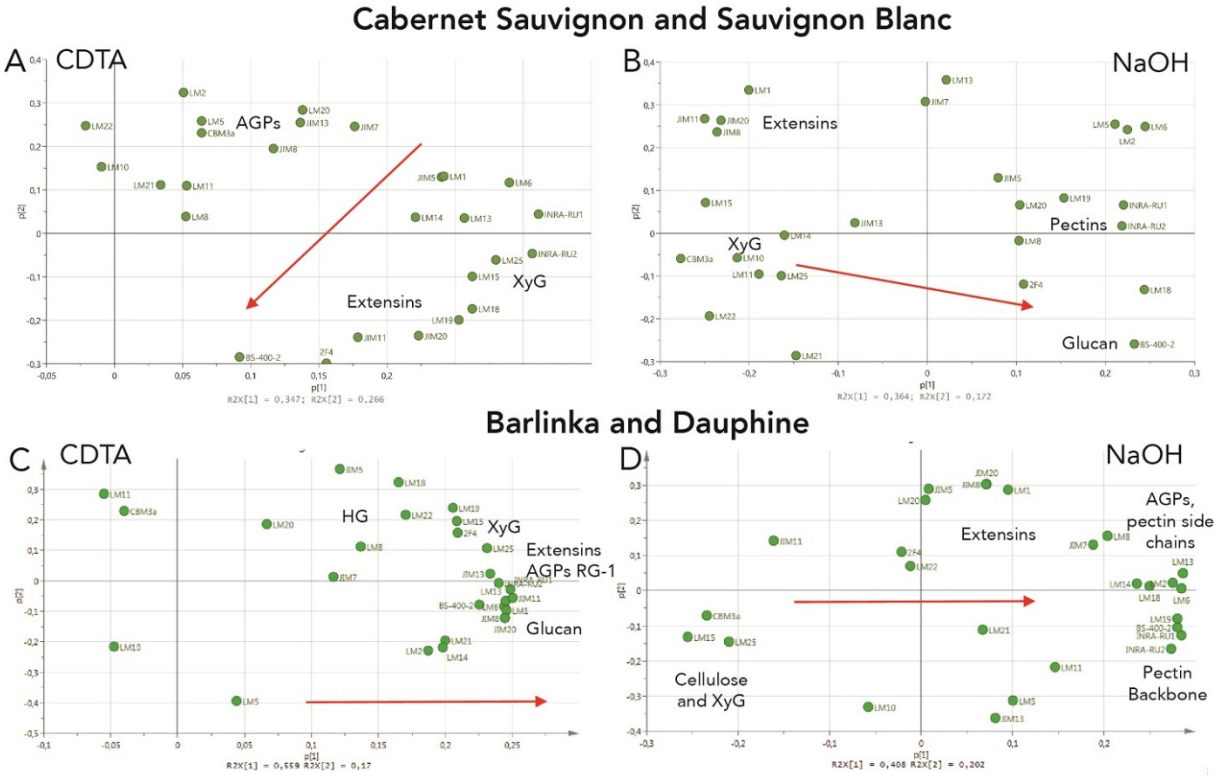

Figure S5.5: Loading plot showing the separation by variables of previously shown PCA analysis of grapes infected by *B. cinerea*. **A**: Loading of the CDTA fraction of CS and SB grapes (Fig. 6B); **B**: Loading of the NaOH fraction of CS and SB grapes (Fig. 6C); Loading of the CDTA fraction of BK and DP grapes (Fig. 8B); **B**: Loading of the NaOH fraction of BK and DP grapes (Fig. 8C). Interesting groupings of antibodies are annotated and circled in blue.

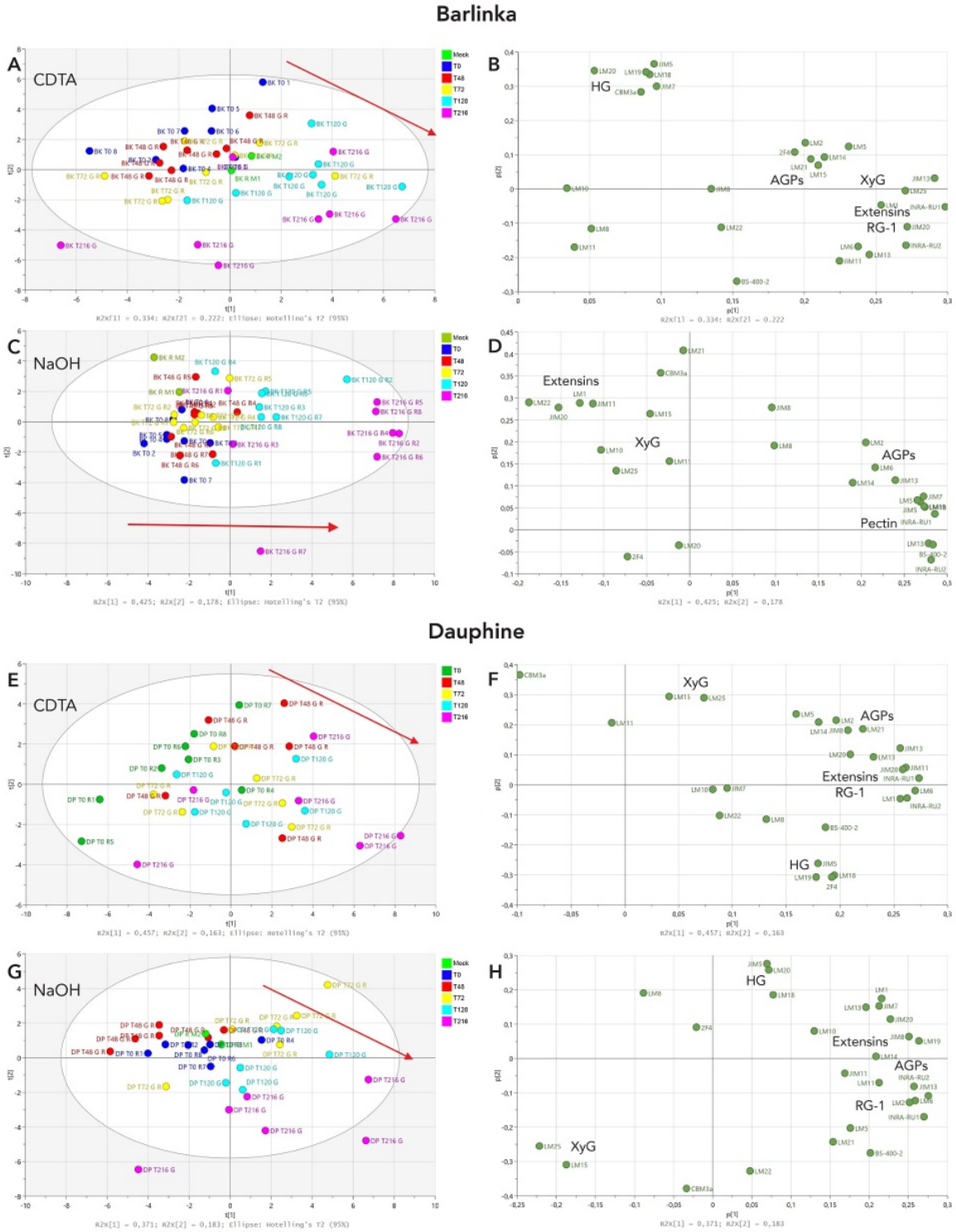

Figure S5.6: PCA of CoMPP results of AIR from Barlinka (**A**, **B**, **C**, **D)** and Dauphine (**E**, **F**, **G**, **H**) ripe grapes infected by *B. cinerea*. **A**, **C**, **E**, **G**: PCA showing sample separation for the CDTA (**A**, **E**) and NaOH (**C**, **G**) extractions. Samples are coloured according to infection progression. **B**, **D**, **F**, **H**: Loading plots of the respective PCA showing the epitopes that drive sample separation. Red arrows show the infection progression. Detailed list of the antibody used is available in Table 1.